DISSERTATION

SYNAPTOTAGMIN IN ASYNCHRONOUS NEUROTRANSMITTER RELEASE AND SYNAPTIC DISEASE

Submitted by

Mallory Catherine Shields

Department of Biomedical Sciences

In partial fulfillment of the requirements

For the Degree of Doctor of Philosophy

Colorado State University

Fort Collins, Colorado

Summer 2018

Doctoral Committee:

Advisor: Noreen Reist

Deborah Garrity
Michael Tamkun
Susan Tsunoda

ABSTRACT

SYNAPTOTAGMIN IN ASYNCHRONOUS NEUROTRANSMITTER RELEASE AND SYNAPTIC DISEASE

The majority of cell-to-cell communication relies on the stimulated release of neurotransmitter. Two forms of Ca^{2+}-dependent stimulated release, synchronous and asynchronous, have been identified. Synchronous release is the initial release that occurs within milliseconds of stimulation. Critical for efficient synaptic communication, synchronous release is the dominant form of release at most synapses. Alternatively, asynchronous release occurs over longer time periods, with implications in synaptic plasticity and development. However, its mechanisms are poorly understood.

Both synchronous and asynchronous release rely on Ca^{2+} sensors to confer their distinct characteristics. Synaptotagmin 1 is widely accepted as the Ca^{2+} sensor for fast, synchronous release, but its role in asynchronous release is unclear. Previous studies have led to the hypothesis that synaptotagmin 1, particularly Ca^{2+} binding by its C_2A domain, is needed to inhibit aberrant asynchronous fusion events. However, recent studies have raised questions regarding the interpretation of the results that led to this conclusion.

In chapter 2, I have directly tested the effect of Ca^{2+} binding by synaptotagmin 1's C_2A domain on asynchronous release utilizing an alternant Ca^{2+}-binding mutant. This novel mutation was designed to block Ca^{2+} binding without introducing the artifacts of the original Ca^{2+}-binding mutation. By investigating asynchronous events *in vivo* at the *Drosophila* neuromuscular junction, I found no significant effect on asynchronous release when C_2A Ca^{2+} binding was

blocked. Thus, I conclude that Ca^{2+} binding by synaptotagmin's C_2A domain is not needed for regulation of asynchronous release, in contrast to the previous study that inadvertently introduced an artifact described below.

To prevent Ca^{2+} binding, the original aspartate to asparagine mutations (*syt*$^{D\text{-}N}$) removed some of the negatively-charged residues that coordinate Ca^{2+}. This simultaneously introduced aberrant fusion events, because it also interrupted the electrostatic repulsion between synaptotagmin's negatively-charged C_2A Ca^{2+}-binding pocket and the negatively-charged presynaptic membrane which is required to clamp constitutive SNARE-mediated fusion. Previous Reist lab results demonstrate that the *syt*$^{D\text{-}N}$ mutations in the C_2A domain are likely behaving as ostensibly constitutively bound Ca^{2+}. Indeed, I report that the *syt*$^{D\text{-}N}$ mutation displays slower release kinetics. To directly test if this mutation is the cause of the increase in asynchronous events, I generated additional mutations that prevent interactions with the presynaptic membrane coupled to the originally published *syt*$^{D\text{-}N}$ mutations.

In chapter 3 of this dissertation, I investigated these novel mutations at the *Drosophila* neuromuscular junction. I reported no increase in asynchronous release relative to control, providing evidence that the increased asynchronous events in *syt*$^{D\text{-}N}$ mutants are a result of the original mutation acting as an asynchronous sensor. Together, my results contradict the current hypothesis in the field and provide the likely mechanism for the increased asynchronous release observed in the original study.

This dissertation also investigated the relatively new role for synaptotagmin mutations in the etiology of neuromuscular disease. With increased availability of high-throughput sequencing, over 20 candidate genes have been implicated in different forms of congential myasthenic syndromes. These inherited disorders are caused by mutations in genes needed for

effective neuromuscular signaling. Two families, presenting with similar myasthenic syndromes, carry point mutations in the C_2B Ca^{2+} binding pocket of synaptotagmin, expressed as an autosomal dominant disorder. One of theses families contains a proline to leucine substitution (*syt*$^{P\text{-}L}$) a residue that had not been previously investigated for synaptotagmin function.

In chapter 4, I investigated the functional importance of this mutation and created a disease model for this familial condition by driving the expression of a homolous proline-leucine synaptotagmin substitution in the central nervous system of *Drosophila*. I demonstrated that the proline residue plays a functional role in efficient transmitter release by testing its function in an otherwise synaptotagmin null genetic background. Additionally, this mutation displayed characteristics similar to the human disorder when expressed in a heterozygous synaptotagmin background, similar to the familial expression. Namely, the *syt*$^{P\text{-}L}$ mutants exhibited a decreased release probability, which resulted in decreased evoked responses that facilitate upon high frequency stimulation, a rightward shift in Ca^{2+} sensitivity, and behavioral deficits, including decreased motor output and increased fatigability. Thus, these studies establish the causative nature of the *syt*$^{P\text{-}L}$ mutation in this rare form of congenital myasthenic syndrome and highlight the utility of the *Drosophila* system for disease modeling.

ACKNOWLEDGEMENTS

As my time at Colorado State University comes to a close, I look back with overwhelming gratitude to the people in my life who have been there to support this dissertation. First and foremost, I acknowledge Dr. Noreen Reist, the quintessential fearless boss lady that all young women scientists dream of becoming. Noreen, your honesty, support, critical intellectual feedback, and overall “science mom” mentality has made my time here unforgettable and nothing short of the best job I can imagine. I feel prepared to face my next endeavor with confidence, and I am proud to say a bit of your fearlessness has worn off on me. I thank you for everything.

Thank you to my committee comprised of Drs. Michael Tamkun, Susan Tsunoda, and Deborah Garitty, for providing feedback and guidance throughout my graduate carreer. I appreciate your edits and suggestions, and of course, your approval signatures.

For the past and current members of the Reist lab: it has been a pleasure to work with each and every one of you. Ben Johnson, Alexa Mumm (Navarro), and Remi Boudreau: you taught me that electrophysiology and western analyses take patience. More importantly, you taught me game nights, bowling Thursdays, pie, birthday cupcakes, and terrible jokes make a new girl feel supported and included. Matt Bowers: I am so grateful you decided to join the Reist lab. Your positive attitude, willingness to grab a beer at the end of a long day, visual eye for figure formatting, and scientific feedback are invaluable. I am proud to call you my colleague and friend. Jasmin Hicks, you make a great new fit in the Reist lab and are a wonderful new friend. I know you will go on to do powerful things.

My family is my main source of unwavering support and love. Mom, Dad, James, Grandmother, Uncle Jay, and Aunt Marilyn: Thank you for hearing the ups and downs of this process and keeping me inspired to finish. To my Pawpaw, Grandmamma, and Grandfather who have passed away: I wish you were still here today. You are missed. I love you all very much.

The friends I have made have made this PhD a whole lot of fun. My roommates Rachel West, Ashley Turnidge, Adam Heck, and Mike Mangalea: You guys are just the best. There are countless other graduate students and post-docs and their families who have stamped a place on my heart, including An Dang, Kristen Brown, Krystle Frahm, Elizabeth Akin, Eric Marr, Nathan Byers, Sarah Wooldridge, Laura Sole, Max Vallejos, Coreen Frawley, and Alli and Jordan Werner. Thanks for all the dress-up parties, ski trips, commiserating, and bike brewery tours.

A special thank you to Erin Bisenius for keeping my paperwork in line and for witty cards and chocolates on my birthday, and Karen Soloman and Shazette Pierce for handling my day-to-day administrative questions. You three made this process run smoothly, and your pleasant personalities make going to work feel less like work.

None of this is possible without funding. Noreen's National Science Foundation grants (IOS-1257362 and IOS-1025966) kept me afloat for years, but there are a few additional sources of funding that are appreciated: the Molecular, Cellular, and Integrative Neuroscience (MCIN) Program for funding my first year, the MCIN travel grants to help support my participation in various meetings, the Thornburg Graduate Excellence Award, and finally, the Vice President for Research Fellowship, which not only supplemented my funding and provided monetary support for meetings, but also offered leadership training throughout this last year.

I had the pleasure to collaborate with both national and international scientists, and would like to address each of them. Rita Horvath, thank you for introducing us to the congenital

myasthenia project and forging our collaboration, Roger Whittaker, for your clinical perspective and feedback, Alysia Vrailes-Mortimer, for opening the doors to your lab and teaching me the *Drosophila* Activity Monitoring Assay and your edits on our manuscript. Moto Yoshihara, thank you and your lab for the *Drosophila* line that spurred my thesis projects. The experts in the Colorado State University Statistics department are unparalleled. Ann Hess and Jim Zumbrunnen, thank you for helping me analyze mounds of data.

Thanks to the Cold Spring Harbor Neurobiology of *Drosophila* course and to the instructors, especially Kate O'Conner-Giles, Greg Macleod, and Adrian Rothenfluh for their time and expertise, and to Stefan Pulver and Richard Daniels for their specialized instruction on two-electrode voltage clamp electrophysiology.

TABLE OF CONTENTS

CHAPTER 1. OVERVIEW OF SYNAPTIC TRANSMISSION AND NEUROMUSCULAR DISEASE

1.1 Overview

Nervous system function relies upon the transmission of signals between neurons. Neurons transmit information across long distances through action potentials, which generally do not propagate between spatially distinct cells. To cross the gap between nerve cells, the majority of cell-to-cell signaling relies on release of neurotransmitters. The majority of neurotransmitter release from active neurons occurs in a Ca^{2+} dependent manner at synapses.

Within synapses, small, synaptic vesicles filled with a quantum of neurotransmitter fuse with the presynaptic membrane in a tightly regulated series of steps. There are two distinct forms of stimulated Ca^{2+}-dependent fusion and subsequent neurotransmitter release, synchronous and asynchronous release. These release events are dependent on Ca^{2+} sensors. One essential protein, synaptotagmin 1, is widely accepted as the Ca^{2+} sensor for synchronous release. Previous studies implicate a regulatory role for synaptotagmin 1 in the other form of stimulated release, asynchronous release, but its precise mechanism is unclear. This dissertation investigates whether synaptotagmin 1 plays a regulatory role in the asynchronous form of Ca^{2+}-dependent release.

This dissertation also investigates the role of synaptotagmin in a newly characterized congenital myasthenic syndrome, a rare subset of neuromuscular disorders caused by genetically inherited synaptic protein mutations. As synaptic transmission is tightly regulated, dysfunction of any protein needed for release or response of neurotransmitter can result in human disease.

Multiple diseases at the neuromuscular junction result from dysfunctional synaptic proteins. Clinicians diagnose neuromuscular disorders using nerve conduction studies, exercise

testing, and genetic sequencing. However, the need to uncover mechanisms mediating these disorders is currently unmet. *Drosophila* offer a quick, economical, and genetically flexible method for investigation of rare human diseases. By modeling this newly characterized synaptotagmin congenital myasthenic disease using *Drosophila*, I investigate a causative role in a synaptotagmin point mutation in the etiology of disease symptoms and uncover some of its mechanistic underpinnings.

1.2 Neuronal structure

Neuronal structure is highly variable, from long projection neurons in the motor system to small bipolar cells of the retina. However, the canonical structure consists of three major structures: dendrites, the cell body, and the axon. Dendrites typically project out from a cell body to neighboring cells and receive neurotransmitter signals from the presynaptic cell terminal. These dendrites respond with small depolarizations or hyperpolarizations that spread passively to the axon hillock. The neuronal cell body houses many components typically found in other cells, such as the nucleus, smooth and rough endoplasmic reticulum, mitochondria, and golgi apparatus. The axon contains the axon hillock, which integrates all depolarizing and hyperpolarizing signals received from the dendrites. If the incoming summative signal reaches the threshold potential, the cell will fire a self-propagating electrical signal, or action potential, down the neuron's axon, stimulating neurotransmitter release at the axon terminal. This release communicates a chemical signal onto the next cell.

1.3 Cellular membranes

The interior and exterior of a neuron is separated by a cellular membrane, which consists of a lipid bilayer with outer hydrophilic head groups and inner hydrophobic fatty acid tails. This lipid bilayer is impermeable to ions. It is responsible for maintaining ionic and electrical gradients between the cytosol and extracellular space. In this way, cellular membranes act as capacitors separating charge.

Controlled ion movement across the membrane is important for electrical activity. Hence, the cellular membrane contains many proteins, which allow ions or other proteins access across the membrane. These gatekeepers can either be passive, or they can use energy to pump ions across the membrane, called active transport. Passive gatekeepers include ion channels, which are gated pores that have some selectivity to ions. Some channels allow specific ions to cross the membrane and others allow more general ion flux. They can be voltage-gated, which only allow ionic flow when the membrane potential is depolarized or hyperpolarized, while others require binding of a ligand before allowing ion passage. Channel properties allow the cell to regulate its ionic concentrations and thus its electrical signaling. Diseases may arise when these channels lose their ability to function correctly, discussed later in this dissertation.

1.4 Action potentials

An action potential propagates down the axon until it reaches the axon terminal. Here, the depolarization opens voltage-gated Ca^{2+} channels. The concentration of Ca^{2+} outside the cell is much greater than inside. Upon Ca^{2+} channel opening, Ca^{2+} enters the presynaptic terminal and results in the fusion of neurotransmitter-filled synaptic vesicles with the presynaptic terminal membrane. This results in the release of neurotransmitter into the synaptic cleft where it can then

generate signals in the next cell. Ca^{2+}-dependent neurotransmitter release will be discussed in detail throughout this dissertation.

1.5 Quantal release

Identification of individually fusing synaptic vesicles as the source of neurotransmitter release was groundbreaking in our understanding of synaptic transmission. Katz and colleagues proposed the quantal release hypothesis in the early 1950s [1-3]. Their studies at the frog neuromuscular junction identified spontaneous, small postsynaptic voltage changes that occurred in the absence of neural activity. These depolarizations resemble end plate potentials (EPPs) following an action potential, but on a smaller scale. These events are referred to as miniature end-plate potentials (mEPPs). The mEPPs appear to be random and between 0.3 and 0.5 mV. This suggests neurotransmitter is being released in discrete packets. Furthermore, they hypothesized that an action potential causes the synchronous release of a large number of these packets and generates a large EPP.

The concept that synaptic transmission could be explained by the quantized release of neurotransmitter was proposed around the same time that small membranous vesicles within nerve terminals were first identified by electron microscopy [4, 5]. Together, these findings led to the vesicular hypothesis for neurotransmitter release, which states that each synaptic vesicle contains a similar amount of neurotransmitter (1 quantum), and that the transmitter release following an action potential results from a discrete number of vesicles fusing synchronously with the plasma membrane.

1.6 Modulation of the chemical synapse

The response of a given postsynaptic cell to the same level of activity in a presynaptic cell can vary depending on the efficacy of the synapse. Synaptic efficacy is based on many factors, including the quantal content (number of neurotransmitter-filled synaptic vesicles that fuse in response to a given stimulus) and the type and number of postsynaptic receptors. Importantly, these pre- and postsynaptic parameters can be regulated by activity patterns. The capacity to modulate synaptic efficacy is an important mechanism underlying learning and memory. These activity-dependent changes in synaptic strength are known as synaptic plasticity.

Experimentally, synaptic plasticity is measured both pre- and postsynaptically. Synapses may have high or low quantal content (m) relative to other synapses. m depends on the number of vesicles available to fuse (n), and the release probability of each vesicle (p). The release probability is dependent on the magnitude and duration of Ca^{2+} influx, the speed of Ca^{2+} clearance, and the proximity of the Ca^{2+} sensor to the channel. Presynaptically, the amount of neurotransmitter released can be decreased or increased, leading to depressed or facilitated responses. Experiments in which two closely spaced stimuli are administered, or paired pulse experiments, are commonly used to monitor changes in release probabilities. When the ratio of the second response to the first response, or paired pulse ratio (PPR) decreases, it is indicative of increased release probability, and decreases are consistent with decreased release probability [6]. High quantal content synapses result in large responses in the postsynaptic cell upon single stimulations, barring any postsynaptic adaptations. Alternatively, low quantal content synapses have the opposite characteristics and result in smaller postsynaptic responses.

Depression can be observed in high quantal content synapses during paired pulse experiments, in which two closely spaced stimuli are administered to a cell [7, 8]. At high

quantal content synapses, the first stimulation is sufficient to release a large fraction of the readily releasable vesicles. Accordingly, there are fewer vesicles available to fuse during the second stimulus, which results in a reduced postsynaptic response. Therefore, the first response is robust, while the second response is reduced. Another example of synaptic depression occurs during presynaptic high-frequency stimulus trains [9, 10]. Since exocytosis is more rapid than endocytosis, such stimulation depletes the readily releasable pool of synaptic vesicles, even at low quantal content synapses, and quantal content is decreased.

Facilitation is an incremental increase in the postsynaptic response to a given presynaptic stimulation observed in paired pulse experiments at low quantal content synapses. Since the first stimulus at such a synapse results in the fusion of only a small fraction of the readily releasable pool, the number of vesicles available for fusion following the second impulse is not significantly reduced. If the delay between the two stimuli is within tens of milliseconds (ms), not all the Ca^{2+} that entered during the first pulse has been removed by the time of the second pulse. Therefore, the $[Ca^{2+}]$ experienced by the release machinery during the second pulse is higher and triggers a greater number of synaptic vesicles to fuse. If the delay between stimuli is long enough to allow the Ca^{2+} from the first pulse to be removed, the second response is not facilitated. This is known as the residual Ca^{2+} hypothesis [11-13], and this form of presynaptic facilitation is very short-lived.

Postsynaptically, changes in synaptic activity can lead to changes in the morphological makeup of the postsynaptic membrane through insertion or removal of receptors. Any change in receptor density results in a change in response strength to a given signal. These changes are referred to as either long-term potentiation, which is characterized by a long-lasting facilitated response in the postsynaptic cell following a brief tetanic stimulation of a strong input or

simultaneous stimulation of multiple weaker inputs, or long-term depression, which is a long-lasting, activity-dependent depressed postsynaptic response induced by prolonged low-frequency stimulation [14].

1.7 Active zones

Functionally, the role of the active zone is to transduce an electrical nerve terminal depolarization into neurotransmitter release. Couteaux and Pecot-Dechavassinein coined the term "active zone" in 1970 when they noticed docked vesicles at the frog neuromuscular junction adjacent to electron dense material at the presynaptic membrane in electron micrographs [15]. Subsequent ultrastructure studies revealed similar morphologies across organisms. The structure of the active zone material (AZM) varies among different types of synapses, but must include the requisite protein machinery for vesicle docking, priming, and fusion. Fusion machinery, Ca^{2+} channels, and Ca^{2+} sensors are all found at active zones.

Fusion machinery

The minimum machinery required to fuse a vesicle with its target membrane is the SNARE (**SNA**P [soluble NSF (n-ethlymaleimide-sensitive factor) attachment protein] **re**ceptor) fusion complex, which is comprised of a vesicle-associated SNARE protein (vSNARE) and target-membrane associated SNARE proteins (tSNAREs). At the synapse, the vSNARE is synaptobrevin-2, also known as vesicle-associated membrane protein 2 (VAMP2) and the tSNAREs are syntaxin-1 and synaptosomal-associated protein of 25 kDa (SNAP-25).

The discovery of SNAREs as the fusion machinery in the late 1980's and early 1990's have been pivotal in our understanding of neurotransmission. Rothman's group originally

discovered the cytosolic proteins NSF [16] and SNAP [17] in the late 1980's and suggested their importance for membrane fusion [18, 19]. They determined interactions between both NSF, SNAP, and an unknown integral membrane protein needed for their interaction [20]. Simultaneously, synaptic vesicle and target membrane proteins were being identified [21-25] and implicated in neurotransmission through the use of neurotoxins [26-30].

Together, the seminal study using NSF and SNAP proteins to extract SNAP receptors, or SNAREs, from brain tissue was performed. Once purified, the proteins were identified as SNAP25, synaptobrevin, and syntaxin [31]. Furthermore, it was shown that without NSF and SNAP, the SNAREs form stable complexes [32] that bind much more efficiently if all three are present [33].

Each SNARE protein contains at least one SNARE motif of ~65 residues with a propensity to form coiled coils [34]. Synaptotobrevin and syntaxin each contain one SNARE motif, and SNAP-25 contains two [35]. Prior to vesicle docking, syntaxin is found in a stable, closed conformation, with its SNARE motif bound to a three-helix-bundle regulatory domain, making it inaccessible for interactions with other SNARE proteins [36]. Syntaxin undergoes a conformational change, which allows its SNARE motif to interact with the SNARE motifs of synaptobrevin and SNAP-25. This creates a *trans*-SNARE complex associated with both the vesicular membrane and the presynaptic plasma membrane. The formation of multiple SNARE complexes [37] contributes to the energy required to drive fusion of the vesicle and target membranes [32, 38]. SNARE complexes mediate both constitutive and regulated vesicle fusion events throughout cells.

The basic concept of the minimal machinery necessary to fuse a vesicular with its target membrane is as follows: SNARE proteins on both the vesicular and target membranes associate

to form a tight coiled-coil configuration. When maximally coiled, *trans*-SNARE complexes force the two membranes together, thereby destabilizing the membranes' natural curvature. Together with additional proteins such as Ca^{2+} sensors, fusion of the two membranes occurs. Once fused, the vSNAREs and tSNAREs form a *cis*-SNARE complex, and the vesicular contents are released.

Ca^{2+} channels and sensors

The presence of voltage-gated Ca^{2+} channels at active zones is necessary to couple neuronal depolarization to vesicle fusion events. Not only do these channels need to be present at active zones, their precise localization within an active zone can have immense effects on the efficacy of synaptic transmission. Ca^{2+} channels are located within 50 nm from docked vesicles [39-41]. When the cell is depolarized, the Ca^{2+} channels briefly open, creating a nanodomain of particularly high [Ca^{2+}] immediately adjacent to each channel. This [Ca^{2+}] reaches hundreds of uM at the mouth of the channel [42] and drops off rapidly with distance [43-46].

As the availability of Ca^{2+} is limited temporally and spatially, the closer the channel is located to a Ca^{2+} sensor, the greater the odds of saturating sensor binding and triggering vesicle fusion. Even a 5 nm change in the distance between the channel and the sensor has profound effects on vesicle release probability [47]. There are multiple Ca^{2+} sensors that transduce Ca^{2+} influx into neurotransmitter release, such as some synaptotagmins and double C_2-containing protein (Doc2). These Ca^{2+} sensors exhibit varying Ca^{2+} affinities and release kinetics and result in differential forms of release, which is a major subject of this dissertation. In particular, I focus on synaptotagmin 1, a Ca^{2+}-sensor postulated to perform distinct roles in multiple forms of Ca^{2+}-dependent release.

1.8 Synaptic vesicle cycle

Before transmitter release, synaptic vesicles must undergo a distinct, tightly regulated series of steps. First, the vesicles are loaded with neurotransmitter and are then transported to the active zone. Vesicles are docked to the presynaptic membrane at the active zone by way of specific molecular interactions, but only a subset of docked vesicles are fusion competent at any given time; namely, those that are maximally primed. In a resting terminal, individual maximally primed vesicles can spontaneously fuse with the presynaptic membrane, resulting in the release of a single quantum of neurotransmitter. In an activated neuron, the influx of Ca^{2+} through voltage-gated Ca^{2+} channels initiates a series of steps essential for the evoked release of neurotransmitter. Ca^{2+}-sensing proteins activate the fusion machinery, which mediates the fusion of multiple maximally primed vesicles with the presynaptic membrane. These fusion events result in the release of neurotransmitter into the synaptic cleft. After neurotransmitter release, the fusion machinery is disassembled and recycled for subsequent use. Concurrently, the synaptic vesicle membrane and associated proteins are retrieved through endocytosis to form new synaptic vesicles. This series of distinct events is known as the synaptic vesicle cycle (Fig 1.1). This dissertation will focus on the priming and fusion steps.

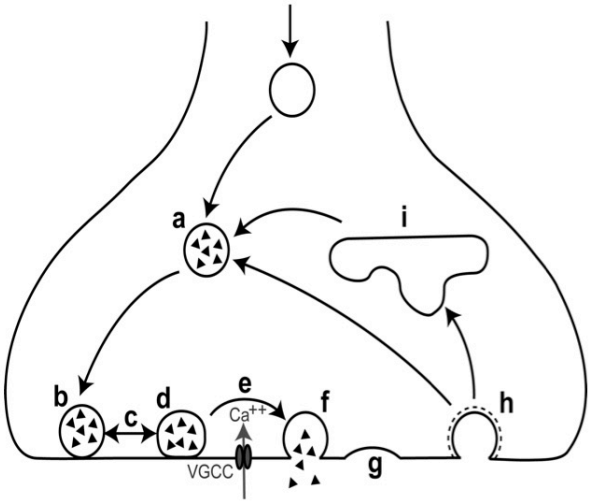

Fig 1.1. Cartoon depiction of the synaptic vesicle cycle. Each tightly regulated step is represented with a letter, including vesicle loading with neurotransmitter (a), vesicle docking (b), variable vesicle priming (c), maximally-primed, docked vesicle (d), depolarization-triggered Ca^{2+} entry (e), vesicle fusion with presynaptic membrane (f), vesicle membrane collapse (g), endocytosis (h), and recycling endosome (i).

1.9 Synaptic vesicle priming

After a vesicle is docked to the presynaptic membrane, additional interactions increase the probability of vesicle fusion. These interactions are termed "priming." Munc13, an essential active zone protein, is thought to orchestrate the first step in fusion machinery assembly (note: Munc13 should not to be confused with the SM protein, Munc18). Munc13 binds to the closed conformation of syntaxin and facilitates the conformational change in syntaxin from its "closed" to its "open" state [36, 48]. Only then can syntaxin's SNARE motif interact with the SNARE motifs of SNAP-25 and synaptobrevin to form the *trans*-SNARE complex.

Recent work suggests that vesicle priming is in a state of dynamic equilibrium, such that only docked vesicles with the largest area of contact with the presynaptic membrane are maximally primed and ready to fuse upon Ca^{2+} influx [49]. One mechanism of accomplishing variable priming would be a balance between the repulsive forces of the vesicular and presynaptic membranes that result in SNARE complex uncoiling to favor minimal priming and SNARE complex coiling to favor maximal priming [49]. At any given moment, only a subpopulation of docked synaptic vesicles has a sufficient number of maximally coiled *trans*-SNARE complexes to produce maximal SV-PM contact area (Fig 1.2). These synaptic vesicles constitute the maximally primed population that is most likely to fuse upon Ca^{2+} influx.

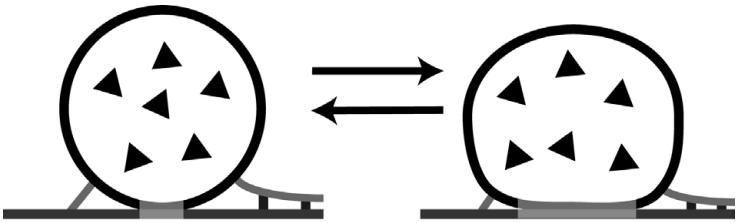

Fig 1.2. Variable priming of synaptic vesicles. *Left*, schematic depicting a docked, minimally primed vesicle at the presynaptic membrane, defined by the small area of contact between the vesicle and plasma membranes. *Right*, SNARE-coiling pulls the vesicle and presynaptic membranes together, increasing the area of contact, resulting in a maximally primed vesicle that has the highest fusion probability. The degree of priming is in a state of dynamic equilibrium (arrows).

1.10 Synaptic vesicle fusion

At the synapse, fusion events can occur in the absence of stimulation or can be evoked when the arrival of an action potential depolarizes the presynaptic terminal. Here, fusion is defined as any time a vesicle membrane combines with the presynaptic membrane, releasing its contents into the synaptic cleft. Evoked release results from depolarization-dependent Ca^{2+} influx that triggers the fusion of maximally primed vesicles with the presynaptic membrane.

Miniature release

Miniature release occurs when a single vesicle fuses with the presynaptic membrane in the absence of experimental stimulation. These events are thought to result from low probability conformational changes that complete coiling of the SNARE proteins. As these spontaneously fusing vesicles are in a maximally primed, fusion-competent state, less energy is required to overcome the fusion barrier.

Discovered by Katz and colleagues and deemed “spontaneous miniature end plate potentials” at the neuromuscular junction [1, 2], these spontaneously occurring events are

observed both peripherally and centrally. Central synapses are innervated by many upstream signaling sources, so all stimulation-independent responses (spontaneous events) are difficult to differentiate from the events that result from one vesicle fusing with the presynaptic membrane (miniature events). To distinguish all spontaneous events from miniature events, researchers employ the use of tetrodotoxin, which blocks voltage-gated Na^+ channels and prevents propagation of upstream action potentials. In this way, only miniature events are recorded.

At the neuromuscular junction, the innervating nerve is isolated and severed to prevent upstream spontaneous signals. Therefore, all recorded events in the absence of stimulation are considered miniature events. To support this, the effect of tetrodotoxin to distinguish spontaneous events and miniature events at the neuromuscular junction in both invertebrate and mammalian systems has been investigated. At these synapses, all recorded spontaneous release is largely analogous to miniature events [50, 51]. As the remainder of this dissertation focuses on events at the neuromuscular junction, spontaneous release and miniature release will be used interchangeably.

Synchronous fusion events

Fast, synchronous release of neurotransmitter is the multiquantal stimulated release that occurs within ms of depolarization. Synchronous fusion events are Ca^{2+} dependent, relying on the large Ca^{2+} influx of open Ca^{2+} channels at active zones. This release is dominant in the majority of synapses, and is the canonical release type typically described in textbooks. It is the dominant form of release at *Drosophila* neuromuscular junctions, but becomes less apparent in certain synaptic mutants. Synaptotagmins 1 and 2 are Ca^{2+} sensors responsible for synchronous fusion events.

Asynchronous fusion events

Asynchronous release is another form of Ca^{2+}-dependent release that continues for 100's of ms up to a second following stimulation. While most synapses exhibit little to no asynchronos release following a single action potential, it is still observed in many synapse types [52-61] and has implications in synaptic plasticity [62-65] and development [66, 67]. In some specialized synapses, such as specific interneurons of the hippocampus and brainstem, asynchronous release is predominant [59-61]. Interestingly, asynchronous release is commonly triggered by a single action potential at synapses in synaptotagmin 1/2 knockouts, when fast, synchronous release is nearly abolished [68]. The total amount of neurotransmitter released remains similar between wild type and synaptotagmin knockout neurons, although the method of release has shifted from predominantly synchronous to predominantly asynchronous [69, 70]. Asynchronous neurotransmitter release is observed in many neuronal types under particular circumstances, such as during and following extended high frequency activity. More research is needed for a full understanding of this release mechanism.

1.11 Ca^{2+} sensors for synchronous and asynchronous release

Synchronous and asynchronous release phases require Ca^{2+} sensors with distinct characteristics. Synchronous release requires a Ca^{2+} sensor with fast Ca^{2+}-binding kinetics to trigger the fusion of multiple quanta within a few ms, thus nearly simultaneously. The tradeoff for these fast binding kinetics is a lower affinity for Ca^{2+}, so more Ca^{2+} is needed to saturate the Ca^{2+} sensors. Therefore, this Ca^{2+} sensor only triggers vesicle fusion when $[Ca^{2+}]$ is high. Alternatively, asynchronous Ca^{2+} sensors must exhibit high affinities for Ca^{2+} with slower Ca^{2+} interaction kinetics, triggering fusion events over a long period of time when $[Ca^{2+}]$ is decreased.

The Ca^{2+} sensors for fast, synchronous release are synaptotagmins 1 and 2. They are both located on synaptic vesicles and play functionally homologous roles in different parts of the nervous system. In mammals, synaptotagmin 1 is expressed predominantly in the cerebral hemispheres, while synaptotagmin 2 is expressed predominantly in the brainstem and spinal cord [71, 72]. *Drosophila* do not have a synaptotagmin 2 gene and synaptotagmin 1 (Dsyt1) is responsible for triggering fast, synchronous neurotransmitter release throughout the nervous system.

Synaptotagmins 1 and 2 are low-affinity Ca^{2+} sensors and only bind Ca^{2+} when intracellular [Ca^{2+}] is very high, as found in Ca^{2+} nanodomains. Without Ca^{2+}, synaptotagmin interacts with SNARE proteins. In the Ca^{2+}-bound state, synaptotagmin interacts with both SNARE proteins [73-78] and negatively charged phospholipid membranes *in vitro* [79-81]. Upon Ca^{2+} binding *in vivo*, synaptotagmins 1 and 2 trigger the fast, synchronous phase of neurotransmitter release [82]. These precise mechanisms are covered in more detail later in this chapter.

The identity of the Ca^{2+} sensor for asynchronous release is still debated. Synaptotagmin 7 and Doc2 are currently the mammalian candidates for the Ca^{2+} sensor for triggering asynchronous neurotransmitter release. They are both enriched at synapses and exhibit high Ca^{2+} affinity and slow Ca^{2+} interaction kinetics [83-85]. The absence of either Doc2 or synaptotagmin 7 attenuates asynchronous release in synaptotagmin 1 knockout models, where asynchronous release is usually elevated [83, 84].

Even in the presence of synaptotagmin 1, synaptotagmin 7 knockouts attenuate asynchronous release under prolonged stimulation [84], although synaptotagmin 7 null mice are viable and fertile [86]. Recently, investigators report synaptotagmin 7's role as a regulator of

asynchronous release at granule cell synapses, also [87]. However, the effect of Doc2 mutants is controversial [88, 89]. Doc2 knockout models are not yet available, but rabphilin, a Doc2-like protein that contains an additional N-terminal zinc finger domain, knockout mice display no obvious phenotype [90]. Additionally, some studies did not observe decreased asynchronous release upon Doc2 knockdown, although differences in experimental procedures can complicate results [88, 89].

The invertebrate candidate for asynchronous release is unknown. There is very little research on the identity of the invertebrate asynchronous sensor. Homologues of mammalian candidates Doc2 and synaptotagmin 7 are intuitive candidates. However, Doc2 is not present in invertebrate systems, and synaptotagmin 7, although present in *Drosophila*, displays expression patterns not consistent with a role as the Ca^{2+} sensor needed at active zones for asynchronous release. In third instar *Drosophila* larvae, synaptotagmin 7 is relegated to neuronal cell bodies in the central nervous system, and not detectable at the neuromuscular junction [91]. In double knockdowns of synaptotagmin 4 and 7, asynchronous release remains intact, eliminating it as the asynchronous sensor [92]. In *C. elegans*, synaptotagmin 7, together with synaptotagmin 4, is implicated in somatodendritic dopamine release, but not vesicle release at synaptic terminals [93]. Within the last year, a *C. elegans* neuronal Ca^{2+}-sensing protein (NCS-2) has been implicated in asynchronous cholinergic release [94]. However, its *Drosophila* homologue frequenin, a high-affinity Ca^{2+} sensor present throughout the nervous system, has not been investigated for this function.

1.12 Synaptotagmin 1 in synchronous release

Synaptotagmin 1's role in synchronous release is well elucidated. Originally discovered and called p65 [95], Sudhof's group suggested it plays a role in membrane interactions during exocytosis by calling attention to p65's cytosolic domain that appeared homologous to the C_2A domain of protein kinase C and could interact with membranes [96]. A year later, they showed that p65 (now deemed synaptotagmin) is highly conserved across species, including *Drosophila* [97]. Much like the studies used to isolate the SNARE proteins, they utilized neurotoxins. Using the spider venom alpha-latrotoxin, which increases neurotransmitter release, Petrenko et al showed the toxin receptor binds specifically to synaptotagmin, suggesting its role in neurotransmitter release [98]. Synaptotagmin's C_2 domains bind Ca^{2+} at physiological levels in a complex that contained negatively charged membranes, providing evidence that synaptotagmin is a Ca^{2+} sensor associated with release [99]. Importantly, synaptotagmin was directly linked to stimulating fast, synchronous release in 1994, when hippocampal cultures from synaptotagmin 1 null mice display abolished synchronous release, but asynchronous and spontaneous release persisted [100].

Synaptotagmin 1 acts as a synchronous Ca^{2+} sensor in stimulated release. It binds Ca^{2+} by its two C_2 domains, C_2A and C_2B. These Ca^{2+} binding domains are lined with highly conserved negatively charged aspartate residues, resulting in a net negative charge before Ca^{2+} is bound. Ca^{2+} binding neutralizes the negative charge of the Ca^{2+} binding pockets and results in a net positive charge. This electrostatic change enhances interactions with the negatively charged presynaptic membrane and potentially with *trans*-SNARE complexes [73, 79, 101, 102]. Thus, Ca^{2+} binding allows synaptotagmin 1 to act as an "electrostatic switch" [103-106] from repulsion at rest to attraction upon Ca^{2+} influx.

Switching from electrostatic repulsion to electrostatic attraction permits hydrophobic residues in synaptotagmin 1's C_2 domains to escape the aqueous cytosol by penetrating into the hydrophobic core of the presynaptic membrane [101, 107]. One of these hydrophobic membrane-penetrating residues in C_2A has been studied *in vivo* and results in a 50% knockdown of function when this phenylalanine (F) is mutated to a glutamate (E, $P[syt^{F\text{-}E}]$) [108]. Moreover, when the hydrophobic residue found in C_2B is mutated to a glutamate, the result is embryonic lethality. Therefore, the membrane interactions via these hydrophobic residues are critical for efficient synchronous fusion [108]. The insertion of these hydrophobic residues is thought to enhance fusion by two mechanisms. First, the inserted side chains occupy space, which induces positive curvature in the presynaptic membrane, bringing it closer to the curvature needed for fusion. Second, the insertion destabilizes the presynaptic membrane, again favoring fusion [81]. Therefore, synaptotagmin 1 can be thought of as providing the final push, much like popping a tightly inflated balloon, to trigger fusion.

1.13 Synaptotagmin 1 in asynchronous release

The role of synaptotagmin 1 in asynchronous release remains unclear. It was originally postulated that the Ca^{2+} binding C_2A domain of synaptotagmin 1 was actively regulating, or inhibiting, asynchronous release. This hypothesis is based on experimental results from two synaptotagmin mutants. Initially, studies reported increased asynchronous release in synaptotagmin 1 knockouts [82, 109-112]. Additionally, another study investigated the role of the C_2A domain in both synchronous and asynchronous release [113]. In this study, Ca^{2+} binding in synaptotagmin's C_2A domain was blocked by mutating two negatively charged aspartates (D) found in the C_2A Ca^{2+}-binding pocket to neutral asparagines (N), here after called the $P[syt^{D\text{-}N}]$

mutation. This mutation effectively prevents Ca^{2+} binding by altering the charge profile of the binding pocket. This *P[syt$^{D\text{-}N}$]* mutant study reports no decrease in evoked release and an increase in asynchronous release. This study and the synaptotagmin 1 knockout studies that report increased asynchronous release led to the hypothesis that Ca^{2+} binding in synaptotagmin 1's C_2A domain is not necessary for fast, synchronous release, but is necessary to regulate, or inhibit, the asynchronous release sensor. I will call this hypothesis the inhibition hypothesis.

Subsequently, Striegel et al [106] determined Ca^{2+} binding by synaptotagmin 1's C_2A domain is needed for efficient synchronous release, contrary to the results in the *P[syt$^{D\text{-}N}$]* study. Striegel generated an alternative C_2A Ca^{2+}-binding mutation in which an essential aspartate (D) was mutated to a negatively charged glutamate (E), here after called the *P[syt$^{D\text{-}E}$]* mutant. This mutant maintains the negative charge of the pocket while structural inhibiting C_2A Ca^{2+} binding [106] and exhibits a significant ~80% decrease in synchronous release.

A major function of synaptotagmin is to act as an electrostatic switch, which alters interactions with SNARE complexes and triggers an interaction with presynaptic membranes. The *P[syt$^{D\text{-}N}$]* mutation effectively trips this electrostatic switch by neutralizing the Ca^{2+} binding pocket [106]. In this light, it is not surprising that in the presence of a wild type C_2B domain, the *P[syt$^{D\text{-}N}$]* mutant exhibits no impact on synchronous release since it is mimicking Ca^{2+} binding [106]. Additionally, the *P[syt$^{D\text{-}N}$]* mutant responds more robustly at lower [Ca^{2+}] for both synchronous and asynchronous release [113], indicating an increased affinity for Ca^{2+}.

Since the *P[syt$^{D\text{-}N}$]* mutation mimics Ca^{2+} binding for synchronous release, its reported effect on asynchronous release also comes into question. An increase in Ca^{2+} affinity and mimicking bound Ca^{2+} may result in increased asynchronous release by triggering release events at lower [Ca^{2+}]. These aberrant asynchronous events would be an artifact of the *P[syt$^{D\text{-}N}$]*

mutation, and not the actual role of C_2A in regulating asynchronous release. This sheds doubt onto the importance of synaptotagmin C_2A Ca^{2+} binding in the regulation of asynchronous release.

Increases in asynchronous events seen in the *P[syt$^{D\text{-}N}$]* mutant may be a result of the *P[syt$^{D\text{-}N}$]* mutation mimicking the asynchronous sensor itself. Asynchronous Ca^{2+} sensors exhibit slower binding and unbinding kinetics for Ca^{2+}, permitting release on a longer timescale [53]. The *P[syt$^{D\text{-}N}$]* mutants exhibit release events over longer time scales [113]. Asynchronous sensors exhibit higher affinities for Ca^{2+}, which would allow the asynchronous sensor to bind Ca^{2+} at lower [Ca^{2+}]. Indeed, the *P[syt$^{D\text{-}N}$]* mutation exhibits increased affinity for Ca^{2+} [113]. In contrast, *P[syt$^{D\text{-}E}$]* mutants exhibit decreased Ca^{2+} affinity [106], again providing evidence that *P[syt$^{D\text{-}N}$]* mutant may be mimicking an asynchronous sensor.

1.14 Clarification of synaptotagmin's role in asynchronous release

In chapter 2 of this dissertation, I directly test the role of Ca^{2+} binding in C_2A in asynchronous release *in vivo* by utilizing the *P[syt$^{D\text{-}E}$]* mutation, which prevents C_2A Ca^{2+} binding while maintaining C_2A's inherently negative charge. If C_2A Ca^{2+} binding is clamping the asynchronous Ca^{2+} sensor, an increase similar to that seen in the *P[syt$^{D\text{-}N}$]* mutant should occur in the *P[syt$^{D\text{-}E}$]* mutant. Such a result would corroborate the current hypothesis in the field. If, however, Ca^{2+} binding in C_2A is not needed to regulate asynchronous events, the *P[syt$^{D\text{-}E}$]* mutation will exhibit no increase in asynchronous events. I compare asynchronous release events in both the C_2A *P[syt$^{D\text{-}N}$]* and *P[syt$^{D\text{-}E}$]* transgenic mutants to a transgenic control in a synaptotagmin null background of *Drosophila*.

In chapter 3, I test the possibility that the *P[syt$^{D\text{-}N}$]* mutant is mimicking the asynchronous Ca^{2+} sensor *in vivo* by generating *Drosophila* mutants that contain the original *P[syt$^{D\text{-}N}$]* mutation with additional mutations of the hydrophobic residues to prevent interactions with the presynaptic membrane. I generate a *P[syt$^{D\text{-}N}$]* mutation coupled to a previously studied *P[syt$^{F\text{-}E}$]* mutation (*P[syt$^{D\text{-}N,F\text{-}E}$]*). I also generated the *P[syt$^{D\text{-}N,F\text{-}E}$]* mutation with an additional hydrophobic mutation, methionine (M) 222, to a glutamate (E), hereafter called *P[syt$^{M\text{-}E,D\text{-}N,F\text{-}E}$]*. If the *P[syt$^{D\text{-}N}$]* mutation is simply mimicking the high-affinity asynchronous sensor, then preventing the downstream membrane interactions needed for triggering fusion events should prevent any aberrant increase in asynchronous release caused by *P[syt$^{D\text{-}N}$]*'s neutralization of the pocket. Conversely, if the synaptotagmin *P[syt$^{D\text{-}N}$]* mutation is not mimicking an asynchronous sensor, but is regulating the asynchronous sensor, consistent with the inhibition hypothesis, the increase in asynchronous release seen in the *P[syt$^{D\text{-}N}$]* mutation should remain.

From these studies, I conclude that C_2A Ca^{2+} binding is not needed to regulate asynchronous release. The *P[syt$^{D\text{-}E}$]* mutation does not exhibit increased asynchronous events. Moreover, I report no changes to asynchronous release in either the *P[syt$^{D\text{-}N,F\text{-}E}$]* or *P[syt$^{M\text{-}E,D\text{-}N,F\text{-}E}$]* mutations, supporting the conclusion that the *P[syt$^{D\text{-}N}$]* mutant is mimicking an asynchronous sensor. These results contradict the inhibition hypothesis. Instead, together these results support an alternative hypothesis, the competition hypothesis, which suggests that synaptotagmin blocks access to SNARE interactions with the asynchronous sensor. The previous synaptotagmin knockout studies also support this hypothesis, as synapses without synaptotagmin 1 would provide more space for asynchronous sensor release interactions.

1.15 Neuromuscular disorders

Many tightly regulated mechanisms are needed to result in efficient release of neurotransmitter and subsequent responses in the postsynaptic cell. When proteins needed for these processes are dysfunctional, synaptic disease may arise. For this dissertation, I will focus primarily on disorders associated with proteins found at the neuromuscular junction. These disorders can be categorized by location of the affected structures, be it presynaptic, synaptic cleft, or postsynaptic. Conditions such as myasthenia gravis affect synaptic proteins in the postsynaptic muscle cell, while neuromyotonia and Lambert-Eaton myasthenic syndrome affect proteins in the presynaptic neuron. They can also be categorized by origin of dysfunction, such as an immune disorder or a congenital disorder. Myasthenia gravis and Lambert-Eaton myasthenic syndrome are both autoimmune disorders, while congenital myasthenic syndromes are associated with rare familial mutations and can exhibit their own distinct symptoms. Neuromuscular diseases in human patients can be diagnosed using a combination of nerve conduction studies, exercise testing, immunological tests, and genetic sequencing.

Nerve conduction studies

Nerve conduction studies (NCS) are performed on patients with clinical presentations that are consistent with neuromuscular disorder. These tests help delineate neuromuscular junction diseases from one another. Clinicians perform NCS by placing surface electrodes over a muscle and the nerve that innervates it. The clinician will stimulate the nerve and progressively increase the stimulus intensity until the muscle response does not increase. This is the supramaximal stimulation used. Once the largest response of the muscle fiber is recorded, one can conclude that all motor nerve fibers are recruited, and therefore all the innervated muscle

fibers within the muscle are responding. This muscle response is called the compound muscle action potential (CMAP) [114].

CMAP amplitude is dependent on two major factors: 1.) the number of innervated muscle fibers available to respond to a given stimulus and 2.) amount of neurotransmission at the neuromuscular junction. The CMAP can detect a gross loss of motor unit innervation to the muscle, indicative of a progressive neurogenic disorder. If this is the case, the CMAP amplitude will be decreased. During the early phases of these disorders, however, the CMAP may appear normal due to compensatory reinnervation. As one motor unit becomes deinnervated, other motor axons send compensatory motor terminal branches to the muscle. If the new motor branches can maintain a similar innervation level to the rate of deinnervation, there may be no detection of deinnervation.

The second factor that affects CMAP amplitude is the efficacy of neurotransmission at the neuromuscular junction. In this case, if there is a normal amount of innervated muscle fibers, but signal transmission from the pre- to postsynaptic cell is hindered, the result is a decreased CMAP amplitude. Unlike progressively deinnervating diseases, the deficits in neuronal transmission can be modulated and recorded through repetitive nerve stimulation tests. These tests are similar to single evoked CMAPs during baseline nerve conduction studies, but stimulations at varying frequencies are administered. These tests can help to localize the deficit. Facilitated amplitudes in response to high frequency stimuli (30 – 50 Hz) indicate a presynaptic deficit, while small amplitudes without facilitation suggests postsynaptic issues.

Lambert-Eaton myasthenic syndrome

Lambert-Eaton Myasthenic Syndrome (LEMS) is an autoimmune disease in which patients experience muscle weakness due to a decrease in Ca^{2+}-triggered neurotransmitter release at the neuromuscular junction [115]. This is the second most common neuromuscular disease, but is still 20 times less prevalent than the other immune-mediated neuromuscular junction disease, myasthenia gravis. As an immune-mediated disorder, IgG antibodies attack the presynaptic voltage-gated Ca^{2+} channels needed for efficient neurotransmission in most patients [116].

Patients experience the most muscle weakness after periods of rest. Strength improves with brief exercise, but does not sustain long periods of activity. Like myasthenia gravis, this disorder is also often co-morbid with cancer. Sixty percent of patients with LEMS experience small cell carcinoma [117]. LEMS usually affects patients over 40 years old.

Nerve conduction studies of LEMS patients result in decreased CMAP amplitudes. Repetitive nerve stimulation (RNS) tests exhibit depression at low frequencies (2-3 Hz) and facilitation at high frequencies (30-50 Hz). A classic hallmark of LEMS is a facilitated CMAP amplitude response after 10 seconds of voluntary muscle contraction [118]. Interestingly, approximately 20% of LEMS patients express antibodies against the intravesicular domain of synaptotagmin, the only portion of the protein exposed to antibodies in the synaptic cleft upon vesicle fusion [119]. This is the first indication that synaptotagmin could be a candidate for synaptic disease.

Congenital myasthenic syndromes

Congenital myasthenic syndromes (CMS) are genetically linked defects in one or multiple proteins found at the neuromuscular junction, including presynaptic, cleft, and postsynaptic proteins [118]. As of 2018, over 20 CMS genes were identified [120]. Some of the affected proteins and their importance have been discussed in this dissertation, including SNAP-25, acetylcholine receptors, postsynaptic Na^+ channels, and cleft enzymes that breakdown acetylcholine (acetylcholinesterase). Importantly for this dissertation, synaptotagmin 2, the fast, synchronous Ca^{2+} sensor at mammalian neuromuscular junctions, has also been implicated in CMS etiology [121, 122]. With the wide variety of proteins, nerve conduction tests, and clinical presentations, clinicians can point to candidate genes. Once candidate genes are identified, genetic testing aides in diagnosis and treatment plans. In patients, however, there is no way to definitively link a mutation to observed symptoms, necessitating the use of model systems to positively identify disease-causing mutations.

1.16 High throughput sequencing

The decreasing cost and increasing availability of DNA sequencing has led to an increased incidence of genomic sequencing during patient diagnoses. This ever-increasing process will undoubtedly lead to the discovery of additional synaptic mutations and associated genetic disorders. The need for a relatively quick and cost effective method to begin elucidating the molecular mechanisms underlying these synaptic disorders is vital.

1.17 Synaptotagmin-related disorders

It is only recently that mutations in the *syt1* and *syt2* genes have been directly implicated in human disease [121-123]. A patient with a *de novo* mutation in the human *syt1* gene presented with an early onset dyskinesia, severe motor delay, and profound cognitive deficits attributed to a single amino acid substitution in the C_2B Ca^{2+}-binding pocket: an isoleucine to threonine (I-T) substitution [123]. This hydrophobic isoleucine residue had been shown previously to mediate Ca^{2+}-dependent membrane penetration by synaptotagmin [79, 81, 124, 125]: an effector interaction critical for coupling Ca^{2+} influx with neurotransmitter release from neurons [83, 108]. Since this *syt* mutation results in the most severe deficits in an animal system [108] and is located in the *syt1* gene, which is preferentially expressed in the cerebral hemispheres [71, 72], this patient experienced extreme cognitive deficits and the most severe motor deficits observed in a synaptotagmin disease to date [123].

Two additional mutations in the human *syt2* gene were implicated in the etiology of congenital myasthenic syndrome patients shortly after: a proline to leucine ($syt^{P\text{-}L}$) mutation and an adjacent aspartate to alanine ($syt^{D\text{-}A}$) mutation. Both of these highly conserved residues are located in synaptotagmin's C_2B Ca^{2+}-binding pocket [96, 126, 127]. The $syt^{P\text{-}L}$ mutation had never been studied. However, previous studies have demonstrated that the C_2B domain Ca^{2+}-binding aspartate (D) residues are essential for synaptotagmin function [82, 121, 125, 128], at times resulting in lethality in animal models [82, 121]. For the $syt^{D\text{-}A}$ familial mutation, expression of the mutant *syt* from a transgene in *syt Drosophila* heterozygotes resulted in lethality in 4 of 6 independent transgenic lines and a dramatic decrease in evoked response in the remaining two lines [121]. It is noteworthy, then, that deficits in the affected human family are comparatively mild [121, 122].

The proline residue affected by the second family is located directly adjacent to one of these previously studied aspartates residues. We speculate that this proline residue may provide conformational rigidity important for stabilizing the C_2B Ca^{2+}-binding pocket. By mutating the proline to a leucine, the rigid R group found in the proline residue would be lost, potentially affecting the precise conformation of the pocket and impacting the ability of the adjacent aspartate to bind Ca^{2+}. Such a mechanism could result in a decreased, albeit not demolished, ability of the C_2B domain to bind Ca^{2+} [82, 108, 113, 121-123]. A decreased ability of synaptotagmin to bind Ca^{2+} would hinder the efficacy of neurotransmission, and potentially to myasthenic disease symptoms. This mutation could be causing the symptoms seen in the affected family, but the correlations between those with the disorder and the mutation provide no direct evidence that the proline mutation leads to disease symptoms.

1.18 *Drosophila* as a model system

One approach to directly assess the responsibility of the proline-leucine mutation in this congenital myasthenia is to leverage the power of *Drosophila* genetics. Rare disorders such as this synaptotagmin-implicated myasthenia are often underfunded and overlooked, as the need for medical research of these diseases does not affect the masses and receive little attention. However, the advances in human genetic sequencing are uncovering more of these rare genetic disorders. *Drosophila* are an ideal organism to investigate these mechanisms. *Drosophila* are economical, rapidly regenerate, and possess a genetic toolbox that allows us to drive the mutation of interest in subsets of cells. By creating a homologous mutation in *Drosophila syt1*, emergence of disease symptoms would create a direct link between the proline-leucine mutation and this congenital myasthenia. Electrophysiological tests where an intracellular electrode is

inserted directly into the fly body wall muscle fiber and its innervating nerve is stimulated can uncover mechanisms of disease etiology. The amplitude of the response can be measured much like a CMAP. Unlike a CMAP, the *Drosophila* tests examine a single muscle fiber, so deficits in the number of innervating nerve cells onto the muscle are not distinguished. This allows a direct investigation of synaptic transmission deficiency. If similar symptoms are detected, researchers can examine the mechanisms mediating this disorder more completely, as there would be a disease model readily available and a causal link between the mutation and disease symptoms.

1.19 Investigation of a synaptotagmin disorder

In chapter 4 of this dissertation I directly test the importance of the previously uninvestigated proline residue *in vivo* by creating a homologous mutation in *Drosophila*. Our *in silico* modeling predicts a conformational change in the C_2B Ca^{2+}-binding pocket, potentially affecting synaptotagmin's efficiency. I report homologous symptoms between the *Drosophila* mutation and human disorder, including: 1) decreased neurotransmission, 2) facilitated neurotransmission in response to high frequency stimulation, and 3) muscle fatigability. This study also provides mechanistic insight into this disease, as the mutation exhibits results consistent with decreased release probability and decreased Ca^{2+} affinity. Therefore, results support a causative role for the $syt^{P\text{-}L}$ mutation in disease etiology.

WORKS CITED

1. Del Castillo, J. and B. Katz, *Quantal components of the end-plate potential.* J Physiol, 1954. **124**(3): p. 560-73.
2. Fatt, P. and B. Katz, *Spontaneous subthreshold activity at motor nerve endings.* J Physiol, 1952. **117**(1): p. 109-28.
3. Fatt, P. and B. Katz, *An analysis of the end-plate potential recorded with an intra-cellular electrode.* J Physiol, 1951. **115**(3): p. 320-70.
4. De Robertis, E.D. and H.S. Bennett, *Some features of the submicroscopic morphology of synapses in frog and earthworm.* J Biophys Biochem Cytol, 1955. **1**(1): p. 47-58.
5. Palay, S.L., *Synapses in the central nervous system.* J Biophys Biochem Cytol, 1956. **2**(4 Suppl): p. 193-202.
6. Zucker, R.S. and W.G. Regehr, *Short-term synaptic plasticity.* Annu Rev Physiol, 2002. **64**: p. 355-405.
7. Thomson, A.M., J. Deuchars, and D.C. West, *Large, deep layer pyramid-pyramid single axon EPSPs in slices of rat motor cortex display paired pulse and frequency-dependent depression, mediated presynaptically and self-facilitation, mediated postsynaptically.* J Neurophysiol, 1993. **70**(6): p. 2354-69.
8. Debanne, D., et al., *Paired-pulse facilitation and depression at unitary synapses in rat hippocampus: quantal fluctuation affects subsequent release.* J Physiol, 1996. **491 (Pt 1)**: p. 163-76.
9. Parnas, I., *Differential block at high frequency of branches of a single axon innervating two muscles.* J Neurophysiol, 1972. **35**(6): p. 903-14.
10. Parker, D., *Depression of synaptic connections between identified motor neurons in the locust.* J Neurophysiol, 1995. **74**(2): p. 529-38.
11. Katz, B. and R. Miledi, *THE EFFECT OF CALCIUM ON ACETYLCHOLINE RELEASE FROM MOTOR NERVE TERMINALS.* Proc R Soc Lond B Biol Sci, 1965. **161**: p. 496-503.
12. Katz, B. and R. Miledi, *The release of acetylcholine from nerve endings by graded electric pulses.* Proc R Soc Lond B Biol Sci, 1967. **167**(1006): p. 23-38.
13. Dodge, F.A., Jr. and R. Rahamimoff, *Co-operative action a calcium ions in transmitter release at the neuromuscular junction.* J Physiol, 1967. **193**(2): p. 419-32.
14. Dudek, S.M. and M.F. Bear, *Homosynaptic long-term depression in area CA1 of hippocampus and effects of N-methyl-D-aspartate receptor blockade.* Proc Natl Acad Sci U S A, 1992. **89**(10): p. 4363-7.
15. Couteaux R, P.-D.M., *Synaptic vesicles and pouches at the level of "active zones" of the neuromuscular junction.* C. R. Hebd. Seances Acad. Sci, 1970. **D271**: p. 2346-2349.
16. Block, M.R., et al., *Purification of an N-ethylmaleimide-sensitive protein catalyzing vesicular transport.* Proc Natl Acad Sci U S A, 1988. **85**(21): p. 7852-6.
17. Weidman, P.J., et al., *Binding of an N-ethylmaleimide-sensitive fusion protein to Golgi membranes requires both a soluble protein(s) and an integral membrane receptor.* J Cell Biol, 1989. **108**(5): p. 1589-96.

18. Malhotra, V., et al., *Role of an N-ethylmaleimide-sensitive transport component in promoting fusion of transport vesicles with cisternae of the Golgi stack.* Cell, 1988. **54**(2): p. 221-7.
19. Beckers, C.J., et al., *Vesicular transport between the endoplasmic reticulum and the Golgi stack requires the NEM-sensitive fusion protein.* Nature, 1989. **339**(6223): p. 397-8.
20. Wilson, D.W., et al., *A multisubunit particle implicated in membrane fusion.* J Cell Biol, 1992. **117**(3): p. 531-8.
21. Trimble, W.S., D.M. Cowan, and R.H. Scheller, *VAMP-1: a synaptic vesicle-associated integral membrane protein.* Proc Natl Acad Sci U S A, 1988. **85**(12): p. 4538-42.
22. Sudhof, T.C., et al., *A synaptic vesicle membrane protein is conserved from mammals to Drosophila.* Neuron, 1989. **2**(5): p. 1475-81.
23. Oyler, G.A., et al., *The identification of a novel synaptosomal-associated protein, SNAP-25, differentially expressed by neuronal subpopulations.* J Cell Biol, 1989. **109**(6 Pt 1): p. 3039-52.
24. Inoue, A., K. Obata, and K. Akagawa, *Cloning and sequence analysis of cDNA for a neuronal cell membrane antigen, HPC-1.* J Biol Chem, 1992. **267**(15): p. 10613-9.
25. Bennett, M.K., N. Calakos, and R.H. Scheller, *Syntaxin: a synaptic protein implicated in docking of synaptic vesicles at presynaptic active zones.* Science, 1992. **257**(5067): p. 255-9.
26. Schiavo, G., et al., *Tetanus and botulinum-B neurotoxins block neurotransmitter release by proteolytic cleavage of synaptobrevin.* Nature, 1992. **359**(6398): p. 832-5.
27. Link, E., et al., *Tetanus toxin action: inhibition of neurotransmitter release linked to synaptobrevin proteolysis.* Biochem Biophys Res Commun, 1992. **189**(2): p. 1017-23.
28. Blasi, J., et al., *Botulinum neurotoxin A selectively cleaves the synaptic protein SNAP-25.* Nature, 1993. **365**(6442): p. 160-3.
29. Blasi, J., et al., *Botulinum neurotoxin C1 blocks neurotransmitter release by means of cleaving HPC-1/syntaxin.* Embo j, 1993. **12**(12): p. 4821-8.
30. Schiavo, G., et al., *Botulinum neurotoxin type C cleaves a single Lys-Ala bond within the carboxyl-terminal region of syntaxins.* J Biol Chem, 1995. **270**(18): p. 10566-70.
31. Sollner, T., et al., *SNAP receptors implicated in vesicle targeting and fusion.* Nature, 1993. **362**(6418): p. 318-24.
32. Sollner, T., et al., *A protein assembly-disassembly pathway in vitro that may correspond to sequential steps of synaptic vesicle docking, activation, and fusion.* Cell, 1993. **75**(3): p. 409-18.
33. Hayashi, T., et al., *Synaptic vesicle membrane fusion complex: action of clostridial neurotoxins on assembly.* Embo j, 1994. **13**(21): p. 5051-61.
34. Lupas, A., *Prediction and analysis of coiled-coil structures.* Methods Enzymol, 1996. **266**: p. 513-25.
35. Sutton, R.B., et al., *Crystal structure of a SNARE complex involved in synaptic exocytosis at 2.4 A resolution.* Nature, 1998. **395**(6700): p. 347-53.
36. Dulubova, I., et al., *A conformational switch in syntaxin during exocytosis: role of munc18.* Embo j, 1999. **18**(16): p. 4372-82.
37. Yersin, A., et al., *Interactions between synaptic vesicle fusion proteins explored by atomic force microscopy.* Proc Natl Acad Sci U S A, 2003. **100**(15): p. 8736-41.

38. Li, F., et al., *Energetics and dynamics of SNAREpin folding across lipid bilayers.* Nat Struct Mol Biol, 2007. **14**(10): p. 890-6.
39. Heuser, J.E., et al., *Synaptic vesicle exocytosis captured by quick freezing and correlated with quantal transmitter release.* J Cell Biol, 1979. **81**(2): p. 275-300.
40. Harlow, M.L., et al., *The architecture of active zone material at the frog's neuromuscular junction.* Nature, 2001. **409**(6819): p. 479-84.
41. Eggermann, E., et al., *Nanodomain coupling between Ca(2)(+) channels and sensors of exocytosis at fast mammalian synapses.* Nat Rev Neurosci, 2011. **13**(1): p. 7-21.
42. Llinas, R., M. Sugimori, and R. Silver, *Microdomains of high calcium concentration in a presynaptic terminal.* Science, 1992. **256**(5057): p. 677-679.
43. Chad, J.E. and R. Eckert, *Calcium domains associated with individual channels can account for anomalous voltage relations of CA-dependent responses.* Biophys J, 1984. **45**(5): p. 993-9.
44. Fogelson, A.L. and R.S. Zucker, *Presynaptic calcium diffusion from various arrays of single channels. Implications for transmitter release and synaptic facilitation.* Biophys J, 1985. **48**(6): p. 1003-17.
45. Simon, S.M. and R.R. Llinas, *Compartmentalization of the submembrane calcium activity during calcium influx and its significance in transmitter release.* Biophys J, 1985. **48**(3): p. 485-98.
46. Naraghi, M. and E. Neher, *Linearized buffered Ca2+ diffusion in microdomains and its implications for calculation of [Ca2+] at the mouth of a calcium channel.* J Neurosci, 1997. **17**(18): p. 6961-73.
47. Shahrezaei, V. and K.R. Delaney, *Consequences of molecular-level Ca2+ channel and synaptic vesicle colocalization for the Ca2+ microdomain and neurotransmitter exocytosis: a monte carlo study.* Biophys J, 2004. **87**(4): p. 2352-64.
48. Ma, C., et al., *Munc13 mediates the transition from the closed syntaxin–Munc18 complex to the SNARE complex.* Nature Structural &Amp; Molecular Biology, 2011. **18**: p. 542.
49. Jung, J.H., et al., *Variable priming of a docked synaptic vesicle.* Proc Natl Acad Sci U S A, 2016. **113**(8): p. E1098-107.
50. F., C. and E.S. D., *Miniature synaptic potentials at frog spinal neurones in the presence of tetrodotoxin.* The Journal of Physiology, 1968. **199**(1): p. 205-221.
51. Elmqvist, D. and D.S. Feldman, *Spontaneous activity at a mammalian neuromuscular junction in tetrodotoxin.* Acta Physiol Scand, 1965. **64**(4): p. 475-6.
52. Chirwa, S.S. and B.R. Sastry, *Asynchronous synaptic responses in hippocampal CA1 neurons during synaptic long-term potentiation.* Neurosci Lett, 1988. **89**(3): p. 355-60.
53. Goda, Y. and C.F. Stevens, *Two components of transmitter release at a central synapse.* Proc Natl Acad Sci U S A, 1994. **91**(26): p. 12942-6.
54. Atluri, P.P. and W.G. Regehr, *Delayed release of neurotransmitter from cerebellar granule cells.* J Neurosci, 1998. **18**(20): p. 8214-27.
55. Yawo, H., *Two components of transmitter release from the chick ciliary presynaptic terminal and their regulation by protein kinase C.* J Physiol, 1999. **516 (Pt 2)**: p. 461-70.
56. Lu, T. and L.O. Trussell, *Inhibitory transmission mediated by asynchronous transmitter release.* Neuron, 2000. **26**(3): p. 683-94.
57. Hagler, D.J., Jr. and Y. Goda, *Properties of synchronous and asynchronous release during pulse train depression in cultured hippocampal neurons.* J Neurophysiol, 2001. **85**(6): p. 2324-34.

58. Kirischuk, S. and R. Grantyn, *Intraterminal Ca2+ concentration and asynchronous transmitter release at single GABAergic boutons in rat collicular cultures.* J Physiol, 2003. **548**(Pt 3): p. 753-64.
59. Hefft, S. and P. Jonas, *Asynchronous GABA release generates long-lasting inhibition at a hippocampal interneuron-principal neuron synapse.* Nat Neurosci, 2005. **8**(10): p. 1319-28.
60. Best, A.R. and W.G. Regehr, *Inhibitory regulation of electrically coupled neurons in the inferior olive is mediated by asynchronous release of GABA.* Neuron, 2009. **62**(4): p. 555-65.
61. Daw, M.I., et al., *Asynchronous transmitter release from cholecystokinin-containing inhibitory interneurons is widespread and target-cell independent.* J Neurosci, 2009. **29**(36): p. 11112-22.
62. Aghajanian, G.K. and G.J. Marek, *Serotonin, via 5-HT2A receptors, increases EPSCs in layer V pyramidal cells of prefrontal cortex by an asynchronous mode of glutamate release.* Brain Res, 1999. **825**(1-2): p. 161-71.
63. Hjelmstad, G.O., *Interactions between asynchronous release and short-term plasticity in the nucleus accumbens slice.* J Neurophysiol, 2006. **95**(3): p. 2020-3.
64. Iremonger, K.J. and J.S. Bains, *Integration of asynchronously released quanta prolongs the postsynaptic spike window.* J Neurosci, 2007. **27**(25): p. 6684-91.
65. Volman, V. and R.C. Gerkin, *Synaptic scaling stabilizes persistent activity driven by asynchronous neurotransmitter release.* Neural Comput, 2011. **23**(4): p. 927-57.
66. Jensen, K., et al., *Developmental increase in asynchronous GABA release in cultured hippocampal neurons.* Neuroscience, 2000. **101**(3): p. 581-8.
67. Kiyosue, K., E. Shimabayashi, and T. Taguchi, *Development of two transmitter release components during the critical period for imprinting in the chick IMHV.* Eur J Neurosci, 2002. **16**(8): p. 1587-92.
68. Yoshihara, M. and J.T. Littleton, *Synaptotagmin I functions as a calcium sensor to synchronize neurotransmitter release.* Neuron, 2002. **36**(5): p. 897-908.
69. Nishiki, T. and G.J. Augustine, *Synaptotagmin I synchronizes transmitter release in mouse hippocampal neurons.* J Neurosci, 2004. **24**(27): p. 6127-32.
70. Liu, H., et al., *Autapses and networks of hippocampal neurons exhibit distinct synaptic transmission phenotypes in the absence of synaptotagmin I.* J Neurosci, 2009. **29**(23): p. 7395-403.
71. Ullrich, B., et al., *Functional properties of multiple synaptotagmins in brain.* Neuron, 1994. **13**(6): p. 1281-91.
72. Marqueze, B., et al., *Cellular localization of synaptotagmin I, II, and III mRNAs in the central nervous system and pituitary and adrenal glands of the rat.* J Neurosci, 1995. **15**(7 Pt 1): p. 4906-17.
73. Chapman, E.R., et al., *Ca2+ regulates the interaction between synaptotagmin and syntaxin 1.* J Biol Chem, 1995. **270**(40): p. 23667-71.
74. Lynch, K.L., et al., *Synaptotagmin C2A loop 2 mediates Ca2+-dependent SNARE interactions essential for Ca2+-triggered vesicle exocytosis.* Mol Biol Cell, 2007. **18**(12): p. 4957-68.
75. Vrljic, M., et al., *Molecular mechanism of the synaptotagmin-SNARE interaction in Ca2+-triggered vesicle fusion.* Nat Struct Mol Biol, 2010. **17**(3): p. 325-31.

76. Zhou, Q., et al., *Architecture of the synaptotagmin-SNARE machinery for neuronal exocytosis.* Nature, 2015. **525**(7567): p. 62-7.
77. Schupp, M., et al., *Interactions Between SNAP-25 and Synaptotagmin-1 Are Involved in Vesicle Priming, Clamping Spontaneous and Stimulating Evoked Neurotransmission.* J Neurosci, 2016. **36**(47): p. 11865-11880.
78. Wang, S., Y. Li, and C. Ma, *Synaptotagmin-1 C2B domain interacts simultaneously with SNAREs and membranes to promote membrane fusion.* Elife, 2016. **5**.
79. Bai, J., P. Wang, and E.R. Chapman, *C2A activates a cryptic Ca(2+)-triggered membrane penetration activity within the C2B domain of synaptotagmin I.* Proc Natl Acad Sci U S A, 2002. **99**(3): p. 1665-70.
80. Li, L., et al., *Phosphatidylinositol phosphates as co-activators of Ca2+ binding to C2 domains of synaptotagmin 1.* J Biol Chem, 2006. **281**(23): p. 15845-52.
81. Hui, E., et al., *Synaptotagmin-mediated bending of the target membrane is a critical step in Ca(2+)-regulated fusion.* Cell, 2009. **138**(4): p. 709-21.
82. Mackler, J.M., et al., *The C(2)B Ca(2+)-binding motif of synaptotagmin is required for synaptic transmission in vivo.* Nature, 2002. **418**(6895): p. 340-4.
83. Yao, J., et al., *Uncoupling the roles of synaptotagmin I during endo- and exocytosis of synaptic vesicles.* Nat Neurosci, 2011. **15**(2): p. 243-9.
84. Bacaj, T., et al., *Synaptotagmin-1 and synaptotagmin-7 trigger synchronous and asynchronous phases of neurotransmitter release.* Neuron, 2013. **80**(4): p. 947-59.
85. Hui, E., et al., *Three distinct kinetic groupings of the synaptotagmin family: candidate sensors for rapid and delayed exocytosis.* Proc Natl Acad Sci U S A, 2005. **102**(14): p. 5210-4.
86. Maximov, A., et al., *Genetic analysis of synaptotagmin-7 function in synaptic vesicle exocytosis.* Proc Natl Acad Sci U S A, 2008. **105**(10): p. 3986-91.
87. Turecek, J. and W.G. Regehr, *Synaptotagmin 7 Mediates Both Facilitation and Asynchronous Release at Granule Cell Synapses.* J Neurosci, 2018. **38**(13): p. 3240-3251.
88. Groffen, A.J., et al., *Doc2b is a high-affinity Ca2+ sensor for spontaneous neurotransmitter release.* Science, 2010. **327**(5973): p. 1614-8.
89. Pang, Z.P., et al., *Doc2 supports spontaneous synaptic transmission by a Ca(2+)-independent mechanism.* Neuron, 2011. **70**(2): p. 244-51.
90. Schluter, O.M., et al., *Rabphilin knock-out mice reveal that rabphilin is not required for rab3 function in regulating neurotransmitter release.* J Neurosci, 1999. **19**(14): p. 5834-46.
91. Adolfsen, B., et al., *Synaptotagmins are trafficked to distinct subcellular domains including the postsynaptic compartment.* J Cell Biol, 2004. **166**(2): p. 249-60.
92. Saraswati, S., B. Adolfsen, and J.T. Littleton, *Characterization of the role of the Synaptotagmin family as calcium sensors in facilitation and asynchronous neurotransmitter release.* Proc Natl Acad Sci U S A, 2007. **104**(35): p. 14122-7.
93. Mendez, J.A., et al., *Somatodendritic dopamine release requires synaptotagmin 4 and 7 and the participation of voltage-gated calcium channels.* J Biol Chem, 2011. **286**(27): p. 23928-37.
94. Zhou, K., et al., *Asynchronous Cholinergic Drive Correlates with Excitation-Inhibition Imbalance via a Neuronal Ca(2+) Sensor Protein.* Cell Rep, 2017. **19**(6): p. 1117-1129.

95. Matthew, W.D., L. Tsavaler, and L.F. Reichardt, *Identification of a synaptic vesicle-specific membrane protein with a wide distribution in neuronal and neurosecretory tissue.* J Cell Biol, 1981. **91**(1): p. 257-69.
96. Perin, M.S., et al., *Phospholipid binding by a synaptic vesicle protein homologous to the regulatory region of protein kinase C.* Nature, 1990. **345**(6272): p. 260-3.
97. Perin, M.S., et al., *Structural and functional conservation of synaptotagmin (p65) in Drosophila and humans.* J Biol Chem, 1991. **266**(1): p. 615-22.
98. Petrenko, A.G., et al., *Binding of synaptotagmin to the alpha-latrotoxin receptor implicates both in synaptic vesicle exocytosis.* Nature, 1991. **353**(6339): p. 65-8.
99. Brose, N., et al., *Synaptotagmin: a calcium sensor on the synaptic vesicle surface.* Science, 1992. **256**(5059): p. 1021-5.
100. Geppert, M., et al., *Synaptotagmin I: a major Ca2+ sensor for transmitter release at a central synapse.* Cell, 1994. **79**(4): p. 717-27.
101. Chapman, E.R. and A.F. Davis, *Direct interaction of a Ca2+-binding loop of synaptotagmin with lipid bilayers.* J Biol Chem, 1998. **273**(22): p. 13995-4001.
102. Zhang, X., et al., *Ca2+-dependent synaptotagmin binding to SNAP-25 is essential for Ca2+-triggered exocytosis.* Neuron, 2002. **34**(4): p. 599-611.
103. Davletov, B., O. Perisic, and R.L. Williams, *Calcium-dependent membrane penetration is a hallmark of the C2 domain of cytosolic phospholipase A2 whereas the C2A domain of synaptotagmin binds membranes electrostatically.* J Biol Chem, 1998. **273**(30): p. 19093-6.
104. Ubach, J., et al., *Ca2+ binding to synaptotagmin: how many Ca2+ ions bind to the tip of a C2-domain?* Embo j, 1998. **17**(14): p. 3921-30.
105. Murray, D. and B. Honig, *Electrostatic control of the membrane targeting of C2 domains.* Mol Cell, 2002. **9**(1): p. 145-54.
106. Striegel, A.R., et al., *Calcium binding by synaptotagmin's C2A domain is an essential element of the electrostatic switch that triggers synchronous synaptic transmission.* J Neurosci, 2012. **32**(4): p. 1253-60.
107. Vermaas, J.V. and E. Tajkhorshid, *Differential Membrane Binding Mechanics of Synaptotagmin Isoforms Observed in Atomic Detail.* Biochemistry, 2017. **56**(1): p. 281-293.
108. Paddock, B.E., et al., *Membrane penetration by synaptotagmin is required for coupling calcium binding to vesicle fusion in vivo.* J Neurosci, 2011. **31**(6): p. 2248-57.
109. Broadie, K., et al., *Absence of synaptotagmin disrupts excitation-secretion coupling during synaptic transmission.* Proc Natl Acad Sci U S A, 1994. **91**(22): p. 10727-31.
110. DiAntonio, A. and T.L. Schwarz, *The effect on synaptic physiology of synaptotagmin mutations in Drosophila.* Neuron, 1994. **12**(4): p. 909-20.
111. Xu, J., et al., *Synaptotagmin-1 functions as a Ca2+ sensor for spontaneous release.* Nat Neurosci, 2009. **12**(6): p. 759-66.
112. Loewen, C.A., J.M. Mackler, and N.E. Reist, *Drosophila synaptotagmin I null mutants survive to early adulthood.* Genesis, 2001. **31**(1): p. 30-6.
113. Yoshihara, M., Z. Guan, and J.T. Littleton, *Differential regulation of synchronous versus asynchronous neurotransmitter release by the C2 domains of synaptotagmin 1.* Proc Natl Acad Sci U S A, 2010. **107**(33): p. 14869-74.
114. Whittaker, R.G., *SNAPs, CMAPs and F-waves: nerve conduction studies for the uninitiated.* Pract Neurol, 2012. **12**(2): p. 108-15.

115. Eaton, L.M. and E.H. Lambert, *Electromyography and electric stimulation of nerves in diseases of motor unit; observations on myasthenic syndrome associated with malignant tumors.* J Am Med Assoc, 1957. **163**(13): p. 1117-24.
116. Lang, B., et al., *The effect of myasthenic syndrome antibody on presynaptic calcium channels in the mouse.* J Physiol, 1987. **390**: p. 257-70.
117. Newsom-Davis, J., *Lambert-Eaton myasthenic syndrome.* Springer Semin Immunopathol, 1985. **8**(1-2): p. 129-40.
118. Howard, J.F., Jr., *Electrodiagnosis of disorders of neuromuscular transmission.* Phys Med Rehabil Clin N Am, 2013. **24**(1): p. 169-92.
119. Takamori, M., *Lambert-Eaton myasthenic syndrome: search for alternative autoimmune targets and possible compensatory mechanisms based on presynaptic calcium homeostasis.* J Neuroimmunol, 2008. **201-202**: p. 145-52.
120. Engel, A.G., *Genetic basis and phenotypic features of congenital myasthenic syndromes.* Handb Clin Neurol, 2018. **148**: p. 565-589.
121. Herrmann, D.N., et al., *Synaptotagmin 2 mutations cause an autosomal-dominant form of lambert-eaton myasthenic syndrome and nonprogressive motor neuropathy.* Am J Hum Genet, 2014. **95**(3): p. 332-9.
122. Whittaker, R.G., et al., *Electrophysiologic features of SYT2 mutations causing a treatable neuromuscular syndrome.* Neurology, 2015. **85**(22): p. 1964-71.
123. Baker, K., et al., *Identification of a human synaptotagmin-1 mutation that perturbs synaptic vesicle cycling.* J Clin Invest, 2015. **125**(4): p. 1670-8.
124. Arac, D., et al., *Close membrane-membrane proximity induced by Ca(2+)-dependent multivalent binding of synaptotagmin-1 to phospholipids.* Nat Struct Mol Biol, 2006. **13**(3): p. 209-17.
125. Martens, S., M.M. Kozlov, and H.T. McMahon, *How synaptotagmin promotes membrane fusion.* Science, 2007. **316**(5828): p. 1205-8.
126. Sutton, R.B., J.A. Ernst, and A.T. Brunger, *Crystal structure of the cytosolic C2A-C2B domains of synaptotagmin III. Implications for Ca(+2)-independent snare complex interaction.* J Cell Biol, 1999. **147**(3): p. 589-98.
127. Fernandez, I., et al., *Three-dimensional structure of the synaptotagmin 1 C2B-domain: synaptotagmin 1 as a phospholipid binding machine.* Neuron, 2001. **32**(6): p. 1057-69.
128. Nishiki, T. and G.J. Augustine, *Dual roles of the C2B domain of synaptotagmin I in synchronizing Ca2+-dependent neurotransmitter release.* J Neurosci, 2004. **24**(39): p. 8542-50.

CHAPTER 2: CLARIFICATION OF CA^{2+} BINDING IN SYNAPTOTAGMIN 1'S C_2A DOMAIN IN ASYNCHRONOUS NEUROTRANSMITTER RELEASE[1]

2.1 Summary

Following nerve stimulation, there are two distinct phases of Ca^{2+}-dependent neurotransmitter release: a fast, synchronous release phase, and a prolonged, asynchronous release phase. Each of these phases is tightly regulated and mediated by distinct mechanisms. Synaptotagmin 1 is the major Ca^{2+} sensor that triggers fast, synchronous neurotransmitter release upon Ca^{2+} binding by its C_2A and C_2B domains. It has also been implicated in the regulation of asynchronous neurotransmitter release. As blocking Ca^{2+} binding by the C_2A domain of synaptotagmin 1 results in a dramatic increase in asynchronous release, C_2A Ca^{2+} binding is postulated to directly inhibit asynchronous release. However, the mutation used to block Ca^{2+} binding in the previous experiments had the unintended side effect of mimicking Ca^{2+} binding, raising the possibility that the increase in asynchronous release was an artifact of ostensibly constitutive Ca^{2+} binding. To test whether Ca^{2+} binding by C_2A is required for the direct regulation of asynchronous release, we utilize an alternate C_2A mutation that we designed to block Ca^{2+} binding without mimicking it. Analysis of both the original mutation and our alternate mutation at the *Drosophila* neuromuscular junction shows opposite effects on: spontanteous release frequency, synchronous release kinetics, and asynchronous release events. Importantly, we found that asynchronous release is not increased in our novel mutant. Thus, our work provides new mechanistic insight into synaptotagmin 1 function during Ca^{2+}-evoked

[1] Authors: Mallory Shields, Matthew Bowers, McKenzie Fulcer, Lara Perinet, Marissa Metz, Noreen Reist

synaptic transmission and demonstrates that Ca^{2+} binding by the C_2A domain of synaptotagmin 1 does not actively inhibit asynchronous neurotransmitter release *in vivo*.

2.2 Introduction

Following nerve stimulation, there are two phases of Ca^{2+}-dependent neurotransmitter release. Fast, synchronous release is the large burst of neurotransmitter release that occurs within milliseconds (ms) of the arrival of the action potential. At most healthy synapses, the majority of release occurs during the synchronous phase [1]. Synaptotagmin 1, which contains two Ca^{2+}-binding C_2 domains, C_2A and C_2B [2], is essential for coupling Ca^{2+} binding to efficient, synchronous release [3-6].

Asynchronous release can last from 10's of ms to 10's of seconds (s) [7], and has been functionally implicated in synaptic plasticity [8-11] and development [12, 13]. While most synapses exhibit little to no asynchronous release, it is observed in many synapse types [7]. In some specialized synapses, such as specific hippocampal and brainstem interneurons, asynchronous release is predominant [14-16].

In addition to being the Ca^{2+} sensor for fast, synchronous release, synaptotagmin 1 is proposed to directly regulate asynchronous release. Increases in asynchronous release are reported in synaptotagmin 1 null mutants [17, 18] and in a synaptotagmin 1 point mutant in which Ca^{2+} binding by the C_2A domain is blocked [19]. Importantly, synchronous release remains intact in this C_2A point mutant. Thus, the authors conclude that Ca^{2+} binding in C_2A is not needed for efficient synchronous release, but does play a role in preventing asynchronous neurotransmission [19]. Together, these studies result in the inhibition hypothesis: that Ca^{2+}

binding by the C_2A domain of synaptotagmin is directly inhibiting asynchronous neurotransmitter release.

More recently, our group demonstrated that Ca^{2+} binding by the C_2A domain *is required* for efficient synchronous release [4], contrary to previous studies [20-22]. The original point mutations used to block Ca^{2+} binding by C_2A removed negative charge from the Ca^{2+} binding pocket; key, negatively-charged aspartate residues (D) essential for coordinating Ca^{2+} were replaced with neutral asparagines (N), sytD-N. Since synaptotagmin 1 functions as an electrostatic switch [23, 24], removing negative charge may mimic Ca^{2+} binding and permit downstream effector interactions [20].

To directly test this hypothesis, we generated a novel Ca^{2+}-binding mutation where an essential C_2A aspartate was mutated to a negatively-charged glutamate (E) [4]. The $syt^{D\text{-}E}$ mutation maintains the negative charge of the pocket but prevents Ca^{2+} binding by steric hindrance resulting in an ~80% decrease in synchronous neurotransmitter release. This finding demonstrated that an intact C_2B Ca^{2+}-binding domain is sufficient to trigger the electrostatic switch in the absence of C_2A Ca^{2+} binding only if the C_2A Ca^{2+}-binding pocket was neutralized. Thus, the failure of $syt^{D\text{-}N}$ mutations to impair synchronous release is an artifact of removing the electrostatic repulsion of the presynaptic membrane.

The current interpretation, that a $syt^{D\text{-}N}$ mutation fails to inhibit asynchronous release because it cannot bind Ca^{2+}, may be subject to the same artifact. By comparing a $syt^{D\text{-}N}$ mutation with the $syt^{D\text{-}E}$ mutation in *Drosophila*, we test whether Ca^{2+} binding by the C_2A domain of synaptotagmin 1 is required to regulate asynchronous release events. If C_2A Ca^{2+} binding clamps asynchronous release, the increased asynchronous release seen in the $syt^{D\text{-}N}$ mutation should also occur in the $syt^{D\text{-}E}$ mutation. However, if increased asynchronous release is an artifact of

ostensibly constitutive Ca^{2+} binding in *syt*$^{D\text{-}N}$, then the *syt*$^{D\text{-}E}$ mutation should not result in increased asynchronous release. We now show the *syt*$^{D\text{-}E}$ mutation had no impact on asynchronous release, demonstrating that C_2A Ca^{2+} binding does not regulate asynchronous neurotransmitter release.

2.3 Results

Synaptotagmin mutations

To test the function of Ca^{2+} binding by the C_2A domain of synaptotagmin during vesicle fusion events, we completed a direct comparison of two disparate mutations that both block Ca^{2+} binding (Fig 2.1). Mutating the third and fourth of the Ca^{2+}-binding Ds to Ns (*syt*$^{D\text{-}N}$, Fig 2.1B) blocks Ca^{2+} binding and Ca^{2+}-dependent C_2A interactions by removing some of the negative charges required to coordinate Ca^{2+}. Mutating the second D to an E (*syt*$^{D\text{-}E}$, Fig 2.1C) in C_2A blocks Ca^{2+} binding by steric hindrance while maintaining the negative charge of the pocket. In all experiments, synaptotagmin 1 was expressed as a transgene (*P[syt]*) in the absence of native synaptotagmin 1.

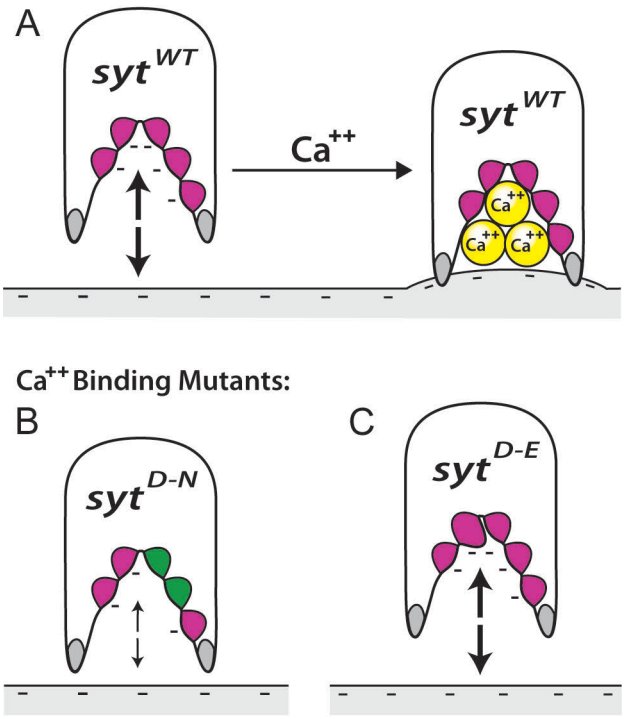

Fig 2.1. C_2A domain of wild type and mutant synaptotagmin and their interactions with the negatively-charged presynaptic membrane. A) Cartoon depicting the C_2A Ca^{2+}-binding pocket of wild type synaptotagmin (*syt^{WT}*) repeling the negatively-charged presynaptic membrane prior to Ca^{2+} entry due to 5 negatively-charged aspartate residues (magenta, left) and penetrating the presynaptic membrane via hydrophobic residues (grey) once Ca^{2+} binding results in a net positive charge that attracts the membrane (right). B) The *syt$^{D\text{-}N}$* mutation in C_2A blocks Ca^{2+} binding by partially neutralizing the pocket when two aspartate residues are replaced with neutral asparagines (green). C) The *syt$^{D\text{-}E}$* mutation in C_2A blocks Ca^{2+} binding by steric hinderance when one aspartate residue deep in the Ca^{2+}-binding pocket is replaced with a larger, negatively-charged glutamate residue (magenta, larger).

Transgenic synaptotagmin expression and targeting

To compare levels of protein expression between *P[syt^{WT}]*, *P[syt$^{D\text{-}N}$]*, and *P[syt$^{D\text{-}E}$]*, western analysis was performed on the central nervous system (CNS) of individual third instar larvae. There were no significant differences in expression of the synaptotagmin transgenes. Mean normalized expression ± standard error of the mean (SEM) in *P[syt$^{D\text{-}N}$]* was 104.6 ± 8.4% of control (Fig 2.2A, p = 0.70, student t-test). Mean expression in *P[syt$^{D\text{-}E}$]* was 112.6 ± 10.4% of control (Fig 2.2B, p = 0.29, student t-test). To assess protein targeting, third instar larval body

wall preparations were labeled with an anti-synaptotagmin antibody, which was visualized with a fluorescent secondary antibody by confocal microscopy. All transgenic synaptotagmin labeling is appropriately localized to the neuromuscular junction (Fig 2.2C).

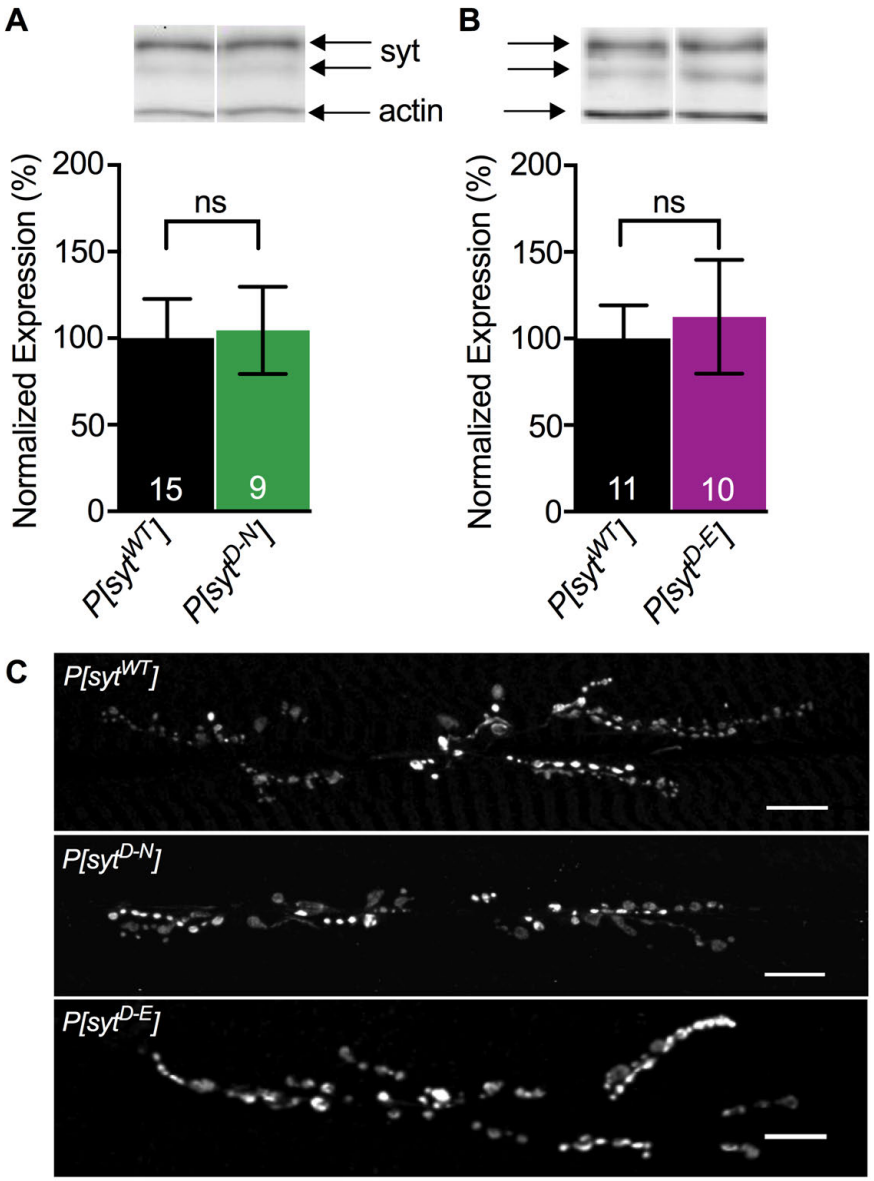

Fig 2.2. Transgenic synaptotagmin expression levels and localization. (A,B) *Above,* Representative western blots showing expression levels of synaptotagmin and the actin loading control. (A) *Below*, *P[syt^{WT}]* (black) and *P[syt^{D-N}]* (green) exhibit similar levels of synaptotagmin expression. (B) *Below*, *P[syt^{WT}]* and *P[syt^{D-E}]* (magenta) exhibit similar levels of synaptotagmin expression. All measurements were normalized to actin levels. Error bars depict SEM, and n's within bars represent number of CNS samples tested. (C) Anti-synaptotagmin labeling of third instar body wall musculature demonstrated that transgenic

synaptotagmin is highly concentrated at the neuromuscular junction in all genotypes. Scale bars = 20 μm.

Opposite effects of Ca^{2+}-binding mutants on synchronous release amplitude

Both the *P[syt^{D-N}]* and *P[syt^{D-E}]* mutations block Ca^{2+} binding by the C_2A domain [4, 19]. We determined the amplitude of excitatory junction potential (EJP) responses in third instars under our recording conditions (Fig 2.3) to ensure that our two electrode voltage clamp (TEVC) recordings attained a ≥ 90% clamp of this response. As previously reported by voltage clamp in embryonic preparations [19], the *P[syt^{D-N}]* mutation supports efficient synchronous neurotransmitter release at the neuromuscular junction in third instar larvae. However, the *P[syt^{D-E}]* mutation does not [4]. ANOVA analysis showed a significant difference between the three genotypes ($p < 0.0001$). There was no significant difference between the mean EJP amplitude in *P[syt^{WT}]* larvae (30.85 ± 1.69 mV, mean ± SEM) and *P[syt^{D-N}]* (Fig 2.3B, 30.88 ± 1.05 mV, $p = 0.99$, Dunnett's correction). The mean EJP amplitude in *P[syt^{D-E}]* larvae was significantly reduced (Fig 2.3B, 7.15 ± 1.01 mV, $p < 0.0001$, Dunnett's correction). Thus, as seen previously [4], the *P[syt^{D-E}]* mutation resulted in ~80% decrease in neurotransmitter release. These results demonstrate Ca^{2+} binding by the C_2A domain is critical for efficient synchronous neurotransmitter release.

The discrepancy in the effects of these two distinct C_2A Ca^{2+}-binding mutations during synchronous neurotransmitter release could be explained by the charge differences within the Ca^{2+}-binding pocket. The *P[syt^{D-N}]* mutation in C_2A may permit downstream effector interactions initiated by Ca^{2+} binding to the C_2B domain, since synaptotagmin acts as an electrostatic switch [4, 18, 23, 25] and this mutation decreases resting repulsion between synaptotagmin and the presynaptic membrane. In contrast, the *P[syt^{D-E}]* mutation in C_2A

maintains the pocket's negative charge and does not allow these interactions despite Ca^{2+} binding by C_2B [4]. This discrepancy during synchronous release highlights the need to re-examine the putative regulatory role of Ca^{2+} binding by C_2A in asynchronous release.

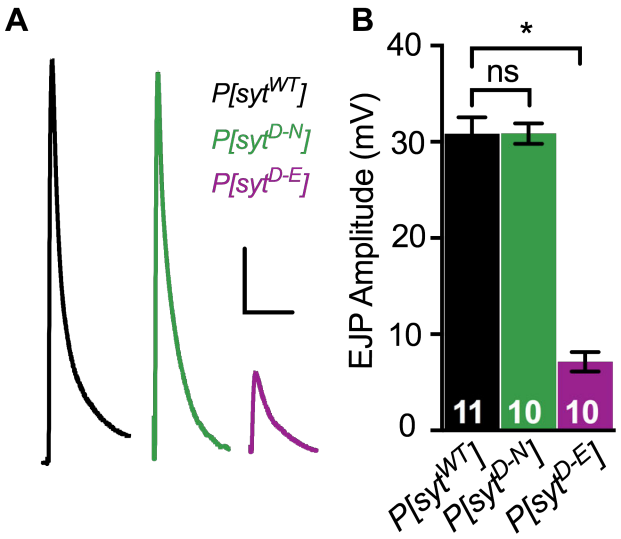

Fig 2.3. Differential effects of C_2A Ca^{2+} binding mutants on amplitude of synchronous release. (A) Representative EJP traces of *P[syt^{WT}]* (black), *P[syt^{D-N}]* (green), and *P[syt^{D-E}]* (magenta). Scale bars = 5 mV, 0.1 s. (B) Mean EJP amplitude in *P[syt^{WT}]* and *P[syt^{D-N}]* was similar, but was significantly decreased in *P[syt^{D-E}]* (*p < 0.0001). Error bars depict SEM, and n's within bars represent number of muscle fibers tested.

Opposite effects of Ca^{2+}-binding mutants on spontaneous release

The decrease in evoked response *P[syt^{D-E}]* could have been a result of decreased quantal size. We compared mean mEJP amplitudes and found no significant differences in any genotype (Fig 2.4B, p = 0.19, Kruskal-Wallis Test).). Mean mEJP amplitude ± SEM in *P[syt^{WT}]* was 0.93 ± 0.05 mV, in *P[syt^{D-N}]* was 0.97 ± 0.03 mV, and in *P[syt^{D-E}]* was 1.02 ± 0.05 mV. Thus, the decrease in synchronous evoked release in the *P[syt^{D-E}]* mutants was not due to a change in quantal size.

Synaptotagmin regulates the rate of spontaneous vesicle fusion events. In synaptotagmin null mutants, the frequency of miniature EJPs (mEJPs) is significantly increased [6, 26-29].

Thus, synaptotagmin acts as a clamp to prevent these spontaneous fusion events. *P[syt$^{D\text{-}N}$]* mutants also exhibited an increased rate of spontaneous fusion events at *Drosophila* embryonic neuromuscular junctions [19]. We verified this effect at third instar neuromuscular junctions and found statistically significant differences in mEJP frequency among genotypes (Fig 2.4C, $p = 0.02$, ANOVA). The mEJP frequency in *P[syt$^{D\text{-}N}$]* mutants was 4.49 ± 0.39 Hz (mean ± SEM) which was significantly increased compared to *P[syt^{WT}]* at 2.81 ± 0.43 Hz ($p = 0.01$, Dunnett's correction). In contrast, mEJP frequency in *P[syt$^{D\text{-}E}$]* was 3.28 ± 0.43 Hz, similar to control ($p = 0.66$, Dunnett's correction). Thus, the negative charge of the Ca^{2+}-binding pocket is the key characteristic required to clamp spontaneous fusion events. The differential effect of these mutations on both spontaneous and synchronous events supports synaptotagmin's role as an electrostatic switch, where electrostatic repulsion between its C_2 domains and the presynaptic membrane is required to prevent vesicle fusion.

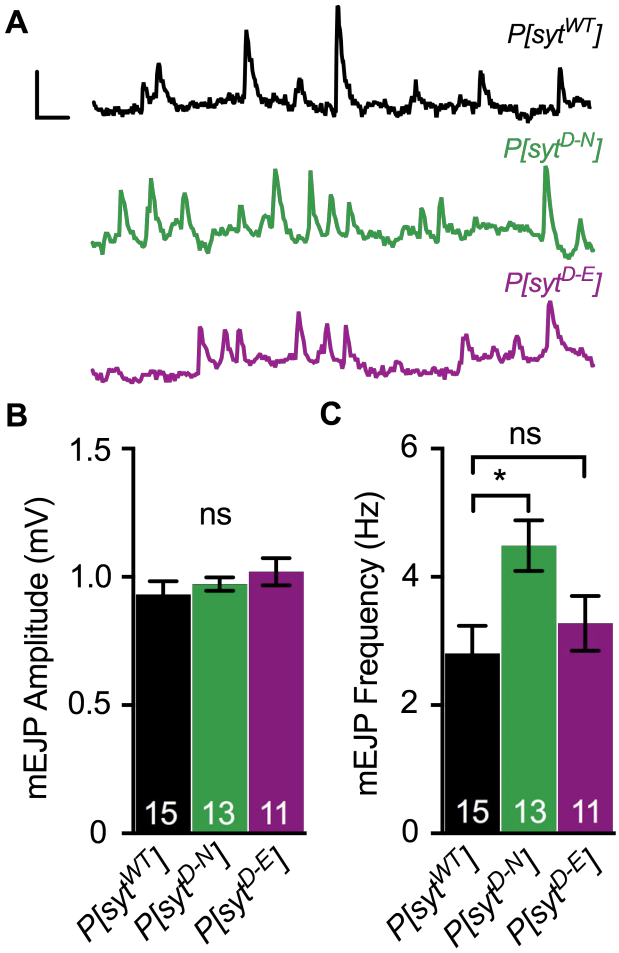

Fig 2.4. The negative charge of the C_2A Ca^{2+}-binding pocket is required to clamp spontaneous vesicle fusion events. (A) Representative mEJP traces from *P[syt^{WT}]* (black,) *P[syt$^{D\text{-}N}$]* (green), and *P[syt$^{D\text{-}E}$]* (magenta) showing 3 consecutive seconds of spontaneous mEJPs. Scale bars = 1 mV, 0.2 s. (B) Mean mEJP amplitude was similar among genotypes. (C) Mean mEJP frequency was increased in *P[syt$^{D\text{-}N}$]* but unchanged in *P[syt$^{D\text{-}E}$]* relative to *P[syt^{WT}]* (*p = 0.01). All error bars depict SEM, and n's within bars represent number of muscle fibers tested.

Readily releasable pool size was unaltered

A decrease in the readily releasable pool of synaptic vesicles could explain the decreased neurotransmitter release seen in the *P[syt$^{D\text{-}E}$]* mutants. Hypertonic solutions stimulate a Ca^{2+}-independent form of release, which has been used to estimate the readily releasable pool of synaptic vesicles [30-32]. To estimate the size of this pool in our lines, we puff applied a 0.3 M sucrose solution to the neuromuscular junction. Sucrose application triggered an increase in the

frequency of fusion events in all genotypes (Fig 2.5A,B). To account for the increase in spontaneous mEJP frequency in *P[syt^{D-N}]* mutants (Fig 2.4C), event frequencies were normalized to the mean mEJP frequency before sucrose application (Fig 2.5C). In all genotypes, sucrose application increased the frequency of fusion events (mean fold increase ± SEM between 0-40 s after sucrose application onset for *P[syt^{WT}]* = 2.55 ± 0.14, for *P[syt^{D-N}]* = 2.55 ± 0.08, and for *P[syt^{D-E}]* = 2.91 ± 0.13). Both *P[syt^{D-N}]* and *P[syt^{D-E}]* mutants displayed similar increases in neurotransmitter release events relative to control during the sucrose response (Fig 2.5C, p = 0.08, Kruskal-Wallis test, p = 0.99 comparing *P[syt^{WT}]* to *P[syt^{D-N}]* and p = 0.13 comparing *P[syt^{WT}]* to *P[syt^{D-E}]*, Dunn's correction). Therefore, the decrease in synchronous release in the *P[syt^{D-E}]* mutants is not the result of a decrease in the size of the readily releasable pool.

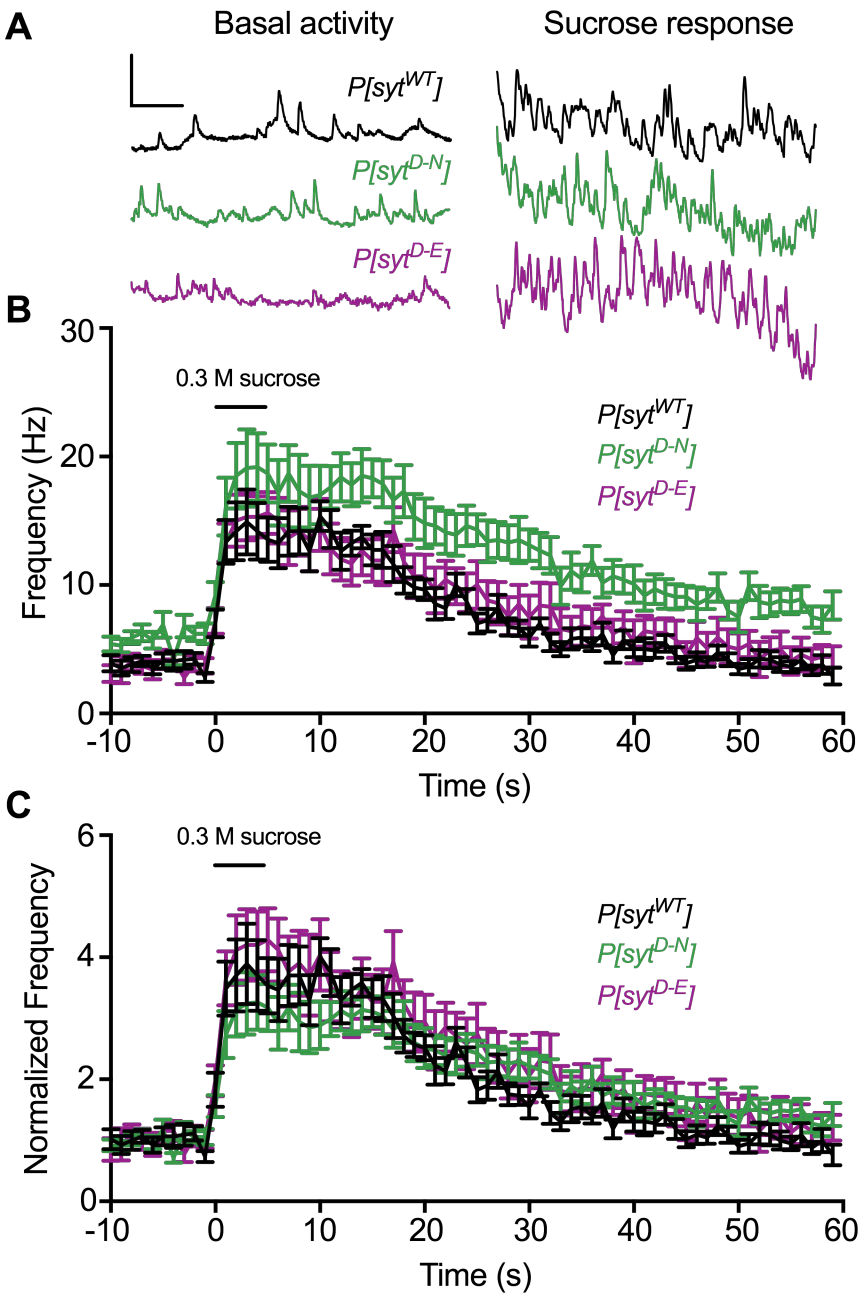

Fig 2.5. The readily releasable pool remains unchanged. (A) Representative traces of event frequency both before and during sucrose-stimulated neurotransmitter release. Scale bars = 2 mV, 0.5 s. (B) Event frequencies over time in response to a 5 s application of a hypertonic sucrose solution. n = 11 fibers for each genotype. (C) Event frequencies over time normalized to the basal mEJP frequency prior to sucrose application. No statistically significant changes were found relative to control during the sucrose response. The black bar above the traces in B,C represents the 5 s sucrose application.

Opposite effects of Ca^{2+}-binding mutants on release probability

Another potential explanation for the decrease in synchronous neurotransmitter release in the *P[syt^{D-E}]* mutants is that this mutation caused a decrease in presynaptic release probability. Since an increase in the paired pulse ratio is correlated to a decrease in release probability [33] we compared paired pulse ratios in each genotype. When muscle fibers were stimulated with two pulses at an interpulse interval of 20 ms, statistically significant differences in paired pulse ratios were seen (Fig 2.6, $p < 0.0001$, ANOVA). While the paired pulse ratio in *P[syt^{D-N}]* (1.09 ± 0.01, mean ± SEM) was nearly identical to *P[syt^{WT}]* (1.09 ± 0.02, $p = 0.99$, Dunnett's correction), the paired pulse ratio in *P[syt^{D-E}]* (1.51 ± 0.05, mean ± SEM) was significantly larger ($p = 0.0001$, Dunnett's correction). The increase in paired pulse ratio indicates that the *syt^{D-E}* mutation caused a decrease in release probability.

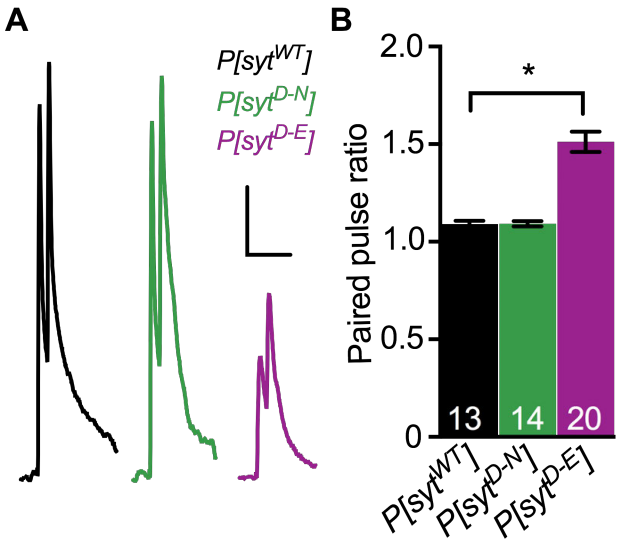

Fig 2.6. Release probability was decreased in *P[syt^{D-E}]* mutants. (A) Representative paired pulse traces with a 20 ms interpulse interval from *P[syt^{WT}]* (black), *P[syt^{D-N}]* (green), and *P[syt^{D-E}]* (magenta). Scale bars = 5 mV, 0.1 s. (B) There was a significant difference in paired pulse ratios among genotypes with a significantly increased paired pulse ratio in *P[syt^{D-E}]* compared to control (*$p < 0.0001$). There was no change in paired pulse ratios between control and *P[syt^{D-N}]* ($p = 0.99$). Error bars are SEM, and n's within bars represent number of fibers tested.

Ca^{2+}-binding mutants display prolonged synchronous release time course

Although the amplitude of synchronous release was unimpaired in the *P[syt$^{D\text{-}N}$]* mutants, we noticed that the kinetics of the synchronous release phase appeared to be slowed. The decay time constant (τ) is a characteristic that provides insight into release kinetics, and is defined as the time it takes for the response to reach *1-1/e*, which is ~ 63.2% of the final value. More simply, it is a measure of how long it takes a trace to recover from peak response to 36.8% of baseline value. We assessed decay time constants using two-electrode voltage clamp analysis, as it provided the adequate temporal resolution that current clamp recordings did not.

There were differences in decay constants (Fig 2.7 left, $p < 0.0001$, ANOVA). The *P[syt$^{D\text{-}N}$]* mutation exhibited a significantly longer decay constant than control (Fig 2.7B left, mean τ ± SEM of *P[syt^{WT}]* = 5.01 ± 0.05 ms, and *P[syt$^{D\text{-}N}$]* = 5.87 ± 0.11 ms, $p < 0.0001$, Tukey's multiple comparisons test). The *P[syt$^{D\text{-}E}$]* mutation also exhibited a significantly longer decay time constant than control (Fig 2.7B, *P[syt$^{D\text{-}E}$]* mean τ ± SEM = 5.56 ± 0.11 ms, $p < 0.0001$, Tukey's multiple comparisons test). Interestingly, differences were also observed between C_2A Ca^{2+}-binding mutants ($p = 0.04$, Tukey's multiple comparisons test).

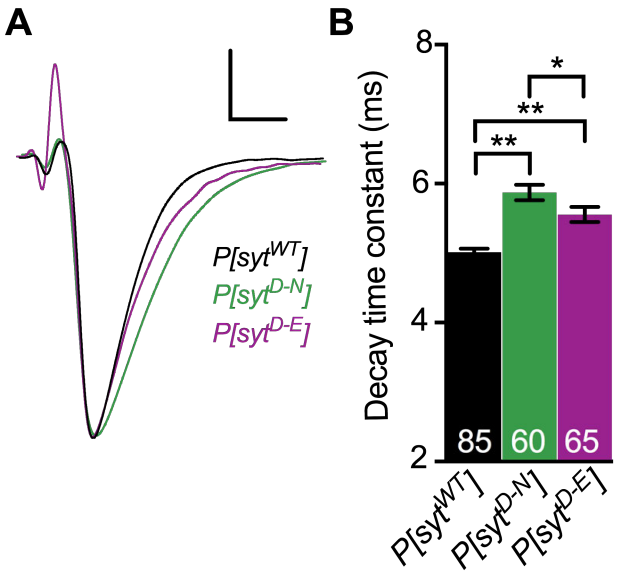

Fig 2.7. Synchronous release kinetics were altered in C_2A Ca^{2+} binding mutants. (A) Representative traces of *P[syt^{WT}]* (black), *P[syt^{D-N}]* (green), and *P[syt^{D-E}]* (magenta). Scale bars = 25% of total response, 5 ms. (B). Both the *P[syt^{D-N}]* and *P[syt^{D-E}]* mutants exhibited longer decay time constants compared to *P[syt^{WT}]* (**p < 0.0001). The *P[syt^{D-N}]* and *P[syt^{D-E}]* mutants also exhibited different decay time constants from one another (*p = 0.04). Error bars are SEM, and n's within bars represent number of fibers tested.

Opposite effects of Ca^{2+}-binding mutants on asynchronous release

We counted release events that occurred from 280 ms before stimulation through 580 ms after stimulation. Latency histograms of the number of events/stimulus before and after stimulation are shown in Fig 2.8. Control larvae and *P[syt^{D-E}]* mutants both showed a trend toward an increase in release events during the 20-300 ms time window compared to the frequency of 280 ms pre-stimulation events (125% increase for control and 111% increase for *P[syt^{D-E}]*), but these increases were not statistically significant (Fig 2.8D, prestimulation event frequency for *P[syt^{WT}]* ± SEM = 3.15 ± 0.36 Hz and during the asynchronous release period was 3.95 ± 0.38 Hz, p = 0.09, paired t-test. Prestimulation event frequency for *P[syt^{D-E}]* was 4.31 ± 0.57 Hz and during asynchronous release was 4.40 ±0.51 Hz, p = 0.52, paired t-test). The *P[syt^{D-N}]* mutants showed a robust and significant increase in asynchronous release of 167% (Fig 2.8D, prestimulation event frequency was 5.06 ± 0.60 Hz and during asynchronous release was 8.45 ± 0.83 Hz , p = 0.001, paired t-test). Release event frequency returned to basal levels approximately 300 ms after the stimulus, as event frequency was not elevated in any genotype from 300 - 580 ms after stimulation compared to prestimulation values (Fig 2.8E, mean event frequencies from 300 – 580 ms after stimulation ± SEM for P[*syt^{WT}*], P[*syt^{D-N}*], and P[*syt^{D-E}*] were 2.44 ± 0.44 Hz, 3.87 ± 0.54 Hz, and 3.19 ± 0.42 Hz, respectively, where p = 0.1, 0.13, and 0.26, respectively, paired t-tests. This is consistent with the timeline of asynchronous release at

Drosophila neuromuscular junctions in synaptotagmin null mutants, where asynchronous release is prevalent [18, 19].

To quantify Ca^{2+}-stimulated, asynchronous release across genotypes while controlling for the variable rate of spontaneous release among genotypes, the mean number of stimulus-*independent* mEJP events that occured during the 280 ms prior to stimulation was subtracted from the mean number of stimulus-*dependent* asynchronous events that occurred during the 280 ms after the synchronous response. In this way, we could assess stimulation-dependent asynchronous release by comparing event differences among genotypes. Directly comparing asynchronous release between genotypes revealed significant differences (Fig 2.8F, $p = 0.03$, Kruskal-Wallis test). Consistent with previous reports [19], the $P[syt^{D\text{-}N}]$ mutants exhibited an increase in the number of asynchronous release events (0.95 ± 0.27 events) compared to control (Fig 2.8F, 0.21 ± 0.13 events, $p = 0.04$, Dunn's correction). Importantly, the $P[syt^{D\text{-}E}]$ mutant exhibited no increase in asynchronous release events (Fig 2.8F, 0.12 ± 0.19 events, $p > 0.99$, Dunn's correction) compared to control. Thus, blocking Ca^{2+} binding by the C_2A domain of synaptotagmin had no impact on asynchronous release provided that the electrostatic repulsion of the presynaptic membrane was maintained.

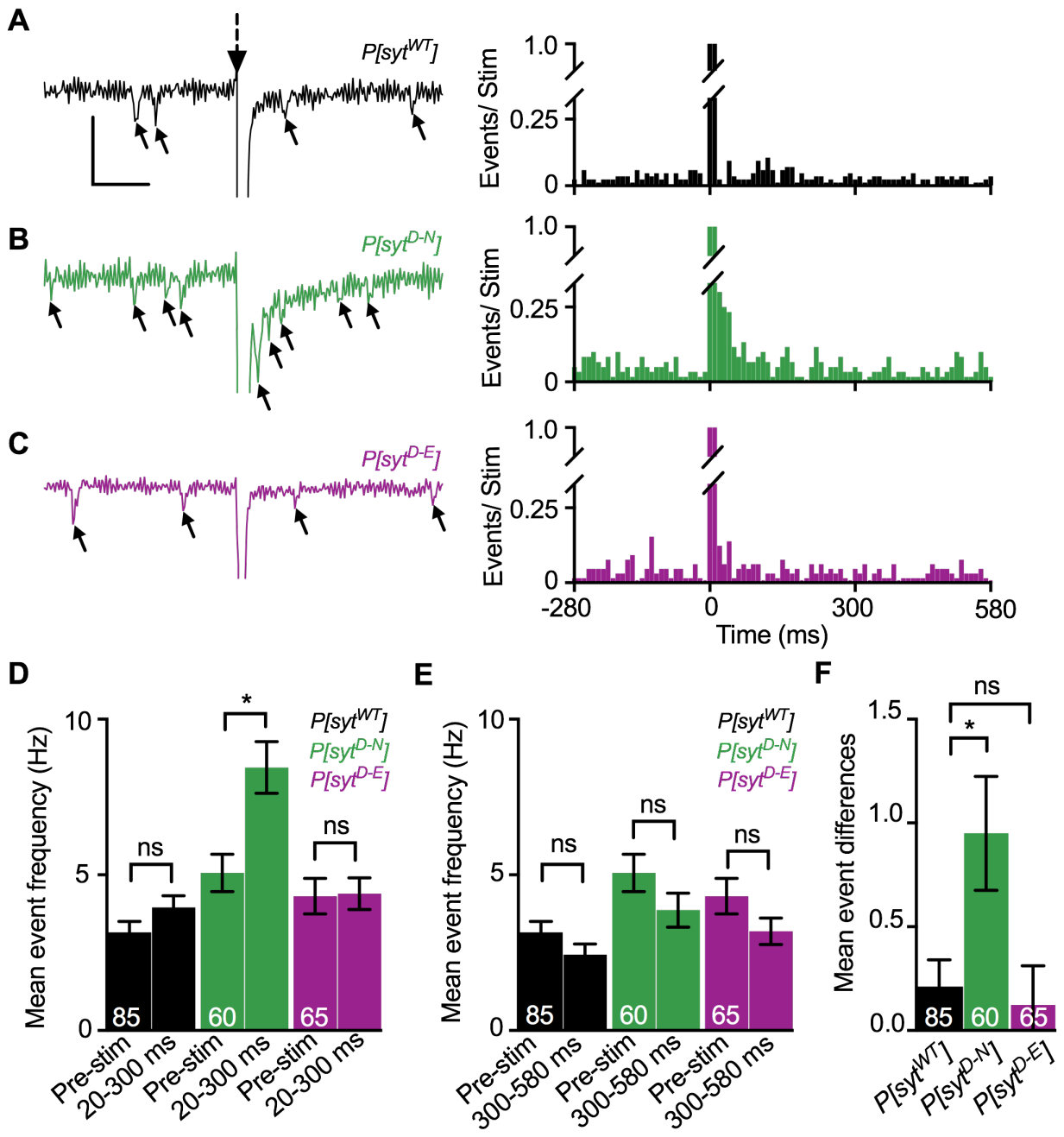

Fig 2.8. Asynchronous release was increased in *P[syt^{D-N}]* mutants but not *P[syt^{D-E}]* mutants. (A-C) Left, Representative traces from *P[syt^{WT}]* (black), *P[syt^{D-N}]* (green), and *P[syt^{D-E}]* (magenta) showing 280 ms before and 300 ms after stimulation (large dotted arrow). Release events before and after the burst of synchronous release are indicated (small arrows). Scale bars = 1 nA, 0.1 s. Right, histograms plotting the mean number of events/stimulus for all genotypes spanning the period of 280 ms before to 580 ms after single stimulations. Data were collected into 10 ms bins and are presented as the number of events/stimulus. A synchronous event occurred within the 0-20 ms bins following every stimulus. (D) Mean frequencies for each genotype 280 ms before stimulation and during the asynchronous time period (20-300 ms post-stimulus) were compared within genotypes. No significant increase in stimulation-dependent

asynchronous release was determined for control (or *P[syt^{D-E}]* larvae. *P[syt^{D-N}]* larvae exhibited a robust asynchronous release response (*p = 0.001). (E) Mean frequencies for each genotype 280 ms before stimulation and 300 – 580 ms post-stimulus were compared within genotypes. No significant increases in stimulation-dependent asynchronous release were determined. (F) Mean event differences between stimulation-dependent asynchronous release events and stimulation-independent spontaneous release reveal increased asynchronous release relative to control in *P[syt^{D-N}]* mutants (*p = 0.04), while *P[syt^{D-E}]* mutants displayed no increase in asynchronous release events. All error bars represent SEM, and n's within bars represent number of traces stimulated.

2.4 Discussion

We investigated the role of Ca^{2+} binding by the C_2A domain of synaptotagmin 1 during neurotransmitter release by comparing two distinct C_2A Ca^{2+}-binding mutations. The *P[syt^{D-N}]* mutant, which blocks Ca^{2+} binding by removing negative charge from the pocket, displayed: no deficits in the amplitude of synchronous release (Fig 2.3) or the pool of readily releasable vesicles (Fig 2.5), an increase in spontaneous release frequency (Fig 2.4), and an increase in asynchronous release events compared to control (Fig 2.8). These findings are consistent with previous reports [19-22]. The paired pulse ratio was similar to control (Fig 2.6), indicating no impact on release probability. However, the slowed kinetics of synchronous release (Fig 2.7) demonstrates that the rate of synchronous vesicle fusion events is impaired.

The *P[syt^{D-E}]* mutants, which block Ca^{2+} binding while maintaining the pocket's negative charge, exhibited: dramatic reduction in the amplitude of synchronous release (Fig 2.3) and no change in spontaneous release frequency (Fig 2.4), as seen previously [4]. In addition, there was no change in the readily releasable pool (Fig 2.5) or in the number of asynchronous release events (Fig 2.8). There was a decrease in release probability (Fig 2.6), and in the kinetics of synchronous release (Fig 2.7).

Why might these two C_2A mutations that block Ca^{2+} binding have opposite effects on the amplitude of synchronous release, release probability, spontaneous release frequency, and asynchronous release? The most likely explanation springs from synaptotagmin's mechanism of action: serving as an electrostatic switch to trigger vesicle fusion events. Once Ca^{2+} binds to C_2A and C_2B, synaptotagmin's electrostatic repulsion of the negatively-charged presynaptic membrane (Fig 1A, left) switches to electrostatic attraction [4, 23-25]. This attraction allows hydrophobic residues at the tips of the C_2 domains to penetrate into the hydrophobic core of the presynaptic membrane (e.g., Fig 1A right, grey residues) [34, 35], favoring fusion.

For synchronous neurotransmitter release, the $syt^{D\text{-}N}$ mutation, by virtue of decreasing the electrostatic repulsion of the presynaptic membrane (Fig 1B), may participate in these downstream effector interactions. Thus, it would support the same level of synchronous release (Fig 3). As there is an intact C_2B domain, the net effect of the $syt^{D\text{-}N}$ mutation is to mimic C_2A Ca^{2+} binding required for synchronous neurotransmitter release. The finding that the kinetics of synchronous release were slowed in the $P[syt^{D\text{-}N}]$ mutant suggests that this ostensibly constitutive Ca^{2+} binding may slow synaptotagmin's association with/disassociation from the membrane. The $syt^{D\text{-}E}$ mutation is expected to have the opposite impact in terms of electrostatic switch function. Since electrostatic repulsion remains intact (Fig 2.1C), the $syt^{D\text{-}E}$ mutation cannot participate in downstream membrane interactions [4]. Therefore, the release probability is significantly reduced (Fig 2.6) and fewer vesicles are triggered to fuse, resulting in decreased synchronous response amplitude (Fig 2.3) [4].

For spontaneous release, the $syt^{D\text{-}N}$ and $syt^{D\text{-}E}$ mutations are also expected to display opposite effects. At rest, SNARE proteins mediate constituitive vesicle-target membrane fusion reactions throughout cells [36]. At the synapse, synaptotagmin is required to prevent aberrent

spontaneous fusion events [6, 26-28] The electrostatic repulsion between the C_2 domains of synaptotagmin and the presynaptic membrane are thought to mediate this inhibitory role. Thus, it is not surprising that the *syt*$^{D\text{-}N}$ mutation, which decreases this electrostatic repulsion resulted in increased spontaneous fusion events, while the *syt*$^{D\text{-}E}$ mutation that maintains the electrostatic repulsion did not (Fig 2.4) [4, 19].

The differential effect on asynchronous release in the Ca^{2+} binding mutants is consistent with synaptotagmin's role as an electrostatic switch. In the *syt*$^{D\text{-}N}$ mutation, the constitutive removal of electrostatic repulsion by C_2A likely mimics bound Ca^{2+}, thereby allowing this mutation to trigger fusion events for a longer period of time, much like an asynchronous sensor. Our alternant *syt*$^{D\text{-}E}$ mutation did not exhibit increased asynchronous release, directly contradicting the current hypothesis that states C_2A Ca^{2+} binding inhibits asynchronous release.

This inhibition hypothesis spawned from two major findings: 1.) that synaptotagmin 1 null mutants showed increased asynchronous release, indicating that synaptotagmin 1 functions to suppress this form of release [17, 18], and 2.) increased asynchronous release in the *syt*$^{D\text{-}N}$ mutation that blocked Ca^{2+} binding by C_2A domains, in either synaptotagmin 1 [19] or Doc2 [37].

Our comparison of the *syt*$^{D\text{-}N}$ to *syt*$^{D\text{-}E}$ mutations refutes the inhibition hypothesis. Therefore, another mechanism must result in the changes in asynchronous release seen in synaptotagmin null mutants and C_2A domain mutations. One simple explanation may be a spatial competition for regulation of SNARE-mediated fusion between synaptotagmin and an asynchronous Ca^{2+} sensor. This competition hypothesis can account for the rates of asynchronous release in synaptotagmin null mutants, as well as various previous manipulations of synaptotagmin 1 at the synapse.

In null mutants, the situation is simple. When synaptotagmin 1 is no longer present at the synapse, the asynchronous sensor has unimpeded access to SNARE complexes to trigger asynchronous release in the absence of synchronous release. Explaining the results reported in the C_2A $syt^{D\text{-}N}$ mutation is more complicated. With an intact C_2B domain, the $syt^{D\text{-}N}$ mutation can function reasonably well during synchronous release and appears to mimic an asynchronous sensor during asynchronous release. Indeed, the $syt^{D\text{-}N}$ mutation triggered more robust release at lower [Ca^{2+}] than control both *in vitro* [20] and *in vivo* [19], consistent with an increased Ca^{2+} affinity and is characteristic of an asynchronous sensor.

The precise subcellular location of the sensor is likely a critical factor for distinct modes of neurotransmitter release [38], further supporting the spatial competition hypothesis. Even a 5 nm difference in distance between the sensor and the Ca^{2+} channel can profoundly affect fusion probability [39]. The current candidates for the mammalian asynchronous sensor are Doc2, a cytosolic protein [40, 41], and synaptotagmin 7, a presynaptic membrane protein [42]. Interestingly, when synaptotagmin 1 was expressed either cytosolically or tethered to the presynaptic membrane, abolished synchronous release and increased asynchronous release were reported [38]. This would be expected if only an asynchronous sensor were present, and provides evidence that competition for optimal space may determine which mode of release is employed.

2.5 Conclusion

Here we show a shift in the current hypothesis regarding the role of *syt* 1's Ca^{2+}-binding role in synchronous, spontaneous, and asynchronous release. Using two distinct C_2A Ca^{2+}-binding mutations, we report opposing effects on synchronous, spontaneous, and asynchronous neurotransmitter release. Using the $syt^{D\text{-}N}$ Ca^{2+}-binding mutation, which inadvertently mimics

Ca^{2+} binding, we observed robust yet kinetically slower synchronous release, increased spontaneous release, and increased asynchronous release, all of which are consistent with this mutation partially flipping the electrostatic switch as a mutational artifact. However, the alternant *P[syt^{D-E}]* mutation that maintains electrostatic repulsion between the C_2A binding pocket and presynaptic membrane displayed opposing results in synchronous, spontaneous, and asynchronous release relative to *syt^{D-N}*. These results indicate that, in contrast to the current inhibition hypothesis in the field, the role of synaptotagmin's C_2A domain does not regulate asynchronous release. Instead, we introduce the spatial competition hypothesis, which resolves the seemingly dischordant results of the differing C_2A Ca^{2+} binding mutations.

2.6 Materials and methods

Drosophila strains

The aspartate to asparagine line used was *syt^{D282,284N}* [generously provided by Motojiro Yoshihara, University of Massachusetts Medical School, Worcester, MA, [19]]. The aspartate to glutamate line used was *syt^{D229E}* [4]. GeneWiz (South Plainfield, New Jersey) synthesized cDNA of the *Drosophila* wild type *syt1* gene flanked by 5' EcoRI and 3' BglII restriction sites. We included some 5' and 3' untranslated sequence [43] to match the mutant *syt* transgenes as closely as possible. This wild type transgene was placed under the control of the UAS promoter by directional subcloning of the synthesized cDNA into the pUAST-attB vector using the EcoRI and BglII restriction sites. The transgene was inserted in the attP2 landing site on the third chromosome in *Drosophila* using the PhiC31 targeted insertion system [44] by Genetivision (Houston, TX). The UAS/Gal4 system was used to drive neuronal expression of our *syt 1* transgenes [45, 46]. To assess the functional significance of the mutations, all transgenes were

expressed in the absence of endogenous synaptotagmin by crossing them into the *syt^{null}* mutant background, *syt^{AD4}* [47]. The genotypes of experimental larvae were the following: *yw; syt^{null}elavGal4/syt^{null}; P[UASsyt^{WT}]/+* line 1 (transgenic control, referred to as *P[syt^{WT}]*), *yw; syt^{null}elavGal4/syt^{null}; P[UASsyt^{D282,284N}]/+* (referred to as *P[syt^{D-N}]*), and *yw; syt^{null}elavGal4/syt^{null}; P[UASsyt^{D229E}]/+* (referred to as *P[syt^{D-E}]*). As no gender selection was employed, experimental larvae included both males and females.

Immunoblotting

The level of synaptotagmin expression was determined by western blot analysis using actin levels as a loading control. Third instar larval central nervous systems (CNSs) were dissected in HL3.1 saline [70 mM NaCl, 5 mM KCl, 4 mM $MgCl_2$, 10 mM $NaHCO_3$, 5 mM Trehalose, 115 mM sucrose, 5 mM HEPES, pH 7.2 [48]]. Individual CNSs were sonified for 5 pulses using a Branson Sonifier 450 (VWR Scientific, Winchester, PA) in Laemmli buffer (Bio-Rad, Hercules, CA) containing 5% β-mercaptoethanol. Each sample was electrophoresed, transferred to Immobilon membranes (Millipore, Bedford, MA), and washed in blocking solution as previously described [49]. Membranes were probed with a 1:2500 dilution of anti-syt antibody, Dsyt-CL1 [3] and 1:10,000 dilution of anti-actin antibody, MAB 1501 (Millipore Bioscience Research Reagents, Billerica, MA), overnight at 4°C. An Epichemi^3 Darkroom and Labworks Imaging Software (UVP BioImaging, Upland, CA) were used to visualize the protein bands. Quantification: for each blot, synaptotagmin/actin ratios were calculated and normalized to the mean synaptotagmin/actin ratio of the control lanes to permit comparison of synaptotagmin signals between blots. Outliers in actin levels were excluded from analysis. Statistical significance was determined using one-way ANOVA.

Immunolabeling

To visualize transgenic synaptotagmin at the neuromuscular junction, third instar larvae were dissected in Ca^{2+}-free HL3.1 saline and fixed in phosphate-buffered saline (PBS, 137 mM NaCl, 1.5 mM KH_2PO_4, 2.7 mM KCl, 8.1 mM Na_2HPO_4) containing 4% formaldehyde for 1 hour. Samples were probed overnight in a 1:400 dilution of Dsyt-CL1 in dilution media [PBS with 0.1% Triton, 1% bovine serum albumin (Millipore-Sigma, Burlington, MA), and 1% normal goat serum (Fitzgerald Industries International, Acton, MA)]. Samples were washed in PBS with 0.1% Triton for 1-3 hours, incubated in dilution media containing a 1:400 dilution of Alexa Fluor 488 goat anti-rabbit antibody (Invitrogen, Carlsbad, CA) for 1 hour at room temperature, washed in PBS with 0.1% Triton for one hour, and mounted on microscope slides in Citifluor (Ted Pella, Redding, CA). Images of neuromuscular junctions of abdominal muscles 6/7 in segments 3 and 4 were acquired using a Zeiss 880 light scanning microscope, a 40X objective, and Zeiss Zen 2.1 acquisition software, version 11,0,3,190.

Electrophysiological experiments and analyses

All electrophysiological events were collected with an Axoclamp 2B amplifier (Molecular Devices, Sunnyvale, CA), a Powerlab 4/35 A/D converter (ADInstuments, Sydney, Australia), and LabChart software (ADInstruments, Sydney, Australia). All statistical analyses were performed using Prism 7 software. 10-20 MΩ intracellular electrodes were pulled using a Sutter model P-97 (Novato, CA) and filled with 3 parts 2 M $K_3C_6H_5O_7$ to 1 part 3 M KCl. Third instar larvae were dissected in Ca^{2+}-free HL3.1 saline to expose the body wall musculature and the CNS was removed. Recordings were made from muscle 6 of abdominal segments 3 and 4. Fibers were held at -55 mV by applying no more than 1 nA of current.

Single evoked excitatory junction potentials (EJPs) were evoked at 0.04 Hz using a stimulating electrode filled with bath solution. Events were evoked in HL3.1 saline containing 1.0 mM Ca^{2+}. The averages of 10 EJPs collected were calculated for each fiber. Statistical significance was determined using a one-way ANOVA with Dunnett's correction.

Miniature excitatory junction potentials (mEJPs) were acquired for 3 minutes in HL3.1 saline. Events were identified manually after recordings had been randomized and blinded to the researcher for analysis. Mean mEJP amplitudes were determined from 50 consecutive events/fiber, beginning after two minutes of recording, from each recording to eliminate bias. Statistical significance was determined using the Kruskal-Wallis test. To determine mEJP frequency, all spontaneous events between the 2nd and 3rd minute of recording from each fiber were counted. Statistical significance for mEJP frequency was determined using a one-way ANOVA with Dunnett's correction.

For paired pulse analysis, stimulations were applied using a 0.02 s interpulse interval. Paired pulse ratios were determined by dividing the EJP amplitude of the second stimulation by the amplitude of the first stimulation. Mean paired pulse ratios were compared between genotypes using a one-way ANOVA with Dunnett's correction.

For hypertonic solution stimulations, a puff application of modified HL3.1 saline containing 0.3 M sucrose was administered to the junctional region of muscles 6/7 in abdominal segments 3 and 4 of third instars using a PicoSpritzer III (Parker Hannifan, Pine Brook, NJ). The puff application was administered for 5 s at ~ 5 pounds per square inch. Recordings were acquired in a bath solution of Ca^{2+}-free HL3.1 saline. All recordings were randomized and blinded to the researcher for analysis. Frequency of mEJP events were counted manually and parsed into 1 s bins for 70 s, including 10 s prior to sucrose application to determine a baseline

mEJP frequency. To determine each genotype's response to the hypertonic solution, the average mEJP frequency during the 40 s following the initiation of the sucrose application was calculated. Statistical significance was determined using a one-way ANOVA with Dunnett's correction to compare mutant genotypes to control.

To quantify asynchronous events, synaptic currents were recorded using two-electrode voltage clamp as described [50]. A second intracellular electrode of 10-15 MΩ resistance was pulled. Following insertion of both intracellular electrodes, recordings with muscle input resistances < 5 MΩ were excluded. Fibers were voltage clamped at -55 mV using no more than 1 nA of current. Traces were acquired in HL3.1 saline containing 1.0 mM Ca^{2+} and fibers were stimulated at 0.2 Hz for 5 stimulations. To measure decay time constants, the mean time to decay 63.2% from the peak EJC response was calculated. ANOVA analysis was performed to determine overall significance, with Tukey's correction to compare all genotypes. Latency analysis of asynchronous release was accomplished by manually binning all miniature EJCs (mEJCs) into 10 ms bins, and graphing the number of events/stimulation in each bin. The difference in mEJC events during the 280 ms before vs. the 20-300 ms after stimulation was calculated (# events after stimulation - # events prior to stimulation) and averaged per genotype. The 20 ms immediately following stimulation was excluded, as synchronous responses occurred during this time period. Statistical significance between genotypes was determined using a Kruskal-Wallis test with Dunn's correction.

WORKS CITED

1. Goda, Y. and C.F. Stevens, *Two components of transmitter release at a central synapse.* Proc Natl Acad Sci U S A, 1994. **91**(26): p. 12942-6.
2. Perin, M.S., et al., *Phospholipid binding by a synaptic vesicle protein homologous to the regulatory region of protein kinase C.* Nature, 1990. **345**(6272): p. 260-3.
3. Mackler, J.M., et al., *The C(2)B Ca(2+)-binding motif of synaptotagmin is required for synaptic transmission in vivo.* Nature, 2002. **418**(6895): p. 340-4.
4. Striegel, A.R., et al., *Calcium binding by synaptotagmin's C2A domain is an essential element of the electrostatic switch that triggers synchronous synaptic transmission.* J Neurosci, 2012. **32**(4): p. 1253-60.
5. Geppert, M., et al., *Synaptotagmin I: a major Ca2+ sensor for transmitter release at a central synapse.* Cell, 1994. **79**(4): p. 717-27.
6. Broadie, K., et al., *Absence of synaptotagmin disrupts excitation-secretion coupling during synaptic transmission.* Proc Natl Acad Sci U S A, 1994. **91**(22): p. 10727-31.
7. Kaeser, P.S. and W.G. Regehr, *Molecular mechanisms for synchronous, asynchronous, and spontaneous neurotransmitter release.* Annu Rev Physiol, 2014. **76**: p. 333-63.
8. Aghajanian, G.K. and G.J. Marek, *Serotonin, via 5-HT2A receptors, increases EPSCs in layer V pyramidal cells of prefrontal cortex by an asynchronous mode of glutamate release.* Brain Res, 1999. **825**(1-2): p. 161-71.
9. Hjelmstad, G.O., *Interactions between asynchronous release and short-term plasticity in the nucleus accumbens slice.* J Neurophysiol, 2006. **95**(3): p. 2020-3.
10. Iremonger, K.J. and J.S. Bains, *Integration of asynchronously released quanta prolongs the postsynaptic spike window.* J Neurosci, 2007. **27**(25): p. 6684-91.
11. Volman, V. and R.C. Gerkin, *Synaptic scaling stabilizes persistent activity driven by asynchronous neurotransmitter release.* Neural Comput, 2011. **23**(4): p. 927-57.
12. Jensen, K., et al., *Developmental increase in asynchronous GABA release in cultured hippocampal neurons.* Neuroscience, 2000. **101**(3): p. 581-8.
13. Kiyosue, K., E. Shimabayashi, and T. Taguchi, *Development of two transmitter release components during the critical period for imprinting in the chick IMHV.* Eur J Neurosci, 2002. **16**(8): p. 1587-92.
14. Hefft, S. and P. Jonas, *Asynchronous GABA release generates long-lasting inhibition at a hippocampal interneuron-principal neuron synapse.* Nat Neurosci, 2005. **8**(10): p. 1319-28.
15. Best, A.R. and W.G. Regehr, *Inhibitory regulation of electrically coupled neurons in the inferior olive is mediated by asynchronous release of GABA.* Neuron, 2009. **62**(4): p. 555-65.
16. Atluri, P.P. and W.G. Regehr, *Delayed release of neurotransmitter from cerebellar granule cells.* J Neurosci, 1998. **18**(20): p. 8214-27.
17. Nishiki, T. and G.J. Augustine, *Synaptotagmin I synchronizes transmitter release in mouse hippocampal neurons.* J Neurosci, 2004. **24**(27): p. 6127-32.
18. Yoshihara, M. and J.T. Littleton, *Synaptotagmin I functions as a calcium sensor to synchronize neurotransmitter release.* Neuron, 2002. **36**(5): p. 897-908.

19. Yoshihara, M., Z. Guan, and J.T. Littleton, *Differential regulation of synchronous versus asynchronous neurotransmitter release by the C2 domains of synaptotagmin 1.* Proc Natl Acad Sci U S A, 2010. **107**(33): p. 14869-74.
20. Stevens, C.F. and J.M. Sullivan, *The synaptotagmin C2A domain is part of the calcium sensor controlling fast synaptic transmission.* Neuron, 2003. **39**(2): p. 299-308.
21. Robinson, I.M., R. Ranjan, and T.L. Schwarz, *Synaptotagmins I and IV promote transmitter release independently of Ca(2+) binding in the C(2)A domain.* Nature, 2002. **418**(6895): p. 336-40.
22. Fernandez-Chacon, R., et al., *Structure/function analysis of Ca2+ binding to the C2A domain of synaptotagmin 1.* J Neurosci, 2002. **22**(19): p. 8438-46.
23. Davletov, B., O. Perisic, and R.L. Williams, *Calcium-dependent membrane penetration is a hallmark of the C2 domain of cytosolic phospholipase A2 whereas the C2A domain of synaptotagmin binds membranes electrostatically.* J Biol Chem, 1998. **273**(30): p. 19093-6.
24. Shao, X., et al., *Synaptotagmin-syntaxin interaction: the C2 domain as a Ca2+-dependent electrostatic switch.* Neuron, 1997. **18**(1): p. 133-42.
25. Murray, D. and B. Honig, *Electrostatic control of the membrane targeting of C2 domains.* Mol Cell, 2002. **9**(1): p. 145-54.
26. DiAntonio, A. and T.L. Schwarz, *The effect on synaptic physiology of synaptotagmin mutations in Drosophila.* Neuron, 1994. **12**(4): p. 909-20.
27. Loewen, C.A., J.M. Mackler, and N.E. Reist, *Drosophila synaptotagmin I null mutants survive to early adulthood.* Genesis, 2001. **31**(1): p. 30-6.
28. Xu, J., et al., *Synaptotagmin-1 functions as a Ca2+ sensor for spontaneous release.* Nat Neurosci, 2009. **12**(6): p. 759-66.
29. Liu, H., et al., *Autapses and networks of hippocampal neurons exhibit distinct synaptic transmission phenotypes in the absence of synaptotagmin I.* J Neurosci, 2009. **29**(23): p. 7395-403.
30. Yu, W. and R.F. Miller, *Hyperosmotic activation of transmitter release from presynaptic terminals onto retinal ganglion cells.* J Neurosci Methods, 1995. **62**(1-2): p. 159-68.
31. Stevens, C.F. and T. Tsujimoto, *Estimates for the pool size of releasable quanta at a single central synapse and for the time required to refill the pool.* Proc Natl Acad Sci U S A, 1995. **92**(3): p. 846-9.
32. Rosenmund, C. and C.F. Stevens, *Definition of the readily releasable pool of vesicles at hippocampal synapses.* Neuron, 1996. **16**(6): p. 1197-207.
33. Regehr, W.G., *Short-term presynaptic plasticity.* Cold Spring Harb Perspect Biol, 2012. **4**(7): p. a005702.
34. Chapman, E.R. and A.F. Davis, *Direct interaction of a Ca2+-binding loop of synaptotagmin with lipid bilayers.* J Biol Chem, 1998. **273**(22): p. 13995-4001.
35. Vermaas, J.V. and E. Tajkhorshid, *Differential Membrane Binding Mechanics of Synaptotagmin Isoforms Observed in Atomic Detail.* Biochemistry, 2017. **56**(1): p. 281-293.
36. Han, J., K. Pluhackova, and R.A. Böckmann, *The Multifaceted Role of SNARE Proteins in Membrane Fusion.* Front Physiol, 2017. **8**.
37. Gaffaney, J.D., R. Xue, and E.R. Chapman, *Mutations that disrupt Ca(2)(+)-binding activity endow Doc2beta with novel functional properties during synaptic transmission.* Mol Biol Cell, 2014. **25**(4): p. 481-94.

38. Lee, J. and J.T. Littleton, *Transmembrane tethering of synaptotagmin to synaptic vesicles controls multiple modes of neurotransmitter release.* Proc Natl Acad Sci U S A, 2015. **112**(12): p. 3793-8.
39. Shahrezaei, V. and K.R. Delaney, *Consequences of molecular-level Ca2+ channel and synaptic vesicle colocalization for the Ca2+ microdomain and neurotransmitter exocytosis: a monte carlo study.* Biophys J, 2004. **87**(4): p. 2352-64.
40. Yao, J., et al., *Doc2 is a Ca2+ sensor required for asynchronous neurotransmitter release.* Cell, 2011. **147**(3): p. 666-77.
41. Xue, R., J.D. Gaffaney, and E.R. Chapman, *Structural elements that underlie Doc2beta function during asynchronous synaptic transmission.* Proc Natl Acad Sci U S A, 2015. **112**(31): p. E4316-25.
42. Bacaj, T., et al., *Synaptotagmin-1 and synaptotagmin-7 trigger synchronous and asynchronous phases of neurotransmitter release.* Neuron, 2013. **80**(4): p. 947-59.
43. DiAntonio, A., et al., *Identification and characterization of Drosophila genes for synaptic vesicle proteins.* J Neurosci, 1993. **13**(11): p. 4924-35.
44. Bischof, J., et al., *An optimized transgenesis system for Drosophila using germ-line-specific phiC31 integrases.* Proc Natl Acad Sci U S A, 2007. **104**(9): p. 3312-7.
45. Brand, A.H. and N. Perrimon, *Targeted gene expression as a means of altering cell fates and generating dominant phenotypes.* Development, 1993. **118**(2): p. 401-15.
46. Yao, K.M. and K. White, *Neural specificity of elav expression: defining a Drosophila promoter for directing expression to the nervous system.* J Neurochem, 1994. **63**(1): p. 41-51.
47. DiAntonio, A., K.D. Parfitt, and T.L. Schwarz, *Synaptic transmission persists in synaptotagmin mutants of Drosophila.* Cell, 1993. **73**(7): p. 1281-90.
48. Feng, Y., A. Ueda, and C.F. Wu, *A modified minimal hemolymph-like solution, HL3.1, for physiological recordings at the neuromuscular junctions of normal and mutant Drosophila larvae.* J Neurogenet, 2004. **18**(2): p. 377-402.
49. Mackler, J.M. and N.E. Reist, *Mutations in the second C2 domain of synaptotagmin disrupt synaptic transmission at Drosophila neuromuscular junctions.* J Comp Neurol, 2001. **436**(1): p. 4-16.
50. Zhang, B. and B. Stewart, *Voltage-clamp analysis of synaptic transmission at the Drosophila larval neuromuscular junction.* Cold Spring Harb Protoc, 2010. **2010**(9): p. pdb.prot5488.

CHAPTER 3: HYDROPHOBIC RESIDUES IN SYNAPTOTAGMIN 1'S C_2A DOMAIN CLARIFY ITS ROLE IN ASYNCHRONOUS NEUROTRANSMITTER RELEASE[2]

3.1 Summary

Synaptotagmin 1 is the proposed Ca^{2+} sensor for fast, synchronous neurotransmitter release, but its role in asynchronous neurotransmitter release remains unclear. Until recently, the Ca^{2+}-binding C_2A domain of synaptotagmin was thought to regulate an asynchronous release sensor. However, a previously published point mutation that led to this hypothesis invited additional asynchronous release events as an artifact of the mutation. Recent studies report that Ca^{2+} binding in the C_2A domain of synaptotagmin in asynchronous release regulation is not needed. Instead, mutational artifacts from the original mutation may function as an asynchronous sensor. We investigated the side effects of the original mutation *in vivo* by introducing additional mutations that prevented C_2A interactions with the presynaptic membrane. These mutations prevented aberrant asynchronous events. We conclude that the original Ca^{2+} binding mutation is mimicking an asynchronous Ca^{2+} sensor, which supports the hypothesis that synaptotagmin's C_2A domain is not actively regulating an asynchronous sensor.

3.2 Introduction

Stimulation-dependent neurotransmitter (NT) release is divided into two temporally distinct phases. The first is a fast, synchronous neurotransmitter release that occurs within milliseconds (ms) of the stimulus. Synchronous release is dominant in the majority of synapses, and is the canonical release type typically described in textbooks. The second is a slower, more

[2] Authors: Mallory C Shields[1,2], Noreen E Reist

prolonged asynchronous phase of release. While most synapses exhibit little to no asynchronous release following a single action potential, it is still observed in many synapse types [1-10] and has implications in synaptic plasticity [11-14] and development [15, 16]. In some specialized synapses, such as specific interneurons of the hippocampus and brainstem, asynchronous release is predominant [8-10]. Both phases require Ca^{2+} sensors with different requisite characteristics.

It has long been established that synaptotagmin 1 is a Ca^{2+} sensor for fast, synchronous NT release. Synaptotagmin 1 is a low affinity Ca^{2+} sensor and exhibits fast binding and unbinding kinetics for Ca^{2+}. Therefore, upon a large influx of Ca^{2+}, synaptotagmin 1 can fully bind and unbind Ca^{2+} quickly and trigger fast, synchronous neurotransmitter release within ms.

Synaptotagmin 1 senses Ca^{2+} via its two Ca^{2+}-binding C_2 domains, C_2A and C_2B. These Ca^{2+}-binding domains contain 5 highly conserved negatively charged aspartate residues, resulting in a resting net negative charge of the binding pocket. Upon high [Ca^{2+}] entry into the cell, each C_2 domain binds Ca^{2+}. Ca^{2+} binding results in a net positive charge of the Ca^{2+}-binding pockets, which enhances interactions with the negatively charged presynaptic membrane and potentially *trans*-SNARE complexes [17-20]. Thus, Ca^{2+} binding allows synaptotagmin 1 to act as an “electrostatic switch” [21-24].

Switching from electrostatic repulsion to electrostatic attraction also permits two hydrophobic residues in each of synaptotagmin 1’s C_2 domains to escape the hydrophilic cytosol by penetrating into the hydrophobic core of the presynaptic membrane and encouraging fusion [18, 25] (Fig 3.1). When one of these hydrophobic residues was mutated in synaptotagmin’s C_2B domain, the result was embryonic lethal, reporting the most severe synaptotagmin phenotype *in vivo* to date [26]. Additionally, when the homologous hydrophobic residue in C_2A is mutated, a

50% knockdown of function was observed [26]. Therefore, hydrophobic residues found in synaptotagmin's C_2 domains are critical for efficient synchronous neurotransmission.

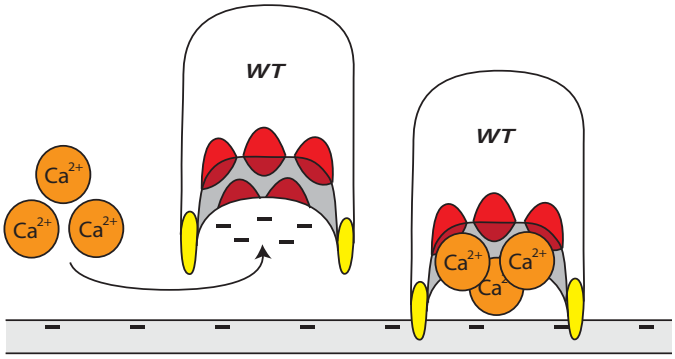

Fig 3.1. Synaptotagmin's C_2A Ca^{2+} binding and membrane penetrating pocket. Left, cartoon of synaptotagmin's C_2A domain, with 5 negatively charged essential aspartate residues (red) that repel the presynaptic membrane at rest and bind Ca^{2+} (orange) upon Ca^{2+} entry into the cell. Right, once bound, the pocket is neutralized, flipping the electrostatic switch to allow hydrophobic resides (yellow) to insert into the presynaptic membrane, favoring fusion.

Alternatively, asynchronous NT release requires a high affinity Ca^{2+} sensor with accompanying slower Ca^{2+} binding and unbinding kinetics. This allows fusion events to occur when [Ca^{2+}] is lower and lasts for 100's of ms. Synaptotagmin 1's role in asynchronous release remains elusive, because previous studies report contradictory results. It was originally postulated that the Ca^{2+} binding C_2A domain of synaptotagmin 1 was actively regulating asynchronous release. This hypothesis is referred to as the inhibition hypothesis. Initial studies resulted in increased asynchronous release in synaptotagmin knockouts [27-30]. Another study investigated the role of the C_2A domain in asynchronous release. In this study, Ca^{2+} binding by C_2A domain was blocked by mutating two C_2A negatively charged aspartates (D) to neutral asparagines (N), referred to as the *P[syt^{D-N}]* mutation [30]. This mutation exhibited increased asynchronous release and led to the hypothesis that synaptotagmin 1's C_2A domain actively regulated the asynchronous sensor.

More recent studies have uncovered inadvertent artifacts of the *P[syt$^{D\text{-}N}$]* mutation ([24] and Shields, unpublished). These studies utilized an alternative C_2A Ca^{2+} binding mutation that structurally blocked Ca^{2+} from binding C_2A while maintaining C_2A's inherently negative charge. These studies demonstrated that the *P[syt$^{D\text{-}N}$]* mutant mimicked Ca^{2+} binding by neutralizing the C_2A pocket [24, 31] and allowed more interaction with both SNARE complexes and the presynaptic membrane (Fig 3.2 left panel). The alternative mutation did not exhibit an increase in asynchronous release, providing evidence that Ca^{2+} binding in the C_2A domain is not necessary to regulate asynchronous NT release (Shields, unpublished). This is contradictory to the inhibition hypothesis.

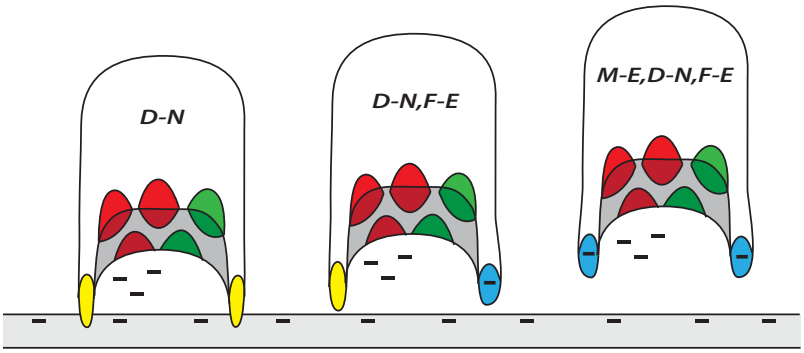

Fig 3.2. C_2A Ca^{2+} binding mutants with and without additional mutations to prevent membrane insertion. *Left*, the *P[syt$^{D\text{-}N}$]* mutation prevented Ca^{2+} binding by removing attractive negative charge to the C_2A pocket by mutating two of five negatively charged aspartate resides (red) to neutral asparagines (green). This partially neutralized the C_2A pocket, which allowed more presynaptic membrane interactions via two hydrophobic residues (yellow). *Middle*, the *P[syt$^{D\text{-}N,F\text{-}E}$]* mutation prevents additional membrane interactions by also mutating the hydrophobic phenylalanine residue (F) to a negatively charged glutamate (blue). *Right*, the *P[syt$^{M\text{-}E,D\text{-}N,F\text{-}E}$]* mutation mutates both membrane-penetrating hydrophobic residues to negatively charged glutamates.

As the *P[syt$^{D\text{-}N}$]* mutant acted as though Ca^{2+} was bound, which flipped the electrostatic switch, additional fusion events in response to Ca^{2+} influx over a longer time course could occur. This resulted in an apparent increase in synaptotagmin 1 Ca^{2+} sensitivity in the *P[syt$^{D\text{-}N}$]*

mutant, as previously reported [30, 31]. This mutation may not only have mimicked Ca^{2+} binding, it may also have mimicked an asynchronous Ca^{2+} sensor.

In this study we directly tested this possibility *in vivo* by generating *Drosophila* mutants that contained the original *P[syt$^{D\text{-}N}$]* mutations with additional hydrophobic residue mutations that prevented interactions with the presynaptic membrane. We generated the *P[syt$^{D\text{-}N}$]* mutation coupled to the previously studied hydrophobic mutation (*P[syt$^{D\text{-}N,F\text{-}E}$]*, Fig 3.2 middle panel). A second mutation with both hydrophobic C_2A membrane penetrating residues mutated to glutamates coupled to the original *P[syt$^{D\text{-}N}$]* mutation was also generated. This mutant is hereafter called *P[syt$^{M\text{-}E,D\text{-}N,F\text{-}E}$]* (Fig 3.2 right panel). Together, these new mutations are referred to as the hydrophobic mutants.

If the *P[syt$^{D\text{-}N}$]* mutation was mimicking the high-affinity asynchronous sensor (e.g., triggering asynchronous release), then preventing membrane interactions needed for triggering fusion events would prevent any aberrant increase in asynchronous release. Conversely, if the synaptotagmin *P[syt$^{D\text{-}N}$]* mutation was not acting as an asynchronous sensor, but was regulating the asynchronous sensor, consistent with the inhibition hypothesis, the increase in asynchronous release would remain. We found no changes to asynchronous release in either newly generated hydrophobic mutant, which supported the hypothesis that the original *P[syt$^{D\text{-}N}$]* was mimicking an asynchronous sensor. Further, our results contradict the inhibition hypothesis and support an alternative hypothesis regarding the role of synaptotagmin in asynchronous release.

3.3 Results

Transgenic synaptotagmin exhibits appropriate expression

We generated transgenic synaptotagmin (*syt*) transgenes and drove pan-neuronal expression of all *syt* transgenes in the syt^{null} background using the *elavGal4* promoter. These genotypes are hereby referred to as $P[syt^{WT}]$ (transgenic control), $P[syt^{D\text{-}N,F\text{-}E}]$ (original Ca^{2+}-binding mutation with one additional hydrophobic mutation that prevented presynaptic membrane interactions), and $P[syt^{M\text{-}E,D\text{-}N,F\text{-}E}]$ (original Ca^{2+}-binding mutation with both mutated hydrophobic residues). See methods for full genotypes. To verify comparable levels of protein expression between $P[syt^{WT}]$, $P[syt^{D\text{-}N,F\text{-}E}]$, and $P[syt^{M\text{-}E,D\text{-}N,F\text{-}E}]$, western analysis was performed on individual central nervous systems (CNSs) of third instar larvae. No significant changes in expression levels were determined for $P[syt^{WT}]$ (n = 21) and $P[syt^{D\text{-}N,F\text{-}E}]$ (n = 14) or $P[syt^{WT}]$ (n = 25) and $P[syt^{M\text{-}E,D\text{-}N,F\text{-}E}]$ (n = 19) (Fig 3.3A, $P[syt^{D\text{-}N,F\text{-}E}]$ was 126.3 % ± 13.5 % of control, p = 0.11, student t-test, and Fig 3.3B, $P[syt^{M\text{-}E,D\text{-}N,F\text{-}E}]$ was 119.6 % ± 9.9 % of control, p = 0.08, student t-test). Transgenic *syt* labeling at the neuromuscular junction in an otherwise syt^{null} background identified correct transgene localization (Fig 3.3C).

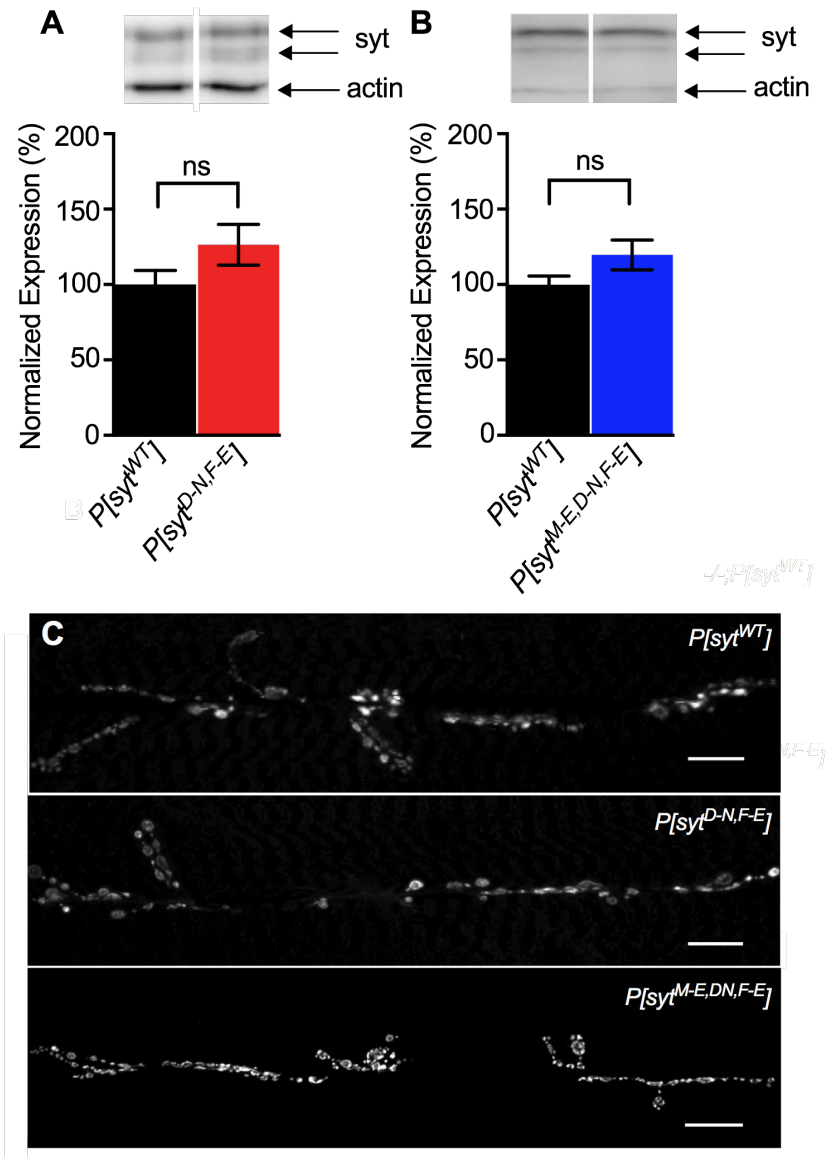

Fig 3.3. Transgenic synaptotagmin expression levels and localization. (A,B) *Above.* Representative blots showing synaptotagmin expression levels and actin loading control. (A) *Below,* western analysis exhibited similar synaptotagmin expression between *P[syt^{WT}]* (black, n = 21) and *P[syt$^{D\text{-}N,F\text{-}E}$]* (red, n = 14, p = 0.11, student t-test) (B) *Below,* western analysis quantification between *P[syt^{WT}]* (black, n = 25 and *P[syt$^{M\text{-}E,D\text{-}N,F\text{-}E}$]* (blue, n = 19, p = 0.08, student t-test) resulted in similar synaptotagmin expression levels. (C) Transgenic third instar larvae with antibodies against synaptotagmin localized at the neuromuscular junction. Scale bars represent 20 µm.

Spontaneous release frequency was increased in P[syt$^{D\text{-}N,F\text{-}E}$] mutants

A known role of *syt* 1 is to clamp stimulation-independent fusion events, or spontaneous miniature excitatory junction potentials (mEJPs), at a relatively low frequency. However, the *P[syt$^{D\text{-}N}$]* mutation mimicked Ca^{2+} binding and resulted in an increase in spontaneous events [24, 30, 31] (also Shields, unpublished). By preventing membrane interaction of synaptotagmin's C_2A domain, the *P[syt$^{D\text{-}N,F\text{-}E}$]* and *P[syt$^{M\text{-}E,D\text{-}N,F\text{-}E}$]* mutations may have clamped this mEJP frequency back to control frequency. Surprisingly, differences were determined between *P[syt^{WT}]* (mean mEJP frequency ± SEM for *P[syt^{WT}]* = 2.81 ± 0.43 Hz, n = 15) and *P[syt$^{D\text{-}N,F\text{-}E}$]* (Fig 3.4C, mean mEJP frequency ± SEM for *P[syt$^{D\text{-}N,F\text{-}E}$]* = 5.09 ± 0.40 Hz, n = 12, $p < 0.0001$, student t-test). However, there were no significant differences between *P[syt^{WT}]* (mean mEJP frequency ± SEM for *P[syt^{WT}]* = 2.72 ± 0.23 Hz, n = 9) and *P[syt$^{M\text{-}E,D\text{-}N,F\text{-}E}$]* (Fig 3.4E, mean mEJP frequency ± SEM for *P[syt$^{M\text{-}E,D\text{-}N,F\text{-}E}$]* = 3.26 ± 0.54 Hz, n = 10, $p = 0.39$, student t-test). Frequency was determined with manual counts of mEJP events for one consecutive minute during recordings. These results support the need for both hydrophobic residues to prevent the aberrant spontaneous release events introduced in the *P[syt$^{D\text{-}N}$]* mutation.

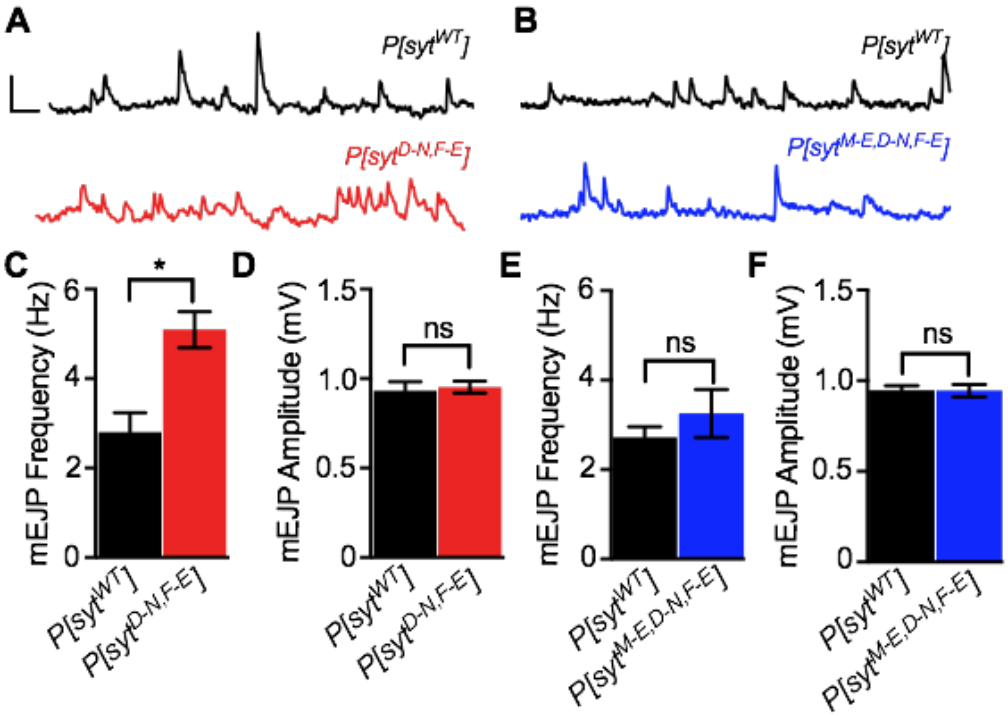

Fig 3.4. Spontaneous release frequency was increased in *P[syt$^{D\text{-}N,F\text{-}E}$]* mutants. (A) Representative mEJP traces of *P[syt^{WT}]* (black) and *P[syt$^{D\text{-}N,F\text{-}E}$]* (red). Scale bar represents 1 mV, 0.2 s. (B) Representative mEJP traces of (black) and *P[syt$^{M\text{-}E,D\text{-}N,F\text{-}E}$]* (blue). (C) Mean mEJP frequency was increased in *P[syt$^{D\text{-}N,F\text{-}E}$]* (n = 12) relative to control (n = 15, $p < 0.0001$, student t-test) (D) Mean mEJP amplitude was unchanged between *P[syt^{WT}]* (n = 9) and *P[syt$^{M\text{-}E,D\text{-}N,F\text{-}E}$]* (n = 10, p = 0.52, Mann-Whitney test). (E) Mean mEJP frequency was similar between *P[syt^{WT}]* and *P[syt$^{M\text{-}E,D\text{-}N,F\text{-}E}$]* (p = 0.39, student t-test). (F) Mean mEJP amplitude was unchanged between *P[syt^{WT}]* and *P[syt$^{M\text{-}E,D\text{-}N,F\text{-}E}$]* (p = 0.78, Mann-Whitney test). Error bars depict SEM.

Quantal size was unaffected

Each of these stimulation-independent events results from one vesicle fusing with the presynaptic membrane, and its response amplitude can be quantified as quantal size, which is sensitive to how much neurotransmitter has been loaded into an individual vesicle, as well as the makeup and density of postsynaptic receptors [32-36]. We calculated the mean amplitudes of individual mEJPs, and no significant changes were determined for any genotype (Fig 3.4D,F). Mean mEJP amplitude ± SEM for *P[syt^{WT}]* was 0.93 ± 0.05 mV (n = 100 mEJPs for 15 fibers)

when compared to *P[syt$^{D\text{-}N,F\text{-}E}$]*, whose mean mEJP amplitude ± SEM was 0.95 ± 0.03 mV (n =100 mEJPs for 12 fibers, p = 0.52, Mann-Whitney test). The mean mEJP amplitude ± SEM for *P[syt^{WT}]* was 0.95 ± 0.02 mV (n = 100 mEJPs for 9 fibers) when compared to *P[syt$^{M\text{-}E,D\text{-}N,F\text{-}E}$]*, whose mean mEJP ± SEM was 1.02 ± 0.05 mV (n = 100 mEJPs for 10 fibers, p = 0.78, Mann-Whitney test). Since quantal size was unchanged, we have no reason to conclude that either vesicle loading or postsynaptic receptor density was affected by these mutations.

Hydrophobic mutants exhibited significant decrease in synchronous release.

As the previously studid *P[syt$^{D\text{-}N}$]* mutation displayed no decrease in synchronous release [30] (also Shields, unpublished), and hydrophobic mutations exhibited significant decreases on synchronous release *in vivo* [26], we tested the effects of the additional hydrophobic mutations on evoked synchronous neurotransmitter release. We measured responses to single stimulations, or excitatory junction potentials (EJPs), at the larval neuromuscular junction. Unlike the *P[syt$^{D\text{-}N}$]* mutation alone, the addition of hydrophobic mutations significantly decreased neurotransmitter release (Fig 3.5B, $p < 0.0001$, ANOVA, $p < 0.0001$ for all comparisons to control, Dunnett's correction). The mean EJP ± SEM for *P[syt^{WT}]* was 29.18 ± 1.39 mV (n = 9) compared to 3.12 ± 0.44 mV and 2.15 ± 0.42 mV in *P[syt$^{D\text{-}N,F\text{-}E}$]* (n = 9) and *P[syt$^{M\text{-}E,D\text{-}N,F\text{-}E}$]* (n = 10) larvae, respectively. These ~90 % decreases in neurotransmitter release are the most severe *syt* C_2A mutations reported to date.

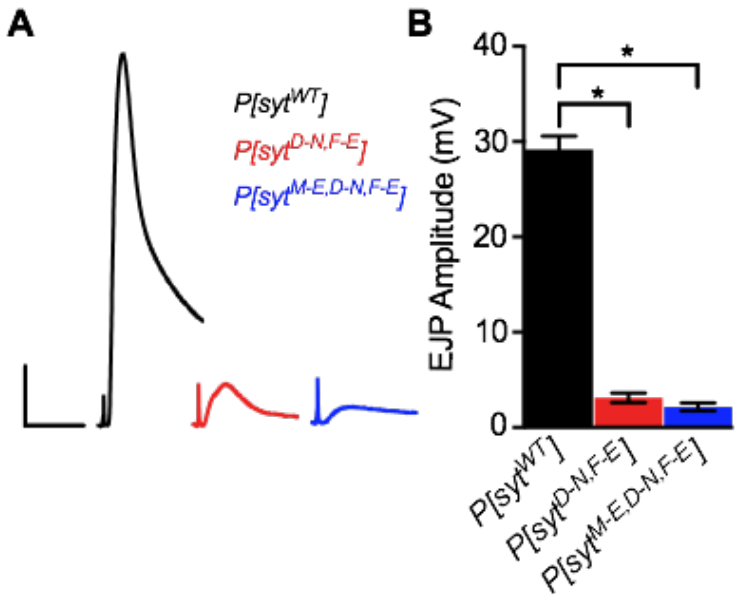

Fig 3.5. Hydrophobic mutations exhibited > 90% knockdown of synchronous release. (A) Representative EJP traces of *P[syt^{WT}]* (black), *P[syt$^{D\text{-}N,F\text{-}E}$]* (red), and *P[syt$^{M\text{-}E,D\text{-}N,F\text{-}E}$]* (blue). Scale bars represent 5 mV, 20 ms. (B) Compared to *P[syt^{WT}]* (n = 9 fibers), mean EJP amplitude was severely impacted in *P[syt$^{D\text{-}N,F\text{-}E}$]* (n = 9 fibers) and *P[syt$^{M\text{-}E,D\text{-}N,F\text{-}E}$]* (n = 10 fibers) ($p < 0.0001$, ANOVA, $p < 0.0001$ comparing *P[syt^{WT}]* to *P[syt$^{D\text{-}N,F\text{-}E}$]*and $p < 0.0001$ comparing *P[syt^{WT}]* to *P[syt$^{M\text{-}E,D\text{-}N,F\text{-}E}$]*, Dunnett's correction). Error bars depict SEM.

The size of the readily releasable pool was unchanged

A decrease in the size of the readily releasable pool could result in decreased NT release. Ringer made hypertonic with the addition of sucrose has been shown to stimulate a Ca^{2+}-independent form of release, which is implicated to correspond to the same pool of releasable vesicles as action-potential triggered release [37-39]. We triggered Ca^{2+}-independent fusion events using puff application of 0.3 M sucrose directly to third instar larval neuromuscular junctions in Ca^{2+}-free saline. During and after sucrose application, increases in mEJP frequency for all genotypes were observed relative to basal frequency (Fig 3.6A,B). As the *P[syt$^{D\text{-}N,F\text{-}E}$]* mutation resulted in increased mEJP frequency (Fig 3.4C), mEJP frequencies were normalized to mEJP frequency before sucrose application (Fig 3.6C). The increases relative to basal mEJP

frequency in all genotypes resulted in similar mEJP frequency increases during the sucrose response (p = 0.09, ANOVA). Normalized mean mEJP fold-change ± SEM for *P[syt^{WT}]* (n = 12) = 2.40 ± 0.16, *P[syt$^{D\text{-}N,F\text{-}E}$]* (n = 14) = 2.33 ± 0.13, and *P[syt$^{M\text{-}E,D\text{-}N,F\text{-}E}$]* (n = 13) = 2.74 ± 0.13). Both *P[syt$^{D\text{-}N,F\text{-}E}$]* and *P[syt$^{M\text{-}E,D\text{-}N,F\text{-}E}$]* mutants displayed similar increases to control during maximal sucrose response (Fig 3.6C, p = 0.99 comparing *P[syt^{WT}]* to *P[syt$^{D\text{-}N,F\text{-}E}$]* and p = 0.15 comparing *P[syt^{WT}]* to *P[syt$^{M\text{-}E,D\text{-}N,F\text{-}E}$]*, Dunnett's correction). These results cannot account for the severe deficits in evoked release.

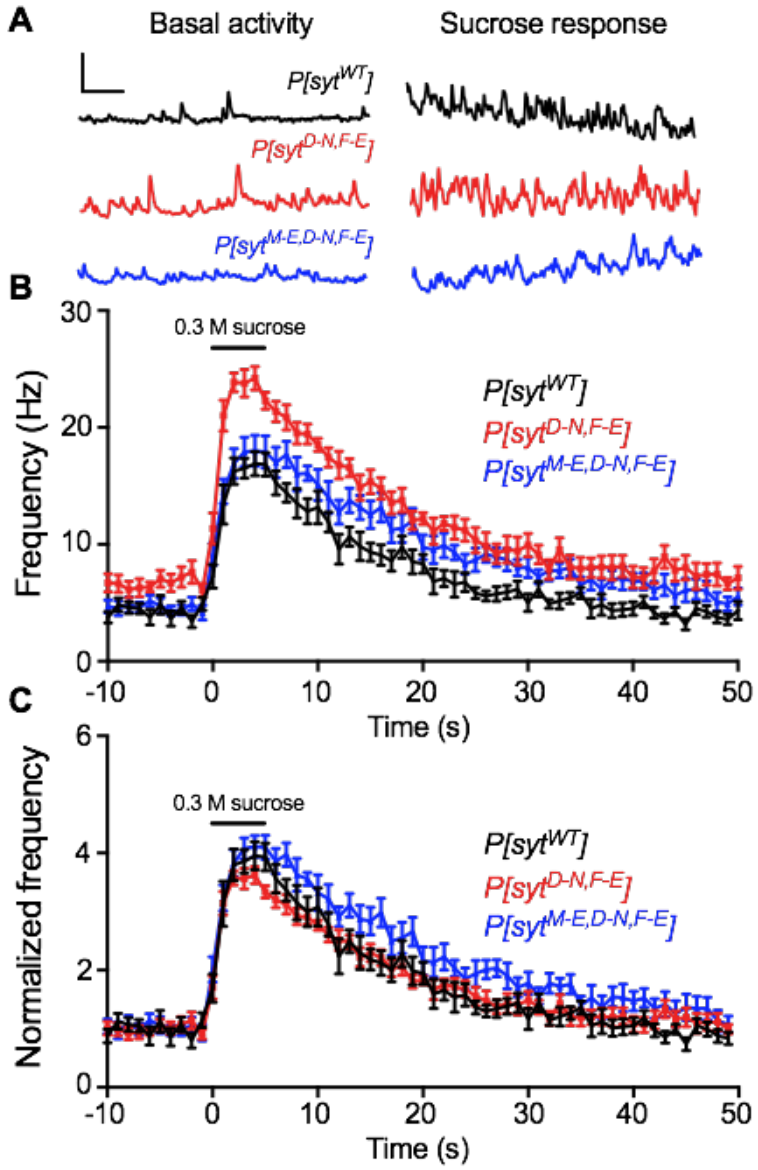

Fig 3.6. The readily releasable pool was unchanged. (A) Representative traces of event frequency before (left) and during sucrose-stimulated responses (right) for *P[syt^{WT}]* (black), *P[syt$^{D\text{-}N,F\text{-}E}$]* (red), and *P[syt$^{M\text{-}E,D\text{-}N,F\text{-}E}$]* (blue). Scale bar 2 mV, 0.4 s. (B) Plotted mEJP frequencies in response to a 5 s application of hypertonic sucrose. The black bar above the traces represents the sucrose application. (C) mEJP frequencies over time in response to sucrose application normalized to basal mEJP frequency. No statistically significant changes were determined between genotypes during sucrose response ($p = 0.09$, ANOVA).

Probability of release was decreased in hydrophobic mutants

A change in release probability could explain the decrease in evoked responses. Experiments in which two closely spaced stimuli are administered, or paired pulse experiments, are commonly used to moniter changes in release probabilities. The ratio of the second response to the first response is called the paired pulse ratio (PPR). PPR decreases as a result of increased release probability, and increases as a result of decreased release probability [31, 40]. Accordingly, we stimulated each fiber with 2 pulses at 20 ms interpulse intervals. We performed a paired pulse analysis in which paired pulse ratios between control (n = 13) and *P[syt$^{D\text{-}N,F\text{-}E}$]* (n = 12) were analyzed. Control (n = 12) and *P[syt$^{M\text{-}E,D\text{-}N,F\text{-}E}$]* (n = 13) mutants were also compared. The *P[syt$^{D\text{-}N,F\text{-}E}$]* mutation exhibits a significantly larger paired pulse ratio when compared to control (Fig 3.7B, mean paired pulse ratio ± SEM for *P[syt^{WT}]* = 1.09 ± 0.02 and *P[syt$^{D\text{-}N,F\text{-}E}$]* = 2.50 ± 0.30, $p < 0.0001$, student t-test). The *P[syt$^{M\text{-}E,D\text{-}N,F\text{-}E}$]* mutation also displayed a significantly larger paired pulse ratio than control (Fig 3.7D, mean paired pulse ratio ± SEM for *P[syt^{WT}]* = 1.08 ± 0.02, and mean paired pulse ratio ± SEM for *P[syt$^{M\text{-}E,D\text{-}N,F\text{-}E}$]* = 1.83 ± 0.10, $p < 0.0001$, student t-test). These significantly larger paired pulse ratios indicate decreased release probability. Therefore, the decreases in synchronous evoked transmission were not due to changes in the readily releasable pool (Fig 3.6C) or quantal size (Fig 3.4D,F), but instead resulted from decreased release probability.

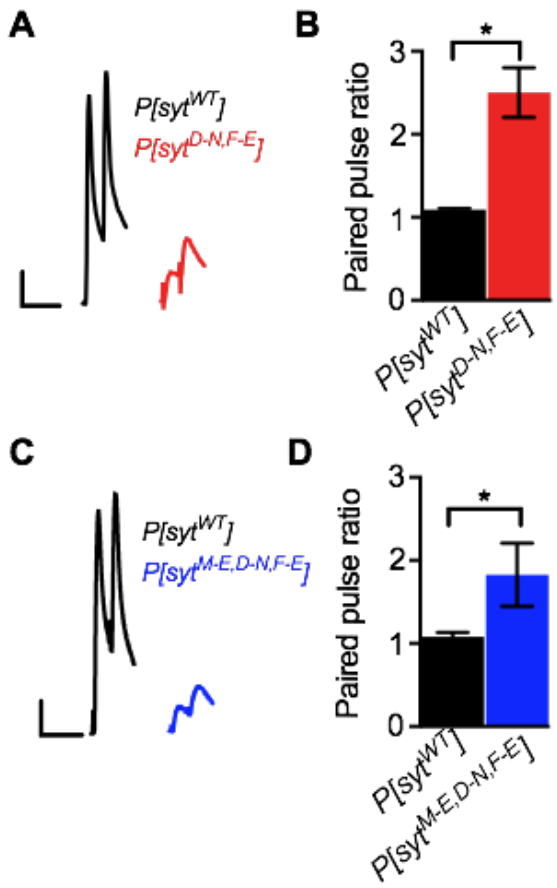

Fig 3.7. Release probability was decreased in hydrophobic mutants. (A) Representative traces between *P[syt^{WT}]* (black) and *P[syt$^{D\text{-}N,F\text{-}E}$]* (red) stimulated with a 20 ms interpulse interval. Scale bars represent 5 mV, 50 ms. (B) Paired pulse analysis indicated statistically different paired pulse ratios between control (n = 13) and *P[syt$^{D\text{-}N,F\text{-}E}$]* (n = 12, $p < 0.0001$, student t-test). Error bars are SEM. (C) Representative responses of *P[syt^{WT}]* (black) and *P[syt$^{M\text{-}E,D\text{-}N,F\text{-}E}$]* (blue) to paired pulse stimulations. Scale bars represent 5 mV, 50 ms. (D) Paired-pulse quantification between control (n = 12) and *P[syt$^{M\text{-}E,D\text{-}N,F\text{-}E}$]* (n = 13) indicated a significantly larger paired pulse ratio in *P[syt$^{M\text{-}E,D\text{-}N,F\text{-}E}$]* ($p < 0.0001$, student t-test). Error bars are SEM.

Asynchronous release was unaffected in hydrophobic mutants

Asynchronous release is thought to occur for ~300 ms at *Drosophila* neuromuscular junctions [30] (and Shields, unpublished). We assessed asynchronous release events using two electrode voltage clamp recordings, as it provides the temporal resolution current clamp cannot. We manually counted the number of individual mEJC events 300 ms before and 300 ms after each stimulation, and quantified the differences for each trace. These differences were summed,

and a ratio of after/before was determined. In this way, a general percentage could be attributed to asynchronous release. The synchronous release event upon stimulation was excluded. Control traces (n = 85) comparing asynchronous release to *P[syt$^{D\text{-}N,F\text{-}E}$]* mutants exhibited a 23% increase in post-stimulation events compared to pre-stimulation events, while the *P[syt$^{D\text{-}N,F\text{-}E}$]* mutation (n = 70) exhibited a 35% increase in events. Control traces (n = 75) comparing asynchronous release to *P[syt$^{M\text{-}E,D\text{-}N,F\text{-}E}$]* mutants exhibited a 29% increase, and *P[syt$^{M\text{-}E,D\text{-}N,F\text{-}E}$]* mutants (n = 80) exhibited a 23% increase.

To statistically analyze asynchronous events between genotypes, trace differences were compared. Mean differences between *P[syt^{WT}]* (n = 85, mean release event differences ± SEM = 0.21 ± 0.14 events) and *P[syt$^{D\text{-}N,F\text{-}E}$]* (n = 70, mean release event differences ± SEM = 0.7 ± 0.23 events) were not statistically different (Fig 3.9C, p = 0.14, Mann-Whitney). Mean differences of release events for *P[syt^{WT}]* (n = 75) are 0.13 ± 0.14 events, and mean differences for *P[syt$^{M\text{-}E,D\text{-}N,F\text{-}E}$]* (n = 80) were 0.28 ± 0.16 events. These genotypes were also not significantly different (Fig 3.9F, p = 0.92, Mann-Whitney). The addition of a second hydrophobic mutation in the *P[syt$^{M\text{-}E,D\text{-}N,F\text{-}E}$]* mutation seemed to prevent aberrant asynchronous release more completely, although this was not determined statistically. Therefore, preventing *syt* from membrane interactions returned asynchronous release to control levels. This supports the hypothesis that the *P[syt$^{D\text{-}N}$]* mutation was mimicking an asynchronous sensor, which created artifacts in release events in response to stimulation.

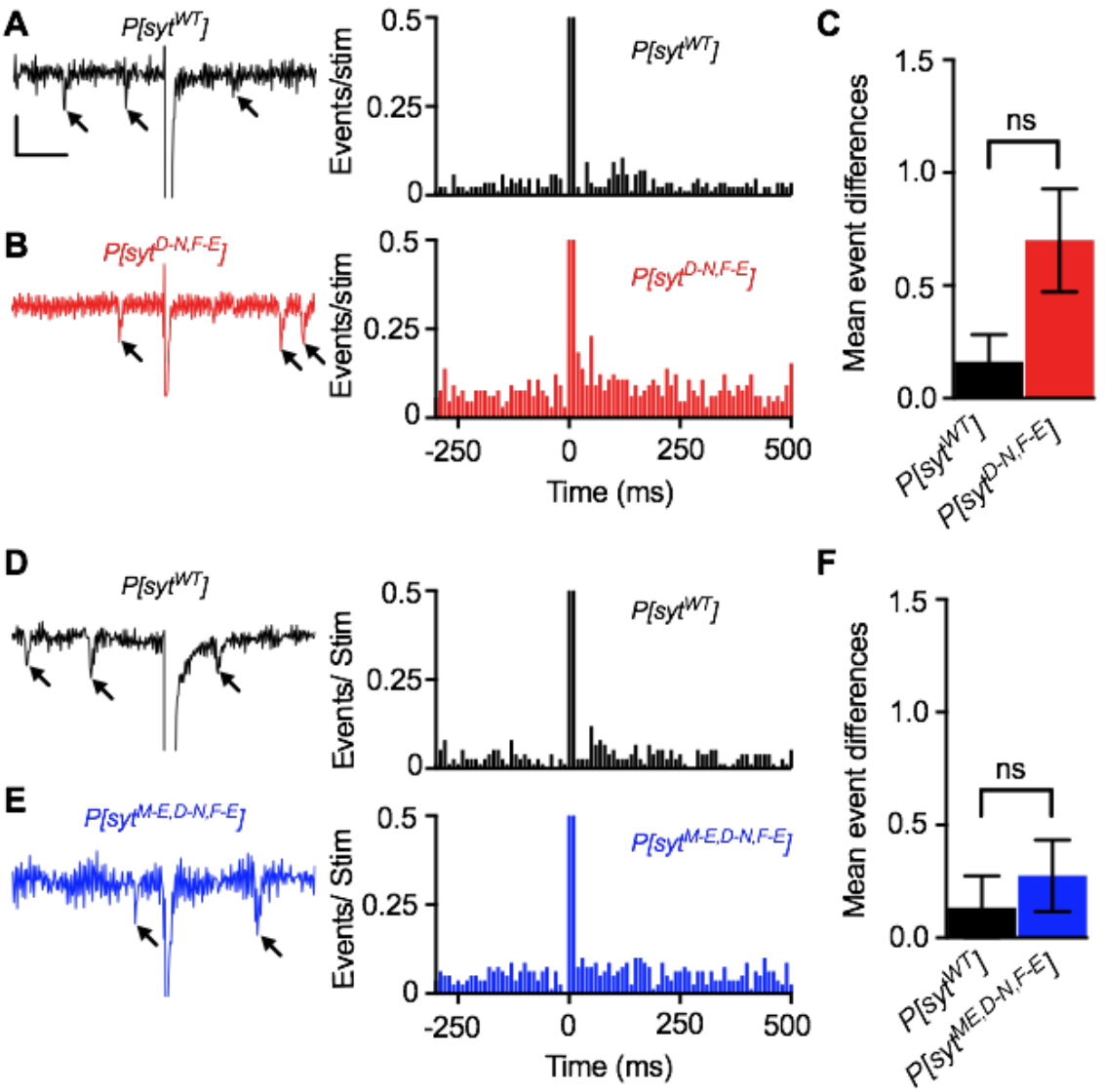

Fig 3.9. Hydrophobic mutations did not alter asynchronous neurotransmitter release. (A-B) *Left*, representative voltage traces for *P[syt^{WT}]* (black) and *P[syt$^{D-N,F-E}$]* (red) exhibiting events both 300 ms before and after single stimulations. Small arrows represent individual events. Scale bars represent 0.5 nA, 0.1 s. *Right*, latencies of mEJCs 0.3 s before and 0.5 s after single stimulations. Each mEJC was categorized into a 10 ms bin. (C) Quantification of mean event differences, or asynchronous release, between *P[syt^{WT}]* (n = 85) and *P[syt$^{D-N,F-E}$]* (n = 70). No significant change was determined between genotypes (p = 0.14, Mann-Whitney). (D-E) *Left*, representative voltage traces for *P[syt^{WT}]* (black) and *P[syt$^{M-E,D-N,F-E}$]* (blue,) exhibiting events 300 ms before and after stimulation. Small arrows represent individual events. *Right*, latencies of mEJCs 0.3 s before and 0.5 s after single stimulations. Each mEJC was categorized into 10 ms bins. Each bin was presented as the number of events/stimulation. (F) Quantification of mean event differences between *P[syt^{WT}]* (n = 75) and *P[syt$^{M-E,D-N,F-E}$]* (n = 80) determined no significant difference between genotypes (p = 0.92, Mann-Whitney).

3.4 Discussion

Here we showed that a previously published mutant introduced asynchronous release artifacts by mimicking an active asynchronous release Ca^{2+} sensor. We accomplished this by adding additional hydrophobic mutations to the previously published mutation, thus preventing presynaptic membrane interactions. If synaptotagmin's C_2A domain was regulating an asynchronous sensor, these mutations would not have affected the increase in asynchronous release seen in the *P[syt$^{D\text{-}N}$]* mutant. However, we reported no increase in asynchronous release events, providing further evidence that synaptotagmin's C_2A domain is not needed to regulate an asynchronous Ca^{2+} sensor.

These newly constructed hydrophobic mutations expressed appropriately to the neuromuscular junction and exhibited similar protein expression to control. The *P[syt$^{D\text{-}N,F\text{-}E}$]* mutation exhibited an increase in mEJP frequency, suggesting interference with only one hydrophobic residue was not sufficient to clamp the increase in mEJP frequency seen in the *P[syt$^{D\text{-}N}$]* mutation alone. However, with interference of both C_2A domain hydrophobic residues in the *P[syt$^{M\text{-}E,D\text{-}N,F\text{-}E}$]* mutation, we reported mEJP frequency similar to control. Therefore, the interference of both hydrophobic residues were sufficient to re-clamp mEJP frequency induced by the *P[syt$^{D\text{-}N}$]* mutation. Evoked events resulted in a > 90% knockdown of function in the hydrophobic mutants. These are the most severe synaptotagmin C_2A mutations reported to date. We conclude that these deficits were due to release probability and not the size of the readily releasable pool or quantal size. Moreover, asynchronous release events were not increased in either the *P[syt$^{D\text{-}N,F\text{-}E}$]* mutant or the *P[syt$^{M\text{-}E,D\text{-}N,F\text{-}E}$]* mutant. Together, these results are inconsistent with the inhibition hypothesis.

If synaptotagmin 1's C_2A domain is not actively regulating an asynchronous sensor, another mechanism must be present to explain the interplay between synaptotagmin knockouts, mutations, and the resultant changes in asynchronous release. One simple explanation may be due to a competition for space between synaptotagmin and the asynchronous Ca^{2+} sensor. This competition hypothesis can explain why synaptotagmin 1 null synapses exhibited increased asynchronous release increases. Here, a lack of competition would allow the asynchronous sensor more access to Ca^{2+} and result in increased asynchronous release.

The competition hypothesis is supported by other studies in which researchers used alternative synaptotagmin C_2A Ca^{2+} binding mutants where they reported no increase in asynchronous release (Shields, unpublished). Synaptotagmin was still present at the active zone and Ca^{2+} binding in C_2A was disabled; yet no increase in asynchronous response. Finally, the present study shows that the *P[syt$^{D\text{-}N}$]* mutation was actually mimicking an asynchronous Ca^{2+} sensor. Therefore, although synaptotagmin was still present, the increased asynchronous release could be explained by artifacts of the *P[syt$^{D\text{-}N}$]* synaptotagmin mutant.

3.5 Conclusion

This study investigates a previously studied Ca^{2+}-binding mutant in synaptotagmin 1's C_2A domain and provides evidence that it mimics an asynchronous sensor due to a mutational artifact. This work supports an alternative hypothesis regarding synaptotagmin 1's affect on asynchronous neurotransmitter release. By introducing additional mutations that prevent interactions with the presynaptic membrane, we showed these new mutants clamp the previously reported increase in asynchronous release. More investigation into this interplay is needed, as there is obvious discord on this mechanism.

3.6 Materials and methods

Drosophila Genotypes

The UAS/Gal4 system was used to drive neuronal expression of our *syt 1* transgenes [41, 42]. The UAS promoter provides strong expression of our *syt* transgenes in any cell expressing galactosidase-4 (Gal4). Expression was localized specifically to the nervous system using the *elav* promoter to drive Gal4 expression, and hence *syt* transgene expression, in all neurons. To assess the functional significance of the mutation, all transgenes were expressed in the absence of endogenous synaptotagmin expression using the syt^{null} mutation, syt^{AD4} [43]. The genotypes of experimental larvae were the following: *yw;* syt^{null}*elavGal4/*syt^{null}*;* $P[UASsyt^{WT}]$/+ line 1 (transgenic control, referred to as $P[syt^{WT}]$), *yw;* syt^{null}*elavGal4/*syt^{null}*;* $P[UASsyt^{D280,282N,F284E}]$/+ (referred to as $P[syt^{D\text{-}N,F\text{-}E}]$), and *yw;* syt^{null}*elavGal4/*syt^{null}*;* $P[UASsyt^{M222E,D280,282N,F284E}]$/+ (referred to as $P[syt^{M\text{-}E,D\text{-}N,F\text{-}E}]$)

Transgenic creation

cDNA of the *Drosophila* wild type *syt1* gene [44], flanked by 5' EcoRI and 3' BgLII restriction sites, was synthesized by GeneWiz (South Plainfield, New Jersey). GeneWiz synthesized cDNA for both hydrophobic mutations, as well. The transgenes were placed under the control of the UAS promoter by directional subcloning of the synthesized cDNA into the pUAST-attB vector using these unique restriction sites. The mutant transgenes were inserted in the attP2 landing site in *Drosophila* using the PhiC31 targeted insertion system [45] at BestGene (Chino Hills, CA).

Immunoblotting

Western analysis on individual larval CNS's was used to determine levels of synaptotagmin relative to an actin loading control. Third instar larval CNSs were dissected in HL3.1 saline (70 mM NaCl, 5 mM KCl, 4 mM $MgCl_2$, 10 mM $NaHCO_3$, 5 mM Trehalose, 115 mM sucrose, 5 mM HEPES, pH 7.2 [46]: Individual CNSs were sonified for 5 pulses using a Branson Sonifier 450 (VWR Scientific, Winchester, PA) in Laemmli buffer (Bio-Rad, Hercules, CA) containing 5% B-mercaptoethanol. Each sample was electrophoresed, transferred to Immobilon membranes (Millipore, Bedford, MA), and washed in blocking solution as previously described [47]. Membranes were probed with a 1:2500 dilution of anti-s*yt* antibody, Dsyt-CL1 [48] and 1:10,000 dilution of anti-actin antibody, MAB 1501 (Millipore Bioscience Research Reagents, Billerica, MA), overnight at 4 degrees. An Epichemi^3 Darkroom and Labworks Imaging Software (UVP BioImaging, Upland, CA) were used to visualize the protein bands. Quantification of blots: *syt*:actin ratios were calculated normalized to the mean *syt*:actin ratios of control lanes for each blot to compare *syt* signals between blots. Outliers in actin levels were excluded from the analysis. Statistical significance was determined using a one-way ANOVA using Prism 7.

Immunolabeling

To visualize transgenic synaptotagmin at the larval neuromuscular junction, third instar larvae were dissected in HL3.1 saline and fixed in phosphate-buffered saline (PBS, 137 mM NaCl, 1.5 mM KH_2PO_4, 2.7 mM KCl, 8.1 mM Na_2HPO_4) containing 4% formaldehyde for 1 hour. Samples were probed overnight in a 1:400 dilution of D*syt*-CL1 in dilution media [PBS with 0.1% Triton, 1% bovine serum albumin (Millipore-Sigma, Burlington, MA) and 1% normal

goat serum (Fitzgerald Industries International, Acton, MA). The next day, the whole mounts were washed in PBS with 0.1% Triton for 1-3 hours, then incubated in dilution media containing a 1:400 dilution of Alexa Fluor 488 goat anti-rabbit antibody (Invitrogen, Carlsbad, CA) for 1 hour at room temperature. Labeled samples were washed in PBS with 0.1% Triton for one additional hour, and mounted on microscope slides in Citifluor (Ted Pella, Redding, CA). Images of neuromuscular junctions of muscle 6/7 in segments 3 and 4 were acquired using a Zeiss 880 light scanning microscope using a 40X objective with Zeiss Zen 2.1 acquisition software, version 11,0,3,190.

Electrophysiological experiments and analyses

All electrophysiological events were collected using an Axoclamp 2B amplifier (Molecular Devices, Sunnyvale, CA), digitized using a Powerlab 4/35 A/D converter (ADInstuments, Sydney, Australia) and recorded in LabChart software (ADInstruments, Sydney, Australia). Intracellular electrodes were pulled using a (Cite puller) to 10-20 MOhms and filled with 3 parts 2 M Kcitrate to 1 part 3 M KCl. Third instar larvae were dissected in HL3.1 saline to expose the body wall and to remove the CNS. Recordings were made from muscle 6 of abdominal segments 3 and 4, and held at -55 mV using up to 1 nA of current. All electrophysiological statistical analyses were calculated using Prism 7 software.

Single EJPs were evoked from in HL3.1 saline containing 1.0 mM Ca^{2+} as previously described [26, 47, 49]. A stimulating electrode was filled with bath solution to directly stimulate the motor nerve innervating the muscle fiber. Averages of 10 EJPs collected at 0.04 Hz were calculated for each fiber. Statistical significance was determined using student t-tests.

Miniature excitatory junction events were acquired for 3 minutes in HL3.1 saline. Events were identified manually after recordings had been randomized and blinded to the researcher for analysis. To determine mEPSP frequency, total events in each fiber were counted for 1 consecutive minute, using consistent time periods from each fiber. Statistical significance for mEJP frequency was determined using student t-tests. Mean mEJP amplitudes were determined from 100 consecutive events/fiber, taken from consistent time periods from each recording to eliminate bias. Statistical significance was determined using Mann-Whitney tests. All recordings were randomized and blinded to the researcher for analysis

For paired pulse experiments, a stimulating electrode was filled with bath solution (HL3.1 saline with 1.0 mM Ca^{2+}) to directly stimulate the motor nerve innervating the muscle fiber. Stimulations were given using a 0.02 s delay between stimulations, and paired pulse ratios were determined by dividing the EJP amplitude of the second stimulation by the amplitude of the first stimulation. Genotype means of the paired pulse ratios were compared using student t-tests.

For hypertonic stimulations, a puff application of modified HL3.1 saline containing 0.3 M sucrose was administered to the junctional region of muscles 6/7 in abdominal segments 3 and 4 of third instars. The puff application was administered for 5 s at ~5 pounds per square inch. Hypertonic stimulation recordings were acquired in a bath solution of Ca^{2+}-free HL3.1 saline. All recordings were randomized and blinded to the researcher for analysis. Frequency of mEJP events were counted manually into 1 s bins for 60 s, with 10 s prior to sucrose application to determine a baseline mEJP frequency, and 50 s to determine each genotype's response to the sucrose up to one minute after puff application. To determine average mEJP frequency during sucrose response, 30 s of mEJP events were averaged during the sucrose response, beginning at

the initiation of the sucrose application. Statistical significance was determined using a one-way ANOVA.

Synaptic currents were recorded using two-electrode voltage clamp as described [50]. Recordings were acquired in HL3.1 saline containing 1.0 mM Ca^{2+}. An additional intracellular electrode was pulled with Sutter model P-97'' to 10-15 MOhm resistance. Upon both intracellular electrodes' insertions, recordings with muscle input resistances < 5 MOhms were excluded. Fibers were voltage clamped to -55 mV using no more than 1 nA of current and stimulated at 0.2 Hz for 5 stimulations. Rise time constants were quantified by determining rise time (time from beginning of current response to peak current response), and then determining the time in which the current had reached 63.2% of its max value. Decay time constants were determined by determining decay time (the time from peak current response back to baseline), and then determining the time for the decay current to decay 63.2% of its peak response. Traces that failed to respond to stimulation were not analyzed for release kinetics. Student t-tests were used to determine significance. Latency analysis was acquired by manually binning each mEJC event into 10 ms bins and presented as the number of events/stimulation for each bin. Statistical analyses for asynchronous release events were determined by calculating the differences in mEJC frequency 300 ms before and after stimulation for each individual stimulation (# events after stimulation - # events prior to stimulation). The synchronous responses found in the first 2 10 ms bins were not included in the asynchronous analysis. These differences were averaged per genotype and a Mann-Whitney was used to determine statistical significance between genotypes.

WORKS CITED

1. Chirwa, S.S. and B.R. Sastry, *Asynchronous synaptic responses in hippocampal CA1 neurons during synaptic long-term potentiation.* Neurosci Lett, 1988. **89**(3): p. 355-60.
2. Goda, Y. and C.F. Stevens, *Two components of transmitter release at a central synapse.* Proc Natl Acad Sci U S A, 1994. **91**(26): p. 12942-6.
3. Atluri, P.P. and W.G. Regehr, *Delayed release of neurotransmitter from cerebellar granule cells.* J Neurosci, 1998. **18**(20): p. 8214-27.
4. Yawo, H., *Two components of transmitter release from the chick ciliary presynaptic terminal and their regulation by protein kinase C.* J Physiol, 1999. **516 (Pt 2)**: p. 461-70.
5. Lu, T. and L.O. Trussell, *Inhibitory transmission mediated by asynchronous transmitter release.* Neuron, 2000. **26**(3): p. 683-94.
6. Hagler, D.J., Jr. and Y. Goda, *Properties of synchronous and asynchronous release during pulse train depression in cultured hippocampal neurons.* J Neurophysiol, 2001. **85**(6): p. 2324-34.
7. Kirischuk, S. and R. Grantyn, *Intraterminal Ca2+ concentration and asynchronous transmitter release at single GABAergic boutons in rat collicular cultures.* J Physiol, 2003. **548**(Pt 3): p. 753-64.
8. Hefft, S. and P. Jonas, *Asynchronous GABA release generates long-lasting inhibition at a hippocampal interneuron-principal neuron synapse.* Nat Neurosci, 2005. **8**(10): p. 1319-28.
9. Best, A.R. and W.G. Regehr, *Inhibitory regulation of electrically coupled neurons in the inferior olive is mediated by asynchronous release of GABA.* Neuron, 2009. **62**(4): p. 555-65.
10. Daw, M.I., et al., *Asynchronous transmitter release from cholecystokinin-containing inhibitory interneurons is widespread and target-cell independent.* J Neurosci, 2009. **29**(36): p. 11112-22.
11. Aghajanian, G.K. and G.J. Marek, *Serotonin, via 5-HT2A receptors, increases EPSCs in layer V pyramidal cells of prefrontal cortex by an asynchronous mode of glutamate release.* Brain Res, 1999. **825**(1-2): p. 161-71.
12. Hjelmstad, G.O., *Interactions between asynchronous release and short-term plasticity in the nucleus accumbens slice.* J Neurophysiol, 2006. **95**(3): p. 2020-3.
13. Iremonger, K.J. and J.S. Bains, *Integration of asynchronously released quanta prolongs the postsynaptic spike window.* J Neurosci, 2007. **27**(25): p. 6684-91.
14. Volman, V. and R.C. Gerkin, *Synaptic scaling stabilizes persistent activity driven by asynchronous neurotransmitter release.* Neural Comput, 2011. **23**(4): p. 927-57.
15. Jensen, K., et al., *Developmental increase in asynchronous GABA release in cultured hippocampal neurons.* Neuroscience, 2000. **101**(3): p. 581-8.
16. Kiyosue, K., E. Shimabayashi, and T. Taguchi, *Development of two transmitter release components during the critical period for imprinting in the chick IMHV.* Eur J Neurosci, 2002. **16**(8): p. 1587-92.
17. Chapman, E.R., et al., *Ca2+ regulates the interaction between synaptotagmin and syntaxin 1.* J Biol Chem, 1995. **270**(40): p. 23667-71.

18. Chapman, E.R. and A.F. Davis, *Direct interaction of a Ca2+-binding loop of synaptotagmin with lipid bilayers.* J Biol Chem, 1998. **273**(22): p. 13995-4001.
19. Bai, J., P. Wang, and E.R. Chapman, *C2A activates a cryptic Ca(2+)-triggered membrane penetration activity within the C2B domain of synaptotagmin I.* Proc Natl Acad Sci U S A, 2002. **99**(3): p. 1665-70.
20. Zhang, X., et al., *Ca2+-dependent synaptotagmin binding to SNAP-25 is essential for Ca2+-triggered exocytosis.* Neuron, 2002. **34**(4): p. 599-611.
21. Davletov, B., O. Perisic, and R.L. Williams, *Calcium-dependent membrane penetration is a hallmark of the C2 domain of cytosolic phospholipase A2 whereas the C2A domain of synaptotagmin binds membranes electrostatically.* J Biol Chem, 1998. **273**(30): p. 19093-6.
22. Ubach, J., et al., *Ca2+ binding to synaptotagmin: how many Ca2+ ions bind to the tip of a C2-domain?* Embo j, 1998. **17**(14): p. 3921-30.
23. Murray, D. and B. Honig, *Electrostatic control of the membrane targeting of C2 domains.* Mol Cell, 2002. **9**(1): p. 145-54.
24. Striegel, A.R., et al., *Calcium binding by synaptotagmin's C2A domain is an essential element of the electrostatic switch that triggers synchronous synaptic transmission.* J Neurosci, 2012. **32**(4): p. 1253-60.
25. Vermaas, J.V. and E. Tajkhorshid, *Differential Membrane Binding Mechanics of Synaptotagmin Isoforms Observed in Atomic Detail.* Biochemistry, 2017. **56**(1): p. 281-293.
26. Paddock, B.E., et al., *Membrane penetration by synaptotagmin is required for coupling calcium binding to vesicle fusion in vivo.* J Neurosci, 2011. **31**(6): p. 2248-57.
27. Nishiki, T. and G.J. Augustine, *Synaptotagmin I synchronizes transmitter release in mouse hippocampal neurons.* J Neurosci, 2004. **24**(27): p. 6127-32.
28. Broadie, K., et al., *Absence of synaptotagmin disrupts excitation-secretion coupling during synaptic transmission.* Proc Natl Acad Sci U S A, 1994. **91**(22): p. 10727-31.
29. Geppert, M., et al., *Synaptotagmin I: a major Ca2+ sensor for transmitter release at a central synapse.* Cell, 1994. **79**(4): p. 717-27.
30. Yoshihara, M., Z. Guan, and J.T. Littleton, *Differential regulation of synchronous versus asynchronous neurotransmitter release by the C2 domains of synaptotagmin 1.* Proc Natl Acad Sci U S A, 2010. **107**(33): p. 14869-74.
31. Stevens, C.F. and J.M. Sullivan, *The synaptotagmin C2A domain is part of the calcium sensor controlling fast synaptic transmission.* Neuron, 2003. **39**(2): p. 299-308.
32. Davis, G.W., et al., *Postsynaptic PKA controls quantal size and reveals a retrograde signal that regulates presynaptic transmitter release in Drosophila.* Neuron, 1998. **20**(2): p. 305-15.
33. DiAntonio, A., et al., *Glutamate receptor expression regulates quantal size and quantal content at the Drosophila neuromuscular junction.* J Neurosci, 1999. **19**(8): p. 3023-32.
34. Lim, R., F.J. Alvarez, and B. Walmsley, *Quantal size is correlated with receptor cluster area at glycinergic synapses in the rat brainstem.* J Physiol, 1999. **516 (Pt 2)**: p. 505-12.
35. Edwards, R.H., *The neurotransmitter cycle and quantal size.* Neuron, 2007. **55**(6): p. 835-58.
36. Takamori, S., *Presynaptic Molecular Determinants of Quantal Size.* Front Synaptic Neurosci, 2016. **8**.

37. Yu, W. and R.F. Miller, *Hyperosmotic activation of transmitter release from presynaptic terminals onto retinal ganglion cells.* J Neurosci Methods, 1995. **62**(1-2): p. 159-68.
38. Stevens, C.F. and T. Tsujimoto, *Estimates for the pool size of releasable quanta at a single central synapse and for the time required to refill the pool.* Proc Natl Acad Sci U S A, 1995. **92**(3): p. 846-9.
39. Rosenmund, C. and C.F. Stevens, *Definition of the readily releasable pool of vesicles at hippocampal synapses.* Neuron, 1996. **16**(6): p. 1197-207.
40. Zucker, R.S. and W.G. Regehr, *Short-term synaptic plasticity.* Annu Rev Physiol, 2002. **64**: p. 355-405.
41. Brand, A.H. and N. Perrimon, *Targeted gene expression as a means of altering cell fates and generating dominant phenotypes.* Development, 1993. **118**(2): p. 401-15.
42. Yao, K.M. and K. White, *Neural specificity of elav expression: defining a Drosophila promoter for directing expression to the nervous system.* J Neurochem, 1994. **63**(1): p. 41-51.
43. DiAntonio, A., K.D. Parfitt, and T.L. Schwarz, *Synaptic transmission persists in synaptotagmin mutants of Drosophila.* Cell, 1993. **73**(7): p. 1281-90.
44. DiAntonio, A., et al., *Identification and characterization of Drosophila genes for synaptic vesicle proteins.* J Neurosci, 1993. **13**(11): p. 4924-35.
45. Bischof, J., et al., *An optimized transgenesis system for Drosophila using germ-line-specific phiC31 integrases.* Proc Natl Acad Sci U S A, 2007. **104**(9): p. 3312-7.
46. Feng, Y., A. Ueda, and C.F. Wu, *A modified minimal hemolymph-like solution, HL3.1, for physiological recordings at the neuromuscular junctions of normal and mutant Drosophila larvae.* J Neurogenet, 2004. **18**(2): p. 377-402.
47. Mackler, J.M. and N.E. Reist, *Mutations in the second C2 domain of synaptotagmin disrupt synaptic transmission at Drosophila neuromuscular junctions.* J Comp Neurol, 2001. **436**(1): p. 4-16.
48. Mackler, J.M., et al., *The C(2)B Ca(2+)-binding motif of synaptotagmin is required for synaptic transmission in vivo.* Nature, 2002. **418**(6895): p. 340-4.
49. Loewen, C.A., J.M. Mackler, and N.E. Reist, *Drosophila synaptotagmin I null mutants survive to early adulthood.* Genesis, 2001. **31**(1): p. 30-6.
50. Zhang, B. and B. Stewart, *Voltage-clamp analysis of synaptic transmission at the Drosophila larval neuromuscular junction.* Cold Spring Harb Protoc, 2010. **2010**(9): p. pdb.prot5488.

CHAPTER 4: *DROSOPHILA* STUDIES SUPPORT A ROLE FOR A PRESYNAPTIC SYNAPTOTAGMIN MUTATION IN A HUMAN CONGENITAL MYASTHENIC SYNDROME[3]

4. 1 Summary

During chemical transmission, the function of synaptic proteins must be coordinated to efficiently release neurotransmitter. Synaptotagmin 2, the Ca^{2+} sensor for fast, synchronized neurotransmitter release at the human neuromuscular junction, has recently been implicated in a dominantly inherited congenital myasthenic syndrome associated with a non-progressive motor neuropathy. In one family, a proline residue within the C_2B Ca^{2+}-binding pocket of synaptotagmin is replaced by a leucine. The functional significance of this residue has not been investigated previously. Here we show that *in silico* modeling predicts disruption of the C_2B Ca^{2+}-binding pocket, and we examine the *in vivo* effects of the homologous mutation in *Drosophila.* When expressed in the absence of native synaptotagmin, this mutation is lethal, demonstrating for the first time that this residue plays a critical role in synaptotagmin function. To achieve expression similar to human patients, the mutation is expressed in flies carrying one copy of the wild type *synaptotagmin* gene. We now show that *Drosophila* carrying this mutation developed neurological and behavioral manifestations similar to those of human patients and provide insight into the mechanisms underlying these deficits. Our *Drosophila* studies support a role for this synaptotagmin point mutation in disease etiology.

---

 1. Shields, M.C., et al., *Drosophila studies support a role for a presynaptic synaptotagmin mutation in a human congenital myasthenic syndrome.* PLoS One, 2017. **12**(9): p. e0184817..

4.2 Introduction

Understanding the mechanisms mediating information transmission across a chemical synapse is essential to understanding brain function. During synaptic transmission, membranous vesicles filled with neurotransmitter must fuse with the presynaptic membrane in response to Ca^{2+} influx, thereby releasing the transmitter into the synaptic cleft. The synaptic vesicle protein, synaptotagmin, is essential for this release [2-4] as it binds the Ca^{2+} that triggers vesicle fusion [5-7]. Synaptotagmin has two Ca^{2+}-binding pockets, C_2A and C_2B [8-10], which have both been extensively studied for their role in synchronizing vesicle fusion *in vivo* [5, 7, 11-13] and in culture [14, 15]. Synaptotagmin 2 is the predominant isoform found at mammalian neuromuscular junctions [16, 17], and until recently, has never been linked to disease. However, whole-exome sequencing techniques have now identified point mutations in the human *synaptotagmin 2 (syt2)* gene in patients with a disease combining congenital myasthenic syndrome and distal motor weakness, suggesting a role for synaptotagmin in neuromuscular disease [18, 19].

Two independent mutations in the C_2B Ca^{2+}-binding pocket of *syt2* have been identified: one in a United States (US) family and one in a United Kingdom (UK) family. Patients in each of the two families exhibit a novel neuromuscular syndrome characterized by foot deformities, fatigable ocular movements, lower limb weakness, and potentiation of tendon reflexes following exercise [18, 19]. In nerve conduction studies, all patients exhibited normal sensory responses. However, motor responses revealed low amplitude compound muscle action potentials (CMAPs) that exhibited significantly less amplitude depression following brief maximum voluntary contraction [18, 19]. These findings are indicative of a presynaptic deficit of neuromuscular junction function.

Interestingly, both familial mutations are located in C_2B Ca^{2+}-binding pocket of *syt2* within the highly conserved "SDPYVK" residue motif (Fig 4.1) [18, 19]. The US family possesses an aspartate 307 (referred to as D2) to alanine substitution within this motif (Fig 4.1D, first *). As D2 is one of the well-ordered C_2B aspartate residues known to coordinate the binding of Ca^{2+} [10, 20, 21] required for triggering neurotransmitter release [5, 12, 15], the function of this residue has been extensively studied. The UK family possesses a proline 308 to leucine substitution within this motif (Fig 4.1D, second *). We investigated the anticipated conformational changes of the proline to leucine (P-L) substitution by modeling this P-L mutation *in silico*. Simulation of the P-L mutation predicts that replacement of the highly conserved proline residue by a leucine would extend β-strand 3 into the Ca^{2+}-binding pocket (Fig 4.1A,B, small arrow). The extension of β-strand 3 is accompanied by a significant distortion of the backbone angles of residues on the amino terminal side of the proline (Fig S4.1). The distortion of upstream residues places this critical D2 Ca^{2+}-binding residue in a non-ideal conformation for Ca^{2+} binding (Fig 4.1C, curved arrow and Fig S4.1). Further, the additional amide proton from the mutant leucine residue forms a new H-bond with neighboring residues in loop 2 (not shown), thereby altering the shape, and likely the flexibility, of the Ca^{2+}-binding pocket. A more rigid Ca^{2+}-binding pocket, as well as the sub-optimally positioned D2 Ca^{2+}-binding residue, predict deficiencies in Ca^{2+} binding in the P-L mutation. Together, our modeling predicts that this mutation would result in conformational changes in synaptotagmin's C_2B domain that would impair Ca^{2+} binding. Although this proline residue is highly conserved (Fig 4.1D), its importance for synaptotagmin function has not been investigated previously.

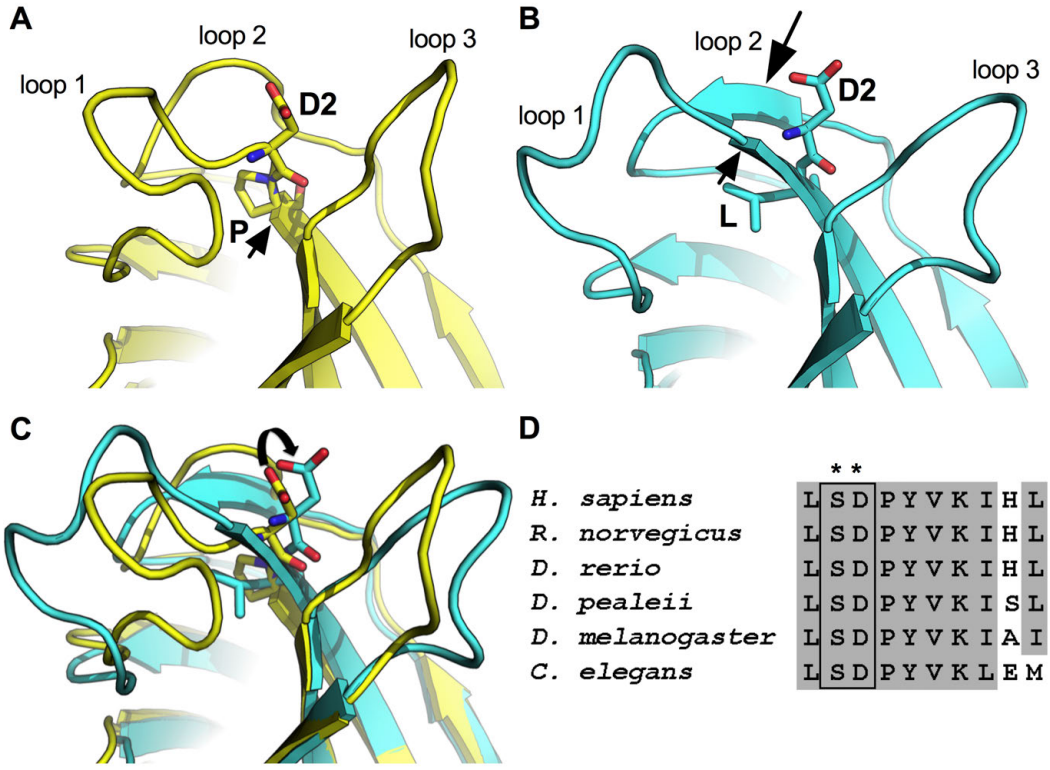

Fig 4.1. Predicted conformational changes in synaptotagmin's C_2B Ca^{2+}-binding pocket. (A) Molecular model depicting the crystal structure of the synaptotagmin C_2B Ca^{2+}-binding pocket. Flexible loops 1, 2, and 3 are indicated. The proline residue under investigation (P) and the adjacent, Ca^{2+}-coordinating aspartate (D2) are shown as stick models. Note that the proline is at one end of β-strand 3 (small arrow) and the aspartate is in loop 1. (B) Predicted structural changes induced by the $syt^{P\text{-}L}$ substitution. The leucine (L) and the adjacent aspartate (D2) residues are shown as stick models and both are now within β-strand 3 (small arrow indicates extension of β-strand 3). The large arrow indicates a newly formed β-strand. (C) Overlay of wild type (yellow) and $syt^{P\text{-}L}$ mutant (turquoise). The curved arrow indicates the displacement of the D2 Ca^{2+}-binding residue. (D) Sequence alignment of the highly conserved SDPYVK amino acid motif of the synaptotagmin C_2B domain from humans, rat, zebra fish, squid, *Drosophila*, and *C. elegans*. *locations of the point mutations in the US and UK families, respectively. Note: *syt1* and *syt2* in mammals are identical in this region.

To directly assess whether the $syt^{P\text{-}L}$ point mutation impacts Ca^{2+}-binding resulting in synaptic deficits *in vivo*, we generated a homologous P-L mutation in the synaptotagmin isoform expressed at the *Drosophila* neuromuscular junction (*$syt^{P\text{-}L}$*). In mammals, the *synaptotagmin 1* gene (*syt1*) is predominantly expressed throughout the cerebral hemispheres while *syt2* is predominantly expressed in the brainstem and spinal cord, and hence at the neuromuscular

junction [16, 17]. There is no *syt2* gene in *Drosophila* [22, 23]; the *syt1* gene is expressed pan-neuronally [24, 25] and codes for the Ca^{2+} sensor for fast, synchronous neurotransmitter release [5, 6] throughout the nervous system. When the $syt^{P\text{-}L}$ mutation is expressed in *Drosophila* in the absence of wild type synaptotagmin, it results in lethality, demonstrating that this proline residue is critical for synaptotagmin function. As the human condition presents as a *syt* heterozygous dominant disorder, with patients carrying one copy of the wild type *syt* gene and one copy of the mutated *syt* gene ($syt^{WT/}syt^{P\text{-}L}$), we simulated this expression pattern by driving pan-neuronal expression from one mutant transgene using *elavGal4* in *syt* heterozygotes ($+/-;P[syt^{P\text{-}L}]/+$). Physiologically, mutant larvae exhibit decreased evoked transmitter release and less synaptic depression during high-frequency stimulus trains, consistent with the human electrophysiological deficits. In addition, the decreased Ca^{2+} affinity of release and the associated decreased release probability documented here are consistent with the predicted disruption to the C_2B Ca^{2+}-binding pocket (Fig 4.1A-C). Behaviorally, mutant adult flies exhibit less overall activity and a marked increase in fatigability, also consistent with the human phenotype. Together, these results indicate that this proline to leucine substitution impairs Ca^{2+} binding and support a role for this substitution in the etiology of this human neuromuscular disease.

4.3 Results

In the absence of wild type synaptotagmin, the $P[syt^{P\text{-}L}]$ mutation increases the lethality rate

To assess the effects of the $syt^{P\text{-}L}$ mutation in the absence of the wild type protein, we drove pan-neuronal expression of *syt* transgenes in the syt^{null} background using the *elavGal4* promoter (referred to as $-/-;P[syt^{WT}]/+$ or $-/-;P[syt^{P\text{-}L}]/+$, see methods for full genotype). Rates of survival to the first instar larval stage were also compared to larvae lacking any synaptotagmin

1 expression (-/-). Balancer chromosomes used in our crossing scheme result in embryonic lethality for any wild type synaptotagmin homozygotes (+/+ for *syt*, included in Table 4.1 under unhatched) due to the presence of a homozygous lethal *Cy* mutation (see methods and Fig S4.2) with an expected frequency of ~25%.

Table 4.1. The $syt^{P\text{-}L}$ mutation negatively impacts survival rate in the absence of native synaptotagmin. Table depicts percentages and raw counts (in parentheses) of first instar larvae in the syt^{null} (-/-, top row) and *syt* heterozygous (+/-, second row) backgrounds and embryonic lethality (unhatched) of progeny containing one copy of synaptotagmin transgenes ($P[syt^{WT}]$ or $P[syt^{P\text{-}L}]$) or of progeny containing no transgenic *syt* (last column). All crosses were carried out using the *CyO* second chromosome balancer such that *syt* homozygotes are lethal (included in unhatched) due to the presence of the homozygous lethal *Cy* mutation (syt^{WT} *Cy*/syt^{WT} *Cy*). There was a significant decrease in the percentage of first instars expressing one copy of $P[syt^{P\text{-}L}]$ in the absence of any wild type synaptotagmin (-/-;$P[syt^{P\text{-}L}]$/+, 12.0%) compared to control (-/-;$P[syt^{WT}]$/+, 25.7%, $p < 0.0001$, Chi-squared test). There was also a significant decrease in the percentage of first instars expressing one copy of the $P[syt^{P\text{-}L}]$ transgene (-/-;$P[syt^{P\text{-}L}]$/+, 12.0%) compared to no synaptotagmin expression at all (-/-; no transgenic *syt*, 18.0%, $p < 0.0001$, Chi-squared test).

	$P[syt^{WT}]$	$P[syt^{P\text{-}L}]$	No transgenic *syt*
-/-	25.7% (365)	12.0% (212)	18.0% (231)
+/-	48.7% (691)	50.1% (888)	49.8% (640)
Unhatched	25.6% (363)	37.9% (671)	32.2% (415)

As expected for a fully functional protein, the wild type transgenic cross resulted in progeny where ~25% were syt^{null} mutants expressing synaptotagmin from the wild type transgene (-/-;$P[syt^{WT}]$/+; Table 1, 25.7%). This is significantly larger than in the $P[syt^{P\text{-}L}]$ cross, in which only 12.0% of progeny were syt^{null} mutants expressing the mutated transgene (-/-;$P[syt^{P\text{-}L}]$/+, Table 1, 12.0%, $p < 0.0001$). As previously shown, syt^{null} mutants are viable [26], and the cross lacking any source of synaptotagmin resulted in 18.0% of progeny that were syt^{null} mutants (Table 1, no transgenic *syt*, 18.0%). Yet the expression of the mutant transgene resulted in a significant decrease in the rate of survival to the 1st instar larval stage (Table 1, 18.0% down

to 12.0%, $p < 0.0001$). Thus, in the absence of wild type synaptotagmin, the expression of *P[syt^{P-L}]* not only fails to rescue synaptotagmin function, it results in a negative impact on survival. This is the first study to show the critical nature of this proline residue for synaptotagmin function.

Transgenic synaptotagmin is expressed appropriately

To verify appropriate transgenic synaptotagmin expression levels for modeling this disease in *Drosophila*, western blot analysis was performed on the central nervous system (CNS) of larvae. Comparison of CNS samples from *syt* heterozygotes (+/-) and *syt* heterozygotes expressing one copy of the mutant transgene (+/-; *P[syt^{P-L}]*/+, hereafter referred to as *P[syt^{P-L}]* heterozygotes) showed significant differences in the level of synaptotagmin expression with an approximate doubling of synaptotagmin levels in the transgenic line (Fig 4.2A, +/- is 46 ± 18% of +/-;*P[syt^{P-L}]*/+, $p = 0.0008$). This finding indicates approximately equal protein expression from the native gene and the transgene. Consistent with this interpretation, CNS samples from wild type *syt* homozygotes (+/+) and from *P[syt^{P-L}]* heterozygotes showed similar levels of synaptotagmin expression (Fig 4.2B, +/-;*P[syt^{P-L}]*/+ is 94 ± 9.0% of +/+, $p = 0.69$). Fig 4.2C demonstrates approximately equal levels of synaptotagmin in *P[syt^{P-L}]* heterozygotes and the *P[syt^{WT}]* heterozygous controls (+/-; *P[syt^{P-L}]*/+ is 121 ± 8.1% of +/-;*P[syt^{WT}]*/+, $p = 0.25$). Thus, our heterozygous transgenic control also expresses appropriate levels of synaptotagmin. Finally, both the transgenic wild type and transgenic mutant protein are appropriately targeted to the synapse (Fig 4.2D-G). As seen in wild type *Drosophila* [24, 25], synaptotagmin staining in muscles is restricted to the neuromuscular junction in third instar larvae of both the *P[syt^{WT}]* heterozygote controls and the *P[syt^{P-L}]* heterozygotes (Fig 4.2D,E, respectively). Staining of

first instar larvae expressing the *syt* transgenes in the absence of native synaptotagmin also revealed that the transgene is appropriately expressed at the neuromuscular junction (Fig 4.2F,G, *-/-;P[syt^{WT}]/+* and *-/-;P[syt$^{P\text{-}L}$]/+*).

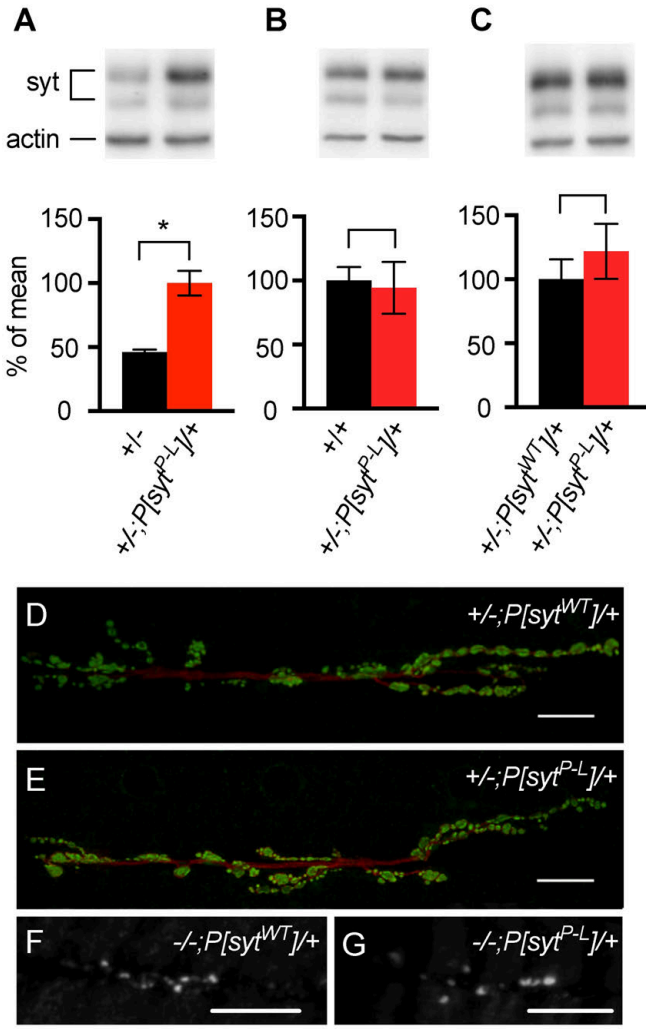

Fig 4.2. Transgenic synaptotagmin is expressed at appropriate levels and exhibits appropriate localization. (A-C) Representative western blots above and average synaptotagmin expression normalized to actin levels below. *Syt* heterozygotes expressing one copy of the mutant transgene (*+/-;P[syt$^{P\text{-}L}$]/+*, n = 6, 5, and 7, respectively) are compared to *syt* heterozygotes (+/-, n = 5, A), *syt* homozygotes (+/+, n = 5, B), and *syt* heterozygotes expressing one copy of the wild type transgene (*+/-;P[syt^{WT}]/+*, n = 8, C). The *P[syt$^{P\text{-}L}$]* heterozygotes had approximately twice as much synaptotagmin expression as *syt* heterozygotes (p = 0.0008, student t-test), while there was no significant difference in expression between the other lines compared (Fig 4.2B, p = 0.69 and Fig 4.2C, p = 0.25). Error bars depict SEM. (D, E) Third instar larvae stained with antibodies against horseradish peroxidase (HRP) as a general axonal stain (red) and synaptotagmin (green). Scale bars represent 10 µm. (F, G) First instar larvae stained with antibodies against synaptotagmin. Scale bars represent 20 µm.

Lifespan is decreased in P[syt$^{P\text{-}L}$] heterozygotes

While *P[syt$^{P\text{-}L}$]* heterozygotes are easily generated and maintained throughout all larval and adult stages, we wanted to ascertain whether this mutation had any impact on lifespan in heterozygotes. Therefore, we performed a longevity assay. Lifespans between *P[syt^{WT}]* heterozygotes (51.4 ± 1.50 days, mean lifespan ± SEM, n = 151) and *P[syt$^{P\text{-}L}$]* heterozygotes (39.2 ± 1.25 days, mean lifespan ± SEM, n = 149) are significantly different (Fig 4.3, $p < 0.0001$, Wilcoxon Rank-Sum test). However, this does not relate directly to the human condition, who show no indication of this P-L mutation impacting longevity, as these flies do not receive any medical intervention. These results support a detrimental role of the proline to leucine mutation in survival.

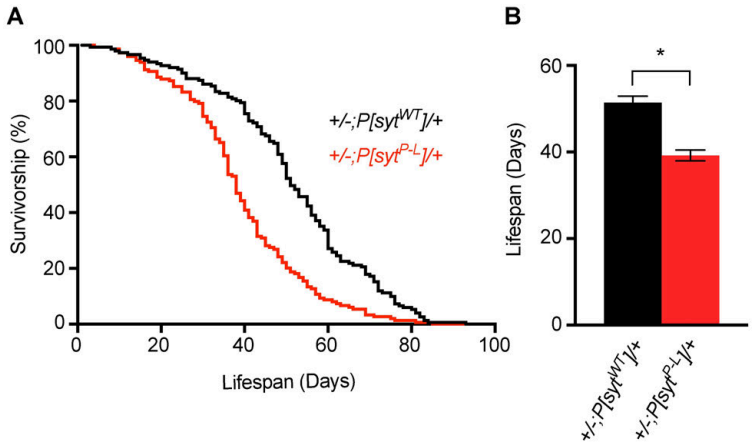

Fig 4.3. Lifespan is decreased in *P[syt$^{P\text{-}L}$]* heterozygotes. (A) Adult lifespan curves of *+/-;P[syt^{WT}]/+* (n = 151, black) and *+/-;P[syt$^{P\text{-}L}$]/+* (n = 149, red). (B) Mean lifespan is significantly decreased in *+/-;P[syt$^{P\text{-}L}$]/+* adults ($p < 0.0001$, Wilcoxon Rank-Sum test).

The syt$^{P\text{-}L}$ mutation disrupts evoked transmitter release

In human motor nerve conduction studies, the summated response of all muscle fibers supplied by a particular motor nerve can be measured as a CMAP. The *syt$^{P\text{-}L}$*-affected family members present with decreased CMAP amplitudes [18, 19], consistent with a decrease in

evoked transmitter release. To test evoked release in *Drosophila P[syt$^{P\text{-}L}$]* heterozygotes, we measured excitatory junction potentials (EJPs) at the larval neuromuscular junction. Upon nerve stimulation, *P[syt$^{P\text{-}L}$]* heterozygotes exhibited a significant decrease in the amount of neurotransmitter released (Fig 4.4A,B). Average EJP ± SEM for *+/-;P[syt^{WT}]/+* was 34.8 ± 0.83 mV, and for *+/-;P[syt$^{P\text{-}L}$]/+* was 29.6 ± 1.5 mV (p = 0.002, student t-test). This decrease in release is consistent with the decrease in baseline amplitude in the human motor nerve conduction studies.

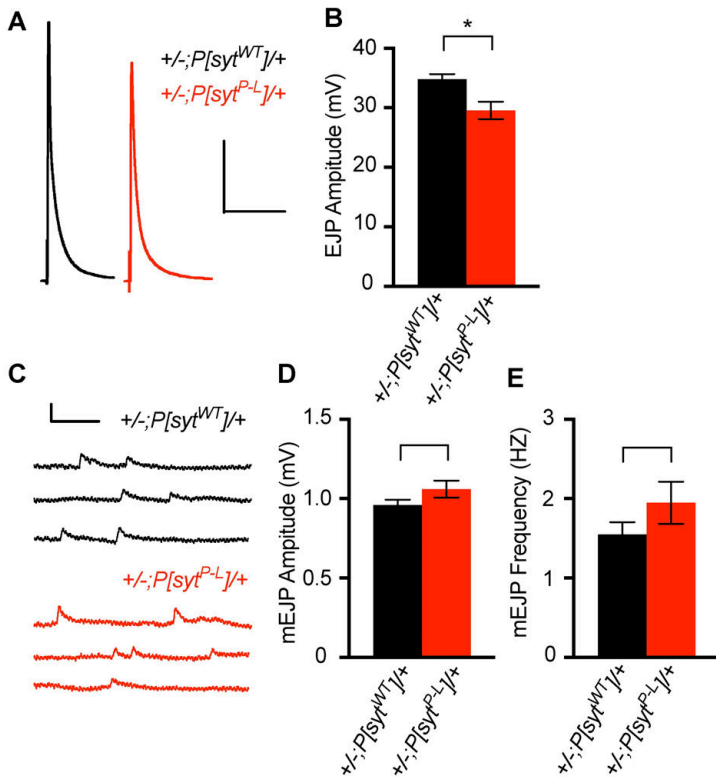

Fig 4.4. Synchronous evoked release is impaired in *P[syt$^{P\text{-}L}$]* heterozygotes, but quantal content is unchanged. (A) Representative EJP traces for control and *P[syt$^{P\text{-}L}$]* heterozygotes. Scale bars represent 10 mV, 0.2 s. (B) Mean EJP amplitude is significantly less in *P[syt$^{P\text{-}L}$]* heterozygotes (n = 19) compared to control (n = 12, *p = 0.002). Error bars depict SEM. (C) Representative consecutive 3 second mEJP traces for control and *P[syt$^{P\text{-}L}$]* heterozygotes. Scale bars represent 1 mV, 0.2 s. (D, E) Neither mean mEJP amplitude (p = 0.09, Wilcoxon Rank-Sum Test, D) nor mean mEJP frequency (p = 0.18, student t-test, E) is significantly different between *P[syt$^{P\text{-}L}$]* heterozygotes (n = 12 fibers) and control (n = 19 fibers). Error bars depict SEM.

One potential explanation for this observed 20% decrease in evoked response could be a decrease in quantal content. To determine quantal size, we calculated the mean amplitudes of Ca^{2+}-independent spontaneous miniature EJPs (mEJPs) in both *P[syt^{P-L}]* heterozygotes and their controls. Each mEJP results from one vesicle fusing with the presynaptic membrane. Thus, the amplitude of the response is an indication of the amount of neurotransmitter loaded into each vesicle. Neither the mean amplitude nor frequency of mEJPs in controls and *P[syt^{P-L}]* heterozygotes were significantly different (Fig 4.4C-E). Mean mEJP amplitude ± SEM for *P[syt^{WT}]* heterozygotes was 0.96 ± 0.03 mV (n = 50 mEJP events from 19 fibers), and for *P[syt^{P-L}]* heterozygotes was 1.06 ± 0.05 mV (n = 50 mEJP events from 12 fibers, p = 0.09, Wilcoxon Rank-Sum Test). Mean mEJP frequency ± SEM for *P[syt^{WT}]* heterozygotes was 1.55 ± 0.15 Hz (n = 19 fibers), and for *P[syt^{P-L}]* heterozygotes was 1.94 ± 0.26 Hz (n = 12 fibers, p = 0.18, student t-test). These results demonstrate that the decrease in evoked release is not due to a change in quantal content.

Transmitter release from an activated nerve terminal is a Ca^{2+}-dependent, cooperative process [27]. Evoked release was measured at a variety of extracellular [Ca^{2+}], ranging from 0.05 mM to 5 mM, to assess whether the Ca^{2+} dependence of release was altered in *P[syt^{P-L}]* heterozygotes. At all [Ca^{2+}] above 0.1 mM, *P[syt^{P-L}]* heterozygotes exhibit a decrease in evoked release compared to controls (Fig 4.5A). A nonlinear regression analysis determined a change in the Ca^{2+} dependence of *P[syt^{P-L}]* heterozygotes. The extracellular [Ca^{2+}] at which a 50% maximum response is reached (EC_{50}) is statistically shifted in *P[syt^{P-L}]* heterozygotes compared to controls. In *+/-;P[syt^{WT}]/+* EC_{50} = 0.33 mM Ca^{2+} (95% confidence intervals from 0.30-0.36 mM Ca^{2+}) and in *+/-;P[syt^{P-L}]/+* EC_{50} = 0.44 mM Ca^{2+} (95% confidence intervals from 0.41-0.48 mM Ca^{2+}, Fig 4.5B). The non-overlapping confidence intervals demonstrate that the proline

to leucine substitution in synaptotagmin results in a significant decrease in the Ca^{2+} affinity of release.

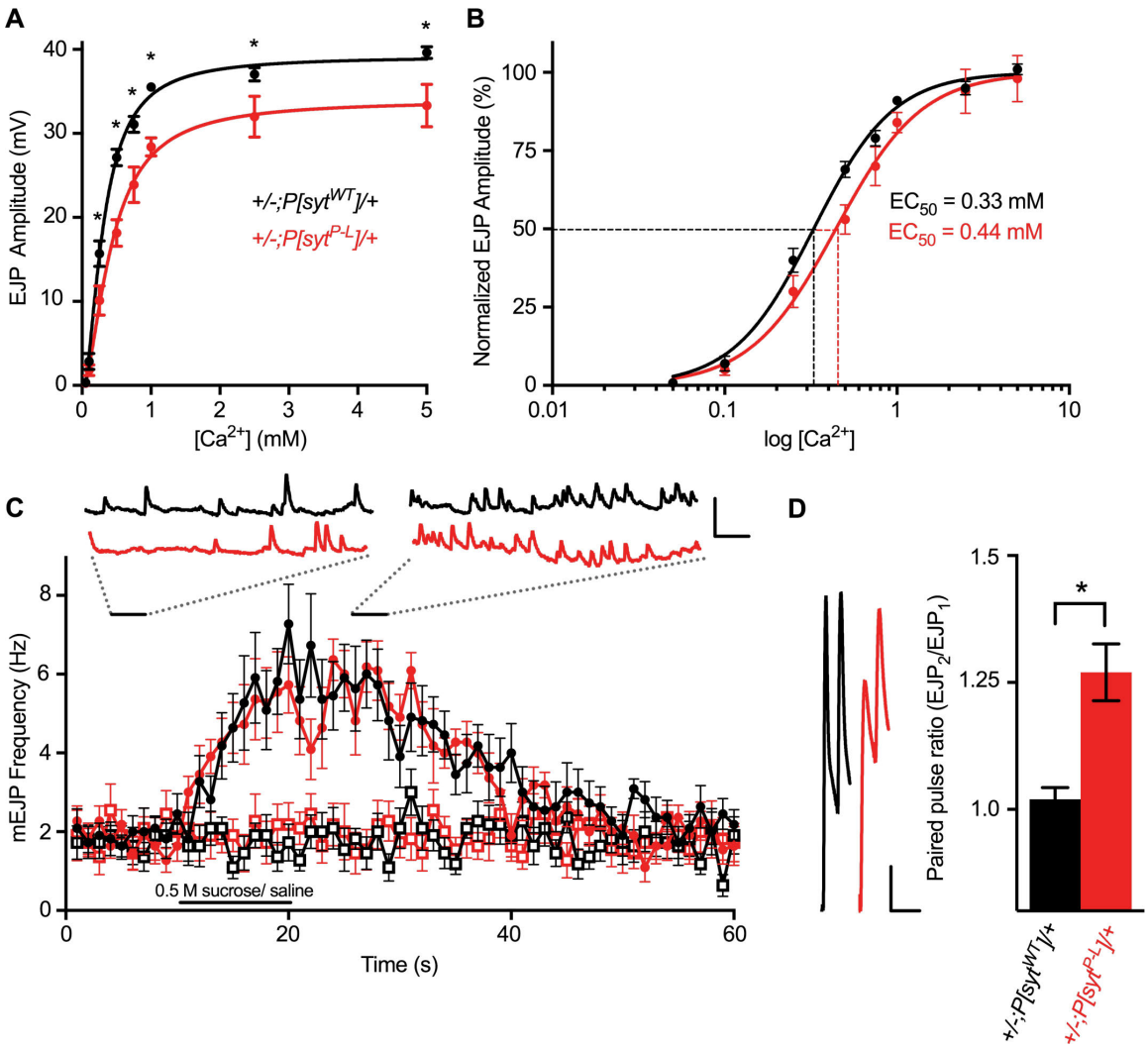

Fig 4.5. The *P[syt^{P-L}]* mutation decreases the Ca^{2+} affinity of release and vesicular release probability, but the readily releasable pool is unchanged. (A) Mean EJP amplitudes from *+/-;P[syt^{WT}]/+* (filled black circles) and *+/-;P[syt^{P-L}]/+* (filled red circles) larvae at Ca^{2+} levels ranging from 0.05 mM - 5.0 mM. At $[Ca^{2+}]$ above 0.1 mM, statistical differences are seen between the two genotypes (*$p < 0.05$ for indicated $[Ca^{2+}]$, see Table S4.1 for specific n's and p-values, student t-tests). Lines of best fit were determined using non-linear regression analyses. (B) Graph depicting normalized EJP responses at log $[Ca^{2+}]$. EC_{50} values were determined using the line of best fit determined by nonlinear regression analyses. Dotted lines depict the shift in the EC_{50} value. (C) Application of hypertonic 0.5 M sucrose to *+/-;P[syt^{WT}]/+* (n = 11 fibers, filled black circles) and *+/-;P[syt^{P-L}]/+* (n = 11 fibers, filled red circles) results in increases in mEJP frequency. Black bar below the traces represents the duration of the 10 s application of 0.5 M sucrose or saline solution. Black bars above the mEJP responses indicate three consecutive seconds of individual traces either before sucrose application (left inset) or during peak sucrose response (right inset). Similar frequencies between *+/-;P[syt^{WT}]/+* and *+/-;P[syt^{P-L}]/+* are

observed both before and during sucrose response (n = 11 fibers for both genotypes, p = 0.28 before sucrose application, p = 0.23 during maximum sucrose response). Application of bath solution does not result in an increase in mEJP frequency in either genotype (open circles) (p = 0.57 for *+/-;P[syt^{WT}]/+* and p = 0.83 for *+/-;P[syt$^{P\text{-}L}$]/+*, student t-test). Scale bar 2mV, 3s. (D) Paired pulse analysis indicates a decrease in release probability in *+/-;P[syt$^{P\text{-}L}$]/+*. Left, representative traces of responses stimulated with a 20 ms interpulse interval. Scale bar 5 mV, 40 ms. Right, in *P[syt$^{P\text{-}L}$]* heterozygotes, the paired pulse ratio is significantly increased (*+/-;P[syt^{WT}]/+* = 1.02 ± 0.02, *+/-;P[syt$^{P\text{-}L}$]/+* = 1.27 ± 0.06, *p = 0.0008, student t-test). Error bars are SEM.

Release probability is decreased in P[syt$^{P\text{-}L}$] heterozygotes

A decrease in the size of the readily releasable pool and/or a decrease in release probability for individual vesicles could result in decreased evoked transmitter release. To determine whether *P[syt$^{P\text{-}L}$]* heterozygotes exhibit alterations in the size of their readily releasable pool of synaptic vesicles, we triggered Ca^{2+}-independent vesicle fusion events using a hypertonic solution (0.5 M sucrose). Before sucrose stimulation, mEJP frequency is similar between both *P[syt^{WT}]* and *P[syt$^{P\text{-}L}$]* heterozygotes [Fig 4.5C, filled symbols, *+/-;P[syt^{WT}]/+* (black), 1.95 ± 0.07 Hz and *+/-;P[syt$^{P\text{-}L}$]/+* (red), 1.81 ± 0.10 Hz, mean mEJP frequency ± SEM, n = 11 fibers for both genotypes, p = 0.28, student t-test). Increases in mEJP frequencies are observed in both controls (p < 0.0001, student t-test) and *P[syt$^{P\text{-}L}$]* heterozygotes (p < 0.0001, student t-test) upon sucrose stimulation. These mEJP frequencies are also similar between genotypes during the maximum sucrose response period (Fig 4.5C, filled symbols, *+/-;P[syt^{WT}]/+*, 5.62 ± 0.23 Hz and *+/-;P[syt$^{P\text{-}L}$]/+*, 5.32 ± 0.23 Hz, mean mEJP frequency ± SEM, p = 0.23, student t-test). When HL3.1 solution is puff applied, mEJP frequency remains similar between *P[syt^{WT}]* and *P[syt$^{P\text{-}L}$]* heterozygotes (Fig 4.5C, open symbols, *+/-;P[syt^{WT}]/+*, 1.71 ±.0.10 Hz and *+/-;P[syt$^{P\text{-}L}$]/+* = 1.96 ± 0.10 Hz, mean mEJP frequency ± SEM, p = 0.23, student t-test, n = 11 for both genotypes). Moreover, no increase is observed for either genotype

during or after saline stimulation (Fig 4.5C, open circles, *+/-;P[syt^{WT}]/+* p = 0.57 and *+/-;P[syt$^{P\text{-}L}$]/+* p = 0.83, student t-test), indicating the increases in mEJP frequencies observed during sucrose stimulation result from hypertonic solution directly, and not a mechanical stimulation due to the puff application. Thus, the size of the readily releasable pool is not significantly altered in *P[syt$^{P\text{-}L}$]* heterozygotes.

To address release probability, we used a paired pulse analysis examining the ratio of the second response divided by the first response using a 20 ms interpulse interval. *P[syt^{WT}]* heterozygotes (n = 18) and *P[syt$^{P\text{-}L}$]* heterozygotes (n = 24) result in significantly different paired pulse ratios [Fig 4.5D, *+/-;P[syt^{WT}]/+* = 1.02 ± 0.02 (first pulse = 34.4 ± 0.84 mV, second pulse = 35.2 ± 0.89 mV, EJP amplitude ± SEM), compared to *+/-;P[syt$^{P\text{-}L}$]/+* = 1.27 ± 0.06 (first pulse = 25.1 ± 1.02 mV, second pulse = 30.6 ± 0.84 mV, EJP amplitude ± SEM), p = 0.0008, student t-test]. The significantly larger paired pulse ratio indicates a decrease in release probability in *P[syt$^{P\text{-}L}$]* heterozygotes. Thus, our electrophysiological analysis of *P[syt$^{P\text{-}L}$]* heterozygotes indicates the decrease in evoked transmitter release is not due to changes in the readily releasable pool, but rather results from a decrease in vesicular release probability.

A distinctive feature of the human condition is that following brief maximal voluntary muscle contraction, the CMAP amplitude is less depressed, typically for several minutes [18, 19]. Since a decrease in release probability could result in less depression, we assessed this unique phenotype in *Drosophila*. We measured the amplitude of evoked release at the larval neuromuscular junction following a 10 Hz stimulation for 2 seconds. Responses were normalized to the initial EJP response to account for the decrease in EJP amplitude seen in the *P[syt$^{P\text{-}L}$]* heterozygotes. Beginning at the fourth pulse of this stimulation period, *P[syt$^{P\text{-}L}$]* heterozygotes exhibited a significant 5-10% decrease in synaptic depression relative to control (Fig 4.6, Table

S4.2). However, when a test stimulation was applied 1 minute after the end of the stimulus train, this effect was no longer observed; the amplitude of the evoked response in both the *P[syt$^{P\text{-}L}$]* heterozygotes and the controls had returned to resting levels (Fig 4.6, Table S4.2).

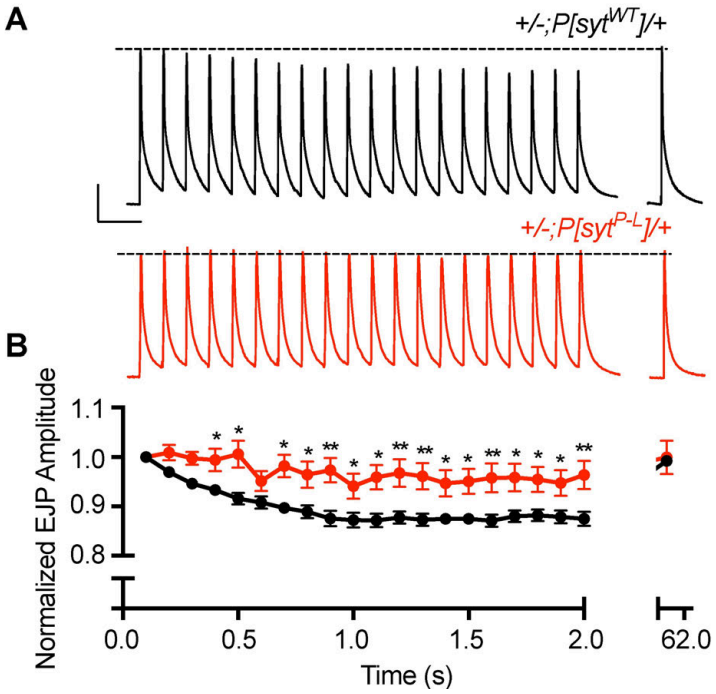

Fig 4.6. *P[syt$^{P\text{-}L}$]* heterozygotes exhibit less depression throughout the course of high frequency stimulation, but fail to maintain this relatively increased response upon cessation of stimulation. (A) Representative traces from control and *P[syt$^{P\text{-}L}$]* heterozygotes during a 2 second, 10 Hz stimulation train, and a single stimulus 1 minute following cessation of the train. Dotted line represents the amplitude of the initial response. Scale bar represents 10 mV, 0.2 s. (B) Mean EJP amplitudes of *P[syt$^{P\text{-}L}$]* heterozygotes (n = 17) showed less depression compared to control (n = 14, *indicates $p < 0.05$, and **indicates $p < 0.001$). However, this relative increase in release is not maintained upon cessation of the stimulus train ($p = 0.87$). Error bars depict SEM.

Since maximum voluntary contraction can produce motor nerve firing rates in excess of 50 Hz [28], larval preparations were stimulated at 50 Hz for 2 seconds in an attempt to more closely approximate the stimulus that results in the prolonged increase in release seen in the affected family members. Normalized post-stimulus train responses were tested at 1 second and then at 30-second intervals out to 4 minutes. This protocol displayed similar results to the 10 Hz stimulation experiment. Both at the end of the stimulus train and at 1 second post-stimulation, there is no synaptic depression in the *P[syt$^{P\text{-}L}$]* heterozygotes, unlike in the control (Fig 4.7,

Table S4.3). However, normalized responses to test stimulations at 30 seconds or longer after cessation of the stimulation train showed no significant differences in release between the *P[syt$^{P\text{-}L}$]* heterozygotes and controls (Fig 4.7, Table S4.3). Thus, our transgenic model system cannot provide insight into the prolonged increase of the CMAP amplitude following maximal voluntary contraction, which can last 10 minutes or longer in humans [18, 19].

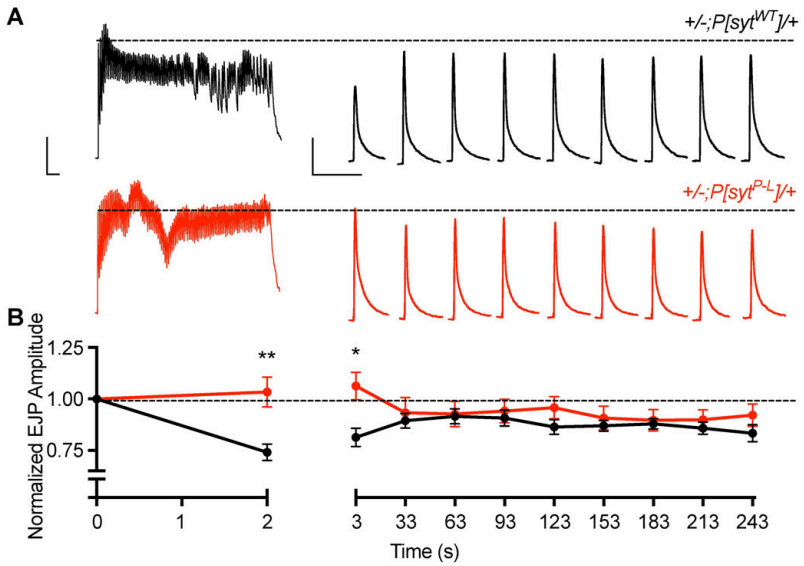

Fig 4.7. The *syt$^{P\text{-}L}$* mutation does not result in synaptic depression during and shortly after a high frequency 50 Hz stimulation, but this relative increase in release is short-lived. (A) Representative traces for control and *P[syt$^{P\text{-}L}$]* heterozygotes showing the initial 2 second 50 Hz train, followed by each post-train pulse at 1 second, then every 30 seconds thereafter for 4 minutes. Dotted line represents the amplitude of the initial response. Scale bar represents 10 mV, 0.1 s. (B) Average EJP amplitude during and after 50 Hz stimulation in control (n = 18) and *P[syt$^{P\text{-}L}$]* heterozygotes (n = 24). Responses were normalized to the amplitude of the initial response. Unlike controls, *P[syt$^{P\text{-}L}$]* heterozygotes do not exhibit synaptic depression at the end of the stimulus train ($p << 0.0001$) and 1 second after cessation of the train ($p = 0.0012$). Error bars depict SEM.

Basal levels of locomotor activity are decreased in P[syt$^{P\text{-}L}$] heterozygotes.

The P-L familial condition presents with distal limb deformities, muscle wasting, and difficulty walking [18, 19]. To assess the impact of this mutation on overall motor function in our model system, the *Drosophila* activity-monitoring (DAM) assay was performed to quantify

basal locomotor activity levels. This assay determines total activity over time. However, as activity levels in *Drosophila* males and females are known to have different circadian cycles [29, 30], males and females were tested separately. Activity level was determined by monitoring individual flies for 6 days in a 12hr light: 12hr dark cycle (Fig 4.8A,B) in age- and sex-matched adult *Drosophila P[syt^{WT}]* or *P[syt$^{P\text{-}L}$]* heterozygotes.

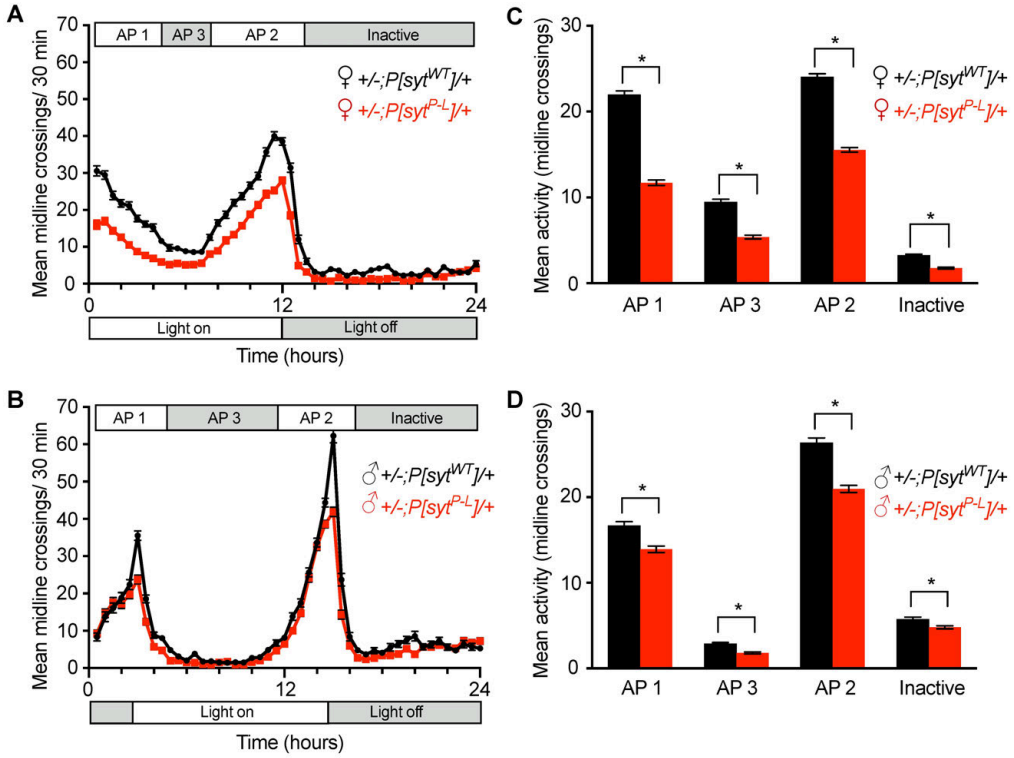

Fig 4.8. The *syt$^{P\text{-}L}$* mutation affects locomotor activity in *Drosophila*. (A, B) Average activity per 30 minutes for an averaged 24-hour day in a 6-day *Drosophila* Activity Monitoring Assay in 5-7 day old females (A) and males (B). (C, D) Distinct activity periods (AP) were averaged for females (C, n = 48 for each genotype) and males (D, n = 48 for *+/-;P[syt$^{P\text{-}L}$]/+*, n = 45 for control). *P[syt$^{P\text{-}L}$]* heterozygotes were significantly less active than controls during all activity periods in both males and females (* indicates $p < 0.001$, student t-tests). Error bars depict SEM.

Drosophila are typically active during periods of light and inactive during periods of dark. Furthermore, flies have an increase in locomotor activity in anticipation of the transition between dark to light and light to dark. We analyzed the locomotor activity at the two anticipatory peaks of activity (Active 1 and 2, respectively), the non-peak period during lights on

(Active 3) and the inactive period approximately corresponding to lights off (Inactive). We find distinct periods of activity between males and females, consistent with published data [29, 30]. During all activity periods, both male and female *P[syt$^{P\text{-}L}$]* heterozygotes displayed significantly less movement (Fig 4.8C,D, Table S4.4).

The rate of muscle fatigue is faster in P[syt$^{P\text{-}L}$] heterozygotes.

Affected individuals with the human disease also present with cramping and pain upon physical exertion, difficulty with sports, and some fatigable eye movements [19]. Since these can all be associated with fatigability in muscle, we analyzed fatigue rate in adult *Drosophila* using a modified climbing assay [31]. Flies were repetitively knocked to the bottom of a vial. This stimulates negative geotaxis, an innate escape response in which flies climb up the vial wall. Vials were dropped (see methods) every 10 seconds for 30 minutes. After each drop, the distance each fly climbed upward within 5 seconds was measured and averaged. As with the DAM assay, we tested age-matched female and male adult flies separately. Differences were observed as early as the first drop for both males and females of *P[syt$^{P\text{-}L}$]* heterozygotes and controls (female *+/-;P[syt^{WT}]/+* = 6.49 ± 0.60 cm, female *+/-;P[syt$^{P\text{-}L}$]/+* = 3.67 ± 0.91 cm, p = 0.017, student t-test, male *+/-;P[syt^{WT}]/+* = 6.99 ± 0.45 cm, and male *+/-;P[syt$^{P\text{-}L}$]/+* = 4.68 ± 0.64 cm, p = 0.009, student t-test, average distance traveled ± SEM after the first drop). To specifically measure fatigue, we controlled for the decreased overall activity in the mutants by normalizing all measurements to the distance traveled after the initial drop. The normalized data was then graphed over time for both females and males (Fig 4.9A,B, respectively). As a measure of the rate of fatigue, we calculated the log of the raw data and used linear regressions to provide predicted lines of best fit (not shown). The slopes of these lines were statistically significantly

different between mutants and controls in both females and males (slopes for female +/-;*P[syt^{WT}]*/+ = -0.013, female +/-;*P[syt$^{P\text{-}L}$]*/+ = -0.039, male +/-;*P[syt^{WT}]*/+ = -0.011, and male +/-;*P[syt$^{P\text{-}L}$]*/+ = -0.069, $p < 0.0001$ for both females and males, see methods). These results demonstrate a faster rate of fatigue in the *P[syt$^{P\text{-}L}$]* heterozygotes, consistent with the muscle fatigability seen in the affected family members.

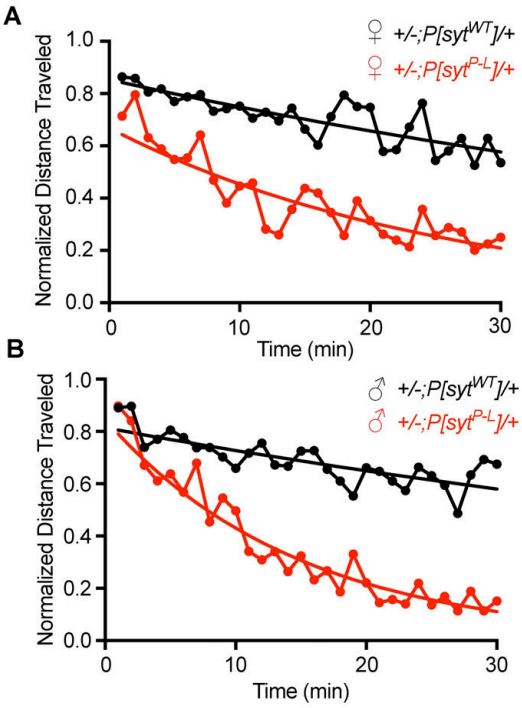

Fig 4.9. The *syt$^{P\text{-}L}$* mutation increases the rate of fatigue in *Drosophila*. (A, B) Normalized values of distance traveled up a vial wall after repetitive drops over time for 5-7 day old females (A) and males (B). Each point is a binned 1 minute average of 6 drops (1 drop every 10 seconds) normalized to the percentage of the distance traveled after the first drop. Statistical analysis indicates different rates of fatigue (see methods) between the two genotypes for both females ($p < 0.0001$) and males ($p < 0.0001$), indicating the *P[syt$^{P\text{-}L}$]* heterozygotes (n = 10) fatigued significantly faster than controls (n = 10).

4.4 Discussion

In this study we have investigated a synaptotagmin point mutation that was implicated in the etiology of a congenital myasthenic syndrome found in a single family. By modeling this

point mutation *in silico*, we predict significant conformation changes to a key, well-ordered Ca^{2+}-binding residue essential for fast, synchronous neurotransmitter release. The role of this conserved proline residue in these C_2 domains could be to punctuate the end of the β-strand leading into the Ca^{2+}-binding pocket thereby providing maximum Ca^{2+} binding volume optimizing Ca^{2+} sensitivity.

We expressed the homologous mutation in *Drosophila* and documented several similar deficits to those seen in the affected patients. In addition, we found a decreased Ca^{2+} affinity for release and decreased release probability that are consistent with the conformational changes predicted by our *in silico* analysis. Notably, this $syt^{P\text{-}L}$ mutation not only fails to rescue synaptotagmin function, it has a negative impact on survival when expressed as the sole source of synaptotagmin ($-/-;P[syt^{P\text{-}L}]/+$); the survival rate is significantly lower than that of larvae with no synaptotagmin expression (-/-). This finding demonstrates for the first time that this proline residue in the C_2B Ca^{2+}-binding pocket is essential for synaptotagmin's Ca^{2+}-sensing function. By driving expression of the mutant transgene in *syt* heterozygotes ($+/-;P[syt^{P\text{-}L}]/+$), we were able to achieve expression levels of syt^{WT} and $syt^{P\text{-}L}$ similar to that in the human disease.

Electrophysiological analyses demonstrated deficits that may help inform the human condition. Consistent with the human nerve conduction tests, the EJP amplitude at the larval neuromuscular junction in $P[syt^{P\text{-}L}]$ heterozygotes is significantly decreased. This decrease in the initial evoked response is not due to a decrease in quantal size or the readily releasable pool. $P[syt^{P\text{-}L}]$ heterozygotes exhibit a decreased Ca^{2+} affinity, as documented by the increased EC_{50} for Ca^{2+}, which resulted in a decreased release probability, as documented by the facilitated responses in paired pulse experiments, and either no, or less, depression during high frequency

stimulations. This decreased probability of release could account for an increased failure rate at the neuromuscular junction, consistent with the decreased CMAP seen in humans.

The *P[syt$^{P\text{-}L}$]* mutation resulted in significant electrophysiological deficits when expressed in a heterozygous background. This is notable, as synaptotagmin heterozygotes previously have been shown to exhibit no significant changes in electrophysiological responses compared to synaptotagmin homozygotes [32]. Although we did not express this mutation in an otherwise wild type background, this would be consistent with a dominant negative phenotype.

This proline to leucine mutation presents with behavioral deficits similar to those in patients, most notably decreased movement and increased fatigability. This similarity of multiple deficits found in the familial disease strongly supports a role for this residue in the etiology of this form of congenital myasthenic syndrome. It is only recently that mutations in the *syt1* and *syt2* genes have been implicated in human disease [18, 19, 33]. A patient with a *de novo* mutation in the human *syt1* gene presented with an early onset dyskinetic movement disorder, severe motor delay, and profound cognitive deficits attributed to a single amino acid substitution in the C_2B Ca^{2+}-binding pocket: an isoleucine to threonine (I-T) substitution [33]. This hydrophobic isoleucine residue had been shown previously to mediate Ca^{2+}-dependent membrane penetration by synaptotagmin [34-37]: an effector interaction critical for coupling Ca^{2+} influx with neurotransmitter release from neurons [38, 39]. Since this *syt* mutation results in the most severe deficits in an animal system [38] and is located in the *syt1* gene, which is preferentially expressed in the cerebral hemispheres [16, 17], it is not surprising that this patient experienced extreme cognitive deficits as well as the most severe motor deficits observed in a synaptotagmin human disease to date [33].

Herrmann et al, 2014 reported two mutations in the human *syt2* gene implicated in the etiology of congenital myasthenic syndrome patients: the proline to leucine ($syt^{P\text{-}L}$) mutation analyzed in this paper and an adjacent aspartate to alanine ($syt^{D\text{-}A}$) mutation. Both of these highly conserved residues are located in synaptotagmin's C_2B Ca^{2+}-binding pocket [10, 20, 40]. While the function of this proline residue had not been previously studied in animal models, previous studies have demonstrated that the Ca^{2+}-binding aspartate residues of the C_2B domain are essential for synaptotagmin function [5, 15, 18, 36], at times resulting in lethality in animal models [5, 18]. The single viable *Drosophila* line from our lab investigating C_2B aspartate mutations had somewhat reduced expression of the mutant transgene [5]. Since these mutations result in a dominant negative decrease in evoked transmitter release (worse than no synaptotagmin at all) [5], the decreased expression level in our line may have contributed to its viability. When driven in the presence of native synaptotagmin, our *Drosophila* lines that disrupted Ca^{2+} binding by C_2B were viable, but they did result in a significant dominant negative knockdown in function [5]. For the $syt^{D\text{-}A}$ familial mutation, expression of the mutant syt from a transgene in *syt* heterozygotes resulted in lethality in 4 of 6 independent transgenic lines. There was a dramatic decrease in the evoked response in the remaining two lines [18]. The $syt^{P\text{-}L}$ mutation investigated here, however, resulted in no viability issues in the heterozygous background, and only a 20% decrease in the evoked response. Thus, it is surprising that both the $syt^{P\text{-}L}$ and the $syt^{D\text{-}A}$ human families present with such similar symptoms [18, 19]. Given the severe consequences of mutating the C_2B Ca^{2+}-binding aspartate residues in animal models, it is noteworthy that the deficits seen in the affected human family are comparatively mild [18, 19].

It has been shown that Ca^{2+}-binding by the aspartate residues [10, 20, 36] as well as membrane penetration by the hydrophobic residue [34-37], both located in the C_2B domain of

synaptotagmin, are of critical importance for proper synchronous transmitter release [5, 15, 18, 19, 33, 38]. Interestingly, the proline residue investigated in this study is located directly adjacent to one of these aspartates residues. We speculate that this proline residue may provide conformational rigidity important for stabilizing the C_2B Ca^{2+}-binding pocket. By mutating the proline to a leucine, the rigid R group found in the proline residue would be lost, potentially affecting the precise conformation of the pocket and impacting the ability of the adjacent aspartate to bind Ca^{2+}. Such a mechanism could result in a decreased, albeit not demolished, ability of the C_2B domain to bind Ca^{2+}, resulting in the less severe phenotype documented here compared to both the aspartate and isoleucine mutations *in vivo* [5, 12, 18, 19, 33, 38].

In our *Drosophila P[syt$^{P\text{-}L}$]* heterozygotes, the impact of high frequency stimulation on EJP amplitude was short-lived. Thus our model system cannot provide insight into the long-lasting decrease in depression of the CMAP seen in the human patients following maximal voluntary contraction. The initial facilitation and following lack of depression observed in our *P[syt$^{P\text{-}L}$]* heterozygotes during and immediately after high frequency stimulation is predicted by the residual Ca^{2+} hypothesis for short-term plasticity [41-43]. The increase in paired pulse facilitation (Fig 4.5D) and lack of depression observed during high frequency stimulation (Fig 4.6 and 4.7) demonstrates that the *syt$^{P\text{-}L}$* mutation decreased release probability compared to wild type. Accordingly, the build-up of Ca^{2+} that occurs during high-frequency stimulation is predicted to contribute to a relatively increased release probability during and shortly after the stimulus train. As this *syt$^{P\text{-}L}$* mutation is predicted to disrupt the critical C_2B Ca^{2+}-binding pocket of synaptotagmin (Fig 4.1A-C), which is the Ca^{2+} sensor for fast, synchronous neurotransmitter release, a decrease in release probability was not unexpected. The note-worthy long-lasting potentiation of the CMAP, which can last up to 60 minutes in human *syt$^{P\text{-}L}$* patients

[19] remains unexplained; mutation of the Ca^{2+} sensor would not be predicted to cause such a long-lasting effect.

The decreasing cost and increasing availability of DNA sequencing has led to an increased incidence of genomic sequencing during patient diagnoses. This ever-increasing process will undoubtedly lead to the discovery of additional synaptic mutations and associated genetic disorders. The need for a relatively quick and cost effective method to begin elucidating the molecular mechanisms underlying these synaptic disorders is vital. Using *Drosophila* to model these newly discovered conditions in highly conserved pathways like synaptic transmission is ideal for elucidating their underlying mechanisms, as *Drosophila* provide a cost-effective and rapid mechanism for analysis.

In summary, we have identified the functional role of a predicted leucine-induced conformational change in the C_2B Ca^{2+}-binding pocket of synaptotagmin. Expression of the homologous human mutation in *Drosophila* resulted in deficits similar to many of the human symptoms. Thus, this work supports a role for this synaptotagmin point mutation in disease etiology and elucidates the molecular mechanisms responsible.

4.5 Conclusion

In this study, we investigate the functional role of a synaptotagmin 2 residue implicated in disease. Recently, a neuromuscular disorder has been reported in which a highly conserved proline residue is mutated to a leucine within synaptotagmin. The functional importance of this residue was unknown. Here we model the impact of this mutation on the structure of synaptotagmin and examine the effects of a homologous mutation *in vivo* using *Drosophila*. We found that this mutation is predicted to produce a conformational change in the C_2B domain of

synaptotagmin that would decrease Ca^{2+} binding. When expressed in flies containing no synaptotagmin, this mutation was lethal, demonstrating the critical nature of the examined residue. When expressed in combination with wild type synaptotagmin, we demonstrated a decreased Ca^{2+} affinity for neurotransmitter release and a decreased release probability. These deficits can account for the defects in neuromuscular function and behavior, which are similar to those of the human patients. Thus, these results support a role for this amino acid substitution in human disease etiology.

4.6 Materials and Methods

Mutagenesis

In *Drosophila*, the *syt1* gene is expressed in all neurons [24, 25] and is homologous to both *syt1* and *syt2* in mammals [22]. Proline residue 363 of *Drosophila syt1* is homologous to proline 308 in human *syt2*, implicated in the human disease, and proline 310 in rat *syt1*, modeled in Fig 4.1. Using the *Drosophila syt1* coding sequence [44, 45], both a wild type control and a P363L mutant cDNA flanked by EcoRI and BglII restriction sites were synthesized by GeneWiz (La Jolla, CA). The synthesized cDNAs were then subcloned into the PUAST-attB vector to place the transgenes under the control of the UAS promoter and the PhiC31 targeted insertion system was used to target the transgene containing vectors to the attP2 landing site on the *Drosophila* third chromosome [BestGene, Chino Hills, CA; [46, 47]]. We refer to the mutant transgene as $P[syt^{P\text{-}L}]$ and the control transgene as $P[syt^{WT}]$.

Fly lines

Expression of the UAS-driven *syt* transgenes was localized to the nervous system using a pan-neuronal source of GAL4 [*elavGAL4* [48, 49]]. Syt^{AD4} was the syt^{null} mutation used [45]. Synaptotagmin is found natively on the second chromosome, and the *syt* transgene used was incorporated into a third chromosome landing site. To directly assess the function of the $syt^{P\text{-}L}$ mutation, the impact of transgene expression on survival was assessed in the syt^{null} background. For these experiments, the following genotype $yw;syt^{null}P[elavGal4w^{+}]/CyO,GFPw^{+}$ was crossed to $yw;syt^{null}/CyO,GFP;P[UASsyt^{WT},y^{+}w^{+}]$ or $yw;syt^{null}/CyO,GFP;P[UASsyt^{P\text{-}L}\ y^{+}w^{+}]$ or $yw;syt^{null}/CyO,GFP$ to generate: 1) the transgenic control in the syt^{null} background $yw;syt^{null}P[elavGAL4w^{+}]/syt^{null};P[UASsyt^{WT}y^{+}w^{+}]/+$ (referred to as *-/-; P[*syt^{WT}*]/+*), 2) the transgenic mutant in the syt^{null} background, $yw;syt^{null}P[elavGAL4w^{+}]/syt^{null};P[UASsyt^{P\text{-}L}y^{+}w^{+}]/+$ (referred to as *-/-;P[*$syt^{P\text{-}L}$*]/+*), and 3) syt^{null} mutants, $yw;syt^{null}P[elavGAL4w^{+}]/syt^{null}$ (referred to as -/-), respectively. Expression of the mutant transgene resulted in embryonic or first instar lethality. Therefore, for most experiments, the *P[*$syt^{P\text{-}L}$*]* transgene was expressed in a *syt* heterozygous background in order to mimic the heterozygous nature of the affected human population ($syt^{P\text{-}L}/syt^{WT}$). This results in synaptotagmin expression from a single copy of the endogenous *syt* gene and from a single copy of the mutant *syt* transgene. For these experiments, the following genotype $yw;syt^{null}P[elavGal4w^{+}]/CyO,GFPw^{+}$ was crossed to $yw;+;P[UASsyt^{P\text{-}L}y^{+}w^{+}]$ or $yw;+;P[UASsyt^{WT}\ y^{+}w^{+}]$ (note: both of these transgenic lines are homozygous for syt^{WT} on the second chromosome) to generate: 4) the transgenic mutant in the *syt* heterozygous background, $yw;syt^{null}P[elavGAL4w^{+}]/syt^{WT};P[UASsyt^{P\text{-}L}y^{+}w^{+}]/+$ (labeled as *+/-;P[*$syt^{P\text{-}L}$*]/+* in the figures and referred to as *P[*$syt^{P\text{-}L}$*]* heterozygotes in the text), and 5) the transgenic control in the *syt*

heterozygous background, *yw;syt^{null}P[elavGAL4w^{+}]/syt^{WT};P[UASsyt^{WT}y^{+}w^{+}]/+* (labeled as *+/-;P[syt^{WT}]/+* in the figure legends and referred to as *P[syt^{WT}]* heterozygotes in the text). For western analyses, the additional genotypes used for comparisons were: 6) *syt* heterozygotes, *yw; syt^{null}/syt^{WT};P[UASsyt$^{P\text{-}L}$y^{+}w^{+}]/+* (labeled as +/- in Fig 4.2A), and 7) *syt* homozygotes, *yw; syt^{WT}/syt^{WT};P[UASsyt$^{P\text{-}L}$y^{+}w^{+}]/+* (labeled as +/+ in Fig 4.2B). The experimental *syt* heterozygotes (+/- in Fig 4.2A) and homozygotes (+/+ in Fig 4.2B) both contained the *P[syt$^{P\text{-}L}$]* transgene but lack the *elavGal4w^{+}* driver, so the transgene was not expressed.

Molecular Dynamics

As the crystal structures of mammalian synaptotagmin 2 proteins have not been solved, we obtained the crystal structures of rat syt1 C_2B (PDB file 1TJX) [21] from the Protein Data Bank. The C_2B domains of mammalian synaptotagmin 1 and synaptotagmin 2 are >90% identical (8 substitutions in the core of 93 C_2B residues) and most of these substitutions are conservative. We generated models of the P-L mutation using the mutagenesis wizard in Pymol Molecular Graphics System, Version 1.8, Schrödinger, LLC. The QuikMD utility in NAMD [50] was used for the simulation. The structures were solvated using the solvate TCL utility in a cube of approximately 7,000 water molecules (TIP3) with a positive and negative padding of 10 Å on each axis. Residue 359 in C_2B was restrained with harmonic constraints to dampen coordinate drift within the simulation box. Both wild type and mutant C_2B models were simulated using NAMD [50] with different random seeds for 50,000,000 frames with a time step of two femtoseconds (total of 100 ns) and a write frequency of 25,000. Periodic boundary conditions were used with PME and a grid spacing of 1.0. We used rigid bonds and constant group pressure control. The pressure was controlled with a Langevin piston set at 1.01325 bar (atmospheric

pressure). The temperature was controlled at 310 K with Langevin dynamics and a dampening coefficient of 5 ps^{-1} was applied to each trajectory. We validated that the trajectories reached equilibrium by calculating the root mean squared displacements of all atoms in the protein after alignment over the course of the run. Each unique simulation setup was run three times.

Lethality assay

The only source of synaptotagmin from the native locus (syt^{WT}) in the crosses used to assess the effect of transgene (*P[syt]*) expression was located on the *CyO,GFP* balancer chromosome (see fly lines section above). Therefore, any progeny that were homozygous for native synaptotagmin are categorized as unhatched since they are also homozygous for *Cy*, which is embryonic lethal (Table 1, S1 File). Based on Mendelian genetics, the expected frequency is ~25% (S1 File). At least three bottle crosses using at least 50 virgin females each were fed on molasses plates supplemented with a dab of yeast/baby food mixture and were left to mate for two days. A fresh molasses plate dabbed with yeast/baby food mixture was then provided and the flies were allowed to lay eggs for 6 hours to provide age-matched progeny. A total of 4476 eggs were collected and observed. First instar progeny were then scored by phenotype, and the number of unhatched eggs was counted. The plates were observed daily for three consecutive days to control for any developmental delays. A chi-squared test between the three genotypes was applied to reject the test of independence. Additional chi-square tests were applied to test for differences between *-/-;P[*syt^{WT}*]/+* and *-/-;P[*$syt^{P\text{-}L}$*]/+*, as well as between *-/-* and *-/-;P[*$syt^{P\text{-}L}$*]/+*.

Immunoblotting

Western analysis of larval CNSs was used to determine relative levels of synaptotagmin expression. The CNS was isolated from third instars dissected in Ca^{2+}-free HL3.1 containing 70 mM NaCl, 5 mM KCl, 4 mM $MgCl_2$, 10mM $NaHCO_3$, 5 mM Trehalose, 115 mM sucrose, 5 mM HEPES, pH 7.2 [51]. Samples were sonified for 10 pulses using a Branson Sonifier 450 (VWR Scientific, Westchester, PA) in Laemmli buffer (Bio-Rad, Hercules, CA) containing 5% 2-mercaptoethanol. The indicated genotype was loaded one CNS per lane. Samples were electrophoresed, transferred to Immobilon membranes (Millipore, Bedford, MA), and washed in blocking solution according as described [32]. Blots were probed overnight at 4°C with an anti-synaptotagmin antibody, Dsyt-CL1 [5], diluted 1:2500 and an anti-actin antibody, MAB 1501 (Millipore Bioscience Research Reagents, Billerica, MA), diluted 1:10,000. Actin levels were used to normalize for equal protein loading. Blots were visualized using an EpiChemi^3 Darkroom and Labworks Imaging software (UVP BioImaging, Upland, CA). The synaptotagmin:actin ratio was determined for each lane, then normalized to the mean synaptotagmin:actin ratio of all control lanes on an individual blot to allow comparison of signal between multiple blots. Outliers in total protein loaded (as indicated by actin levels) were not included in the analysis. Statistical significance for each comparison was determined using a student's t-test.

Immunolabeling

For immunolabeling of the neuromuscular junction, third instars of *P[syt^{WT}]* heterozygotes and *P[syt$^{P\text{-}L}$]* heterozygotes were dissected in Ca^{2+}-free HL3.1 saline to expose their body wall muscles and fixed in phosphate-buffered saline (PBS, 137 mM NaCl, 1.5 mM KH_2PO_4, 2.7 mM KCl, 8.1 mM Na_2HPO_4) containing 2% formaldehyde for 1 hour. Whole-

mounts were incubated overnight in Dsyt-CL1 diluted 1:400 in dilution media [PBS with 0.1% Triton, 1% bovine serum albumin, and 1% normal goat serum (NGS from Jackson ImmunoResearch, West Grove, PA)], washed in PBST (PBS with 0.1% Triton) for 3 hours, incubated in Alexa Fluor 488 goat-anti-rabbit antibody (Invitrogen, Carlsbad, CA) diluted 1:400 and Texas Red anti-HRP (Jackson ImmunoResearch, West Grove, PA) diluted 1:50 in dilution media for 1 hour, washed in PBST for 1 hour, and mounted in Citifluor (Ted Pella, Redding, CA). To label transgenic synaptotagmin expressed in the syt^{null} background, the above protocol was applied to first instars rather than third instars with the following changes: first instars were fixed in PBS containing 4% formaldehyde for 2 hours and Texas Red anti-HRP was omitted. Neuromuscular junctions at the muscle 6/7 junction were imaged for both first and third instars with a Zeiss 880 light scanning microscope using a 40X objective, and acquired using Zeiss Zen 2.1 acquisition software, version 11,0,3,190.

Longevity Assay

Lifespans between *+/-;P[syt^{WT}]/+* and *+/-;P[syt$^{P\text{-}L}$]/+* were recorded from at least three separate crosses using at least 50 virgins in each cross. Lenth's analysis was used to determine adequate sample size. N = 151 for *+/-;P[syt^{WT}]/+* and n = 149 for *+/-;P[syt$^{P\text{-}L}$]/+*. Ten newly hatched adult flies/vial were observed/flipped into fresh food every Monday/Wednesday/Friday and number of living or dead flies were recorded. Flies that were found alive but stuck in the food were omitted from analysis. Any flies that escaped during flipping were also omitted from analysis, as there was no way to determine the length of natural life. The Wilcoxon (two-sample) Rank-Sum test was used to determine significance between genotypes.

Excitatory Junction Potentials

Third instars were dissected in Ca^{2+}-free HL3.1 saline. EJPs were evoked from muscle fiber 6 of abdominal segments 3 and 4 in HL3.1 containing 1.0 mM Ca^{2+} using standard techniques [26, 32, 38]. Intracellular electrodes of 10–25 MΩ contained 3 parts 2M potassium citrate to 1 part 3M potassium chloride. The resting membrane potential of each fiber was maintained at -55 mV by passing no more than 1 nA of current. Nerves were stimulated with a suction electrode filled with HL3.1 containing 1.0 mM Ca^{2+}. All events were collected using an AxoClamp 2B (Molecular Devices, Sunnyvale, CA) amplifier and digitized using a Powerlab 4/35 A/D converter (ADInstruments, Sydney, Australia). EJPs were recorded in LabChart software (ADInstruments, Sydney, Australia). For single evoked responses, averages of 10 EJPs collected at 0.04 Hz were calculated for each individual fiber. Statistical significance was determined using a student's t-test. Spontaneous events were identified manually after recordings had been randomized and blinded to the researcher. Average mEJP amplitudes were determined from 50 consecutive mEJP events/fiber, taken from consistent time periods across fibers. Statistical significance for mEJP amplitude was determined by the Wilcoxon Rank-Sum test. Frequency of spontaneous events was determined by manually counting number of mEJP events during one minute of baseline activity/fiber. Each fiber was analyzed for the same time period during the recording to eliminate bias.

Ca^{2+} dependence of release

Individual fibers were bathed in HL3.1 saline containing Ca^{2+} levels varying from 0.05 mM – 5.0 mM. Each fiber was recorded in at least three different [Ca^{2+}] to be included in analysis. At each [Ca^{2+}], the mean response of 5 EJPs collected at 0.5 Hz were calculated. Lines

of best fit were calculated using a nonlinear regression analysis, which provided EC_{50} values and their confidence intervals for each genotype.

Paired pulse

Experiments were conducted using a 0.02 second delay between stimulations, and averages of EJP responses were normalized to the first stimulation. Statistical significance was determined using a student t-test.

High frequency stimulation

Assays to observe depression or facilitation were first assessed by stimulating the nerve at 10 Hz for 2 seconds followed by a test pulse 60 sec post-stimulus train. EJP amplitudes were normalized to that of the first EJP prior to calculating the average response within a genotype. A repeated measures analysis of variance was used to compare the two genotypes at each stimulus. Post-hoc t-tests were then used to determine significance. To more closely mimic maximal voluntary contraction at the human neuromuscular junction, another protocol was designed using 50 Hz stimulation for 2 seconds, followed by test pulses at 1 second post-stimulus train, and then at 30 second intervals to 4 minutes. Similar statistical methods as above were applied to determine significant differences between amplitudes at each individual time point.

Hypertonic solution stimulations

A PicoSpritzer III was used to administer a puff application of either 0.5M sucrose or HL3.1 bath solution to the junctional region of muscle fibers 6 at 5 pounds per square inch (psi) for 10 seconds. Hypertonic stimulations were conducted in Ca^{2+}-free HL3.1. mEJP events were

counted manually for all time points analyzed. To determine baseline mEJP frequency, 10 seconds of mEJP events immediately prior to sucrose or HL3.1 application were analyzed. To determine average mEJP frequency during maximum sucrose stimulation, 15 seconds of mEJP events were analyzed, beginning 5 seconds into the sucrose or HL3.1 application. Statistical significance was determined by student t-tests.

For all electrophysiological experiments, post-hoc Lenth's analyses were performed to ensure adequate sample size. If fibers were unable to maintain a physiological potential when injected with a maximum of 1 nA of current, they were excluded.

Drosophila Activity Monitoring

The basal locomotor activity of adult *Drosophila* was assessed using the TriKinetics Locomotor Activity Monitoring System (Trikinetics, Waltham, MA). Age-matched 5-7 day old adult flies of the indicated genotypes were loaded into DAM2 *Drosophila* activity monitors. Males and females were tested separately to control for sex differences in circadian rhythms [29, 30]. Animals were placed on a 12hr light: 12hr dark cycle on standard fly food media and activity was recorded for 7 days using DAM system Acquisition Software. Data from the first day were not included in the analysis to allow flies to acclimate to their new environment. Activity levels were binned into 30-minute intervals and uploaded into Microsoft Excel using DAM Filescan software. Using these 30-minute intervals, an averaged 24-hour day was created for each genotype and sex. Four distinct activity periods were determined post-hoc that correspond to *Drosophila*'s two anticipatory peaks (Active 1 and 2), a lights-on active period (Active 3), and a lights off-inactive period (Inactive). T-tests were performed to compare genotypes during each activity period for both males and females. Flies that died during the

course of the experiment were excluded from the analysis. Post-hoc Lenth's analysis was performed to ensure adequate sample size.

Fatigability assay

To assess fatigue, a modified negative geotaxis assay was used [31]. For each genotype, 10 un-anesthetized, sex- and age-matched 5-7 day old adult flies were loaded by aspiration into a 9 cm tall standard *Drosophila* vial. Flies were not exposed to CO_2 to avoid possible side effects and were left to acclimate for 1 hour. Experimental and control vials were secured side by side in a vial rack, raised 6-8 inches above a table, and then dropped, causing all flies to fall to the bottom of the vial. Vials were dropped every 10 seconds for 30 minutes, and a picture was recorded 5 seconds after every drop. Each picture was analyzed in ImageJ for the distance each fly had traveled up the side of the vial. The average for each sex and genotype was calculated for each picture, and the data was binned into 1 minute averages. To control for any genotype-dependent decrease in mobility and thereby specifically assess fatigue, all average distances were normalized to the average distance traveled after the first drop. Linear regressions of the log of the raw data provided predicted lines of best fit for each sex and genotype. A significant interaction between time and genotype (for both sexes) in the log of the raw data indicates that there is a difference between the slopes for the two genotypes. Fitted curves, after back transformation, are shown in Fig 4.9. Post-hoc Lenth's analysis was performed to ensure adequate sample size.

WORKS CITED

1. Shields, M.C., et al., *Drosophila studies support a role for a presynaptic synaptotagmin mutation in a human congenital myasthenic syndrome.* PLoS One, 2017. **12**(9): p. e0184817.
2. DiAntonio, A. and T.L. Schwarz, *The effect on synaptic physiology of synaptotagmin mutations in Drosophila.* Neuron, 1994. **12**(4): p. 909-20.
3. Littleton, J.T., et al., *Calcium dependence of neurotransmitter release and rate of spontaneous vesicle fusions are altered in Drosophila synaptotagmin mutants.* Proc Natl Acad Sci U S A, 1994. **91**(23): p. 10888-92.
4. Geppert, M., et al., *Synaptotagmin I: a major Ca2+ sensor for transmitter release at a central synapse.* Cell, 1994. **79**(4): p. 717-27.
5. Mackler, J.M., et al., *The C(2)B Ca(2+)-binding motif of synaptotagmin is required for synaptic transmission in vivo.* Nature, 2002. **418**(6895): p. 340-4.
6. Nishiki, T. and G.J. Augustine, *Synaptotagmin I synchronizes transmitter release in mouse hippocampal neurons.* J Neurosci, 2004. **24**(27): p. 6127-32.
7. Chapman, E.R., *How does synaptotagmin trigger neurotransmitter release?* Annu Rev Biochem, 2008. **77**: p. 615-41.
8. Brose, N., et al., *Synaptotagmin: a calcium sensor on the synaptic vesicle surface.* Science, 1992. **256**(5059): p. 1021-5.
9. Sutton, R.B., et al., *Structure of the first C2 domain of synaptotagmin I: a novel Ca2+/phospholipid-binding fold.* Cell, 1995. **80**(6): p. 929-38.
10. Fernandez, I., et al., *Three-dimensional structure of the synaptotagmin 1 C2B-domain: synaptotagmin 1 as a phospholipid binding machine.* Neuron, 2001. **32**(6): p. 1057-69.
11. Robinson, I.M., R. Ranjan, and T.L. Schwarz, *Synaptotagmins I and IV promote transmitter release independently of Ca(2+) binding in the C(2)A domain.* Nature, 2002. **418**(6895): p. 336-40.
12. Yoshihara, M., Z. Guan, and J.T. Littleton, *Differential regulation of synchronous versus asynchronous neurotransmitter release by the C2 domains of synaptotagmin 1.* Proc Natl Acad Sci U S A, 2010. **107**(33): p. 14869-74.
13. Striegel, A.R., et al., *Calcium binding by synaptotagmin's C2A domain is an essential element of the electrostatic switch that triggers synchronous synaptic transmission.* J Neurosci, 2012. **32**(4): p. 1253-60.
14. Tucker, W.C., T. Weber, and E.R. Chapman, *Reconstitution of Ca2+-regulated membrane fusion by synaptotagmin and SNAREs.* Science, 2004. **304**(5669): p. 435-8.
15. Nishiki, T. and G.J. Augustine, *Dual roles of the C2B domain of synaptotagmin I in synchronizing Ca2+-dependent neurotransmitter release.* J Neurosci, 2004. **24**(39): p. 8542-50.
16. Ullrich, B., et al., *Functional properties of multiple synaptotagmins in brain.* Neuron, 1994. **13**(6): p. 1281-91.
17. Marqueze, B., et al., *Cellular localization of synaptotagmin I, II, and III mRNAs in the central nervous system and pituitary and adrenal glands of the rat.* J Neurosci, 1995. **15**(7 Pt 1): p. 4906-17.

18. Herrmann, D.N., et al., *Synaptotagmin 2 mutations cause an autosomal-dominant form of lambert-eaton myasthenic syndrome and nonprogressive motor neuropathy.* Am J Hum Genet, 2014. **95**(3): p. 332-9.
19. Whittaker, R.G., et al., *Electrophysiologic features of SYT2 mutations causing a treatable neuromuscular syndrome.* Neurology, 2015. **85**(22): p. 1964-71.
20. Sutton, R.B., J.A. Ernst, and A.T. Brunger, *Crystal structure of the cytosolic C2A-C2B domains of synaptotagmin III. Implications for Ca(+2)-independent snare complex interaction.* J Cell Biol, 1999. **147**(3): p. 589-98.
21. Cheng, Y., et al., *Crystallographic identification of Ca2+ and Sr2+ coordination sites in synaptotagmin I C2B domain.* Protein Sci, 2004. **13**(10): p. 2665-72.
22. Lloyd, T.E., et al., *A genome-wide search for synaptic vesicle cycle proteins in Drosophila.* Neuron, 2000. **26**(1): p. 45-50.
23. Adolfsen, B., et al., *Synaptotagmins are trafficked to distinct subcellular domains including the postsynaptic compartment.* J Cell Biol, 2004. **166**(2): p. 249-60.
24. Littleton, J.T., H.J. Bellen, and M.S. Perin, *Expression of synaptotagmin in Drosophila reveals transport and localization of synaptic vesicles to the synapse.* Development, 1993. **118**(4): p. 1077-88.
25. DiAntonio, A., et al., *Identification and characterization of Drosophila genes for synaptic vesicle proteins.* J Neurosci, 1993. **13**(11): p. 4924-35.
26. Loewen, C.A., J.M. Mackler, and N.E. Reist, *Drosophila synaptotagmin I null mutants survive to early adulthood.* Genesis, 2001. **31**(1): p. 30-6.
27. Dodge, F.A. and R. Rahamimoff, *Co-operative action of calcium ions in transmitter release at the neuromuscular junction.*
28. Bellemare, F., et al., *Motor-unit discharge rates in maximal voluntary contractions of three human muscles.* J Neurophysiol, 1983. **50**(6): p. 1380-92.
29. Helfrich-Forster, C., *Differential control of morning and evening components in the activity rhythm of Drosophila melanogaster--sex-specific differences suggest a different quality of activity.* J Biol Rhythms, 2000. **15**(2): p. 135-54.
30. Vrailas-Mortimer, A.D., et al., *p38 MAP kinase regulates circadian rhythms in Drosophila.* J Biol Rhythms, 2014. **29**(6): p. 411-26.
31. Gargano, J.W., et al., *Rapid iterative negative geotaxis (RING): a new method for assessing age-related locomotor decline in Drosophila.* Exp Gerontol, 2005. **40**(5): p. 386-95.
32. Mackler, J.M. and N.E. Reist, *Mutations in the second C2 domain of synaptotagmin disrupt synaptic transmission at Drosophila neuromuscular junctions.* J Comp Neurol, 2001. **436**(1): p. 4-16.
33. Baker, K., et al., *Identification of a human synaptotagmin-1 mutation that perturbs synaptic vesicle cycling.* J Clin Invest, 2015. **125**(4): p. 1670-8.
34. Bai, J., P. Wang, and E.R. Chapman, *C2A activates a cryptic Ca(2+)-triggered membrane penetration activity within the C2B domain of synaptotagmin I.* Proc Natl Acad Sci U S A, 2002. **99**(3): p. 1665-70.
35. Arac, D., et al., *Close membrane-membrane proximity induced by Ca(2+)-dependent multivalent binding of synaptotagmin-1 to phospholipids.* Nat Struct Mol Biol, 2006. **13**(3): p. 209-17.
36. Martens, S., M.M. Kozlov, and H.T. McMahon, *How synaptotagmin promotes membrane fusion.* Science, 2007. **316**(5828): p. 1205-8.

37. Hui, E., et al., *Synaptotagmin-mediated bending of the target membrane is a critical step in Ca(2+)-regulated fusion.* Cell, 2009. **138**(4): p. 709-21.
38. Paddock, B.E., et al., *Membrane penetration by synaptotagmin is required for coupling calcium binding to vesicle fusion in vivo.* J Neurosci, 2011. **31**(6): p. 2248-57.
39. Yao, J., et al., *Uncoupling the roles of synaptotagmin I during endo- and exocytosis of synaptic vesicles.* Nat Neurosci, 2011. **15**(2): p. 243-9.
40. Perin, M.S., et al., *Phospholipid binding by a synaptic vesicle protein homologous to the regulatory region of protein kinase C.* Nature, 1990. **345**(6272): p. 260-3.
41. Katz, B. and R. Miledi, *The role of calcium in neuromuscular facilitation.* J Physiol, 1968. **195**(2): p. 481-92.
42. Regehr, W.G., *Short-term presynaptic plasticity.* Cold Spring Harb Perspect Biol, 2012. **4**(7): p. a005702.
43. Jackman, S.L. and W.G. Regehr, *The Mechanisms and Functions of Synaptic Facilitation.* Neuron, 2017. **94**(3): p. 447-464.
44. Perin, M.S., et al., *Structural and functional conservation of synaptotagmin (p65) in Drosophila and humans.* J Biol Chem, 1991. **266**(1): p. 615-22.
45. DiAntonio, A., K.D. Parfitt, and T.L. Schwarz, *Synaptic transmission persists in synaptotagmin mutants of Drosophila.* Cell, 1993. **73**(7): p. 1281-90.
46. Groth, A.C., et al., *Construction of transgenic Drosophila by using the site-specific integrase from phage phiC31.* Genetics, 2004. **166**(4): p. 1775-82.
47. Bischof, J., et al., *An optimized transgenesis system for Drosophila using germ-line-specific phiC31 integrases.* Proc Natl Acad Sci U S A, 2007. **104**(9): p. 3312-7.
48. Brand, A.H. and N. Perrimon, *Targeted gene expression as a means of altering cell fates and generating dominant phenotypes.* Development, 1993. **118**(2): p. 401-15.
49. Yao, K.M. and K. White, *Neural specificity of elav expression: defining a Drosophila promoter for directing expression to the nervous system.* J Neurochem, 1994. **63**(1): p. 41-51.
50. Phillips, J.C., et al., *Scalable molecular dynamics with NAMD.* J Comput Chem, 2005. **26**(16): p. 1781-802.
51. Feng, Y., A. Ueda, and C.F. Wu, *A modified minimal hemolymph-like solution, HL3.1, for physiological recordings at the neuromuscular junctions of normal and mutant Drosophila larvae.* J Neurogenet, 2004. **18**(2): p. 377-402.

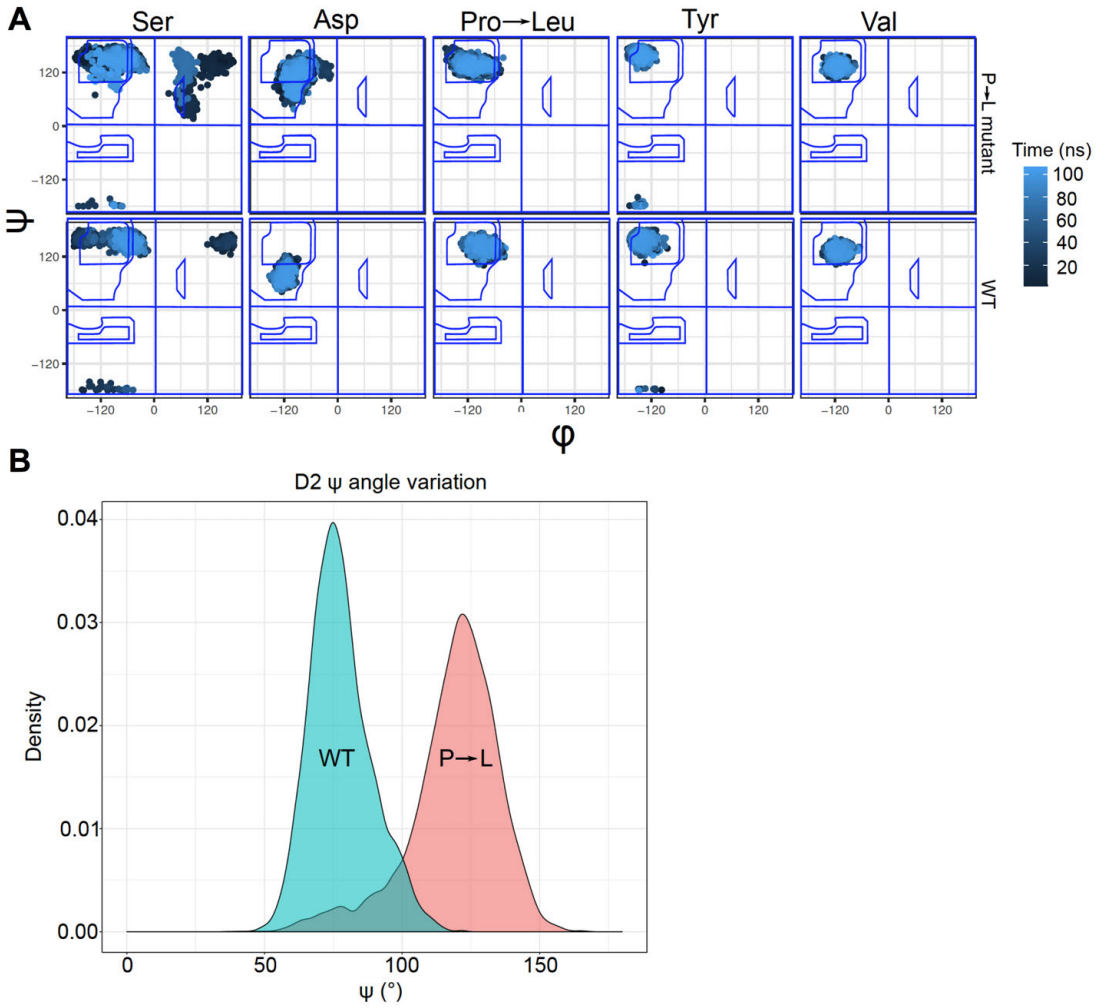

Fig S4.1. Molecular modeling predicts conformational changes in the C_2B Ca^{2+}-binding domain of synaptotagmin. (A) Dynamic Ramachandran Plot of the residues surrounding the P-L mutation in *syt* C_2B. The top panels are taken from the trajectories from the P-L simulations. The bottom panels are taken from the wild type *syt1* C_2B simulations. Each dot in each plot represents a time progression from 0 – 100 ns. Zero ns being the darkest spot and 100 ns being the bluest. Standard Ramachandran boundaries for alpha and beta secondary structure are provided. (B) Histogram showing the range and variation of phi angles of the D2 aspartate residue in wild type and the P-L mutation throughout the 100 ns molecular dynamics trajectories.

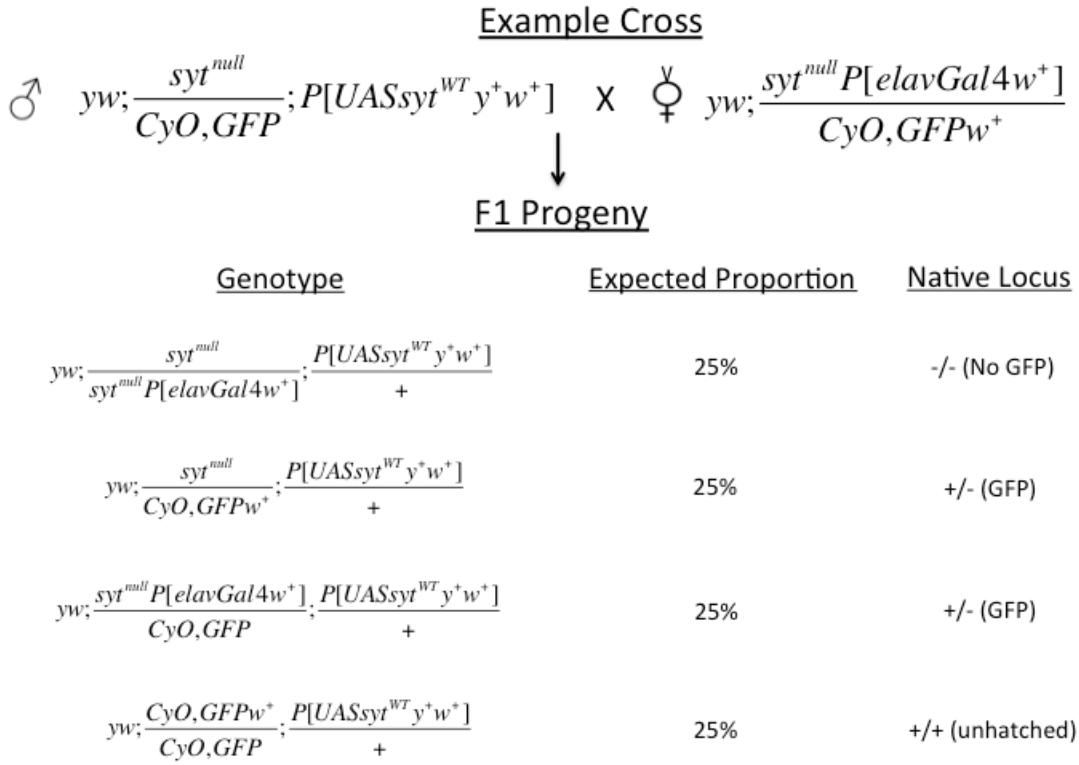

Fig S4.2. Example cross used for lethality assay in *syt*^{null} background. Potential F1 progeny are shown with the expected Mendelian distribution of each genotype, and identification of null, heterozygotes, and homozygotes at the native locus. Due to the use of the CyO balancer, ~25% of F1 progeny in control crosses (*syt* homozygotes at the native locus) are expected to remain unhatched, as they are also homozygous for Cy, which is embryonic lethal. The remaining progeny should present as ~25% lacking GFP (*syt*^{null} at the native locus) and ~50% GFP (*syt* heterozygotes at the native locus).

APPENDIX 2: SUPPLEMENTAL TABLES

Table S4.1. *P[syt^{P-L}]* heterozygotes exhibit decreased EJP amplitudes at most [Ca^{2+}]. Table providing p-values for each [Ca^{2+}] tested in Fig 4.5. *depicts statistical significance.

	+/-;P[syt^{WT}]/+			*+/-;P[syt^{P-L}]/+*			
[Ca^{2+}] (mM)	Mean EJP (mV)	SEM	n =	Mean EJP (mV)	SEM	n =	p =
0.05	0.32	0.04	12	0.28	0.06	12	0.60
0.1	2.86	0.95	12	1.81	0.63	12	0.37
0.25	15.70	1.53	16	10.10	1.74	16	0.02*
0.5	27.17	0.98	23	18.16	1.60	22	<0.0001*
0.75	31.09	0.95	12	23.88	2.12	10	0.003*
1.0	35.52	0.50	15	28.40	1.08	16	<0.0001*
2.5	37.05	0.81	11	31.99	2.43	11	0.05*
5.0	39.63	0.69	13	33.32	2.51	12	0.02*

Table S4.2. *P[syt$^{P\text{-}L}$]* heterozygotes exhibit less synaptic depression relative to the control throughout a 10 Hz stimulation, but fail to maintain this relative increase in release upon cessation of the stimulus train. Table providing normalized mean responses, SEM, and p-values for all points tested during and after a 10 Hz stimulation train (Fig 4.6), where *p < 0.05, and **p < 0.001.

	+/-;P[syt^{WT}]/+		*+/-;P[syt$^{P\text{-}L}$]/+*		
Time	Normalized Mean	SEM	Normalized Mean	SEM	p-value
0.1	1.00	0.00	1.00	0.00	1.0
0.2	0.97	0.01	1.01	0.02	0.28
0.3	0.95	0.01	1.00	0.01	0.13
0.4	0.93	0.01	0.99	0.02	0.033*
0.5	0.92	0.01	1.01	0.03	0.0013*
0.6	0.91	0.01	0.95	0.02	0.10
0.7	0.90	0.01	0.98	0.02	0.0030*
0.8	0.89	0.01	0.96	0.03	0.0071*
0.9	0.88	0.02	0.97	0.02	0.0004**
1.0	0.87	0.02	0.94	0.03	0.0083*
1.1	0.87	0.01	0.96	0.02	0.0010*
1.2	0.88	0.01	0.97	0.03	0.0007**
1.3	0.87	0.01	0.96	0.03	0.0008**
1.4	0.87	0.01	0.95	0.02	0.0046*
1.5	0.87	0.01	0.95	0.03	0.0029*
1.6	0.87	0.01	0.96	0.03	0.0005**
1.7	0.88	0.01	0.96	0.03	0.0012*
1.8	0.88	0.01	0.95	0.03	0.0037*
1.9	0.88	0.01	0.95	0.03	0.0063*
2.0	0.87	0.01	0.96	0.03	0.0005**
62.0	0.99	0.01	1.00	0.03	0.87

Table S4.3. *P[syt$^{P\text{-}L}$]* heterozygotes do not exhibit synaptic depression during and shortly after 50 Hz stimulation, but this increase in release relative to controls is not prolonged. Table providing normalized mean responses, SEM, and p-values during and after a 50 Hz stimulation train (Fig 4.7), where **p << 0.0001, and *p < 0.01.

	+/-;P[syt^{WT}]/+		*+/-;P[syt$^{P\text{-}L}$]/+*		
Time	Normalized Mean	SEM	Normalized Mean	SEM	p-value
0	1.00	0.00	1.00	0.00	1.00
2	0.74	0.04	1.03	0.07	<<0.0001**
3	0.81	0.05	1.06	0.07	0.0012*
33	0.89	0.04	0.93	0.07	0.50
63	0.91	0.04	0.93	0.06	0.54
93	0.91	0.04	0.94	0.06	0.62
123	0.86	0.04	0.96	0.05	0.19
153	0.87	0.03	0.91	0.06	0.60
183	0.88	0.02	0.90	0.05	0.73
213	0.86	0.03	0.90	0.05	0.52
243	0.83	0.04	0.92	0.05	0.21

Table S4.4. *P[syt$^{P\text{-}L}$]* heterozygotes display decreased motor output compared to controls. Table providing mean sensor crossings and SEM acquired during the *Drosophila* Activity Monitoring assay (Fig 4.8).

		+/-;P[syt^{WT}]/+		*+/-;P[syt$^{P\text{-}L}$]/+*	
	Sex	Mean crossings /30 min	SEM	Mean crossings /30 min	SEM
Active Period 1	F M	21.97 16.70	0.43 0.45	11.71 13.91	0.31 0.38
Active Period 3	F M	9.48 2.89	0.32 0.13	5.38 1.80	0.22 0.11
Active Period 2	F M	24.06 26.38	0.35 0.55	15.54 20.96	0.27 0.42
Inactive Period	F M	3.28 5.77	0.12 0.23	1.77 4.8	0.10 0.18

APPENDIX 3: SYNAPTIC TRANSMISSION CHAPTER IN CELL PHYSIOLOGY SOURCE BOOK, 5TH EDITION[4]

I. Summary

Most communication between neurons is mediated by release of chemical signals. This release takes place at specialized structures called synapses, consisting of a presynaptic element, a synaptic cleft, a postsynaptic element, and surrounding glial cells. Presynaptic cells are specialized to transduce an electrical signal into a chemical signal through the synthesis, packaging and release of neurotransmitter. The synaptic cleft contains molecules that direct the formation of synaptic specializations, enzymes that break down neurotransmitter, and scaffolding proteins that maintain the synaptic superstructure. The postsynaptic cell is responsible for transducing the chemical signal back into an electrical response. Chemical synapses can be modulated in an activity-dependent manner, resulting in physiological, morphological, and behavioral changes

II. Introduction

Nervous system function relies upon the transmission of signals between neurons. Neurons transmit information across long distances through the nervous system by sending an electrical impulse, known as an action potential, down its axon. However, these electrical signals generally do not propagate between spatially distinct cells. To cross the gap between nerve cells, the majority of cell-to-cell signaling relies on small diffusible chemicals known as neurotransmitters. These neurotransmitters are released from active neurons in a calcium dependent manner at specialized cell-to-cell contact sites called synapses. It is important to note

[4] Authors: Mallory Shields*[,1,2], Matthew Bowers*[,1,2], Noreen Reist[1,2] *equally contributing

that direct electrical communication can occur between nerve cells through specialized structures called gap junctions. Chemical synaptic transmission is primarily unidirectional. Thus, the transmission of information required for canonical neuronal processes, such as sensation, movement, and thought, is primarily from the presynaptic cell to the postsynaptic cell. Retrograde signaling from the postsynaptic cell back to the presynaptic cell occurs, but will not be addressed in this chapter. Slower and less-directed release of chemical transmitters occurs in the autonomic nervous system and neuroendocrine pathways, including release of proteinaceous signals from large dense core vesicles. These mechanisms will not be addressed here. This chapter is focused on the Ca^{2+}-dependent, release of classical chemical neurotransmitters from an activated presynaptic neuron and their effects on their postsynaptic target.

Pioneering studies by Bernard Katz and colleagues in the 1950s first identified that the release of neurotransmitters from nerve cells at the frog neuromuscular junction occurrs via unitary packets [1-3]. These studies were foundational to the modern understanding of chemical synaptic transmission (section IV.b). In the 1960s and 1970s, experiments in rabbits and *Aplasia* demonstrated that synaptic transmission was highly plastic in response to activity by documenting changes in synaptic strength underlying changes in behavior [4-6] (section VIII). In the 1970s, extracellular molecules located in the synaptic cleft were discovered to direct the differentiation of synaptic contacts [7, 8]. Throughout the 1970-1980s, many postsynaptic receptor proteins were identified [9-15]. Essential players in the synaptic cleft began to be identified throughout the 1980s and 1990s. These include extracellular molecules such as agrin, the neural cadherins, and others [16-24]. Also in the 1980s and 1990s, the molecular identity of the presynaptic neurotransmitter release machinery was identified using a combination of

purification and cloning techniques in conjunction with clostridial neurotoxin studies [25-29]. Since then, these mechanisms have been found to be conserved at the majority of synapses.

III. Structure of the Chemical Synapse

While synaptic structure varies between cell types, many basic features are relatively conserved. This chapter will focus on generalized neuron-to-neuron synapses in the central nervous system (AF 1.1A,B) and neuron-to-muscle synapses peripherally (AF 1.1C,D). Chemical synapses possess a pool of small, clear synaptic vesicles clustered around electron dense synaptic machinery in the presynaptic cell. The pre- and postsynaptic cells are separated by a narrow space, the synaptic cleft, and are insulated by glial cells. Finally, the postsynaptic cells have defined, electron-dense domains containing receptors positioned opposite release sites.

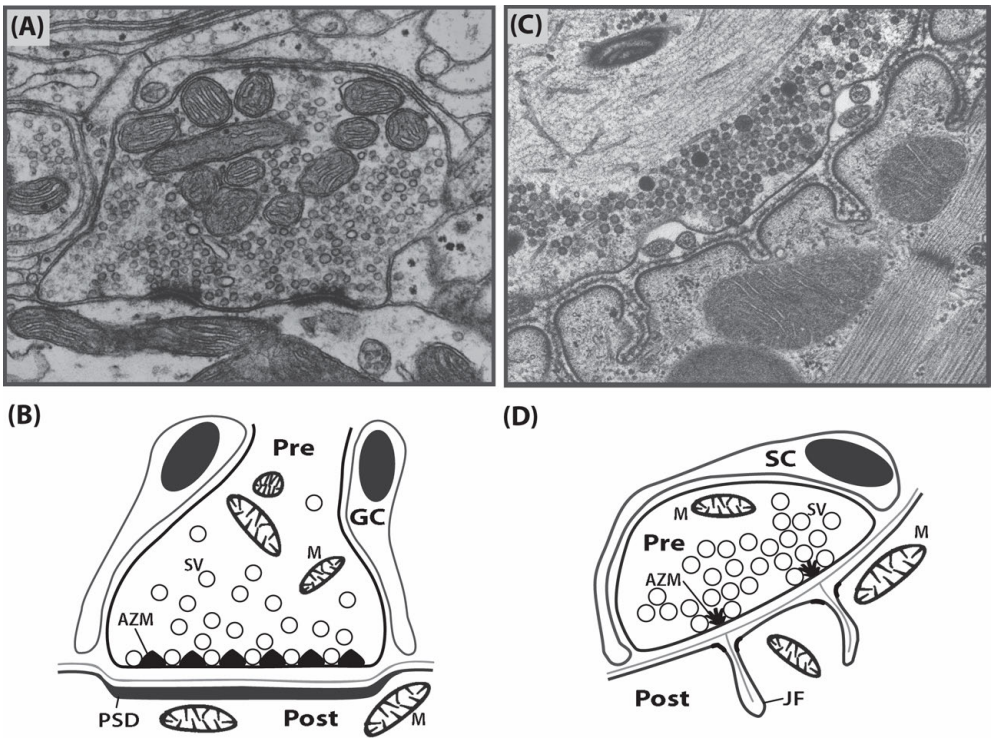

AF 1.1. Synaptic structure. (A) Electron micrograph of a synapse in the central nervous system (CNS). (B) The presynaptic (PRE) and postsynaptic (POST) neurons of a CNS synapse mediating fast synaptic transmission showing mitochondria (M) and a population of small, clear

synaptic vesicles (SV) containing neurotransmitter. Some vesicles are docked on the presynaptic membrane adjacent to dense material containing the protein machinery for vesicle fusion, active zone material (AZM). Opposite the docked vesicles and AZM, the membrane of the postsynaptic neuron appears thickened due to the presence of neurotransmitter receptors and scaffolding proteins, referred to as the postsynaptic density (PSD). Glial cells (GC) envelop and insulate the synapse. (C) Electron micrograph of a neuromuscular junction. (D) The presynaptic neuron (PRE) and postsynaptic striated muscle fiber (POST) of a neuromuscular junction showing similar mitochondria and neurotransmitter filled SVs with a subset docked adjacent to AZM. Invaginations of the postsynaptic membrane, junctional folds (JF), are found immediately opposite the AZM. Receptors for neurotransmitter and scaffolding proteins are especially concentrated near the tops of the JFs. The insulating glial cell is a Schwann Cell (SC). (Micrographs courtesy of John Heuser).

III.a. Presynaptic Structure

The presynaptic terminal is generally a distinct bouton or varicosity filled with synaptic vesicles containing small, fast-acting chemical neurotransmitters (section IV.a). Synaptic vesicles must fuse with the presynaptic membrane to release their neurotransmitters into the synaptic cleft and initiate synaptic transmission. Thus, presynaptic terminals contain the machinery required to: 1) synthesize neurotransmitter, 2) package neurotransmitter into vesicles, 3) couple incoming electrical signals with an increase in cytosolic [Ca^{2+}], 4) fuse the vesicles with the presynaptic membrane in response to this Ca^{2+} influx, and 5) recycle the vesicle membrane and associated proteins back into the presynaptic terminal to make new synaptic vesicles.

Within presynaptic terminals, vesicles are clustered at specialized fusion sites along the presynaptic membrane, called active zones [30]. Active zones consist of specialized scaffolding proteins that organize the presynaptic machinery required for the Ca^{2+}-dependent, vesicular fusion events that release neurotransmitter. Electron microscopy has shed light onto the precise structural organization at the active zone (section V.a). This organization provides precise alignment of synaptic vesicles with the fusion machinery complex and Ca^{2+} channels. This

highly ordered structure is critical for proper triggering of neurotransmitter release in response to action potentials.

III.b. Synaptic Cleft Structure

The synaptic cleft contains structural proteins that control the surface area of the synaptic interface and the proximity between the pre- and postsynaptic membranes. Synaptic cleft width is related to the type of transmission at the synapse. Small synapses, with closer apposition of the pre- and post-synaptic cells (20-50 nm), are fast acting with localized effects. Larger synapses with wide synaptic clefts can have slower time scales and a wider range of postsynaptic targets [31]. Cell-adhesion molecules and scaffolding proteins control cleft width [32]. Regulatory proteins align domains on the pre- and postsynaptic membranes and direct the organization of the pre- and postsynaptic specializations required for efficient synaptic communications [18, 33].

Other synaptic cleft molecules provide clearance of neurotransmitter. Following release, neurotransmitters must be efficiently removed to terminate the signal from the pre- to the postsynaptic cell. Neurotransmitter may be enzymatically cleaved within the cleft or removed by uptake machinery on the surface of the surrounding glial cells, the presynaptic terminal, or the postsynaptic cell (section VI).

III.c. Postsynaptic Structure

The postsynaptic cell must transduce the chemical signal of the neurotransmitter back into an electrical signal. Required specializations within the postsynaptic membrane include a high concentration of neurotransmitter receptors, regulatory molecules, and ion channels to produce the electrical signal (reviewed in [34]). The postsynaptic response may be a fast, specific

response or a slower, more generalized response. It can be excitatory (depolarizing) or inhibitory (hyperpolarizing). The postsynaptic response depends on the specific neurotransmitter receptors present in the postsynaptic membrane, which are highly variable between cell populations, but generally fall into two main categories: ionotropic and metabotropic (section VII.a). Ionotropic receptors are ligand-gated ion channels; the binding of neurotransmitter opens the channel allowing specific ions to cross the membrane. The selective permeability for specific ions determines whether the cell is depolarized or hyperpolarized. Metabotropic receptors are integral membrane proteins that bind G-proteins, called G-protein coupled receptors (GPCRs). Neurotransmitter binding to GPCRs results in activation of the coupled G-protein, triggering second messenger cascades that cause downstream secondary effects. These include opening of ion channels, posttranslational modification of proteins, or transcriptional changes.

IV. Neurotransmitters

The presynaptic element is specialized to synthesize and release neurotransmitters. The type of neurotransmitter released varies between neuron types, with many neurons releasing more than one kind of neurotransmitter. During synaptic transmission, neurotransmitter-filled synaptic vesicles undergo a stereotypical cycle: docking at active zones, priming, Ca^{2+}-triggered fusion, vesicle reformation, refilling with neurotransmitter, and trafficking back to the active zone (AF 1.2). This continuous cycle provides a constantly replenished supply of neurotransmitter ready for release.

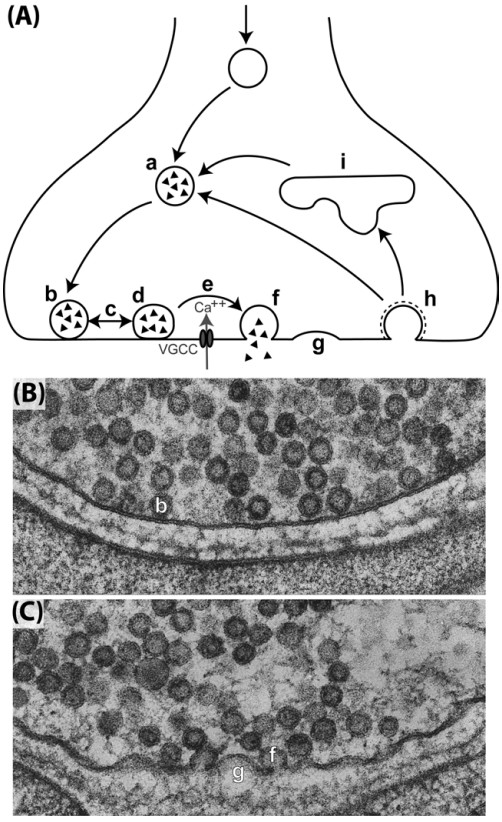

AF 1.2. The synaptic vesicle cycle. (A) Schematic of the synaptic vesicle cycle depicting vesicle loading with neurotransmitter (a), vesicle docking (b), variable vesicle priming (c), maximally-primed, docked vesicle (d), depolarization-triggered Ca^{2+} entry (e), vesicle fusion with presynaptic membrane (f), vesicle membrane collapse (g), endocytosis (h), and recycling endosome (i). (B) Electron micrograph showing docked vesicles (b) at a neuromuscular junction. (C) Electron micrograph showing fusing vesicles with omega morphology (f) and vesicle membrane collapse (g). (Micrographs courtesy of John Heuser).

IV.a. Neurotransmitter Synthesis, Loading and Clearance

To be classified as a neurotransmitter, a chemical must meet several criteria. There must be enzymatic machinery located at the synapse to synthesize the neurotransmitter. It must be released from the terminal in response to an electrical signal. Finally, there must be machinery to degrade or clear the neurotransmitter from the synaptic cleft.

The small, fast-acting neurotransmitters, shown in AT 1.1, can be grouped into a few general classes: cholinergic, amino acidergic, monoaminergic, and purinergic. While each has its

own specific synthesis, loading, and clearance machinery (reviewed in [35]), they share many common characteristics.

Vesicle loading for these neurotransmitters relies on a proton (H^+) gradient driving force. A proton pump, or vesicular-ATPase, hydrolyzes ATP to transport H^+ ions into the vesicles. Transporters for specific neurotransmitters rely on the resultant proton gradient to move neurotransmitter into the vesicle in exchange for allowing protons to exit (reviewed in [36, 37]).

AT 1.1. Table title and caption go here above the table.

Neurotransmitters and receptors			
Category	Neurotransmitter	Ionotropic receptors	Metabotropic receptors
Cholinergic	Acetylcholine	nAChR	mAChR
Amino	Glutamate	Kainate, AMPA,	mGluR
	Glycine	Gly-R	
	GABA	GABAa, GABAc	GABAb
Monoaminergic	Dopamine		D_1, D_2
	Norepinepherine		α_1, α_2, β_1, β_2
	Serotonin	5-HT_3	5-HT_1, 5-HT_2
Purinergic	ATP, Adenosine	P_{2x}	P_1, P_{2y}

Cholinergic Neurons

Cholinergic neurons synthesize and release the neurotransmitter acetylcholine (ACh). In mammals, ACh is present in the central, peripheral and autonomic nervous systems. ACh is the neurotransmitter in motor neurons that innervate skeletal muscle, making it essential for movement. It is one of two predominant transmitters in the parasympathetic division of the autonomic nervous system and is increasingly thought to play an important role in cognition. ACh is synthesized by choline acetyltransferase, which attaches choline to acetyl coenzyme A.

Acetyl coenzyme A and choline acetyltransferase are synthesized in cholinergic neurons, but choline must be transported into these neurons by a Na^+-dependent carrier. Following synthesis of ACh, the neurotransmitter is loaded into vesicles by the vesicular acetylcholine transporter using the proton gradient mentioned above. Once released, ACh is cleared from the synaptic cleft by acetylcholinesterases that hydrolyze ACh. This produces acetate and choline, much of which is recaptured by the presynaptic terminal for synthesis of new ACh (reviewed in [38, 39]).

Amino Acidergic Neurons

Amino acidergic neurons release glycine, glutamate, or gamma-aminobutyric acid (GABA), which are common neurotransmitters released broadly throughout the CNS. Neurons synthesize glycine from serine using the enzyme serine hydroxymethyltransferase. Glycine can have excitatory or inhibitory effects on the postsynaptic cell depending on the receptor types present. Following release, specific transporters sequester it into glia or back into nerve terminals. Neurons are unable to synthesize glutamate or GABA *de novo* from glucose. They rely on glutamine production in surrounding glia as sources of the precursors for neurotransmitter production and reuptake of released neurotransmitter. In glia, alpha-ketoglutaric acid of the tricarboxylic acid cycle is converted to glutamate by the enzyme transaminase. This glutamate is then converted to glutamine, which is transported to the nerve terminal. Once there, the enzyme glutaminase catalyzes the conversion of glutamine back to glutamate. GABA is generated from glutamate by the enzyme glutamic acid dehydrogenase. Once synthesized, each is loaded into synaptic vesicles, again utilizing the proton gradient. Following release, they are transported from the cleft back into the nerve terminal for reuse or into surrounding glial cells. In glial cells, the neurotransmitter is converted back to glutamine for transport back to the

presynaptic cell. This glutamine-glutamate cycle between the neuron and glial cell provides the synapse with the necessary pool of neurotransmitter (reviewed in [40, 41]).

Monoaminergic Neurons

Monoaminergic neurons release a wide array of neurotransmitters (reviewed in [42, 43]). One class, known as catecholaminergic neurons, release dopamine, norepinephrine, or epinephrine. The catecholamines are synthesized from tyrosine through multiple intermediaries. Tyrosine is initially converted to L-dihydroxyphenylalanine (L-DOPA) by tyrosine hydroxylase, the rate-limiting step in catecholamine production. L-DOPA is decarboxylated to dopamine by l-amino acid decarboxylase. In dopaminergic neurons, dopamine is loaded into vesicles via its specific monoamine transporter. In neurons that release norepinephrine, dopamine is loaded into vesicles containing the enzyme dopamine-β-hydroxylase which converts the dopamine into norepinephrine. In epinephrine-releasing neurons, norepinephrine leaks out of vesicles, where it is converted to epinephrine by the cytosolic enzyme phenolethanolamide-N-methyltransferase. This epinepherine is then loaded into its own vesicle population. Following release, dopamine, norepinephrine and epinephrine are cleared from the cleft by Na^+- and Cl^--dependent monoamine transporters that move them back into nerve terminals. In the terminal, these monoamines are either broken down by mitochondrial monoamine oxidase (MAO) or reloaded into new synaptic vesicles.

Other monoaminergic neurons release the indoleamine, serotonin. In serotonergic terminals, tryptophan-hydroxylase converts the amino acid tryptophan into 5-hydroxytryptophan, which is decarboxylated by 5-hydroxytryptophan decarboxylase to serotonin (5-hydroxytryptamine or 5-HT). Serotonin is loaded into vesicles via vesicular monoamine

transporters. Following release, serotonin is cleared from the cleft and degraded in the cytosol of the presynaptic terminal by MAO or reloaded into synaptic vesicles.

Purinergic Neurons

Purinergic neurons synthesize and release the nucleotides ATP and adenosine (reviewed in [44, 45]). ATP and adenosine are important for numerous cellular processes, and are therefore sequestered into different populations. At the synapse, they are loaded into vesicles to prevent other cellular processes from depleting the supply necessary for release. This class of neurotransmitter is often co-released with other neurotransmitters throughout the peripheral and central nervous systems. Once released, ATP and adenosine are degraded in the cleft by cell surface enzymes known as ectonucleotidases.

IV.b. Quantal Release Hypothesis

Identification of synaptic vesicles as the source of neurotransmitter release was a groundbreaking step in our understanding of synaptic transmission. Bernard Katz and his colleagues proposed the quantal release hypothesis in the early 1950s [1-3]. In pioneering electrophysiological studies at the frog neuromuscular junction, they identified spontaneous, small postsynaptic changes (AF 1.3A) that occurred in the absence of neural activity. These depolarizations resembled end plate potentials (EPPs) following an action potential (AF 1.3B), albeit on a much smaller scale. These small, spontaneous events are referred to as miniature end-plate potentials (mEPPs). Since mEPPs appeared to be random and similarly-sized (between 0.3 and 0.5 mV), this suggested neurotransmitter was being released in discrete packets, or quanta. When they evoked EPPs with presynaptic action potentials in the presence of excess Mg^{2+},

which decreases Ca^{2+} entry, the amplitude of the EPP was decreased and highly variable (AF 1.3C). Importantly, they noticed that the EPP amplitudes fell in roughly even steps, with the step height being multiples of the spontaneous mEPP amplitude. These findings led to the hypothesis that neurotransmitter was being released in multimolecular quantized packets. Furthermore, an action potential causes the synchronous release of a large number of these packets, generating a large EPP (AF 1.3B) in the postsynaptic cell. Later studies at the mammalian neuromuscular junction clearly demonstrated the step-wise distribution of EPP amplitudes under similar conditions (AF 1.3D).

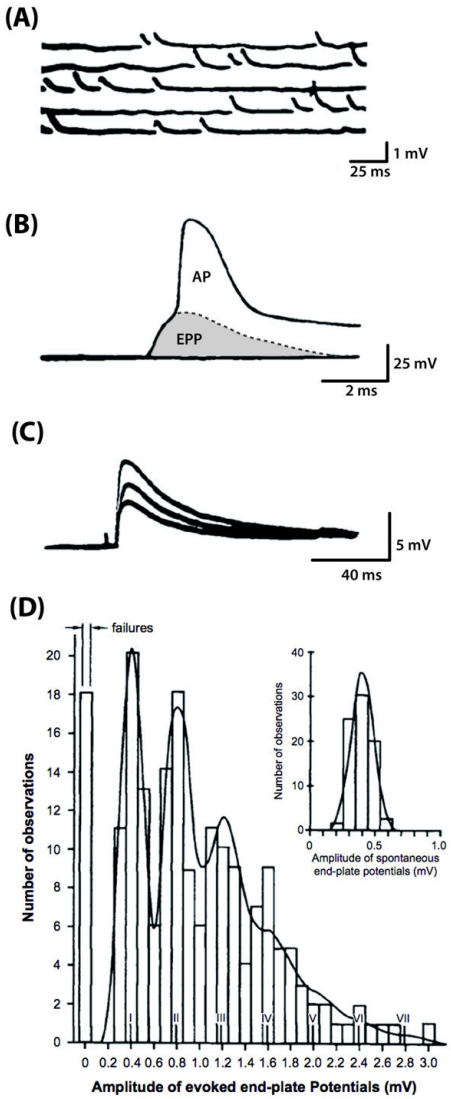

AF 1.3. Intracellular recordings at the neuromuscular junction. (A) Spontaneous, mEPPs recorded from a resting (not stimulated) frog neuromuscular junction. Note that these small depolarizing potentials are less than 1 mV in amplitude and occur randomly. (B) Postsynaptic response to a presynaptic action potential. The initial hump on the recorded waveform is the EPP elicited by ACh released from the presynaptic terminal. Note that the EPP is a large depolarization (> 40 mV), sufficient to bring the end-plate to threshold and trigger a muscle action potential (AP) (A,B adapted with permission from [2], ©1952 The Physiological Society). (C) Fluctuations in EPPs when neurotransmitter output has been reduced by adding 10 mM Mg^{2+} to the bathing medium. (C adapted with permission from [3] ©1954 The Physiological Society). (D) Distribution of EPP amplitudes recorded from a mammalian end-plate under conditions of reduced transmitter release in high (12.5 mM) Mg^{2+}. The inset shows a histogram of spontaneous mEPPs recorded from a resting junction. Note that EPP amplitudes group around multiples of mean mEPP amplitude. The number of experimentally observed failures (0 quanta released) and single, double, triple, or more quantal responses, fit the theoretical distribution (solid curve) calculated from the Poisson equation. (Adapted with permission from [46] ©1956 The Physiological Society).

The concept that synaptic transmission could be explained by the quantized release of neurotransmitter was proposed around the same time that small membranous vesicles within nerve terminals were first identified by electron microscopy [47, 48]. Together, these findings led to the vesicular hypothesis for neurotransmitter release, which states that each synaptic vesicle contains a similar amount of neurotransmitter (1 quantum), and that the transmitter release following an action potential results from a discrete number of vesicles fusing synchronously with the plasma membrane.

This hypothesis allows for neurotransmitter release at the synapse to be understood in terms of the relatively simple equation $m=np$, where m is the average number of quanta released following a single nerve impulse (referred to as quantal content). The parameter m depends on the number of vesicles immediately available for release (n) and the probability (p) that any given vesicle will fuse with the membrane after a single impulse. This probability depends on multiple factors, including how “ready” the vesicle is to fuse, which we will refer to as its degree of priming, and the amount of Ca^{2+} influx into the presynaptic terminal (see sections V.a and

V.b). Statistical analysis of neurotransmitter release extends beyond this foundational concept (reviewed in [49]).

V. Presynaptic Vesicle Cycle

As introduced above, synaptic vesicles must undergo a distinct, tightly regulated series of steps. They must be loaded with neurotransmitter (AF 1.2A.a), transported to the active zone, and docked to the presynaptic membrane by way of specific molecular interactions (AF 1.2A.b and 1.2B.b). The population of docked vesicles at a synapse is thought to constitute a readily releasable pool of neurotransmitter. However, only a subset of docked vesicles are fusion competent at any given time, namely, those that are maximally primed (AF 1.2A.d). In a resting terminal, individual maximally-primed vesicles can spontaneously fuse with the presynaptic membrane, resulting in the release of a single quantum of neurotransmitter. In an activated neuron, the influx of Ca^{2+} through voltage-gated Ca^{2+} channels (AF 1.2A.e) triggers the fusion of multiple maximally-primed vesicles with the presynaptic membrane and results in a larger release of neurotransmitter (AF 1.2A.f,g and 1.2C.f,g). This is accomplished by Ca^{2+}-sensing proteins activating the fusion machinery. Neurotransmitter release occurs in two temporally distinct Ca^{2+}-dependent phases: synchronous and asynchronous. After neurotransmitter release, the fusion machinery is disassembled and recycled for subsequent use. Concurrently, the synaptic vesicle membrane and associated proteins are retrieved through endocytosis (AF 1.2A.h) to form new synaptic vesicles. These vesicles are reloaded with neurotransmitter and transported back to active zones, completing the cycle. The proteins covered in this and subsequent sections can be found in AT 1.2.

AT 1.2. Table title and caption go here above the table.

Compartment	Protein	Function
Presynaptic	RIM	Active zone material
	Munc13	Active zone material
	RIM-BP	Active zone material
	Alpha-liprin	Active zone material
	ELKS/CAST	Active zone material
	Synaptobrevin 2	Fusion machinery
	SNAP-25	Fusion machinery
	Syntaxin	Fusion machinery
	Munc18	SM protein
	Synaptotagmin 1/2	Ca^{2+} sensor, synchronous
	Synaptotagmin 7	Ca^{2+} sensor, asynchronous
	Doc2	Ca^{2+} sensor, asynchronous
	NSF	SNARE disassembly
	Clathrin	Endocytosis
	Dynamin	Endocytosis
Synaptic Cleft	Agrin	Synaptogenesis
	MuSK	Synaptogenesis
	LRP4	Synaptogenesis
	Neuroligins	Synaptogenesis/plasticity
	Neurexins	Synaptogenesis/plasticity
	Cadherins	Scaffolding/plasticity
	Eph Tyrosine Kinases	Scaffolding/plasticity
	Epherins	Scaffolding/plasticity
Postsynaptic	Ionotropic receptors	Changes in postsynaptic potential
	Metabotropic receptors	Changes in postsynaptic potential/ second messenger cascades

V.a. The Active Zone

Functionally, the role of the active zone is to transduce an electrical nerve terminal depolarization into neurotransmitter release. Couteaux and Pecot-Dechavassinein coined the term “active zone” in 1970 when they noticed synaptic vesicles at the frog neuromuscular junction docked to the presynaptic membrane adjacent to electron dense material in electron micrographs [30]. Subsequent ultrastructural studies revealed similar morphologies across organisms. The structure of this active zone material (AZM) varies among different types of synapses, but must

include the requisite protein machinery for vesicle docking, priming, and fusion. The major constituents of active zones include: active zone core proteins, essential fusion machinery, Sec1/Munc18-like (SM) proteins, Ca^{2+} channels, and Ca^{2+} sensors. The core proteins covered in this chapter are Rab3-interacting molecules (RIM), Munc13, RIM binding protein (RIM-BP), alpha-liprin, and ELKS/CAST [50]. The essential fusion machinery consists of the soluble N-ethlymaleimide sensitive factor adaptor protein receptors, or SNAREs. The Ca^{2+}-sensing proteins covered in this chapter that trigger evoked neurotransmitter release are synaptotagmin 1, 2, 7, and double C_2 containing protein (Doc2). Numerous additional regulatory and adaptor molecules are present at or near active zones, but are not covered.

The AZM holds a cluster of synaptic vesicles near release sites, including those docked against the presynaptic membrane. The precise structure of the AZM can vary in size and shape, depending on synaptic type and/or organism. In certain visual and auditory neurons, ribbon-like structures have been observed across several species. In contrast, neuromuscular junction ultrasturcture varies across organisms. In *Drosophila,* the neuromuscular AZM has a “T-bar” shape surrounded by synaptic vesicles. At mammalian neuromuscular junctions, the AZM contains short bars of electron-dense material located on either side of two adjacent docked vesicles with additional associated vesicles above. Frog neuromuscular junctions exhibit a long midline AZM with two rows of docked vesicles on either side (see AF 1.6) surrounded by additional synaptic vesicles. Despite their differences, *Drosophila*, frog, and mammalian neuromuscular junctions share common synaptic machinery. Recent electron tomography studies at the frog and mouse neuromuscular junctions reveal similar ultrastructural AZM components [51, 52]. The molecular identity of the individual proteins comprising these structures remains an active area of synaptic research.

Active Zone Core Proteins

Some of the proteins that are located in the core of the active zone include RIM, Munc13, RIM-BP, alpha-liprin, and ELKS/CAST. Together with additional adaptor proteins, they recruit synaptic vesicles, fusion machinery, and Ca^{2+} channels to the active zone. RIM and Munc13 work together to link synaptic vesicles to active zones, as discussed below. In addition, RIM binds Ca^{2+} channels, which are concurrently bound by RIM-BP and ELKS/CAST, creating a trimeric complex essential for recruiting Ca^{2+} channels to active zones. Munc13 is additionally involved in enhancing vesicle fusion competence (see section V.b). Alpha-liprins interact with multiple proteins that regulate active zone formation [53]. They are scaffold proteins that may act as anchors to recruit and stabilize molecules at the active zone, as they are critical for recruiting RIM [54, 55] and trafficking synaptic vesicles [56]. Studies in invertebrates suggest a role for alpha liprin in active zone morphogenesis as mutants exhibit larger, less dense active zones [57]. The invertebrate homolog of ELKS/CAST is implicated in active zone cytoskeletal formation [58] and Ca^{2+} channel recruitment [59].

Fusion Machinery

The minimum machinery required to fuse a vesicle with its target membrane is the SNARE fusion complex, which is comprised of a vesicle-associated SNARE protein (vSNARE) and target-membrane associated SNARE proteins (tSNAREs). At the synapse, the vSNARE is synaptobrevin-2, also known as vesicle-associated membrane protein 2 (VAMP2) and the tSNAREs are syntaxin-1 and synaptosomal-associated protein of 25 kDa (SNAP-25) (AF 1.4).

Each SNARE protein contains at least one SNARE motif of ~65 residues with a propensity to form coiled coils [60]. Synaptotobrevin and syntaxin each contain one SNARE

motif, and SNAP-25 contains two [61]. Prior to vesicle docking, syntaxin is found in a stable, closed conformation, with its SNARE motif bound to an internal three-helix-bundle regulatory domain, making it inaccessible for interactions with other SNARE proteins [62]. Syntaxin undergoes a conformational change triggered by Munc13 (see section V.b), which allows its SNARE motif to interact with the SNARE motifs of synaptobrevin and SNAP-25. This creates a *trans*-SNARE complex which is associated with both the vesicular membrane and the presynaptic plasma membrane. On any given vesicle, tight coiling of multiple SNARE complexes [63] provides the energy required to drive fusion of the vesicle and target membranes (AF 1.4) [64, 65]. Following membrane fusion, all members of the SNARE complex are located in the target membrane, and the complex is referred to as a *cis*-SNARE complex.

SNARE complexes mediate both constitutive and regulated vesicle fusion events throughout cells. At the synapse, multiple regulatory elements suppress constitutive SNARE-mediated fusion events and facilitate the fast, synchronous fusion of multiple synaptic vesicles upon Ca^{2+} influx. Synchronous fusion of multiple vesicles is essential for neuronal signaling and relies on the docking of vesicles at the active zone and their priming to a fusion ready state (section V.b).

The basic concept of the minimal machinery necessary to fuse a vesicular with its target membrane is as follows: SNARE proteins on both the vesicular and target membranes associate to form tight coiled-coil configurations. When maximally coiled, *trans*-SNARE complexes force the two membranes together, thereby destabilizing the membranes' natural curvature (AF 1.4). The coiling of *trans*-SNARE complexes all the way into their transmembrane domains provides the energy to drive fusion of the membranes [64, 66, 67]. Following fusion, the vSNAREs and tSNARES are now in a *cis*-SNARE complex, and the vesicular contents are released.

AF 1.4. Minimal fusion machinery. Schematic of a vesicle just prior to fusion showing two (of multiple) maximally-coiled, *trans*-SNARE complexes pulling the vesicle membrane flat against the presynaptic membrane. (Reprinted by permission from [61], Springer Nature: Springer, Nature, Crystal structure of a SNARE complex involved in synaptic exocytosis at 2.4 Å resolution. R Brian Sutton, Dirk Fasshauer, Reinhard Jahn, Axel T. Brunger, ©1998).

SM Proteins

SM proteins function during virtually all SNARE-dependent fusion reactions. These soluble proteins fold into general "clasp" shapes [68] with a propensity to bind four helix bundles. At least one SM protein is necessary for any SNARE-mediated fusion event to occur. SM proteins are believed to be essential to stabilize SNARE complexes spatially and support SNARE complex assembly. Munc18, a member of the SM protein family, binds the N-terminal region of syntaxin in its closed conformation [62, 68, 69]. This SM/SNARE interaction prevents SNARE complex assembly, thereby inhibiting fusion events. Once syntaxin undergoes a conformational change to its open configuration (see section V.b), Munc18 remains bound but alters its binding to interact directly with the four helix bundle of the assembling *trans*-SNARE complex, aiding in fusion [70, 71]. In this way, SM proteins are both negative and positive regulators of SNARE-mediated fusion.

Ca^{2+} Channels

The presence of voltage-gated Ca^{2+} channels at active zones is necessary to couple neuronal depolarization to vesicle fusion events. Not only do these channels need to be present at

active zones, their precise localization within an active zone can have immense effects on the efficacy of synaptic transmission. Ca^{2+} channels are located within 50 nm from docked vesicles [72-74]. When the cell is depolarized, the Ca^{2+} channels briefly open, creating a nanodomain of particularly high [Ca^{2+}] immediately adjacent to each channel. This [Ca^{2+}] reaches hundreds of μM at the mouth of the channel [75] and drops off rapidly with distance (AF 1.5) [76-79]. As the availability of Ca^{2+} is limited temporally and spatially, the closer the channel is located to the Ca^{2+} sensor, the greater the odds of saturating sensor binding and triggering vesicle fusion. Since the sensor for fast, synchronous neurotransmitter release is a low affinity sensor (see below), even a 5 nm change in the distance between the channel and the sensor has profound effects on vesicle release probability [80].

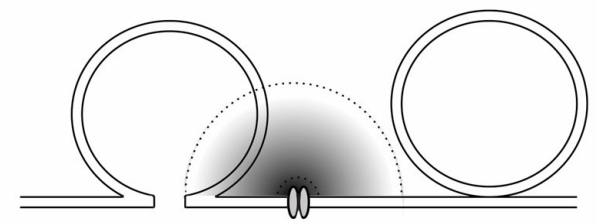

AF 1.5. Ca^{2+} nanodomains. Schematic depicting the rapid decay of [Ca^{2+}] with distance from the Ca^{2+} channel. The darker the gradient, the higher the [Ca^{2+}]. A Ca^{2+} sensor on the left vesicle would experience a very high [Ca^{2+}], which would maximize the probability of fusion. A Ca^{2+} sensor on the right vesicle would be exposed to a much lower [Ca^{2+}] and have a correspondingly lower probability of fusion.

Ca^{2+} Sensors

Synaptotagmins 1, 2, and 7, as well as Doc2 regulate two distinct forms of Ca^{2+}-dependent neurotransmitter release: fast, synchronous release and a longer lasting, asynchronous release (section V.c). While other Ca^{2+} sensors exist, only the previously mentioned proteins will be covered as they are currently the best understood.

Synaptotagmins are a large family of integral membrane proteins that contain two Ca^{2+}-binding motifs called C_2 domains. Synaptotagmin 1 and 2 are located on synaptic vesicles and play functionally homologous roles in different parts of the nervous system. In mammals, synaptotagmin 1 is expressed predominantly in the cerebral hemispheres, while synaptotagmin 2 is expressed predominantly in the brainstem, spinal cord, and at the neuromuscular junction [81, 82]. Synaptotagmins 1/2 are low-affinity Ca^{2+} sensors, meaning they only bind Ca^{2+} when intracellular [Ca^{2+}] is very high, as found in the Ca^{2+} nanodomains discussed above. In the Ca^{2+}-bound state, the C_2 domains of synaptotagmin interact with both SNARE proteins [83-88] and negatively-charged phospholipid membranes *in vitro* [89-91]. Upon Ca^{2+} binding *in vivo*, synaptotagmins 1/2 trigger the fast, synchronous phase of neurotransmitter release [92] primarily through membrane interactions [93, 94], although Ca^{2+}-dependent SNARE interactions likely contribute as well.

Synaptotagmin 7 is another member of the synaptotagmin family enriched at synapses. It is an integral membrane protein localized in the presynaptic membrane [95] that binds Ca^{2+} with a higher affinity than synaptotagmins 1/2. Doc2 is also enriched at synapses and contains two Ca^{2+}-binding C_2 domains with a high affinity for Ca^{2+} [96]. Unlike the synaptotagmins, Doc2 is a cytosolic protein. Both synaptotagmin 7 and Doc2 are attractive candidates for triggering asynchronous release (section V.c) due to their high Ca^{2+} affinities and slow Ca^{2+}-interaction kinetics [97].

V.b. Docking and Priming at the Active Zone

To become fusion competent, synaptic vesicles must be precisely targeted to the active zone and held in direct contact with the presynaptic membrane. First, vesicles are tethered near

the presynaptic membrane at active zones. When the vesicle membrane touches the presynaptic membrane, the vesicle is considered docked at the release site. Once docked, additional interactions, referred to as priming, increase the probability of vesicle fusion.

Adaptor proteins piccolo/bassoon are thought to guide synaptic vesicles toward active zones in vertebrates [98, 99]. Once there, RIM and Munc13 contribute to vesicle docking [100]. RIM binds to Munc13, creating a RIM/Munc13 heterodimer. This heterodimer binds an accessory protein, either Rab3 or Rab27, and this complex provides the scaffold needed to precisely target and hold synaptic vesicles to active zones (AF 1.2A.b) [101]. These vesicles are now considered docked.

Additional intermolecular interactions are required before vesicles are maximally primed and fully fusion competent. Munc13, an essential active zone protein, is thought to orchestrate the first step in fusion machinery assembly (note: Munc13 should not to be confused with the SM protein, Munc18, discussed in section V.a). Munc13 binds to the closed conformation of syntaxin and facilitates a conformational change in syntaxin from its “closed” to its “open” state [62, 102]. Only then can syntaxin’s SNARE motif interact with the SNARE motifs of SNAP-25 and synaptobrevin to form a *trans*-SNARE complex. Upon syntaxin’s conformational change, the Munc18 interaction adjusts to facilitate the assembly of the *trans*-SNARE complex [70, 71], thereby contributing to the fusion-competency of the vesicle.

Recent work in the McMahan lab suggests that vesicle priming is in a state of dynamic equilibrium (AF 1.6A, arrows), such that only docked vesicles with the largest area of contact with the presynaptic membrane are maximally primed and ready to fuse upon Ca^{2+} influx [52]. One mechanism of accomplishing variable priming would be a balance between the repulsive forces of the vesicular and presynaptic membranes that result in SNARE complex uncoiling to

favor minimal priming (AF 1.6A, left) and SNARE complex coiling to favor maximal priming (AF 1.6A, right) [52]. At any given moment, only a subpopulation of docked synaptic vesicles have a sufficient number of maximally-coiled *trans*-SNARE complexes to produce maximal SV-PM contact area. These synaptic vesicles constitute the maximally-primed population that is most likely to fuse upon Ca^{2+} influx. Once triggered by Ca^{2+}, these maximally-primed synaptic vesicles complete the SNARE coiling process all the way into the transmembrane domains of syntaxin and synaptobrevin [103]. The synaptic vesicle membrane merges with the presynaptic membrane, resulting in *cis*-SNARE complex formation. Thus, the coiling of SNARE complexes provides the energy needed to induce membrane fusion.

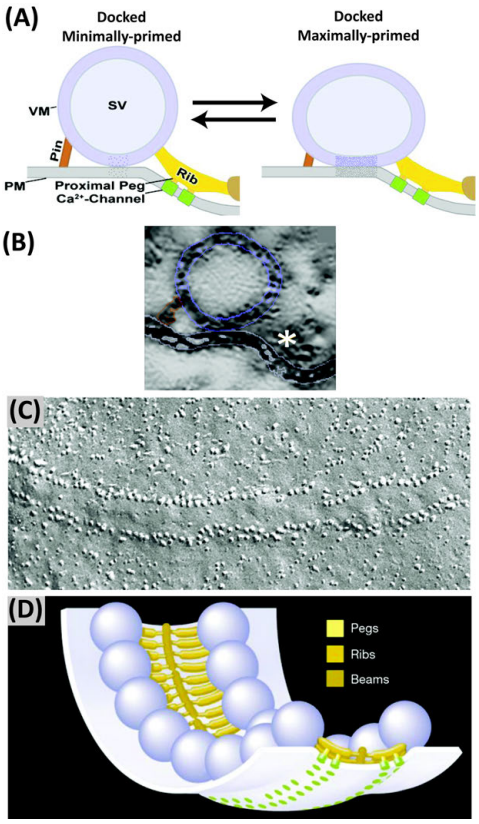

AF 1.6. Docking and variable priming of synaptic vesicles. (A) Left, schematic depicting a docked, minimally-primed vesicle at the presynaptic membrane, defined by the small area of contact between the vesicle and plasma membranes. Right, the fusion machinery located in the AZM (ribs, pegs) and in pins pulls the vesicle and presynaptic membranes together, increasing the area of contact, resulting in a maximally-primed vesicle that has the highest fusion probability. The degree of priming is in a state of dynamic equilibrium (arrows). Those vesicles

that happen to be maximally primed when Ca^{2+} influx occurs are thought to be the vesicles that fuse. (Adapted from [52]). (B) A docked synaptic vesicle viewed by electron tomography. White * represents AZM. (Adapted from [104]). (C) Freeze-fracture electron micrograph at the frog neuromuscular junction showing the characteristic parallel double-rows of particles that comprise the pegs of the AZM and include the voltage-gated Ca^{2+} channels required for triggering fusion. (Adapted from [72] ©1979 Journal of Cell Biology. 81:275-300. DOI:10.1083/jcb.81.2.275). (D) Schematic showing the relationship of docked synaptic vesicles, the AZM, and the double row of particles that include Ca^{2+} channels at the frog neuromuscular junction. (Reprinted with permission from [73], Springer Nature: Springer, Nature, The Architecture of active zone material at the frog's neuromuscular junction. Mark L Harlow, David Ress, Arne Stoschek, Robert M Marshall, Uel J McMahan, ©2001).

V.c. Vesicle Fusion

Fusion events can occur spontaneously or can be evoked. When an action potential depolarizes the presynaptic terminal, voltage-gated Ca^{2+} channels open. The subsequent influx of Ca^{2+} triggers a series of intermolecular interactions that results in the fusion of multiple maximally-primed vesicles with the presynaptic membrane (AF 1.2A,C and 1.7).

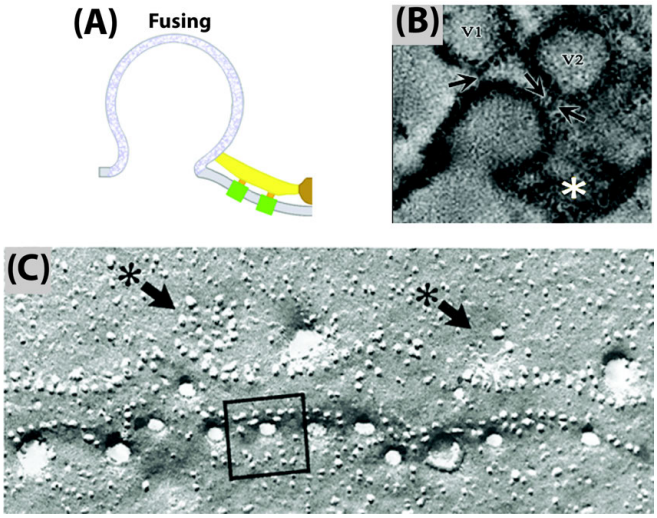

AF 1.7. Vesicle fusion. (A) Schematic depicting a vesicle that has just fused with the presynaptic membrane such that the vesicle membrane is now incorporated into the plasma membrane, forming an omega figure. (B) Electron tomograph of a fusing vesicle. V1 and V2 represent additional synaptic vesicles located near the active zone that are linked to the fusing vesicle (arrows). White * represents AZM. (A,B adapted from [104]). (C) Freeze-fracture electron micrograph showing the openings of fusing vesicles (box) just lateral to the double-rows of particles found at active zones. Cluster of particles characteristic of fully-collapsed vesicles (black * bold arrows) are also found lateral to the double-row of particles. (Adapted from [72] ©1979 Journal of Cell Biology. 81:275-300. DOI:10.1083/jcb.81.2.275).

Ca^{2+}-independent Neurotransmitter Release

Ca^{2+}-independent neurotransmitter release is referred to as spontaneous release. This form of neurotransmitter release occurs in resting nerve terminals when a single vesicle fuses with the presynaptic membrane in the absence of presynaptic Ca^{2+} influx (AF 1.3A). Classically, spontaneous release is considered to be random fusion events caused by low-probability conformational changes that complete coiling of the SNARE proteins and result in fusion. Since these spontaneously fusing vesicles would be in a maximally-primed, fusion-competent state, little energy is required to overcome the fusion barrier.

Spontaneous and evoked fusion events can occur at distinct active zones [105, 106] from separate recycling pools [107, 108]. Thus, location may partially determine the probability of a vesicle participating in spontaneous versus evoked neurotransmitter release. These recent studies, together with the classic spontaneous release hypothesis, suggest multiple mechanisms occurring during spontaneous fusion, with a subpopulation originating from maximally-primed vesicles reacting to transient changes in their environment, and another subpopulation occurring at specialized, Ca^{2+}-independent fusion sites.

Ca^{2+}-dependent Neurotransmitter Release

Ca^{2+}-dependent neurotransmitter release is differentiated temporally into two phases: fast, synchronous release and a slower, asynchronous release (AF 1.8) [109, 110]. The fast, synchronous phase is the large burst of neurotransmitter release that occurs within milliseconds of the arrival of the action potential and constitutes the classical neurotransmitter release pathway typically described in textbooks (AF 1.8, upper trace). However, there is an additional slower, or asynchronous, phase of elevated release that is still Ca^{2+}-dependent and lasts for tens

to hundreds of milliseconds [109, 110]. This phase of release is most notable following periods of high frequency stimulation, at specialized synapses, and at synaptotagmin 1 knock out synapses (FA 1.8, lower trace) [110-114].

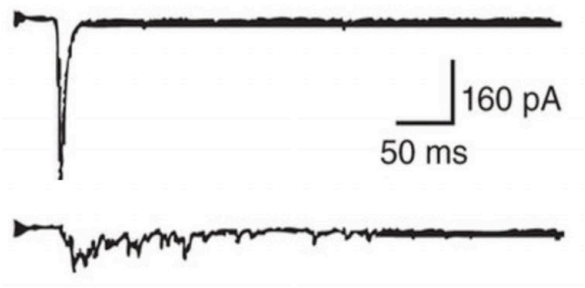

AF 1.8. Ca^{2+}-dependent neurotransmitter release at cultured hippocampal synapses. Upper, voltage trace depicts the fast, synchronous neurotransmitter release in cultures from wild type mice. Lower, voltage trace depicts the slower, asynchronous neurotransmitter release in cultures from synaptotagmin 1 knock out mice. (Reprinted from [115], Cell, 79/4, Martin Geppert, Yukiko Goda, Robert E Hammer, Cai Li, Thomas W Rosahl, Charles F Stevens, Thomas C Sudhof, Synaptotagmin I: a major Ca^{2+} sensor for transmitter release at a central synapse, p. 717-27. ©1994, with permission from Elsevier).

Fast, synchronous release of neurotransmitter occurs when multiple synaptic vesicles fuse within milliseconds of depolarization (AF 1.8, upper trace). The structure of the active zone provides optimal conditions to accomplish this task. Synaptotagmin 1/2 is a low-affinity Ca^{2+} sensor with fast binding/unbinding kinetics. Thus, saturated Ca^{2+} binding requires the exceptionally high [Ca^{2+}] that only occurs in nanodomains around open Ca^{2+} channels. Since this high [Ca^{2+}] drops off rapidly in time and space by diffusion [76-79], only synaptotagmin 1/2 located within such a nanodomain would be expected to trigger fusion; the rapid decrease in high [Ca^{2+}] ensures that the signal to fuse is terminated. Therefore, synaptotagmin's precise location relative to the presynaptic Ca^{2+} channels has profound effects on the release probability of the vesicle. As the SNAREs coil and pull the vesicle and plasma membranes together, not only does the membrane contact area increase, the distance between the Ca^{2+} channel and synaptotagmin is predicted to decrease [52]. According to this hypothesis, only the subpopulation of docked

synaptic vesicles that are maximally primed would situate synaptotagmin at its closest to Ca^{2+} channels. The closer synaptatogamin 1/2 is to the Ca^{2+} channel at the time of Ca^{2+} influx, the higher the [Ca^{2+}] that reaches its C_2B domains, favoring fusion.

Upon Ca^{2+} binding, the net charge of the Ca^{2+} binding pockets of synaptotagmin changes from negative to positive. This enhances interactions with the negatively charged presynaptic membrane and potentially with *trans*-SNARE complexes [83, 89, 116, 117]. Thus, Ca^{2+} binding allows synaptotagmin 1/2 to act as an "electrostatic switch" [118-121]. Switching from electrostatic repulsion to electrostatic attraction permits hydrophobic residues in the C_2 domains of synaptotagmin 1/2 to escape the hydrophilic cytosol by penetrating into the hydrophobic core of the presynaptic membrane. Therefore, synaptotagmin 1/2 can be thought of as providing the final push, much like popping a tightly-inflated balloon, to trigger fusion. This hypothesis can account for both the spatial and temporal restriction observed during fast, synchronous neurotransmitter release.

Asynchronous Release

Asynchronous release continues for several 100's of milliseconds up to a second (AF 1.8, lower trace). Asynchronous neurotransmitter release is observed in many neuronal types during and following extended high frequency activity [111]. Under these circumstances, the [Ca^{2+}] builds up since Ca^{2+} clearance is slower than Ca^{2+} entry. During the prolonged Ca^{2+} clearance phase, the residual [Ca^{2+}] is thought to drop below saturating binding levels for synaptotagmin 1/2 [109], but it remains high enough to activate a high-affinity Ca^{2+} sensor. While most synapses exhibit little to no asynchronous release following a single action potential,

asynchronous release is predominant in some specialized synapses [112-114]. Asynchronous release has been implicated in modulating postsynaptic responses [122].

The identity of the Ca^{2+} sensor(s) for asynchronous release is still debated. Like the fast, synchronous Ca^{2+} sensor, the asynchronous Ca^{2+} sensor needs be present at synapses and enriched at fusion sites. However, it must have a higher affinity for Ca^{2+} so that it can bind at lower [Ca^{2+}], permitting this protein to trigger release over a longer time course. Synaptotagmin 7 and Doc2 are current candidates for the Ca^{2+} sensor for triggering asynchronous neurotransmitter release, as they exhibit these characteristics [96, 97, 123].

V.d. SNARE and Vesicle Recycling

After a synaptic vesicle fuses, the SNARE complex is in a *cis* conformation since the vesicle membrane is incorporated into the presynaptic membrane. Cytosolic adaptor proteins specifically recognize and bind to *cis*-SNARE complexes and recruit N-ethylmaleimide-sensitive factor (NSF). NSF is an ATPase responsible for disassembling the SNARE complex [64]. This disassembly is required before the vSNAREs can be endocytosed for incorporation into new vesicles and before the tSNAREs can be reused in subsequent rounds of fusion events.

The synaptic vesicle membrane and all associated vesicle proteins must be rapidly recycled within nerve terminals to maintain the pool of vesicles available for fusion. There are multiple proposed mechanisms of synaptic vesicle recycling, but clathrin-mediated endocytosis (CME) is currently the best understood. CME was first described over 50 years ago [124] and occurs in many cell types (reviewed in [125]). It was first implicated in synaptic vesicle recycling in 1973 when it was shown to occur away from active zones following full collapse of the synaptic vesicle membrane into the presynaptic membrane (AF 1.2A,h) [124]. During CME,

a plethora of adaptor and accessory proteins facilitate appropriate membrane invagination and recruitment of clathrin to form spherical clathrin-coated membrane pits that project into the presynaptic cytoplasm [126]. The GTPase, dynamin, is then recruited to mediate a scission event that separates the clathrin-coated pit from the presynaptic membrane. The new vesicle is uncoated, targeted to endosomes or synapses, reloaded with neurotransmitter, and transported back to active zones. This completes the synaptic vesicle cycle, and can occur as fast as ~20-40 seconds [127].

Recently, a clathrin-independent endocytic mechanism was reported in both invertebrate [128] and vertebrate [129] neurons. This mechanism, called ultrafast endocytosis, occurs 200 times faster than CME. However, it must be stressed that this pathway still requires the action of clathrin for reformation of synaptic vesicles. The clathrin-independent bulk internalization of membrane produces large vesicles that form endosomes. The reformation of synaptic vesicles requires clathrin-mediated vesicle budding from these endosomes [130]. Another mechanism postulated to mediate vesicle recycling is known as “kiss and run”, where vesicles undergo a transient connection to the plasma membrane via a fusion pore, but the vesicle never collapses [131]. While this mechanism occurs in endocrine cells [132], its role in nerve terminals is questionable (reviewed in [133]).

VI. Synaptic Cleft

The synaptic cleft contains proteins and glycoproteins that support cell adhesion and regulate synaptic development and stability. Cleft proteins also clear neurotransmitter. The vast majority of proteins in the synaptic cleft provide structural support to the pre- and postsynaptic membranes from development through maturity. Many of these proteins are transmembrane cell

adhesion molecules (reviewed in [32]). Their cytosolic domains generally interact with intracellular synaptic proteins while their extracellular domains bind to transmembrane synaptic proteins of the opposing cell. Some extracellular and transmembrane synaptic proteins direct synaptogenesis, while others are important for neurotransmitter clearance, including enzymes that break them down and transporters that sequester them.

The protein machinery and organization varies by synapse type and location. A CNS synapse connects two neurons, and in some locations, it is functionally important for the strength of CNS synapses to be easily modified. At the neuromuscular junction, the postsynaptic cell is a muscle fiber where there is less need for rapid changes in synaptic strength. Nevertheless, many general processes are conserved across synapses. Machinery for synaptogenesis, scaffolding, and neurotransmitter clearance are universally required, but the individual molecular interactions will be synapse specific.

VI.a. Synaptogenesis

A specific role for an extracellular matrix molecule in regulating the formation and maintenance of synaptic connections has been best elucidated at the frog neuromuscular junction. Dr. U.J. McMahan and colleagues discovered that the synaptic basal lamina contains molecules that direct the formation of synaptic specializations in both regenerating nerve terminals [7] and regenerating muscle fibers [8]. They purified the basal lamina molecule responsible for directing postsynaptic specializations and named it agrin [19].

Agrin is a critical signal for synaptogenesis and synaptic maintenance [134, 135]. It is secreted from presynaptic nerve terminals and is stably incorporated into the synaptic basal lamina. It binds to and activates a receptor complex in the plasma membrane of the muscle fiber,

which then induces postsynaptic specializations [134]. This receptor complex is composed of the low-density lipoprotein receptor-related protein 4 (LRP4), which binds agrin, and a muscle-specific kinase (MuSK), which triggers a postsynaptic signaling cascade [136-138]. This cascade recruits acetylcholine receptors, acetylcholinesterase (AChE), and numerous other components of the postsynaptic apparatus to postsynaptic sites immediately opposite the nerve terminal [139]. Precise alignment is critical for the formation, organization, maintenance, and function of the neuromuscular junction.

CNS synaptogenesis is not well understood. However, the neuroligin and neurexin families of proteins may play a role. The neuroligins are postsynaptic cell adhesion molecules [140] that bind to the presynaptic cell adhesion molecules, the neurexins [141]. This heterotypic interaction across the cleft aggregates the machinery (both pre- and postsynaptic) necessary for a functional synapse [142, 143]. Neuroligin-1 is present exclusively in excitatory synapses [144], while neuroligin-2 is present exclusively in inhibitory synapses [145]. Knockdown of neuroligins [146] or interference with neuroligin-neurexin signaling [147] diminishes the number of fully developed synapses. This research has led to the hypothesis that in addition to offering the structural stability of cell adhesion molecules at developing synapses, the postsynaptic neuroligins and presynaptic neurexins are critical for aggregating synaptic components and assigning the valence of the synapse.

VI.b. Scaffolding

The stability of synaptic connections is tightly regulated based on the functional requirements of the particular synapse. Some synapses, like neuromuscular junctions, are relatively stable and provide reliable transmission for proper locomotion over long time periods.

While there is minor synaptic remodeling, the function at this synapse remains relatively constant in healthy individuals. Other synapses are short lived or exhibit synaptic strengths that vary widely within seconds. In the cerebral cortex, synaptic plasticity may strengthen some synapses in response to heavy activity while pruning others that are less active. Such alterations in synaptic strength are foundational to the mechanisms of learning and memory first posited by Donald Hebb [148]. Scaffolding molecules spanning the synaptic cleft can either maintain and support a synapse or promote retraction and weakening.

The cadherins are a family of transmembrane cell adhesion molecules (reviewed in [149]) present at most synapses. They are thought to provide critical support for synapse stability, particularly in dendritic spines [150, 151]. They are present both pre- and postsynaptically and bridge the synaptic cleft through homotypic binding interactions. Cadherins are generally concentrated around the edges of synapses [152]. This localization may form a diffusion barrier that helps sequester receptors and maintain the structural integrity of the synapse [153].

Other classes of transmembrane proteins have more varied affects. The Eph receptor tyrosine kinases and their binding partners, epherins, interact across the cleft through heterotypic interactions. Signals in both antero- and retrograde directions are postulated to promote remodeling of synaptic structure [154, 155]. Different subtypes of Eph receptors and epherins have alternate affects. Knockdown of EphB2 leads to decreased synapse number and loss of synaptic superstructure [156]. Therefore, EphB2 signaling encourages the stability of synapses [157]. Ephrin-A3 and EphA4 signaling, on the other hand, results in decreased synapse number and retraction of synaptic ultrastructure [158]. Thus, these scaffolding molecules are critical for both maintenance and alteration of existing synapses across time, and their trans-synaptic signaling is necessary during many neurological processes.

VI.c. Neurotransmitter Clearance

Removal and/or breakdown of neurotransmitter by cleft proteins is pivotal for regulating the temporal aspects of the signal strength between neurons. The dopamine transporter, a well-defined example of this role [159], is the primary regulator of dopamine concentration in the synaptic cleft in a key reward center in the brain. Inhibition of this transporter by cocaine prevents the removal of dopamine from the presynaptic cell into the cleft [160]. The resulting build up causes increased signaling to the postsynaptic cell and consequent over-activity of the reward circuitry, leading to addiction.

Enzymatic breakdown is the other way to clear neurotransmitter after release. A well-characterized example of this clearance mechanism is the enzyme AChE [161], which hydrolyzes ACh. The action of AChE is so fast that the rate-limiting step in the breakdown of ACh is diffusion of the transmitter. This rapid breakdown is critical for proper synaptic function as it regulates ACh concentration and thus the postsynaptic response. AChE inhibitors provide effective treatment for diseases involving deficits in ACh signaling. In myasthenia gravis, the immune system attacks ACh receptors such that normal ACh release from motor neurons cannot provide sufficient muscle stimulation. By slowing down the clearance of ACh, AChE inhibitors counteract the muscle's decreased ability to respond [162]. Presynaptic defects are similarly amenable to treatment. According to the cholinergic hypothesis of Alzheimer's disease [163], loss of cholinergic neurons may underlie some cognitive deficits. AChE inhibitors are again used to slow down clearance, resulting in an accumulation of the ACh released by the remaining cholinergic neurons. Thus, it is essential that proteins specific for clearance of each type of neurotransmitter(s) released are present in the synaptic cleft.

VII. Postsynaptic Function

The postsynaptic membrane is uniquely specialized to detect neurotransmitters and transduce this chemical signal back into an electrical signal. Binding of neurotransmitters to receptors can elicit either a fast, transient or slower, longer-lasting response which may activate or inhibit electrical signaling in the postsynaptic cell. The specific response depends on the neurotransmitter released as well as the postsynaptic receptor subtype(s) present. Ionotropic receptors are ion channels that open upon neurotransmitter binding. Metabotropic receptors are GPCRs that activate G-protein second messenger systems, leading to changes in ion channel opening. Activating either type of receptor can result in postsynaptic depolarization or hyperpolarization depending on the ion selectivity of the activated channels.

VII.a. Postsynaptic Receptors

Ionotropic Receptors

Ionotropic receptors are ligand-gated ion channels that form pores in the membrane allowing the passage of ions down their electrochemical gradients [164]. Ion channels are generally closed at rest. Binding of their specific neurotransmitter causes a conformational change, opening the pore and allowing ion influx. Early studies at the frog neuromuscular junction measured ACh-induced changes in ion conductances in muscle fibers demonstrating channel opening in response to a ligand [165]. This process is extremely rapid, allowing immediate ion influx that abruptly ceases when the ligand unbinds, and the channel closes. In addition, some channels inactivate, stopping ionic conductance even while a ligand remains bound. In this way, ionotropic channels generate fast and transient electrical signals in response to the presence of neurotransmitter.

Metabotropic Receptors

Metabotropic receptors have extracellular binding sites for specific neurotransmitters and bind to intracellular G-proteins [166]. Binding of neurotransmitter to these GPCRs causes activation of the intracellular G-protein, which dissociates from the receptor and may activate intracellular kinase cascades, phosphatases, and/or other second messengers, which then act on various downstream effectors, including opening of ion channels. The necessity of multiple protein interactions before the opening of an ion channel means that the time scale of metabotropic receptor effects will be much slower than those of ionotropic receptors. Second messenger cascades can also amplify the original signal. One neurotransmitter molecule can activate a G-protein, which can activate multiple kinases, which can activate multiple ion channels. In addition, the downstream second messengers may remain activated after the ligand comes unbound from the GPCR. Thus, the postsynaptic response generated by metabotropic receptors, though slower, tend to be larger and more persistent.

Second messenger systems can have additional wide-ranging affects independent of electrical changes in the postsynaptic cell. Some second messengers act as transcription factors, altering gene expression [167]. Others cause release of internal Ca^{2+} stores and lead to changes in synaptic strength [168]. The potential downstream effects of multiple, simultaneously activated signaling pathways can vary widely depending on the downstream machinery present in the postsynaptic cell.

VII.b. Generation of Postsynaptic Potentials

The postsynaptic membrane's ability to transduce the chemical signal into an electrical signal is dependent on the opening of ion channels (either ionotropic receptors, or downstream

effectors of GPCRs) that allow ions to travel down their electrochemical gradients. Thus, the ion selectivity of the activated channels determines the net potential generated in the postsynaptic cell. At a typical excitatory synapse, the open ion channels allow positively-charged ions, such as Na^+ and Ca^{2+}, to flow down their electrochemical gradients into the postsynaptic cell. The influx of positive charge depolarizes the post-synaptic cell, otherwise known as an excitatory postsynaptic potential (EPSP). If the activated channels are permeable to either Cl^- or K^+, the postsynaptic membrane will be hyperpolarized. The concentration gradient for each of these ions is great enough to drive them against the electrical gradient, so Cl^- will enter or K^+ will leave the cell, which drives the membrane potential to a more negative value. Such a hyperpolarization is called an inhibitory postsynaptic potential (IPSP).

The net change in membrane potential depends on the summation of all synaptic inputs. Mammalian neuromuscular junctions are exclusively excitatory. At these synapses, sufficient ACh is released to ensure that the postsynaptic muscle fiber is depolarized past threshold, resulting in muscle fiber contraction (AF 1.3B). In the CNS, all synaptic inputs to the postsynaptic neuron, which may include both EPSPs and IPSPs, are summated. If the postsynaptic neuron is sufficiently depolarized at its axon initial segment, its firing rate will increase. If the net effect at the axon initial segment is a hyperpolarization, its firing rate will decrease. Thus, it is the net activity that determines the overall response in the postsynaptic cell (reviewed in [169]).

VIII. Modulation of the Chemical Synapse

The response of a given postsynaptic cell to the same level of activity in a presynaptic cell can vary depending on the efficacy of the synapse. Synaptic efficacy is based on many

factors, including the quantal content (number of neurotransmitter-filled synaptic vesicles that fuse in response to a given stimulus, discussed in section IV.b) and the type and number of postsynaptic receptors. Importantly, these pre- and postsynaptic parameters can be regulated by activity patterns. The capacity to modulate synaptic efficacy is an important mechanism underlying learning and memory. These activity-dependent changes are known as synaptic plasticity.

Experimentally, synaptic plasticity is measured both pre- and postsynaptically. Presynaptically, the amount of neurotransmitter released can be decreased or increased, leading to depressed or facilitated responses, respectively. Specifically, the quantal content of a synapse (m) depends on the number of vesicles available to fuse (n), and the release probability of each vesicle (p) (section IV.b). The release probability is dependent on the magnitude and duration of Ca^{2+} influx, the speed of Ca^{2+} clearance, and the proximity of the Ca^{2+} sensor to the channel (section V.a). Higher quantal content causes larger responses in the postsynaptic cell, barring any postsynaptic adaptations. Synapses with a high quantal content result from some combination of a large readily releasable pool of vesicles, high vesicle release probability, high Ca^{2+} influx, and/or slow Ca^{2+} clearance. Alternatively, low quantal content synapses have the opposite characteristics and result in smaller postsynaptic responses.

Postsynaptically, changes in synaptic activity can lead to changes in the morphological makeup of the postsynaptic membrane through insertion or removal of receptors. Any change in receptor density results in a change in response strength to a given signal. Therefore, activity-dependent alteration of the postsynaptic machinery allows for flexible modulation of postsynaptic responses to neurotransmitter release.

VIII.a. Depression

Synaptic depression is defined as a reduction in the amplitude of the postsynaptic response following a given presynaptic stimulus. This can be observed at high quantal content synapses during paired pulse experiments, in which two closely spaced stimuli are administered to a cell [170, 171]. The first response, or EPSP, is robust, while the second response is reduced. At a high quantal content synapse, the first stimulation is sufficient to release a large fraction of the readily releasable vesicles. Accordingly, there are fewer vesicles available to fuse during the second stimulus, which results in a reduced EPSP. Another example of synaptic depression is seen during a high-frequency stimulus train to the presynaptic cell [172, 173]. Since exocytosis is more rapid than endocytosis, such stimulation depletes the readily releasable pool of synaptic vesicles, even at low quantal content synapses, and quantal content is decreased.

VIII.b. Facilitation

Facilitation is an incremental increase in the postsynaptic response to a given presynaptic stimulation observed in paired pulse experiments at low quantal content synapses. Since the first stimulus at such a synapse results in the fusion of only a small fraction of the readily releasable pool, the number of vesicles available for fusion following the second impulse is not significantly reduced. If the delay between the two stimuli is within tens of milliseconds, not all the Ca^{2+} that entered during the first pulse has been removed by the time of the second pulse. Therefore, the $[Ca^{2+}]$ experienced by vesicles during the second pulse is higher and triggers a greater number of synaptic vesicles to fuse. If the delay between stimuli is long enough to allow the Ca^{2+} from the first pulse to be removed, the second response is not facilitated. This is known

as the residual Ca^{2+} hypothesis [174-176], and this form of presynaptic facilitation is very short-lived.

VIII.c. Long-term Potentiation

Long-term potentiation (LTP) is characterized by a long-lasting facilitated response in the postsynaptic cell following a brief tetanic stimulation of a strong input (AF 1.9A) or simultaneous stimulation of multiple weaker inputs. Since its discovery in the rabbit hippocampus in 1966 [4], the study of LTP has grown into an immense field. In the intervening 50 years, multiple forms of LTP have been detected in many different cells and brain regions. These changes can last from hours to days and rely on presynaptic and postsynaptic mechanisms (reviewed in [67, 177]). Here we describe a prototypic form of postsynaptic LTP, namely NMDA receptor-dependent LTP at excitatory synapses in the hippocampus (reviewed in [178]).

In this form of LTP, the postsynaptic neuron contains two classes of ionotropic glutamate receptors, AMPA receptors and NMDA receptors. NMDA receptors have extracellular Mg^{2+} bound in their pores at the resting membrane potential. Following a single stimulus, glutamate binds to both types of receptors. The AMPA receptors open, which allows Na^{+} influx and results in an EPSP. However, little to no current passes through the NMDA receptors due to the voltage-dependent Mg^{2+} block [179, 180].

During tetantic stimulation, the postsynaptic cell is sufficiently depolarized to remove the Mg^{2+} block from the NMDA receptor pore. With the block removed, glutamate binding results in a robust influx of Ca^{2+} through the NMDA receptor [181]. This is the essential step in the induction of LTP [182-184]. The increase in intracellular Ca^{2+} activates Ca^{2+}/calmodulin-dependent kinase II (CaMKII), resulting in the addition of more AMPA receptors in the

postsynaptic membrane [185-187]. This is an essential step in the expression of LTP [188-192], and AMPA receptor phosphorylation is likely involved [193-196]. The additional AMPA receptors may be locally inserted from intracellular pools and/or captured by the postsynaptic density from extrasynaptic receptors already in the membrane. While the precise mechanisms mediating the increase in AMPA receptors remain an active area of research, the presence of additional AMPA receptors in the postsynaptic membrane causes a given amount of glutamate release to elicit a potentiated response in the postsynaptic cell.

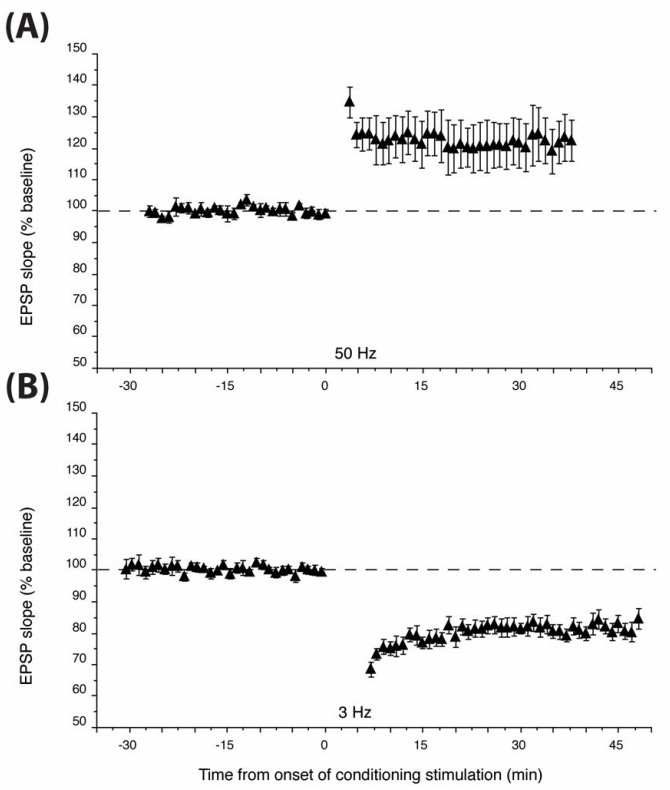

AF 1.9. Long-term potentiation and long-term depression. (A) Example of long-term potentiation induced by a brief high frequency stimulation (50 Hz for 900 pulses). (B) Example of long-term depression induced by a longer low frequency stimulation (3 Hz for 900 pulses). (Adapted from [197]).

VIII.d. Long-term Depression

Much like LTP, long-term depression (LTD) consists of multiple forms found in many different cell types and brain regions (reviewed in [198-200]). This chapter covers NMDA

receptor-dependent LTD in the hippocampus. LTD is a long-lasting, activity-dependent change in the efficacy of a synapse that results in a depressed postsynaptic response to a given presynaptic stimulus. It can be induced by prolonged low-frequency stimulation (AF 1.9B) [197]. As in LTP, this form of LTD requires both AMPA and NMDA receptors and is dependent on Ca^{2+} entry through unblocked NMDA receptors [197, 201-205]. Long duration, low-frequency synaptic stimulation results in a consistent, long-lasting, but smaller Ca^{2+} influx than the large, short-lived Ca^{2+} influx that causes LTP. This lower [Ca^{2+}] does not activate CaMKII [204]. Instead, it activates the phosphatases calcineurin and protein phosphatase 1 [66, 204, 206-208]. These phosphatases modify the phosphorylation state of AMPA receptors [196, 204, 209, 210] and tag them for internalization by clathrin and dynamin-dependent endocytosis [211-214]. The decrease in the number of AMPA receptors causes a depressed postsynaptic response. The structural changes in the number of postsynaptic AMPA receptors following either LTP or LTD induction allow the change in synaptic strength to last for a prolonged period of time.

WORKS CITED

1. Fatt, P. and B. Katz, *An analysis of the end-plate potential recorded with an intra-cellular electrode.* J Physiol, 1951. **115**(3): p. 320-70.
2. Fatt, P. and B. Katz, *Spontaneous subthreshold activity at motor nerve endings.* J Physiol, 1952. **117**(1): p. 109-28.
3. Del Castillo, J. and B. Katz, *Quantal components of the end-plate potential.* J Physiol, 1954. **124**(3): p. 560-73.
4. Lomo, T., *Frequency potentiation of excitatory synaptic activity in the dentate area of the hippocampal formation.* Acta Physiologica Scandinavia, 1966. **277**: p. 128.
5. Pinsker, H., et al., *Habituation and dishabituation of the gill-withdrawal reflex in Aplysia.* Science, 1970. **167**(3926): p. 1740-2.
6. Bliss, T.V. and T. Lomo, *Long-lasting potentiation of synaptic transmission in the dentate area of the anaesthetized rabbit following stimulation of the perforant path.* J Physiol, 1973. **232**(2): p. 331-56.
7. Sanes, J.R., L.M. Marshall, and U.J. McMahan, *Reinnervation of muscle fiber basal lamina after removal of myofibers. Differentiation of regenerating axons at original synaptic sites.* J Cell Biol, 1978. **78**(1): p. 176-98.
8. Burden, S.J., P.B. Sargent, and U.J. McMahan, *Acetylcholine receptors in regenerating muscle accumulate at original synaptic sites in the absence of the nerve.* J Cell Biol, 1979. **82**(2): p. 412-25.
9. Changeux, J.P., et al., *[Extraction from electric tissue of gymnotus of a protein presenting several typical properties characteristic of the physiological receptor of acetylcholine].* C R Acad Sci Hebd Seances Acad Sci D, 1970. **270**(23): p. 2864-7.
10. Takeuchi, A. and K. Onodera, *Effect of bicuculline on the GABA receptor of the crayfish neuromuscular junction.* Nat New Biol, 1972. **236**(63): p. 55-6.
11. Nickel, E. and L.T. Potter, *Ultrastructure of isolated membranes of Torpedo electric tissue.* Brain Res, 1973. **57**(2): p. 508-17.
12. Cartaud, J., et al., *Presence of a lattice structure in membrane fragments rich in nicotinic receptor protein from the electric organ of Torpedo marmorata.* FEBS Lett, 1973. **33**(1): p. 109-13.
13. Pfeiffer, F., D. Graham, and H. Betz, *Purification by affinity chromatography of the glycine receptor of rat spinal cord.* J Biol Chem, 1982. **257**(16): p. 9389-93.
14. Honore, T., J. Lauridsen, and P. Krogsgaard-Larsen, *The binding of [3H]AMPA, a structural analogue of glutamic acid, to rat brain membranes.* J Neurochem, 1982. **38**(1): p. 173-8.
15. Bradley, P.B., P.P. Humphrey, and R.H. Williams, *Evidence for the existence of 5-hydroxytryptamine receptors, which are not of the 5-HT2 type, mediating contraction of rabbit isolated basilar artery.* Br J Pharmacol, 1986. **87**(1): p. 3-4.
16. Hatta, K., T.S. Okada, and M. Takeichi, *A monoclonal antibody disrupting calcium-dependent cell-cell adhesion of brain tissues: possible role of its target antigen in animal pattern formation.* Proc Natl Acad Sci U S A, 1985. **82**(9): p. 2789-93.
17. Hirai, H., et al., *A novel putative tyrosine kinase receptor encoded by the eph gene.* Science, 1987. **238**(4834): p. 1717-20.

18. Magill, C., et al., *Agrin.* Prog Brain Res, 1987. **71**: p. 391-6.
19. Nitkin, R.M., et al., *Identification of agrin, a synaptic organizing protein from Torpedo electric organ.* J Cell Biol, 1987. **105**(6 Pt 1): p. 2471-8.
20. Ushkaryov, Y.A., et al., *Neurexins: synaptic cell surface proteins related to the alpha-latrotoxin receptor and laminin.* Science, 1992. **257**(5066): p. 50-6.
21. Bartley, T.D., et al., *B61 is a ligand for the ECK receptor protein-tyrosine kinase.* Nature, 1994. **368**(6471): p. 558-60.
22. Beckmann, M.P., et al., *Molecular characterization of a family of ligands for eph-related tyrosine kinase receptors.* Embo j, 1994. **13**(16): p. 3757-62.
23. Cheng, H.J. and J.G. Flanagan, *Identification and cloning of ELF-1, a developmentally expressed ligand for the Mek4 and Sek receptor tyrosine kinases.* Cell, 1994. **79**(1): p. 157-68.
24. Ichtchenko, K., et al., *Neuroligin 1: a splice site-specific ligand for beta-neurexins.* Cell, 1995. **81**(3): p. 435-43.
25. Block, M.R., et al., *Purification of an N-ethylmaleimide-sensitive protein catalyzing vesicular transport.* Proc Natl Acad Sci U S A, 1988. **85**(21): p. 7852-6.
26. Clary, D.O., I.C. Griff, and J.E. Rothman, *SNAPs, a family of NSF attachment proteins involved in intracellular membrane fusion in animals and yeast.* Cell, 1990. **61**(4): p. 709-21.
27. Clary, D.O. and J.E. Rothman, *Purification of three related peripheral membrane proteins needed for vesicular transport.* J Biol Chem, 1990. **265**(17): p. 10109-17.
28. Sollner, T., et al., *SNAP receptors implicated in vesicle targeting and fusion.* Nature, 1993. **362**(6418): p. 318-24.
29. Schiavo, G., et al., *Identification of the nerve terminal targets of botulinum neurotoxin serotypes A, D, and E.* J Biol Chem, 1993. **268**(32): p. 23784-7.
30. Couteaux R, P.-D.M., *Synaptic vesicles and pouches at the level of "active zones" of the neuromuscular junction.* C. R. Hebd. Seances Acad. Sci, 1970. **D271**: p. 2346-2349.
31. Hall, Z.W. and J.R. Sanes, *Synaptic structure and development: the neuromuscular junction.* Cell, 1993. **72 Suppl**: p. 99-121.
32. Missler, M., T.C. Sudhof, and T. Biederer, *Synaptic cell adhesion.* Cold Spring Harb Perspect Biol, 2012. **4**(4): p. a005694.
33. Specht, C.G. and A. Triller, *The dynamics of synaptic scaffolds.* Bioessays, 2008. **30**(11-12): p. 1062-74.
34. Sheng, M. and E. Kim, *The postsynaptic organization of synapses.* Cold Spring Harb Perspect Biol, 2011. **3**(12).
35. McMahon, H.T. and D.G. Nicholls, *The bioenergetics of neurotransmitter release.* Biochim Biophys Acta, 1991. **1059**(3): p. 243-64.
36. Marshansky, V. and M. Futai, *The V-type H+-ATPase in vesicular trafficking: targeting, regulation and function.* Curr Opin Cell Biol, 2008. **20**(4): p. 415-26.
37. Blakely, R.D. and R.H. Edwards, *Vesicular and Plasma Membrane Transporters for Neurotransmitters.* Cold Spring Harb Perspect Biol, 2012. **4**(2).
38. Sarter, M. and V. Parikh, *Choline transporters, cholinergic transmission and cognition.* Nat Rev Neurosci, 2005. **6**(1): p. 48-56.
39. Soreq, H., *Checks and balances on cholinergic signaling in brain and body function.* Trends Neurosci, 2015. **38**(7): p. 448-58.

40. Bak, L.K., A. Schousboe, and H.S. Waagepetersen, *The glutamate/GABA-glutamine cycle: aspects of transport, neurotransmitter homeostasis and ammonia transfer.* J Neurochem, 2006. **98**(3): p. 641-53.
41. Schousboe, A., et al., *Glutamate metabolism in the brain focusing on astrocytes.* Adv Neurobiol, 2014. **11**: p. 13-30.
42. Carlsson, A., *Perspectives on the discovery of central monoaminergic neurotransmission.* Annu Rev Neurosci, 1987. **10**: p. 19-40.
43. Ng, J., et al., *Monoamine neurotransmitter disorders--clinical advances and future perspectives.* Nat Rev Neurol, 2015. **11**(10): p. 567-84.
44. Abbracchio, M.P., et al., *Purinergic signalling in the nervous system: an overview.* Trends Neurosci, 2009. **32**(1): p. 19-29.
45. Burnstock, G., *Purinergic signalling: from discovery to current developments.* Exp Physiol, 2014. **99**(1): p. 16-34.
46. Boyd, I.A. and A.R. Martin, *The end-plate potential in mammalian muscle.* J Physiol, 1956. **132**(1): p. 74-91.
47. De Robertis, E.D. and H.S. Bennett, *Some features of the submicroscopic morphology of synapses in frog and earthworm.* J Biophys Biochem Cytol, 1955. **1**(1): p. 47-58.
48. Palay, S.L., *Synapses in the central nervous system.* J Biophys Biochem Cytol, 1956. **2**(4 Suppl): p. 193-202.
49. Bennett, M.R. and J.L. Kearns, *Statistics of transmitter release at nerve terminals.* Prog Neurobiol, 2000. **60**(6): p. 545-606.
50. Südhof, Thomas C., *The Presynaptic Active Zone.* Neuron, 2012. **75**: p. 11-25.
51. Nagwaney, S., et al., *Macromolecular connections of active zone material to docked synaptic vesicles and presynaptic membrane at neuromuscular junctions of mouse.* J Comp Neurol, 2009. **513**(5): p. 457-68.
52. Jung, J.H., et al., *Variable priming of a docked synaptic vesicle.* Proc Natl Acad Sci U S A, 2016. **113**(8): p. E1098-107.
53. Zhen, M. and Y. Jin, *Presynaptic terminal differentiation: transport and assembly.* Curr Opin Neurobiol, 2004. **14**(3): p. 280-7.
54. Schoch, S., et al., *RIM1α forms a protein scaffold for regulating neurotransmitter release at the active zone.* Nature, 2002. **415**: p. 321.
55. Spangler, S.A., et al., *Liprin-alpha2 promotes the presynaptic recruitment and turnover of RIM1/CASK to facilitate synaptic transmission.* J Cell Biol, 2013. **201**(6): p. 915-28.
56. Miller, K.E., et al., *Direct Observation Demonstrates that Liprin-α Is Required for Trafficking of Synaptic Vesicles.* Current Biology, 2005. **15**: p. 684-689.
57. Kaufmann, N., et al., *Drosophila Liprin-α and the Receptor Phosphatase Dlar Control Synapse Morphogenesis.* Neuron, 2002. **34**: p. 27-38.
58. Wagh, D.A., et al., *Bruchpilot, a protein with homology to ELKS/CAST, is required for structural integrity and function of synaptic active zones in Drosophila.* Neuron, 2006. **49**(6): p. 833-44.
59. Kittel, R.J., et al., *Bruchpilot promotes active zone assembly, Ca2+ channel clustering, and vesicle release.* Science, 2006. **312**(5776): p. 1051-4.
60. Lupas, A., *Prediction and analysis of coiled-coil structures.* Methods Enzymol, 1996. **266**: p. 513-25.
61. Sutton, R.B., et al., *Crystal structure of a SNARE complex involved in synaptic exocytosis at 2.4 A resolution.* Nature, 1998. **395**(6700): p. 347-53.

62. Dulubova, I., et al., *A conformational switch in syntaxin during exocytosis: role of munc18.* Embo j, 1999. **18**(16): p. 4372-82.
63. Yersin, A., et al., *Interactions between synaptic vesicle fusion proteins explored by atomic force microscopy.* Proc Natl Acad Sci U S A, 2003. **100**(15): p. 8736-41.
64. Sollner, T., et al., *A protein assembly-disassembly pathway in vitro that may correspond to sequential steps of synaptic vesicle docking, activation, and fusion.* Cell, 1993. **75**(3): p. 409-18.
65. Li, F., et al., *Energetics and dynamics of SNAREpin folding across lipid bilayers.* Nat Struct Mol Biol, 2007. **14**(10): p. 890-6.
66. Kameyama, K., et al., *Involvement of a postsynaptic protein kinase A substrate in the expression of homosynaptic long-term depression.* Neuron, 1998. **21**(5): p. 1163-75.
67. Castillo, P.E., *Presynaptic LTP and LTD of excitatory and inhibitory synapses.* Cold Spring Harb Perspect Biol, 2012. **4**(2).
68. K.M.S. Misura, R.H.S., W.I Weiss, *Three-dimensional structure of the neuronal Sec1-syntaxin 1a complex.* Nature, 2000. **404**(6776): p. 355-62.
69. Yang, B., et al., *nSec1 binds a closed conformation of syntaxin1A.* J Cell Biol, 2000. **148**(2): p. 247-52.
70. Shen, J., et al., *Selective Activation of Cognate SNAREpins by Sec1/Munc18 Proteins.* Cell. **128**(1): p. 183-195.
71. Dulubova, I., et al., *Munc18-1 binds directly to the neuronal SNARE complex.* Proceedings of the National Academy of Sciences, 2007. **104**(8): p. 2697-2702.
72. Heuser, J.E., et al., *Synaptic vesicle exocytosis captured by quick freezing and correlated with quantal transmitter release.* J Cell Biol, 1979. **81**(2): p. 275-300.
73. Harlow, M.L., et al., *The architecture of active zone material at the frog's neuromuscular junction.* Nature, 2001. **409**(6819): p. 479-84.
74. Eggermann, E., et al., *Nanodomain coupling between Ca(2)(+) channels and sensors of exocytosis at fast mammalian synapses.* Nat Rev Neurosci, 2011. **13**(1): p. 7-21.
75. Llinas, R., M. Sugimori, and R. Silver, *Microdomains of high calcium concentration in a presynaptic terminal.* Science, 1992. **256**(5057): p. 677-679.
76. Chad, J.E. and R. Eckert, *Calcium domains associated with individual channels can account for anomalous voltage relations of CA-dependent responses.* Biophys J, 1984. **45**(5): p. 993-9.
77. Fogelson, A.L. and R.S. Zucker, *Presynaptic calcium diffusion from various arrays of single channels. Implications for transmitter release and synaptic facilitation.* Biophys J, 1985. **48**(6): p. 1003-17.
78. Simon, S.M. and R.R. Llinas, *Compartmentalization of the submembrane calcium activity during calcium influx and its significance in transmitter release.* Biophys J, 1985. **48**(3): p. 485-98.
79. Naraghi, M. and E. Neher, *Linearized buffered Ca2+ diffusion in microdomains and its implications for calculation of [Ca2+] at the mouth of a calcium channel.* J Neurosci, 1997. **17**(18): p. 6961-73.
80. Shahrezaei, V. and K.R. Delaney, *Consequences of molecular-level Ca2+ channel and synaptic vesicle colocalization for the Ca2+ microdomain and neurotransmitter exocytosis: a monte carlo study.* Biophys J, 2004. **87**(4): p. 2352-64.
81. Ullrich, B., et al., *Functional properties of multiple synaptotagmins in brain.* Neuron, 1994. **13**(6): p. 1281-91.

82. Marqueze, B., et al., *Cellular localization of synaptotagmin I, II, and III mRNAs in the central nervous system and pituitary and adrenal glands of the rat.* J Neurosci, 1995. **15**(7 Pt 1): p. 4906-17.
83. Chapman, E.R., et al., *Ca2+ regulates the interaction between synaptotagmin and syntaxin 1.* J Biol Chem, 1995. **270**(40): p. 23667-71.
84. Lynch, K.L., et al., *Synaptotagmin C2A loop 2 mediates Ca2+-dependent SNARE interactions essential for Ca2+-triggered vesicle exocytosis.* Mol Biol Cell, 2007. **18**(12): p. 4957-68.
85. Vrljic, M., et al., *Molecular mechanism of the synaptotagmin-SNARE interaction in Ca2+-triggered vesicle fusion.* Nat Struct Mol Biol, 2010. **17**(3): p. 325-31.
86. Zhou, Q., et al., *Architecture of the synaptotagmin-SNARE machinery for neuronal exocytosis.* Nature, 2015. **525**(7567): p. 62-7.
87. Schupp, M., et al., *Interactions Between SNAP-25 and Synaptotagmin-1 Are Involved in Vesicle Priming, Clamping Spontaneous and Stimulating Evoked Neurotransmission.* J Neurosci, 2016. **36**(47): p. 11865-11880.
88. Wang, S., Y. Li, and C. Ma, *Synaptotagmin-1 C2B domain interacts simultaneously with SNAREs and membranes to promote membrane fusion.* Elife, 2016. **5**.
89. Bai, J., P. Wang, and E.R. Chapman, *C2A activates a cryptic Ca(2+)-triggered membrane penetration activity within the C2B domain of synaptotagmin I.* Proc Natl Acad Sci U S A, 2002. **99**(3): p. 1665-70.
90. Li, L., et al., *Phosphatidylinositol phosphates as co-activators of Ca2+ binding to C2 domains of synaptotagmin 1.* J Biol Chem, 2006. **281**(23): p. 15845-52.
91. Hui, E., et al., *Synaptotagmin-mediated bending of the target membrane is a critical step in Ca(2+)-regulated fusion.* Cell, 2009. **138**(4): p. 709-21.
92. Mackler, J.M., et al., *The C(2)B Ca(2+)-binding motif of synaptotagmin is required for synaptic transmission in vivo.* Nature, 2002. **418**(6895): p. 340-4.
93. Paddock, B.E., et al., *Ca2+-dependent, phospholipid-binding residues of synaptotagmin are critical for excitation-secretion coupling in vivo.* J Neurosci, 2008. **28**(30): p. 7458-66.
94. Paddock, B.E., et al., *Membrane penetration by synaptotagmin is required for coupling calcium binding to vesicle fusion in vivo.* J Neurosci, 2011. **31**(6): p. 2248-57.
95. Sugita, S., et al., *Synaptotagmin VII as a plasma membrane Ca(2+) sensor in exocytosis.* Neuron, 2001. **30**(2): p. 459-73.
96. Yao, J., et al., *Uncoupling the roles of synaptotagmin I during endo- and exocytosis of synaptic vesicles.* Nat Neurosci, 2011. **15**(2): p. 243-9.
97. Bacaj, T., et al., *Synaptotagmin-1 and synaptotagmin-7 trigger synchronous and asynchronous phases of neurotransmitter release.* Neuron, 2013. **80**(4): p. 947-59.
98. Mukherjee, K., et al., *Piccolo and bassoon maintain synaptic vesicle clustering without directly participating in vesicle exocytosis.* Proc Natl Acad Sci U S A, 2010. **107**(14): p. 6504-9.
99. Hallermann, S., et al., *Bassoon speeds vesicle reloading at a central excitatory synapse.* Neuron, 2010. **68**(4): p. 710-23.
100. Weimer, R.M., et al., *UNC-13 and UNC-10/Rim Localize Synaptic Vesicles to Specific Membrane Domains.* The Journal of Neuroscience, 2006. **26**(31): p. 8040-8047.
101. Dulubova, I., et al., *A Munc13/RIM/Rab3 tripartite complex: from priming to plasticity?* The EMBO Journal, 2005. **24**(16): p. 2839-2850.

102. Ma, C., et al., *Munc13 mediates the transition from the closed syntaxin–Munc18 complex to the SNARE complex.* Nature Structural &Amp; Molecular Biology, 2011. **18**: p. 542.
103. Stein, A., et al., *Helical extension of the neuronal SNARE complex into the membrane.* Nature, 2009. **460**(7254): p. 525-8.
104. Szule, J.A., et al., *Regulation of synaptic vesicle docking by different classes of macromolecules in active zone material.* PLoS One, 2012. **7**(3): p. e33333.
105. Melom, J.E., et al., *Spontaneous and Evoked Release Are Independently Regulated at Individual Active Zones.* The Journal of Neuroscience, 2013. **33**(44): p. 17253-17263.
106. Peled, E.S., Z.L. Newman, and E.Y. Isacoff, *Evoked and spontaneous transmission favored by distinct sets of synapses.* Curr Biol, 2014. **24**(5): p. 484-93.
107. Chung, C., et al., *Acute dynamin inhibition dissects synaptic vesicle recycling pathways that drive spontaneous and evoked neurotransmission.* J Neurosci, 2010. **30**(4): p. 1363-76.
108. Fawley, J.A., M.E. Hofmann, and M.C. Andresen, *Cannabinoid 1 and transient receptor potential vanilloid 1 receptors discretely modulate evoked glutamate separately from spontaneous glutamate transmission.* J Neurosci, 2014. **34**(24): p. 8324-32.
109. Goda, Y. and C.F. Stevens, *Two components of transmitter release at a central synapse.* Proc Natl Acad Sci U S A, 1994. **91**(26): p. 12942-6.
110. Atluri, P.P. and W.G. Regehr, *Delayed release of neurotransmitter from cerebellar granule cells.* J Neurosci, 1998. **18**(20): p. 8214-27.
111. Jensen, K., J.D. Lambert, and M.S. Jensen, *Tetanus-induced asynchronous GABA release in cultured hippocampal neurons.* Brain Res, 2000. **880**(1-2): p. 198-201.
112. Hefft, S. and P. Jonas, *Asynchronous GABA release generates long-lasting inhibition at a hippocampal interneuron-principal neuron synapse.* Nat Neurosci, 2005. **8**(10): p. 1319-28.
113. Daw, M.I., et al., *Asynchronous transmitter release from cholecystokinin-containing inhibitory interneurons is widespread and target-cell independent.* J Neurosci, 2009. **29**(36): p. 11112-22.
114. Best, A.R. and W.G. Regehr, *Inhibitory regulation of electrically coupled neurons in the inferior olive is mediated by asynchronous release of GABA.* Neuron, 2009. **62**(4): p. 555-65.
115. Geppert, M., et al., *Synaptotagmin I: a major Ca2+ sensor for transmitter release at a central synapse.* Cell, 1994. **79**(4): p. 717-27.
116. Chapman, E.R. and A.F. Davis, *Direct interaction of a Ca2+-binding loop of synaptotagmin with lipid bilayers.* J Biol Chem, 1998. **273**(22): p. 13995-4001.
117. Zhang, X., et al., *Ca2+-dependent synaptotagmin binding to SNAP-25 is essential for Ca2+-triggered exocytosis.* Neuron, 2002. **34**(4): p. 599-611.
118. Davletov, B., O. Perisic, and R.L. Williams, *Calcium-dependent membrane penetration is a hallmark of the C2 domain of cytosolic phospholipase A2 whereas the C2A domain of synaptotagmin binds membranes electrostatically.* J Biol Chem, 1998. **273**(30): p. 19093-6.
119. Ubach, J., et al., *Ca2+ binding to synaptotagmin: how many Ca2+ ions bind to the tip of a C2-domain?* Embo j, 1998. **17**(14): p. 3921-30.
120. Murray, D. and B. Honig, *Electrostatic control of the membrane targeting of C2 domains.* Mol Cell, 2002. **9**(1): p. 145-54.

121. Striegel, A.R., et al., *Calcium binding by synaptotagmin's C2A domain is an essential element of the electrostatic switch that triggers synchronous synaptic transmission.* J Neurosci, 2012. **32**(4): p. 1253-60.
122. Iremonger, K.J. and J.S. Bains, *Integration of asynchronously released quanta prolongs the postsynaptic spike window.* J Neurosci, 2007. **27**(25): p. 6684-91.
123. Hui, E., et al., *Three distinct kinetic groupings of the synaptotagmin family: candidate sensors for rapid and delayed exocytosis.* Proc Natl Acad Sci U S A, 2005. **102**(14): p. 5210-4.
124. Heuser, J.E. and T.S. Reese, *Evidence for recycling of synaptic vesicle membrane during transmitter release at the frog neuromuscular junction.* J Cell Biol, 1973. **57**(2): p. 315-44.
125. Kaksonen, M. and A. Roux, *Mechanisms of clathrin-mediated endocytosis.* Nat Rev Mol Cell Biol, 2018.
126. Reider, A. and B. Wendland, *Endocytic adaptors--social networking at the plasma membrane.* J Cell Sci, 2011. **124**(Pt 10): p. 1613-22.
127. Loerke, D., et al., *Cargo and dynamin regulate clathrin-coated pit maturation.* PLoS Biol, 2009. **7**(3): p. e57.
128. Watanabe, S., et al., *Ultrafast endocytosis at Caenorhabditis elegans neuromuscular junctions.* Elife, 2013. **2**: p. e00723.
129. Watanabe, S., et al., *Ultrafast endocytosis at mouse hippocampal synapses.* Nature, 2013. **504**(7479): p. 242-247.
130. Watanabe, S., et al., *Clathrin regenerates synaptic vesicles from endosomes.* Nature, 2014. **515**(7526): p. 228-33.
131. Ceccarelli, B., W.P. Hurlbut, and A. Mauro, *Depletion of vesicles from frog neuromuscular junctions by prolonged tetanic stimulation.* J Cell Biol, 1972. **54**(1): p. 30-8.
132. Neher, E. and A. Marty, *Discrete changes of cell membrane capacitance observed under conditions of enhanced secretion in bovine adrenal chromaffin cells.* Proc Natl Acad Sci U S A, 1982. **79**(21): p. 6712-6.
133. He, L. and L.G. Wu, *The debate on the kiss-and-run fusion at synapses.* Trends Neurosci, 2007. **30**(9): p. 447-55.
134. McMahan, U.J., *The agrin hypothesis.* Cold Spring Harb Symp Quant Biol, 1990. **55**: p. 407-18.
135. Tintignac, L.A., H.R. Brenner, and M.A. Ruegg, *Mechanisms Regulating Neuromuscular Junction Development and Function and Causes of Muscle Wasting.* Physiol Rev, 2015. **95**(3): p. 809-52.
136. Weatherbee, S.D., K.V. Anderson, and L.A. Niswander, *LDL-receptor-related protein 4 is crucial for formation of the neuromuscular junction.* Development, 2006. **133**(24): p. 4993-5000.
137. Zhang, B., et al., *LRP4 serves as a coreceptor of agrin.* Neuron, 2008. **60**(2): p. 285-97.
138. Kim, N., et al., *Lrp4 is a receptor for Agrin and forms a complex with MuSK.* Cell, 2008. **135**(2): p. 334-42.
139. Okada, K., et al., *The muscle protein Dok-7 is essential for neuromuscular synaptogenesis.* Science, 2006. **312**(5781): p. 1802-5.
140. Lise, M.F. and A. El-Husseini, *The neuroligin and neurexin families: from structure to function at the synapse.* Cell Mol Life Sci, 2006. **63**(16): p. 1833-49.

141. Missler, M. and T.C. Sudhof, *Neurexins: three genes and 1001 products.* Trends Genet, 1998. **14**(1): p. 20-6.
142. Scheiffele, P., et al., *Neuroligin expressed in nonneuronal cells triggers presynaptic development in contacting axons.* Cell, 2000. **101**(6): p. 657-69.
143. Graf, E.R., et al., *Neurexins induce differentiation of GABA and glutamate postsynaptic specializations via neuroligins.* Cell, 2004. **119**(7): p. 1013-26.
144. Song, J.Y., et al., *Neuroligin 1 is a postsynaptic cell-adhesion molecule of excitatory synapses.* Proc Natl Acad Sci U S A, 1999. **96**(3): p. 1100-5.
145. Varoqueaux, F., S. Jamain, and N. Brose, *Neuroligin 2 is exclusively localized to inhibitory synapses.* Eur J Cell Biol, 2004. **83**(9): p. 449-56.
146. Chih, B., H. Engelman, and P. Scheiffele, *Control of excitatory and inhibitory synapse formation by neuroligins.* Science, 2005. **307**(5713): p. 1324-8.
147. Levinson, J.N., et al., *Neuroligins mediate excitatory and inhibitory synapse formation: involvement of PSD-95 and neurexin-1beta in neuroligin-induced synaptic specificity.* J Biol Chem, 2005. **280**(17): p. 17312-9.
148. Hebb, D.O., *The Organization of Behavior*. 1949, New York: John Wiley and Sons, Inc.
149. Pokutta, S. and W.I. Weis, *Structure and mechanism of cadherins and catenins in cell-cell contacts.* Annu Rev Cell Dev Biol, 2007. **23**: p. 237-61.
150. Saglietti, L., et al., *Extracellular interactions between GluR2 and N-cadherin in spine regulation.* Neuron, 2007. **54**(3): p. 461-77.
151. Mendez, P., et al., *N-cadherin mediates plasticity-induced long-term spine stabilization.* J Cell Biol, 2010. **189**(3): p. 589-600.
152. Uchida, N., et al., *The catenin/cadherin adhesion system is localized in synaptic junctions bordering transmitter release zones.* J Cell Biol, 1996. **135**(3): p. 767-79.
153. Renner, M., et al., *Diffusion barriers constrain receptors at synapses.* PLoS One, 2012. **7**(8): p. e43032.
154. Arvanitis, D. and A. Davy, *Eph/ephrin signaling: networks.* Genes Dev, 2008. **22**(4): p. 416-29.
155. Lai, K.O. and N.Y. Ip, *Synapse development and plasticity: roles of ephrin/Eph receptor signaling.* Curr Opin Neurobiol, 2009. **19**(3): p. 275-83.
156. Henkemeyer, M., et al., *Multiple EphB receptor tyrosine kinases shape dendritic spines in the hippocampus.* J Cell Biol, 2003. **163**(6): p. 1313-26.
157. Kayser, M.S., et al., *Intracellular and trans-synaptic regulation of glutamatergic synaptogenesis by EphB receptors.* J Neurosci, 2006. **26**(47): p. 12152-64.
158. Murai, K.K., et al., *Control of hippocampal dendritic spine morphology through ephrin-A3/EphA4 signaling.* Nat Neurosci, 2003. **6**(2): p. 153-60.
159. Vaughan, R.A. and J.D. Foster, *Mechanisms of dopamine transporter regulation in normal and disease states.* Trends in Pharmacological Sciences. **34**(9): p. 489-496.
160. Huang, X., H.H. Gu, and C.G. Zhan, *Mechanism for Cocaine Blocking the Transport of Dopamine: Insights from Molecular Modeling and Dynamics Simulations.* J Phys Chem B, 2009. **113**(45): p. 15057-66.
161. Soreq, H. and S. Seidman, *Acetylcholinesterase--new roles for an old actor.* Nat Rev Neurosci, 2001. **2**(4): p. 294-302.
162. Pohanka, M., *Acetylcholinesterase inhibitors: a patent review (2008 - present).* Expert Opin Ther Pat, 2012. **22**(8): p. 871-86.

163. Francis, P.T., et al., *The cholinergic hypothesis of Alzheimer's disease: a review of progress.* Journal of Neurology, Neurosurgery & Psychiatry, 1999. **66**(2): p. 137-147.
164. Smart, T.G. and P. Paoletti, *Synaptic neurotransmitter-gated receptors.* Cold Spring Harb Perspect Biol, 2012. **4**(3).
165. Anderson, C.R. and C.F. Stevens, *Voltage clamp analysis of acetylcholine produced end-plate current fluctuations at frog neuromuscular junction.* J Physiol, 1973. **235**(3): p. 655-91.
166. Huang, Y. and A. Thathiah, *Regulation of neuronal communication by G protein-coupled receptors.* FEBS Lett, 2015. **589**(14): p. 1607-19.
167. Kvachnina, E., et al., *5-HT7 receptor is coupled to G alpha subunits of heterotrimeric G12-protein to regulate gene transcription and neuronal morphology.* J Neurosci, 2005. **25**(34): p. 7821-30.
168. Miyata, M., et al., *Local Calcium Release in Dendritic Spines Required for Long-Term Synaptic Depression.* Neuron, 2000. **28**(1): p. 233-244.
169. Blomfield, S., *Arithmetical operations performed by nerve cells.* Brain Res, 1974. **69**(1): p. 115-24.
170. Thomson, A.M., J. Deuchars, and D.C. West, *Large, deep layer pyramid-pyramid single axon EPSPs in slices of rat motor cortex display paired pulse and frequency-dependent depression, mediated presynaptically and self-facilitation, mediated postsynaptically.* J Neurophysiol, 1993. **70**(6): p. 2354-69.
171. Debanne, D., et al., *Paired-pulse facilitation and depression at unitary synapses in rat hippocampus: quantal fluctuation affects subsequent release.* J Physiol, 1996. **491 (Pt 1)**: p. 163-76.
172. Parnas, I., *Differential block at high frequency of branches of a single axon innervating two muscles.* J Neurophysiol, 1972. **35**(6): p. 903-14.
173. Parker, D., *Depression of synaptic connections between identified motor neurons in the locust.* J Neurophysiol, 1995. **74**(2): p. 529-38.
174. Katz, B. and R. Miledi, *THE EFFECT OF CALCIUM ON ACETYLCHOLINE RELEASE FROM MOTOR NERVE TERMINALS.* Proc R Soc Lond B Biol Sci, 1965. **161**: p. 496-503.
175. Katz, B. and R. Miledi, *The release of acetylcholine from nerve endings by graded electric pulses.* Proc R Soc Lond B Biol Sci, 1967. **167**(1006): p. 23-38.
176. Dodge, F.A., Jr. and R. Rahamimoff, *Co-operative action a calcium ions in transmitter release at the neuromuscular junction.* J Physiol, 1967. **193**(2): p. 419-32.
177. Malenka, R.C. and M.F. Bear, *LTP and LTD: an embarrassment of riches.* Neuron, 2004. **44**(1): p. 5-21.
178. Herring, B.E. and R.A. Nicoll, *Long-Term Potentiation: From CaMKII to AMPA Receptor Trafficking.* Annu Rev Physiol, 2016. **78**: p. 351-65.
179. Nowak, L., et al., *Magnesium gates glutamate-activated channels in mouse central neurones.* Nature, 1984. **307**(5950): p. 462-5.
180. Mayer, M.L., G.L. Westbrook, and P.B. Guthrie, *Voltage-dependent block by Mg2+ of NMDA responses in spinal cord neurones.* Nature, 1984. **309**(5965): p. 261-3.
181. Dingledine, R., *N-methyl aspartate activates voltage-dependent calcium conductance in rat hippocampal pyramidal cells.* J Physiol, 1983. **343**: p. 385-405.

182. Collingridge, G.L., S.J. Kehl, and H. McLennan, *Excitatory amino acids in synaptic transmission in the Schaffer collateral-commissural pathway of the rat hippocampus.* J Physiol, 1983. **334**: p. 33-46.
183. Wigstrom, H. and B. Gustafsson, *A possible correlate of the postsynaptic condition for long-lasting potentiation in the guinea pig hippocampus in vitro.* Neurosci Lett, 1984. **44**(3): p. 327-32.
184. Morris, R.G., et al., *Selective impairment of learning and blockade of long-term potentiation by an N-methyl-D-aspartate receptor antagonist, AP5.* Nature, 1986. **319**(6056): p. 774-6.
185. Liao, D., N.A. Hessler, and R. Malinow, *Activation of postsynaptically silent synapses during pairing-induced LTP in CA1 region of hippocampal slice.* Nature, 1995. **375**(6530): p. 400-4.
186. Durand, G.M., Y. Kovalchuk, and A. Konnerth, *Long-term potentiation and functional synapse induction in developing hippocampus.* Nature, 1996. **381**(6577): p. 71-5.
187. Shi, S.H., et al., *Rapid spine delivery and redistribution of AMPA receptors after synaptic NMDA receptor activation.* Science, 1999. **284**(5421): p. 1811-6.
188. Malinow, R., H. Schulman, and R.W. Tsien, *Inhibition of postsynaptic PKC or CaMKII blocks induction but not expression of LTP.* Science, 1989. **245**(4920): p. 862-6.
189. Malenka, R.C., et al., *An essential role for postsynaptic calmodulin and protein kinase activity in long-term potentiation.* Nature, 1989. **340**(6234): p. 554-7.
190. Silva, A.J., et al., *Alpha calcium/calmodulin kinase II mutant mice: deficient long-term potentiation and impaired spatial learning.* Cold Spring Harb Symp Quant Biol, 1992. **57**: p. 527-39.
191. Pettit, D.L., S. Perlman, and R. Malinow, *Potentiated transmission and prevention of further LTP by increased CaMKII activity in postsynaptic hippocampal slice neurons.* Science, 1994. **266**(5192): p. 1881-5.
192. Lledo, P.M., et al., *Calcium/calmodulin-dependent kinase II and long-term potentiation enhance synaptic transmission by the same mechanism.* Proc Natl Acad Sci U S A, 1995. **92**(24): p. 11175-9.
193. McGlade-McCulloh, E., et al., *Phosphorylation and regulation of glutamate receptors by calcium/calmodulin-dependent protein kinase II.* Nature, 1993. **362**(6421): p. 640-2.
194. Tan, S.E., R.J. Wenthold, and T.R. Soderling, *Phosphorylation of AMPA-type glutamate receptors by calcium/calmodulin-dependent protein kinase II and protein kinase C in cultured hippocampal neurons.* J Neurosci, 1994. **14**(3 Pt 1): p. 1123-9.
195. Barria, A., et al., *Regulatory phosphorylation of AMPA-type glutamate receptors by CaM-KII during long-term potentiation.* Science, 1997. **276**(5321): p. 2042-5.
196. Barria, A., V. Derkach, and T. Soderling, *Identification of the Ca2+/calmodulin-dependent protein kinase II regulatory phosphorylation site in the alpha-amino-3-hydroxyl-5-methyl-4-isoxazole-propionate-type glutamate receptor.* J Biol Chem, 1997. **272**(52): p. 32727-30.
197. Dudek, S.M. and M.F. Bear, *Homosynaptic long-term depression in area CA1 of hippocampus and effects of N-methyl-D-aspartate receptor blockade.* Proc Natl Acad Sci U S A, 1992. **89**(10): p. 4363-7.
198. Bellone, C., C. Luscher, and M. Mameli, *Mechanisms of synaptic depression triggered by metabotropic glutamate receptors.* Cell Mol Life Sci, 2008. **65**(18): p. 2913-23.

199. Gladding, C.M., S.M. Fitzjohn, and E. Molnar, *Metabotropic glutamate receptor-mediated long-term depression: molecular mechanisms.* Pharmacol Rev, 2009. **61**(4): p. 395-412.
200. Heifets, B.D. and P.E. Castillo, *Endocannabinoid signaling and long-term synaptic plasticity.* Annu Rev Physiol, 2009. **71**: p. 283-306.
201. Christie, B.R. and W.C. Abraham, *NMDA-dependent heterosynaptic long-term depression in the dentate gyrus of anaesthetized rats.* Synapse, 1992. **10**(1): p. 1-6.
202. Mulkey, R.M. and R.C. Malenka, *Mechanisms underlying induction of homosynaptic long-term depression in area CA1 of the hippocampus.* Neuron, 1992. **9**(5): p. 967-75.
203. Kandler, K., L.C. Katz, and J.A. Kauer, *Focal photolysis of caged glutamate produces long-term depression of hippocampal glutamate receptors.* Nat Neurosci, 1998. **1**(2): p. 119-23.
204. Lee, H.K., et al., *NMDA induces long-term synaptic depression and dephosphorylation of the GluR1 subunit of AMPA receptors in hippocampus.* Neuron, 1998. **21**(5): p. 1151-62.
205. Yang, S.N., Y.G. Tang, and R.S. Zucker, *Selective induction of LTP and LTD by postsynaptic [Ca2+]i elevation.* J Neurophysiol, 1999. **81**(2): p. 781-7.
206. Mulkey, R.M., C.E. Herron, and R.C. Malenka, *An essential role for protein phosphatases in hippocampal long-term depression.* Science, 1993. **261**(5124): p. 1051-5.
207. Mulkey, R.M., et al., *Involvement of a calcineurin/inhibitor-1 phosphatase cascade in hippocampal long-term depression.* Nature, 1994. **369**(6480): p. 486-8.
208. Kirkwood, A. and M.F. Bear, *Homosynaptic long-term depression in the visual cortex.* J Neurosci, 1994. **14**(5 Pt 2): p. 3404-12.
209. Roche, K.W., et al., *Characterization of multiple phosphorylation sites on the AMPA receptor GluR1 subunit.* Neuron, 1996. **16**(6): p. 1179-88.
210. Lee, H.K., et al., *Regulation of distinct AMPA receptor phosphorylation sites during bidirectional synaptic plasticity.* Nature, 2000. **405**(6789): p. 955-9.
211. Carroll, R.C., et al., *Dynamin-dependent endocytosis of ionotropic glutamate receptors.* Proc Natl Acad Sci U S A, 1999. **96**(24): p. 14112-7.
212. Heynen, A.J., et al., *Bidirectional, activity-dependent regulation of glutamate receptors in the adult hippocampus in vivo.* Neuron, 2000. **28**(2): p. 527-36.
213. Man, H.Y., et al., *Regulation of AMPA receptor-mediated synaptic transmission by clathrin-dependent receptor internalization.* Neuron, 2000. **25**(3): p. 649-62.
214. Wang, Y.T. and D.J. Linden, *Expression of cerebellar long-term depression requires postsynaptic clathrin-mediated endocytosis.* Neuron, 2000. **25**(3): p. 635-47.